

https://dspace.org/

Low NOx coal burner temperature profile evaluation

Smit, Dewan

2016

http://hdl.handle.net/10539/22689

Smit, Dewan (2016) Low NOx coal burner temperature profile evaluation, University of Witwatersrand, Johannesburg, <http://wiredspace.wits.ac.za/handle/10539/22689>

Downloaded from a DSpace repository. https://dspace.org/

LOW NO_x COAL BURNER TEMPERATURE PROFILE EVALUATION

Dewan Smit

A dissertation submitted to the Faculty of Engineering and the Built Environment, University of the Witwatersrand, Johannesburg, in fulfilment of the requirements for the degree of Master of Science in Engineering.

Johannesburg 2016

Declaration

I declare that this dissertation is my own unaided work. It is being submitted for the degree of Master of Science in Engineering to the University of Witwatersrand, Johannesburg. It has not been submitted before for any degree or examination to any other university.



(Signature of Candidate)

On the **15th** day of **October 2016**

Abstract

Stringent worldwide emissions legislation, the drive to lower carbon emissions, together with the ever increasing demand to preserve the environment has led to a considerable demand for cleaner and more efficient coal combustion technologies. A primary technology for the reduction of emissions of oxides of nitrogen (NO_x) is the installation of low NO_x coal combustion burners. Extensive research into various burner characteristics and, in particular, the aerodynamic characteristics required to improve combustion performance of low NO_x coal burners has been extensively undertaken and is ongoing.

In this work the aerodynamic behaviour of a full-scale, aerodynamically staged, single low-NO_x coal burner was numerically investigated. The objective of the study was to develop a single low NO_x burner CFD model in Ansys Fluent, to better characterize and understand the flame shape in terms of the temperature profile achieved. CFD serve as an additional tool to assist with plant optimization, design proposals and occurrence investigations. To have confidence in the single burner coal combustion CFD model, the results of the model were compared to data obtained from an existing operational low NO_x burner on site during a pre-defined load condition. To further improve on the theoretical CFD combustion model, drop tube furnace (DTF) experiments have been done to calculate the single rate Arrhenius kinetic parameters (pre-exponential factor and activation energy) for coal devolatilization and char combustion of the specific South African coal used.

The combustion CFD simulations showed with a lower than design air flow through the burner, a reduced amount of swirl was achieved. This reduced amount of swirl produces a jet like flame and influences the way in which the combustion species are brought together. Under these operating conditions the flame distance from the burner mouth was predicted to be 1.2 (m). A very promising result was obtained through CFD and compared well with the in-flame temperature measurement obtained through the burner centre-line of approximately 1.4 (m). In an attempt to improve the aerodynamic profile of the burner under the same operating conditions the swirl angle on the tertiary air (TA) inlet was increased. The increased swirl on the TA inlet of the burner showed an improvement on the aerodynamic profile and had a significant impact on the temperature distribution within the flame. The increased swirl resulted in an improved flame distance of approximately 0.5 (m) from the burner mouth. The effect of increased swirl on the temperature profile of the flame displayed the aerodynamic dependence of the low NOx burner on combustion performance.

Acknowledgements

I would like to extend my gratitude to the many people who helped to bring this research project to fulfilment.

First, I would like to thank my academic mentors Professor Walter Schmitz and Reshendren Naidoo, and my industrial mentor Sandile Peta for your passionate participation and inputs into the research. Thank you for your professionalism and valuable guidance you gave me throughout the research.

Then I would like to thank Bonny Nyangwa and Kganuwi Kekana at the Eskom Research, Testing and Development (RT&D) centre for allowing me access to their drop tube furnace facility and their guidance regarding the drop tube furnace tests.

I would also like to thank Notemba Sobuwa, Makgwanya Maringa, and Justice Tshikomba for allowing me to take part in the master's program and for the financial support. I will forever be grateful for the opportunity you gave me.

I would also like to acknowledge the Eskom Power Plant Engineering Institute (EPPEI) management team and it's Combustion Specialisation Centre at Wits University. My thanks also go to the EPPEI, Emission Control Specialisation Centre at North West University regarding the PC coal lab calculations.

Finally, I must express my very profound gratitude to my wife Alida for providing me with unfailing support and continuous encouragement throughout my years of study and through the process of researching and writing this dissertation. This accomplishment would not have been possible without you.

Table of Contents

Declaration I

Abstract II

Acknowledgements III

Table of Contents IV

List of Figures IX

List of Tables XIV

Nomenclature XV

Chapter 1: INTRODUCTION 1

1.1. Research Background 1

1.2. Research Motivation 2

1.3. Power Plant Overview 3

1.4. Research Objectives 5

1.5. Research Methodology 5

1.6. Structure of Dissertation 7

Chapter 2: LITERATURE REVIEW 8

2.1. Introduction 8

2.2. Low NOx Coal Combustion 9

2.2.1. NOx Environmental Concerns 9

2.2.2. Different NOx Formations 10

2.3. In-Flame NOx reduction 11

2.4. Flame Temperature Measurements 12

2.4.1. Non-Contact Methods 13

2.4.2. Contact Methods 15

2.5. Drop Tube Furnace Experiments 17

2.5.1. Devolatilization 18

2.5.2. Char Burnout 23
2.5.3. Ash Tracer Method 25
2.6. FLASHCHAIN 26
2.6.1. Devolatilization 27
2.6.2. Char Combustion 28
2.6.3. Combustion Kinetics Calculation 30
2.7. Numerical Simulations 32
2.7.1. Combustion Computational Models 33
2.7.2. Ansys Fluent 40
Chapter 3: BURNER IN-FLAME TEMPERATURE MEASUREMENTS 44
3.1. Introduction 44
3.2. Low NO_x Burner Operation 45
3.3. In-Flame Burner Measurements: 46
3.3.1. Parameters Measured 47
3.3.2. Equipment Used 47
3.3.3. Radiation Shield 49
3.3.4. Measurement Location 50
3.4. Burner Selection Process 51
3.4.1. Burner Condition 52
3.4.2. PF Distribution 52
3.4.3. Geometric Analysis 53
3.4.4. Fire Hydrant 55
3.5. Burner In-flame Measurements Procedure: 56
3.5.1. Swirl Settings 56
3.5.2. Operating Procedure 57
3.5.3. Burner In-flame Measurements Method 58
3.5.4. Additional Measurements 59

3.6. Experimental Error Analysis 59
3.6.1. Measurement Fluctuation: 59
3.6.2. Measurement Error Analysis 61
3.6.3. Final Error Percentage 64
3.7. Results 64
3.7.1. Operational Values 64
3.7.2. Temperature Results 65
3.8. Flame Profile Measurement Discussion 68
Chapter 4: DEVOLATILIZATION DTF EXPERIMENTS 69
4.1. Introduction 69
4.2. Experimental Setup 70
4.3. Coal Properties & Preparation: 73
4.4. Devolatilization Experimental Procedure 74
4.5. DTF Experiments Results 76
4.6. DTF Devolatilization Discussion 78
Chapter 5: DEVOLATILIZATION DTF NUMERICAL ANALYSIS 80
5.1. Introduction 80
5.2. PC Coal Lab Simulation (Initial Run) 82
5.3. DTF CFD Model 85
5.3.1. Geometry 85
5.3.2. Mesh 85
5.3.3. CFD Simulation Model Setup 86
5.3.4. CFD Wall Temperature User Defined Function 88
5.3.5. CFD Inlet Temperature Calculation 89
5.4. CFD Results – Default Kinetics (Initial Run) 90
5.5. PC Coal Lab Simulation (Improved User Defined Profile) 94
5.6. CFD Results – Updated Kinetics 99

5.7. PC Coal Lab Simulation (Final Kinetics Calculation) 101
5.8. Devolatilization Numerical Analysis Discussion 102
Chapter 6: CHAR BURNOUT DTF EXPERIMENTS 103
6.1. Introduction 103
6.2. Char Burnout Procedure 103
6.3. Coal Properties & Preparation 104
6.4. DTF Experiment Equations 105
6.4.1. Calculation of particle temperature (Tp): 105
6.4.2. Calculation particle residence time: 108
6.5. Measured Wall Temperature 110
6.6. Char Burnout Results 111
6.7. DTF Experiment Char Burnout Kinetics 112
6.8. DTF Char Burnout Discussion 113
Chapter 7: CHAR BURNOUT DTF NUMERICAL ANALYSIS 114
7.1. Introduction 114
7.2. PC Coal Lab Char Burnout Simulation – Initial Run 116
7.3. DTF CFD Char Burnout Model 119
7.3.1. Geometry & Mesh 119
7.3.2. Model Boundary Conditions 120
7.3.3. CFD Wall Temperature User Defined Function 121
7.4. CFD Char Burnout Results – Default Kinetics (Initial Run) 122
7.5. CFD Char Burnout Results – Updated Kinetics 123
7.6. PC Coal Lab Char Burnout Simulation – User Defined Conditions 125
7.7. Char Burnout Numerical Analysis Discussion 128
Chapter 8: LOW NO_x BURNER COMBUSTION CFD SIMULATION 130
8.1. Introduction 130
8.2. CFD Geometry 131

8.3. Mesh 132
8.4. Model Physics 134
8.5. Boundary Conditions 136
8.6. Stoichiometric Air Calculation 137
8.7. Inlet Swirl Calculation 140
8.8. Single Burner Combustion CFD Results 142
8.8.1. Baseline vs Design Simulation Results 143
8.8.2. Comparison to Measurements 146
8.8.3. Case Study 1: Kinetics Input Effect on Numerical Result 149
8.8.4. Case Study 2: Swirl Effect on Numerical Result 151
8.9. Mesh Sensitivity 157
8.10. CFD Results Discussion 158
Chapter 9: CONCLUSION AND RECOMMENDATION 160
9.1. Conclusion 160
9.2. Recommendations 161
Chapter 10: REFERENCES 164
APPENDIX A 169
APPENDIX B 171
APPENDIX C 173
APPENDIX D 174
APPENDIX E 176
APPENDIX F 177
APPENDIX G 178
APPENDIX H 179
APPENDIX I 180
APPENDIX J 181

List of Figures

Figure 1-1: Simplified power plant schematic **3**
Figure 1-2: Method used in terms of the burner temperature profile evaluation **5**
Figure 2-1: Structure of a low NO_x coal burner's flame [8] **11**
Figure 2-2: Electromagnetic spectrum [17] **13**
Figure 2-3: Construction of a radiation pyrometer [17] **14**
Figure 2-4: Typical experimental setup of a suction pyrometer [14] **15**
Figure 2-5: IFRF Standard suction pyrometer scheme [15] **16**
Figure 2-6: DTF facility set up at the laboratory GRE at the University of Haute-Alsace [18] **18**
Figure 2-7: Measurement of gas temperature along the DTF heights as a function of reference temperature (from 800 to 1400 (°C)) [18] **19**
Figure 2-8: AG-coal mass loss as a function of time and reference temperature in DTF [18] .. **20**
Figure 2-9: C-coal mass loss as a function of time and reference temperature in DTF [18] **21**
Figure 2-10: DTF volatile yield results at various temperatures (Δ 800 (°C), o 900 (°C), □ 1000 (°C), ∨ 1300(°C), 0 1450(°C)) [19] **22**
Figure 2-11: DTF char combustion efficiency results at various temperatures (o 900 (°C), □ 1000 (°C), Δ 1200 (°C), ∨ 1300(°C), 0 1450(°C)) [19] **24**
Figure 2-12: Effect of oxygen concentration on the mass fraction of char remaining after each experiment [25] **25**
Figure 2-13: Mechanistic features in CBK/E [36] **28**
Figure 2-14: PC coal lab coal combustion results for three different quality coals. Showing particle temperatures, mass loss profiles, scaled particle sizes and bulk densities [36] **29**
Figure 2-15: Arrhenius plots at increasing heating rates [36] **31**
Figure 2-16: (Left) - Coal's proximate and ultimate analysis. (Right) - Specific coal's single rate Arrhenius parameters [31] **32**
Figure 2-17: (Left) - An example of a typical mesh created for CFD application. (Right) - An example of the conservation of mass on a single cell in the domain [28][29] **33**
Figure 2-18: Typical CFD results of a low NO_x coal burner. a) Temperature, b) CO_2, c) CO, d) Particle tracks (K) [35] **35**
Figure 2-19: Horizontal furnace with low NOx burner [63] **36**
Figure 2-20: (Left) – CFD gas temperature results, (Right) – CFD oxygen concentration [63] **37**
Figure 2-21: Comparison of CFD predictions of near burner flow behaviour and burner performance with a decrease in TA vane angle [64] **39**
Figure 3-1: Low NO_x coal burner **46**

Figure 3-2: Actual water cooled suction pyrometer used 47
Figure 3-3: CAD of the probe used 48
Figure 3-4: Temporary ceramic tip added to the suction probe in order to shield the thermocouple from radiation 49
Figure 3-5: Basic burner schematic showing probe entry points into the furnace 50
Figure 3-6: Location of burner E3 in relation to furnace front wall and windbox. 51
Figure 3-7: Summary of complete PF distribution (21 October 2014) done during measurements 53
Figure 3-8: CAD distance from burner outlet to probe cross point through centre-line was calculated at 1994 (mm). CAD distance from the outer windbox wall to the probe cross point through the bottom inspection port was calculated at 3205 (mm) 54
Figure 3-9: Probe cross point in the furnace indicated by point x viewed from the side furnace inspection door 55
Figure 3-10: Burner sleeve setting 56
Figure 3-11: Percentage fluctuation from the mean value at each point measured through the bottom inspection port 60
Figure 3-12: Percentage fluctuation from the mean value at each point measured through the burner centre-line 60
Figure 3-13: Burner in-flame temperature measurement results through the centre-line and bottom inspection port combined 66
Figure 4-1: DTF experimental setup [26] 70
Figure 4-2: DTF gas inlet experimental setup 71
Figure 4-3: (Left) - Mechanical feeder. (Right) - Alumina tube together with the six surrounding heating elements 71
Figure 4-4: DTF gas outlet experimental setup 72
Figure 4-5: DTF experimental particle distribution 74
Figure 4-6: (Left) - DTF devolatilization experiment wall temperature profiles [26], (Right) - Illustration of measuring points down the furnace wall 76
Figure 4-7: DTF volatile yield experimental results 78
Figure 5-1: Method followed in the numerical calculation of devolatilization reaction kinetics 81
Figure 5-2: PC coal lab devolatilization simulation input values 83
Figure 5-3: PC coal lab particle temperature result @ 1400 (°C) (initial run) 83
Figure 5-4: PC coal lab volatile yield compared to DTF experimental results at 1400 (°C) set point 84
Figure 5-5: DTF CAD 85

Figure 5-6: (Left) - Expanded view of mesh at the injector inlet. (Right) – Mesh of the complete DTF furnace 86
Figure 5-7: C^{++} UDF Interpreted Into CFD 89
Figure 5-8: Secondary gas temperatures measured at the collection probe inlet during the experiments 90
Figure 5-9: CFD Wall Temperature UDF Result 91
Figure 5-10: Temperature Contours (K) 91
Figure 5-11: CFD particle temperature compared to PC coal lab @ 1400 (°C) - initial run .. 92
Figure 5-12: Volatile yield mass fraction contour 93
Figure 5-13: CFD volatile yield (%) result compared to PC coal lab and experimental results @ 1400 (°C) (initial run) 93
Figure 5-14: (Left) - PC coal lab user defined profiles for the DTF wall and centre-line gas temperatures - ("Dvol.inp"), (Right) – Complete profile obtained from CFD 94
Figure 5-15: Improved PC coal lab result compared to initial PC coal lab and CFD results @ 1400 (°C) (UDF defined) 95
Figure 5-16: Improved PC coal lab volatile yield (%) compared to initial PC coal lab simulation, initial CFD results, and experimental results @ 1400 (°C) 96
Figure 5-17: PC coal lab single rate parameters 97
Figure 5-18: Arrhenius plot 98
Figure 5-19: Updated volatile yield mass fraction contour @ 1400 (°C) 99
Figure 5-20: Single rate kinetics CFD volatile yield (%) compared to default kinetics CFD volatile yield (%) @ 1400 (°C) 100
Figure 5-21: Complete development of the numerical volatile yield (%) results compared to experimental result @ 1400 (°C) 101
Figure 6-1: DTF char burnout experiments wall temperature profile [26] 110
Figure 6-2: DTF experiments char burnout percentage 111
Figure 6-3: Arrhenius plot (char burnout) 112
Figure 7-1: Numerical calculation of char reaction kinetics method followed 115
Figure 7-2: PC coal lab "Coalpc" input file 116
Figure 7-3: PC coal lab "Testplan" input file 116
Figure 7-4: PC coal lab char burnout (%) 117
Figure 7-5: PC coal lab initial run char burnout (%) compared to experimental results @ 1400 (°C) (initial run) 118
Figure 7-6: (Left) - Expanded view of injection probe inlet showing the polyhedral mesh, (Right) - DTF char burnout furnace CAD 119
Figure 7-7: 1320 (mm) char DTF experiments furnace wall temperature UDF 121

Figure 7-8: Temperature contours (K) of the furnace wall 121
Figure 7-9: CFD initial char burnout result compared to experimental data @ 1400 (°C) .. 122
Figure 7-10: Mass fraction percentage oxygen concentration contour - default kinetics 123
Figure 7-11: CFD char burnout (%) result with updated kinetics compared to initial CFD result, and experimental data @ 1400 (°C) 124
Figure 7-12: Mass fraction percentage oxygen concentration contour - updated kinetics 124
Figure 7-13: PC coal lab "CBKE.inp" input file created for char burnout simulation 125
Figure 7-14: Complete user defined input profiles for the centre-line temperature, centre-line oxygen, and wall temperature 126
Figure 7-15: PC coal lab char burnout % result with user defined input profiles compared to initial PC coal lab result, and experimental data @ 1400 (°C) 127
Figure 7-16: Complete development of numerical char burnout results compared to experimental data @ 1400 (°C) 129
Figure 8-1: Simplified single burner geometry 131
Figure 8-2: Single burner geometry inlet boundaries expanded 132
Figure 8-3: (Left) - Body of influence added, (Right) – Tetrahedral mesh created as a result of body of influence 133
Figure 8-4: Final polyhedral mesh created 133
Figure 8-5: Detailed burner CFD model geometry per burner pair [59] 141
Figure 8-6: Final velocity vectors (m/s) achieved with simplified geometry (isometric view) 142
Figure 8-7: Contours of velocity magnitude (m/s) during baseline simulation, reduced flow 143
Figure 8-8: Contours of velocity magnitude (m/s) during design flows 144
Figure 8-9: (Top) - Contours of static temperature (K) during baseline flows. (Bottom) - Contours of static temperature (K) during design flows 145
Figure 8-10: (Top) - Measurement results obtained in Chapter 3: . (Bottom) – Expanded view of temperature contour showing probe angles used in CFD to compare to measurements taken 146
Figure 8-11: Numerical result with probe inserted through centre-line compared to in-flame measurements 147
Figure 8-12: Numerical result with probe inserted through bottom-port compared to in-flame measurements 148
Figure 8-13: Kinetic input results through burner centre-line 150
Figure 8-14: Kinetic input results through burner bottom-port 150

Figure 8-15: Contours of velocity magnitude (m/s) of baseline simulation with an increased amount of swirl through tertiary burner tube **152**
Figure 8-16: (Left) – Extended view of the increased swirl simulation velocity magnitude (m/s) result. (Right) – Design flow CFD velocity results (m/s) **152**
Figure 8-17: (Top) - Velocity vectors coloured by velocity magnitude (m/s) baseline simulation. (Bottom) - Velocity vectors coloured by velocity magnitude (m/s) increased swirl **153**
Figure 8-18: (Top) - Contours of static temperature (K) during baseline simulation. (Middle) - Contours of static temperature (K) with an improved swirl. (Bottom) - Contours of static temperature (K) during design simulation **154**
Figure 8-19: (Top) Contours of DPM concentration during baseline simulation. (Bottom) - Contours of DPM concentration with an improved swirl **155**
Figure 8-20: (Top) - Contours of mass fraction of CO during baseline simulation. (Bottom) - Contours of mass fraction of CO with an improved swirl **156**
Figure 8-21: Temperature obtained through burner centre-line **157**
Figure 10-1: Oxygen concentration through bottom-port **169**
Figure 10-2: Carbon dioxide concentration through bottom-port **169**
Figure 10-3: Carbon monoxide concentration through bottom-port **170**
Figure 10-4: NOx concentration through bottom-port **170**
Figure 10-5: PF sampling & grading **171**
Figure 10-6: PF sampling results **172**
Figure 10-7: Rosin-Rammler graph **172**
Figure 10-8: Measurements carried out by Eskom RT&D **173**
Figure 10-9: Unit critical operating values **174**
Figure 10-10: Mill E & RH Air Heater outlet temperatures **174**
Figure 10-11: PA fan E PA air flow per burner pair **175**
Figure 10-12: Winbox & burner pressure **175**
Figure 10-13: (Left) – "Dvol.inp" file containing wall and gas temperature profiles. (Right) - PC coal lab volatile yield result **177**
Figure 10-14: PC coal lab devolatilization coal combustion kinetics result **177**
Figure 10-15: Contours of static temperature (K) - updated kinetics **178**
Figure 10-16: Contours of static temperature (K) - default kinetics **178**
Figure 10-17: Contours of static temperature (K) - diffusion limited **178**
Figure 10-18: Mesh 1 ..... **179**
Figure 10-19: Mesh 2 ..... **179**
Figure 10-20: Mesh 3 ..... **179**
Figure 10-21: Mesh 4 ..... **179**

Figure 10-22: (Top) - Contours of mass fraction of O_2 during baseline flows. (Bottom) - Contours of mass fraction of O_2 during design flows **180**
Figure 10-23: (Top) - Contours of mass fraction of CO during baseline flows. (Bottom) - Contours of mass fraction of CO during design flows **180**

List of Tables

Table 2-1: Coal properties used during DTF experiments [18] **20**
Table 2-2: Proximate and ultimate analysis of selected coals [19] **22**
Table 2-3: Proximate and ultimate analysis results of charred sample of the selected coals to be used in char burnout experiments [19] **23**
Table 2-4: List of products available in PC coal lab [36] **27**
Table 3-1: Instruments used during the in-flame measurements **48**
Table 3-2: CAD compared to on-site measurements **55**
Table 3-3: Operational data **65**
Table 4-1: Devolatilization experiment coal proximate analysis **73**
Table 4-2: Proximate ash percentages (dry basis) of product remaining after each DTF experiment **77**
Table 4-3: Particle volatile yield percentage (ash tracer method) **77**
Table 5-1: Devolatilization CFD model input boundary conditions **87**
Table 5-2: Single rate kinetic parameters **98**
Table 5-3: Single rate kinetic parameters comparison **99**
Table 5-4: Final single rate kinetic parameters **102**
Table 6-1: DTF sample proximate analysis **104**
Table 6-2: DTF calculated particle temperature and particle residence time at each operating condition **108**
Table 6-3: DTF experimental results **111**
Table 6-4: Arrhenius single rate kinetic parameters **113**
Table 7-1: Char CFD model boundary conditions **120**
Table 7-2: Default single rate char combustion kinetic parameters **122**
Table 7-3: Final char combustion single rate kinetic parameters **127**
Table 8-1: Combustion CFD boundary conditions **136**
Table 8-2: Final combustion kinetics during the baseline CFD simulations **137**
Table 8-3: Coal ultimate analysis (as received) **137**
Table 8-4: Velocity components calculated from detailed geometry CFD model [59] **141**

Table 8-5: Design vs baseline simulation single burner flow [3][12] 143
Table 8-6: Summary of the different single rate kinetic input values used..... 149
Table 8-7: Mesh sensitivity information..... 157
Table 10-1: In-Flame burner temperature results 169
Table 10-2: Arrhenius equation parameters used in devolatilization kinetics calculation.... 176
Table 10-3: Gas phase mass balance 181

Nomenclature

List of symbols

E_a	*Activation Energy ((J/Kmol))*
k_s	*Arrhenius Rate Constant*
ΔT_a	*Ash Temperature Increase (K)*
x	*Average Particle Diameter (m)*
C	*Carbon*
CO_2	*Carbon Dioxide*
CO	*Carbon Monoxide*
D	*Characteristic Diameter (m)*
h_c	*Convective Heat Transfer Coefficient (W/m2.K)*
ΔT_f	*Flue Gas Temperature Increase (K)*
k_f	*Fluid Thermal Conductivity (W/m .K)*
V	*Fluid Velocity (m/s)*
V_p	*Free Fall Velocity in Gas (m/s)*
A	*Frequency Factor (1/s)*
P_0	*Gas Inlet Pressure (atm),*
T_0	*Gas Inlet Temperature (K)*
P_1	*Gas Outlet Pressure (atm),*
T_1	*Gas Outlet Temperature (K)*
g	*Gravitational Acceleration (m/s2)*
CV_{coal}	*Gross Calorific Value of Coal (kJ/kg)*
H_g	*Heat Gained (J/m2.s)*

H_c	*Heat Gained by Conduction (J/m2.s)*
H_r	*Heat Gained by Radiation (J/m2.s)*
H_l	*Heat Lost (J/m2.s)*
CH_i	*Hydrocarbon Radicals*
H	*Hydrogen*
H_2	*Hydrogen Gas*
A_i	*Initial Proximate Ash Percentage of Coal*
F_0	*Inlet Volumetric Flow (m3/s)*
$V_{(t)}$	*Instantaneous Yield*
L_i	*Length of Slice (m)*
V_g	*Linear Velocity of Gas (m/s)*
T_b	*Local Bulk Gas Temperature (K)*
T_w	*Local DTF Wall Temperature (K)*
m_{ash}	*Mass Flow of Ash (kg/s)*
m_{coal}	*Mass Flow of Coal (kg/s)*
$m_{flue\ gas}$	*Mass Flow of Flue Gas (kg/s)*
x	*Mean Particle Diameter of Coal Fired (m)*
T_m	*Measured Gas Temperature (K)*
HNO_3	*Nitric Acid*
N	*Nitrogen*
NO_2	*Nitrogen Dioxide*
N_2	*Nitrogen Gas*
NH	*Nitrogen Monohydrate*
NO	*Nitrogen Oxide*
HNO_2	*Nitrous Acid*
NO_x	*Oxides of Nitrogen*
O_2	*Oxygen*
O_3	*Ozone*
D	*Particle Diameter (m)*

t_p	*Particle Residence Time (s)*
T_p	*Particle Surface Temperature (K)*
A_e	*Percentage of Ash Remaining In Coal*
q	*Rate of Carbon Removal per Unit Surface Area (g/m2.s)*
R_v	*Reactor Volume per Meter (m3/m)*
Cp_{ash}	*Specific Heat of Ash (kJ/kg.K)*
$Cp_{flue\ gas}$	*Specific Heat of Flue Gas (kJ/kg.K)*
V_A	*Suction Velocity (m/s)*
S	*Sulphur*
SO_2	*Sulphur Dioxide*
T_g	*True Gas Temperature (K)*
V_G	*True Gas Velocity*
V_{ult}	*Ultimate Yield*
R	*Universal Gas Constant (J/mol.K)*
F	*Volumetric Flow (m3/s)*
H_2O	*Water*

Greek Symbols

ε	*Dissipation Rate*
ε_s	*Emissivity of Surface*
ρ	*Fluid Density (kg/m3)*
μ	*Fluid Viscosity (kg.s/m)*
ρ_g	*Gas Density (kg/m3)*
δ_g	*Gas Viscosity (kg/m.s)*
ρ_p	*Particle Density (kg/m3)*
a	*Recovery Factor ~ 0.85*
σ	*Stefan-Boltzmann Constant*
λ	*Thermal Conductivity of Reactant Gas (J/m.s.K)*
k	*Turbulence Kinetic Energy*

Abbreviations/Acronyms

CBK	*Carbon Burnout Kinetics*
CFD	*Computational Fluid Dynamics*
CAD	*Computer-aided Design*
DO	*Discrete Ordinate*
DPM	*Discrete Phase Model*
DCS	*Distributed Control System*
DTF	*Drop Tube Furnace*
DAF	*Dry Ash Free*
EDC	*Eddy-Dissipation-Concept*
ERZ	*External Re-circulation Zone*
FD	*Forced Draft*
ID	*Induced Draft*
IFRF	*International Flame Research Foundation*
IRZ	*Internal Re-circulation Zones*
LAR	*Limited Access Register*
LES	*Large Eddy Simulation*
MCR	*Maximum Continuous Rating*
NEA	*Niksa Energy Associates*
OEM	*Original Equipment Manufacturer*
PVC	*Polyvinyl Chloride*
PHD	*Process History Database*
PDF	*Probability Density Function*
PA	*Primary Air*
PF	*Pulverized Fuel*
RT&D	*Research, Testing, and Development*
SNLL	*Sandia National Laboratories, Livermore*
SA	*Secondary Air*
SCR	*Selective Catalytic Reduction*

SFOR	*Single-first Order Reaction*
TOI	*Temporary Operating Instruction*
TA	*Tertiary Air*
TGA	*Thermal Gravimetric Analysis*
UDF	*User Defined Function*
UBC	*Unburnt Carbon in Fly Ash*
WSGGM	*Weighted-Sum-of-Gray-Gases Model*

Chapter 1: INTRODUCTION

1.1. Research Background

The coal-fired power plant under investigation during the past few years has replaced their conventional type coal burners with upgraded low NO_x coal burners. The power plant frequently suffers from poor flame stability and incomplete and/or delayed combustion with associated high super-heater metal temperatures. The poor flame stability affects the power plant in the way that the power plant frequently requires fuel oil support, especially during low-load conditions which lead to high fuel oil usage and high associated costs involved. A thorough investigation has been done where possible causes of the poor flame stability and delayed combustion were identified [1].

Apart from low-quality coal resulting in longer burnout times the main factor possibly contributing to flame stability and delayed combustion was identified as the air flow requirements to the windbox supplying air to the burners.

Three methods have been used to investigate and properly validate the current air flow measurements to the burners. These three methods were:

1. Boiler mass and energy balance including taking the global boiler and air pre-heater parameters into account.
2. Direct measurements from the Distributed Control System (DCS) control panel.
3. CFD flow model correlating burner pressure difference to mass flow.

All three methods were in agreement that the air flow to the burners was well below the required design value [1]. Therefore, the importance of establishing the effect reduced air flows conditions have on the low NOx burner both aerodynamically and subsequent temperature distribution achieved.

1.2. Research Motivation

According to the National Environmental Management: Air Quality Act (No 39 of 2004) the allowed plant limit for NO_x emissions will reduce from 1100 mg/Nm³ @ 10 (%) dry flue gas O_2 in 2015 to 750 mg/Nm³ @ 10 (%) dry flue gas O_2 in 2020 [2]. Modern coal combustion technologies show a reduction in NO_x emissions with the installation of low NO_x coal burners. Compared to conventional type coal burners, low NO_x burners delay the mixing of air and fuel at the burner outlet thereby lowering the average flame temperature and creating an oxygen lean environment for volatile combustion [3].

Improvement in a low NO_x coal burner's combustion performance requires extensive research into the aerodynamic characteristics of the burner's flame. Coal properties and aerodynamics play a major role in the chemical reactions (and thus the pollutant formation) in the flame. The air flow patterns within the burner control the rate and conditions at which the active combustion species are brought together.

There is a need in coal power plant generation to optimize its low NO_x coal burners in terms of combustion efficiency. At the specific power plant under investigation, the air flow to the burners is lower than design expectations and the effect thereof on combustion stability needs to be thoroughly investigated.

In South Africa, the recent power supply and funding constraints limit the opportunity to perform utility-scale online coal burner analysis to make sensible adjustments. Computational fluid dynamics (CFD) is a definite tool to aid with analysis, design and development of pulverized coal combustion burners. This method is capable of providing detailed information on the distributions of temperature and chemical species and the behaviour of pulverized coal particles over the entire combustion spectrum that cannot easily be obtained by experimental or other means. CFD modelling offers a substantially lower cost solution and, more importantly, zero risk to production loss. A reliable capability to accurately simulate coal combustion scenarios will give power plants the ability to optimize and troubleshoot plant performance without requiring shut-downs. This capability will also be instrumental in the development of existing and new coal-fired power station burner designs. An accurate single low NO_x coal burner combustion CFD model will contribute to defining parameters for improved combustion stability at below design air flow conditions. This will produce better turndown capability to be able to

operate under two shifting/load following operation without oil support with resulting fuel oil cost savings. Optimum burner swirl settings could also result in lower unburnt carbon in ash levels and reduced emissions.

1.3. Power Plant Overview

Figure 1-1 below shows a simplified schematic of the power plant identified to perform the in-flame measurements on.

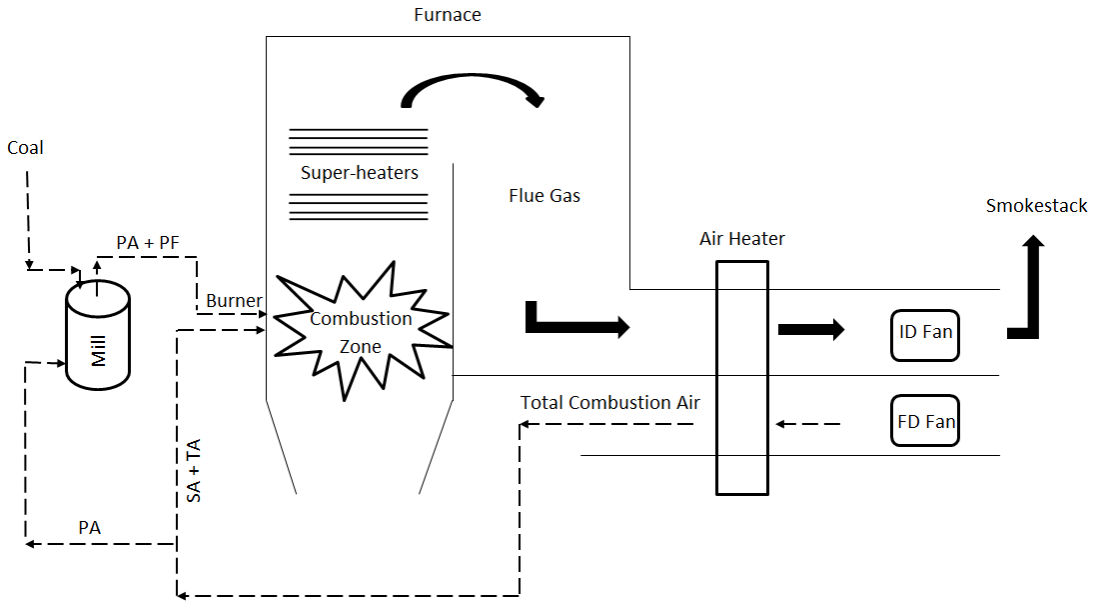


Figure 1-1: Simplified power plant schematic

Figure 1-1 is an illustration of the main components and process involved and does not necessarily show the correct orientation and flow path as found on the power plant. The power plant under consideration has a maximum operating capacity of 200 MWe (electrical output). The super-heaters above the combustion zone provide the final superheated steam required to be supplied to the turbine which rotates the generator to produce electricity. The super-heaters provide a thermodynamic gain and ensure minimum wetness in the turbine.

The power plant is equipped with twenty-four low NO_x coal burners equally distributed along the front and rear furnace wall. For combustion to take place fuel and oxygen are required at the correct temperature and in the correct quantities.

The required fossil fuel in the form of coal is stored in a coal stockyard and two coal staiths. From the staiths, the coal is transported to the station via three incline conveyor belts and gets distributed to the mill coal bunkers situated above each mill on the unit. The power plant has six mills with five mills in service and a one mill on standby philosophy during full load.

Coal from the coal bunkers falls through a coal feeder which controls the fuel feed rate into the centre of the mill where the coal is ground into a fine powder called pulverized fuel (PF). The vertical spindle mills make use of an upper and lower grinding ring with 9 grinding balls in-between. The coal is ground to PF by passing between these grinding elements. The process continues until the PF is fine enough to be picked up by the sweeping primary air (PA) entering the mill from the side. The mill classifier at the top of the mill rejects heavier particles back to the grinding elements in the flow stream depending on the particle's momentum. The particle fineness, therefore, can be controlled by adjusting the classifier blade angle. PF fuel is an essential part and plays an important role in combustion efficiency. Each mill is able to produce a minimum of twenty-five tons of PF per hour and uses air to dry, heat and transport the PF through four PF pipes supplying four burners per mill.

The air required for transporting pulverised fuel to the burners and to supply oxygen to the combustion process is supplied by two forced draft (FD) fans situated on the left and right hand side of the boiler. To improve combustion and boiler efficiency the air from the FD fans passes through two Rothemule type air heaters which heat the inlet air with heat transferred from the hot flue gas after the combustion process. The hot air from the air heaters flows into the windbox situated on the left and right, front and rear side of the furnace and supplies secondary (SA) and Tertiary (TA) air per burner pair on each row. Six primary air fans supply transport air to each of the six mills which draw hot air after the air heaters from the FD ducts and supply the air to the mills.

The combustion furnace is being kept at a slightly negative pressure of approximately -100 (Pa). This is to ensure suction through the furnace at all times to prevent hot gasses and combustion products from being blown into the boiler house thus creating an unsafe

environment. This pressure is maintained by drawing the combustion products out of the furnace and eventually discharging it through the smokestack by two induced draft (ID) fans on the left and right hand side of the boiler.

1.4. Research Objectives

- Determine the devolatilization and char single rate reaction kinetics of the specific coal both numerically and through DTF experiments to better characterise the coal for combustion CFD modelling.
- Perform in-flame temperature measurements on an industrial low NO_x coal burner in order to determine the combustion CFD model's accuracy.
- Develop a complete combustion CFD model of a single low NO_x coal burner installed at the specific power plant to determine the aerodynamic flame profile and temperature distribution achieved during the identified load conditions.

1.5. Research Methodology

The temperature profile of the low NOx coal burner was evaluated through a combination of experimental and numerical methods.

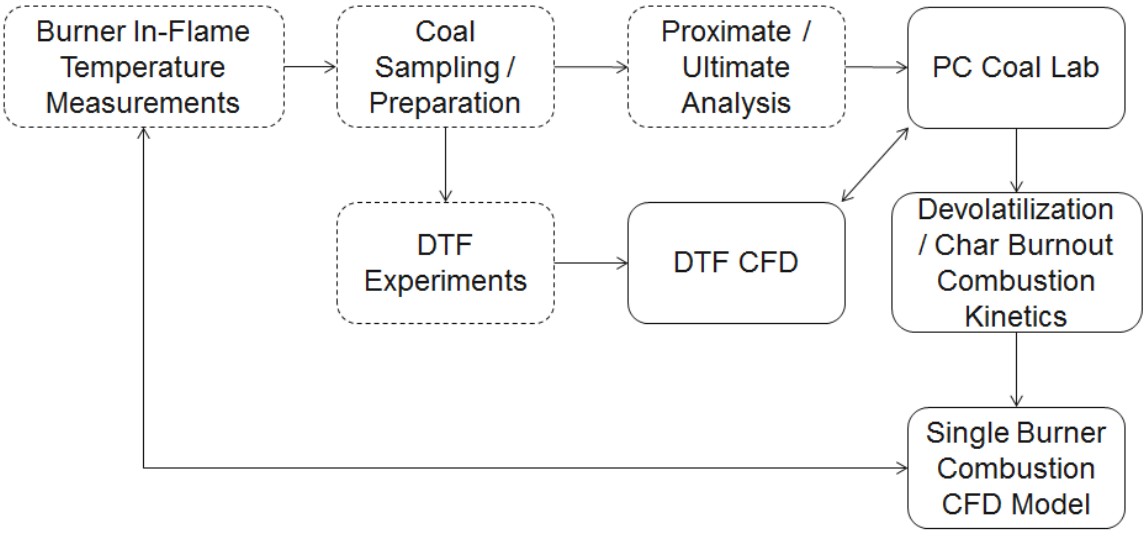


Figure 1-2: Method used in terms of the burner temperature profile evaluation

The experimental methods are shown by the dashed lines in Figure 1-2 and involved the following:

- *Burner in-flame temperature measurements:* In-flame temperature measurements were done on an industrial low NO_x coal burner by making use of a water-cooled suction probe. The temperature results were compared to the combustion CFD simulation results to establish CFD accuracy.
- *Coal sampling and preparation:* Since the coal quality received by the power plant changes constantly over time it was required to take a coal sample in combination with the in-flame temperature measurements to ensure the most representative coal sample was collected to be used during the DTF experiments.
- *Coal proximate and ultimate analysis:* A coal quality analysis was done on the coal sample to determine the proximate and ultimate analysis of the coal which was required as input for all subsequent numerical simulations.
- *DTF experiments:* Drop tube furnace experiments were done to determine the devolatilization and char burnout rate of the specific coal. These results were used to be compared to the numerical simulations.

The numerical section, in turn, involved the development of a complete single burner low NO_x coal combustion CFD model. The numerical methods are shown by the solid lines in Figure 1-2 and involved the following:

- *DTF CFD:* A CFD model of the drop tube furnace used during the experimental section was created. The model was mainly used to calculate the particle residence time, the centre-line gas temperature profile, and the centre-line oxygen concentration of the DTF at each operating condition. These values were required as input into PC coal lab.
- *PC coal lab:* PC coal lab harnesses the reaction mechanisms for solid fuel conversion into the convenient format of a virtual fuels laboratory. PC coal lab numerically predicts a fuel's devolatilization, combustion, and gasification behaviour. During the current study PC coal lab was used to calculate the devolatilization and char single rate combustion kinetics through a series of numerical iteration between PC coal lab and CFD. The devolatilization and char combustion kinetics were required as input into the single burner combustion CFD model.

- *Single burner combustion CFD model:* A complete single burner combustion CFD model was developed. The CFD model was mainly used to evaluate the burner's flame temperature profile during the currently received reduced air flow conditions, and to establish the level of the temperature dependence of the flame on TA swirl velocity.

1.6. Structure of Dissertation

This dissertation includes 10 chapters including the introduction and background sections. Chapter 1: provides a background and gives a motivation of why the specific topic was covered. Chapter 2: provides a literature study of all the elements involved in the low NO_x coal burner temperature profile study. Chapter 3: gives the methods used in performing the in-flame temperature measurements on an industrial low NO_x coal burner together with its corresponding results. The development of an accurate CFD combustion model included the calculation of the coal's devolatilization and char single rate combustion kinetic parameters. The coal combustion kinetics have been calculated numerically by making use of NEA's PC coal lab software and the results validated through DTF experiments. This section was divided into two separate parts. The first part examined the initial homogenous devolatilization phase of coal combustion. Chapter 4: and Chapter 5: detail this section and its findings. The second part examined the heterogeneous char burnout phase of coal combustion. Chapter 6: and Chapter 7: detail this section and its findings. The complete single burner coal combustion CFD model is described in Chapter 8: . Chapter 9: gives the final conclusions together with recommendations for the way forward. Chapter 10: includes the references together with appendixes.

Chapter 2: LITERATURE REVIEW

2.1. Introduction

The literature study describes low NO_x coal combustion in terms of the different types of NO_x formation during coal combustion and the negative impacts NO_x emissions has on the environment. The principles of how NO_x emissions are reduced by means of the in-flame NO_x reduction technique of a low NO_x coal burner was also investigated. In performing industrial in-flame temperature measurements, different temperature measurement techniques were considered including contact and non-contact type measurements. In determining the coal devolatilization and char single rate combustion kinetics a study was done on drop tube furnace experiments together with the Arrhenius single rate kinetics model and possible numerical solutions such as Flashchain. The literature study concludes with a section expanding on combustion CFD modelling. This section identifies common combustion CFD models used within the literature and provides technical information on how Ansys Fluent solve them.

2.2. Low NOx Coal Combustion

Coal is an energy source with abundant reserves and will remain the main energy source for coal-fired boilers for years to come [35][51]. Compared with gas or oil, coal produces higher CO_2 emissions per unit of combustion energy in the fuel and contains larger amounts of nitrogen and ash, making environmental measures such as flue gas treatment plants (selective catalytic reduction (SCR), flue gas desulphurization, electrostatic precipitators, fabric filter bags, CO_2 Capture and Sequestration) and the installation of low NO_x coal burners ever more essential [4]. The development of NO_x reduction technologies will continue to play a significant role in power generation [5].

2.2.1. NOx Environmental Concerns

NOx is a major environmental burden and is controlled because of [7]:

Health hazards: NO is poisonous and in the most extreme cases could be fatal to humans. More common causes of NO on humans are irritation of the eyes and throat, tightness in the chest, nausea, headache, and gradual loss of strength.

NO2, in turn, is a reddish-brown gas with a strong odour and highly reactive properties. It is highly toxic and hazardous because of its ability to cause delayed chemical pneumonitis and pulmonary edema.

Ground-level ozone: Ozone (O3), although very desirable in the upper atmosphere as it shields the earth against high-intensity radiation from the sun, is also just as undesirable in the lower atmosphere of the earth. Ozone formed in the lower atmosphere through the reaction of NO and oxygen also imposes a health risk to humans. Ozone could cause irritation to the eyes, nose, and throat, and in more serious instances also could lead to respiratory problems in humans.

Acid rain: When NO2 comes in contact with water in the form of rain it decomposes and reacts with the water to form nitric (HNO3) or nitrous (HNO2) acid called acid rain. Acid

rain is very undesirable and highly damaging and corrosive to any material it comes in contact with.

Smog: Smog is a combination of smoke and fog and impacts the visibility through the atmosphere. Smog is formed when high concentrations of pollutants such as NOx combine with fog.

2.2.2. Different NOx Formations

In coal combustion furnaces there are three opportunities for NO_x formation [49]:

- Thermal NO_x (± 20 (%) Contribution) - Thermal NO_x is formed when the oxygen concentration in the air react with the nitrogen concentration in the air at high temperatures. The reaction of thermal NO_x depends on the temperature and the formation increases as the temperature increases. Thermal NO_x formation becomes more prominent at temperatures above 1300 (°C). The mechanism of the formation of thermal NO_x is widely studied and is called the extended Zeldovitch mechanism [50].

- Fuel NO_x (± 75 (%) Contribution) - The main source of NO_x formation in coal combustion is the formation of NO_x which results from the nitrogen contained in the fuel reacting with the available oxygen to form fuel NO_x. Fuel NO_x is being formed during the devolatilization and char oxidation stage of the combustion process [37].

- Prompt NO_x (± 5 (%) Contribution) - Prompt NO_x is formed in the flame front through the reaction of molecular nitrogen in the air combining with CH_i radicals in the fuel. The nitrogen oxidizes along with the fuel and becomes NO_x during the combustion process. Prompt NO_x within the flame contribute only a few percent of the total NO_x formed and is often neglected [6][37].

2.3. In-Flame NOx reduction

In-flame NO_x reduction mechanism used in low NO_x coal burner technologies is based on reduction reactions in the high temperature, oxygen-deficient flame zone, close to the burner mouth. The low NO_x burner is designed to promote mixing near the burner mouth by means of recirculating flow produced by the straight motion of primary air and the strong swirling motion of the secondary and tertiary air. This recirculation flow lengthens the residence time of pulverized coal particles in the high-temperature field near the burner outlet and accelerates the evolution of volatile matter and the progress of char oxidation.

Figure 2-1 shows the basic flame structure of a low NO_x coal burner together with a figure comparing the NO_x formation rate of a low NO_x coal burner to a conventional coal burner.

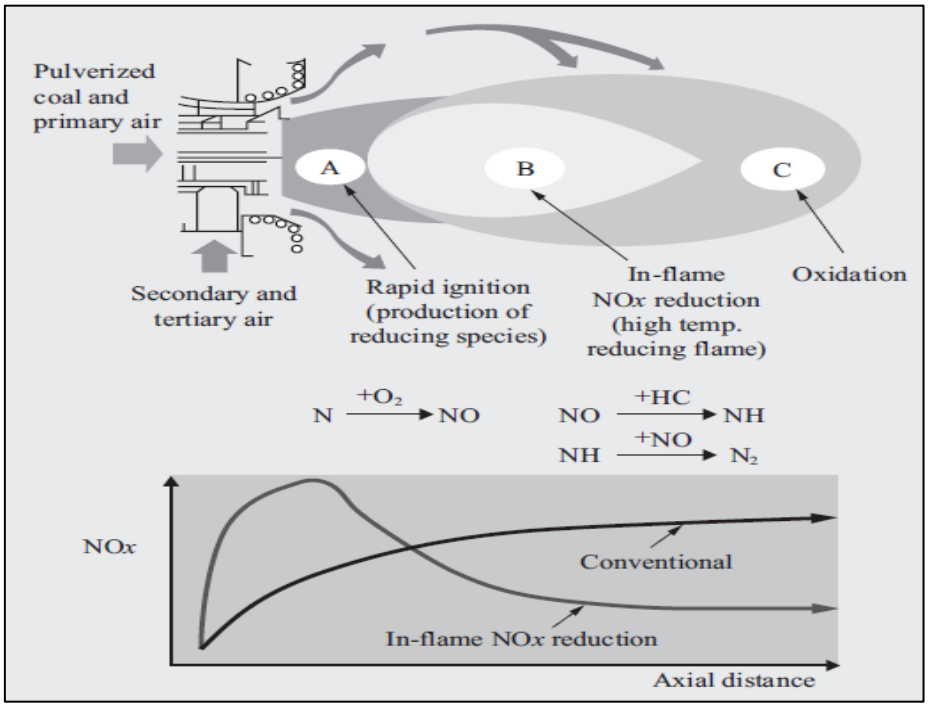


Figure 2-1: Structure of a low NO_x coal burner's flame [8]

Figure 2-1 shows that although the NO_x formation of a low NO_x coal burner is higher compared to a conventional type coal burner in the early stages of combustion, the in-flame NO_x reduction mechanism of a low NO_x coal burner soon after the ignition point reduce the NO_x emitted to atmosphere to much lower than the a conventional type coal burner.

The NO_x concentration during low NO_x combustion increases rapidly at point A just after the burner mouth. This is where devolatilization and rapid fuel ignition takes place in the form of homogenous volatile oxidation reactions. Point A is vital in maintaining a stable flame. For optimum burner settings one would strive to find the minimum amount of oxygen in this region to still maintain stable combustion but at the same time to reduce the amount of NO_x formed [12]. NO_x reducing species also formed during this stage of the combustion process are mainly in the form of Hydrocarbon radicals (CHi) and Nitrogen Monohydrate (NH). Establishing a stable flame at the early stages of combustion at point A promotes consumption of the available oxygen within the flame and enlarges the reduction zone developing to point B. The reduction zone created at point B has a low oxygen concentration as a result of staged combustion and ensures that fuel rich conditions are maintained at point B. This fuel-rich reducing atmosphere at point B is where the NO_x concentration already formed during early stages of combustion immediately reduces to N_2 because of the fuel rich conditions which promote the formation of N_2 instead of NO_x [37]. The reaction time during point B should be as long as possible to ensure the NO_x reducing reactions have completed before the additional oxygen is supplied at point C [12]. Point C is the final oxidation step of the low NO_x combustion process. This is where the staged tertiary air of the burner returns to the centre of the flame after the NO_x reduction reaction has completed and mixes with the flame to supply the additional oxygen required and complete the char combustion process [8].

2.4. Flame Temperature Measurements

Temperature measurements play a vital role in evaluating the thermodynamic characteristics of the flame. Gas temperatures directly relate to the combustion process efficiency and influence the many processes that take place within the flame. Gas temperature measurements can be obtained through various techniques depending on the required application. The measuring of gas temperature within the flame is extremely difficult due to the harsh and dusty conditions that exist. Essentially two types of temperature measurement techniques exist: A non-contact type measurement technique which is based on infrared emissions or acoustic pyrometry, and a traditional contact-type

measurement technique which involves physical contact with the gas such as suction pyrometers [13].

2.4.1. Non-Contact Methods

The main advantages of non-contact temperature measurement are the following [16]:

- It supports temperature measurements of moving or overheated objects.
- It supports temperature measurements in hazardous surroundings.
- It has a fast response and exposure time.
- Measures without interaction, with no influence on the measuring object.
- They are able to measure at high operating temperatures above 1300 (°C). In such applications, contacting thermometers will have a limited life span.
- Equipment is long lasting, with no mechanical wear.

The most commonly used and best-known type of radiation pyrometers is the infrared pyrometer which measures the intensity of the heat radiation emitted from a surface or region (in the case of combustion) [13]. Any object or region with a temperature exceeding absolute zero emits radiation from its surface. This heat radiation emits radiation at wavelengths that lie predominantly in the infrared range above visible light in the electric-magnetic spectrum shown in Figure 2-2 and, therefore, termed infrared pyrometry [17].

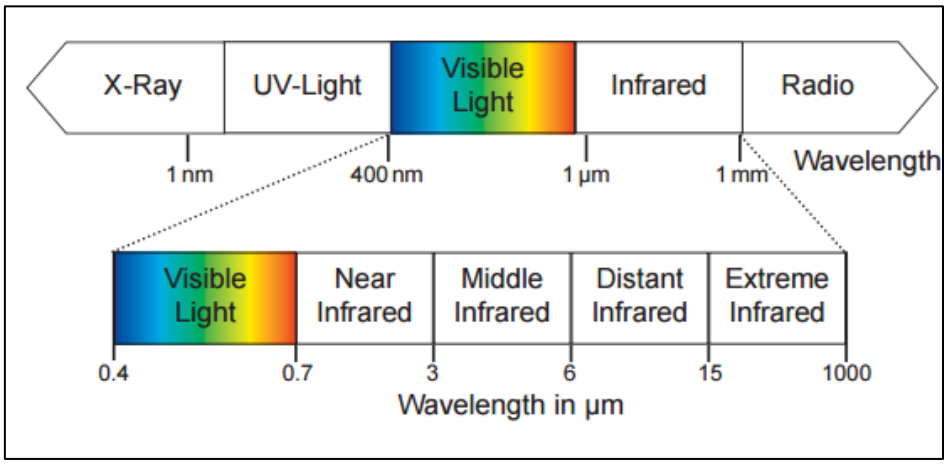


Figure 2-2: Electromagnetic spectrum [17]

The basic construction of the radiation pyrometer is shown in Figure 2-3 below:

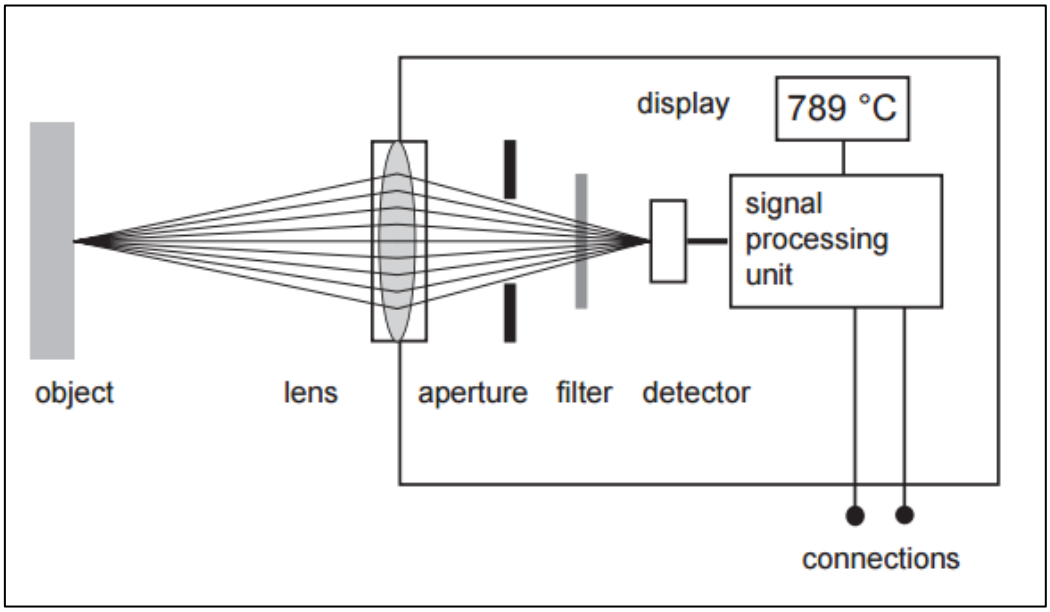


Figure 2-3: Construction of a radiation pyrometer [17]

The pyrometer basically consists of a lens, aperture, filter, detector, and the signal processing unit. The infrared radiation emitted from the desired object or region enters the lens of the pyrometer which collects the radiating wavelengths and directs the emitted radiation to the detector. The aperture behind the lens blocks unwanted rays at the edges of the radiation field. The filter before the detector ensures only the desired spectral range wavelengths enters the detector. The detector then transforms the infrared radiation into electric signals which are then linearized in the signal processing unit and converted into a standard output signal which can then be read on the display.

The aim of the measurements was to investigate the flame temperature at various locations within the flame. Although non-contact type temperature measurement techniques provide several advantages over the contact type techniques it provides the bulk temperature of the combustion system which was not required during the in-flame temperature measurements. An average temperature of the total flame would not serve the purpose and, therefore, the choice of a contact type measurement technique.

2.4.2. Contact Methods

In comparing the in-flame measurements with the CFD results the exact locations of the measurements within the flame were required. Contact type measurement techniques serve this particular purpose well.

Contact type devices are limited in their capabilities when dealing with extremely high temperatures and further limited in dusty conditions [13]. The typical experimental setup of a suction pyrometer is shown in Figure 2-4 below.

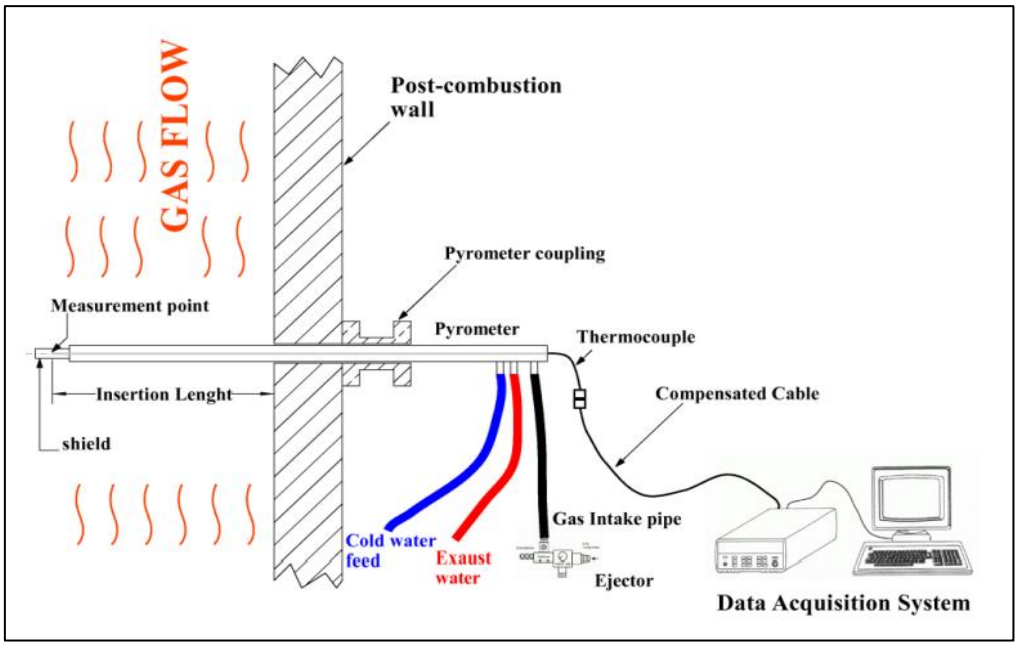


Figure 2-4: Typical experimental setup of a suction pyrometer [14]

The experimental setup shown in Figure 2-4 consists of a water-cooled suction pyrometer extended into the furnace in contact with the gas to be measured. The measurement system is made up of a thermocouple, compensated extension cable and data acquisition system [14].The thermocouple is placed in the centre of the suction probe which draws the hot gas at high velocity through the radiation shield by means of a compressed air ejector where it comes in contact with the thermocouple tip.

The standard probe used by the international flame research foundation (IFRF) is shown in Figure 2-5 below.

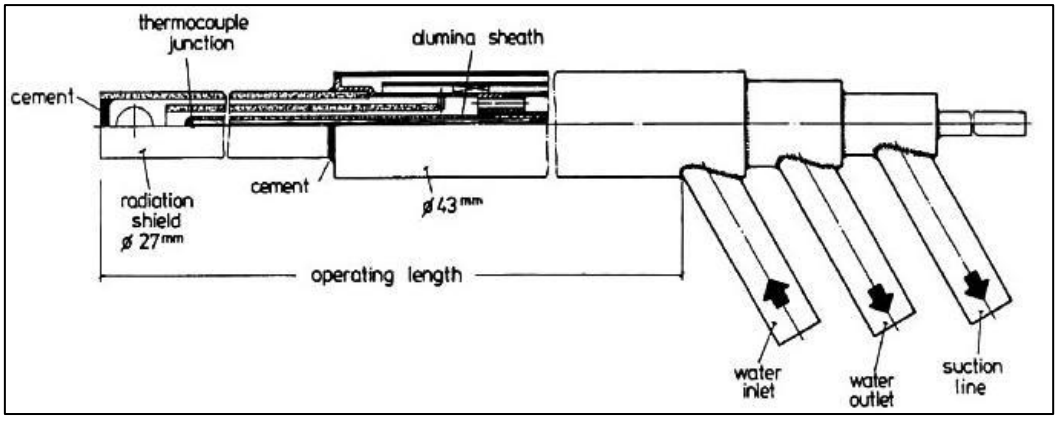


Figure 2-5: IFRF Standard suction pyrometer scheme [15]

To protect the thermocouple from radiation emitted by the surroundings the thermocouple is surrounded by two concentric cement radiation shields. The thermocouple is also further protected against chemical attack with the inclusion of a sintered alumina sheath. The gasses are drawn from the 14 (mm) hole drilled at the side of the radiation shield at high velocity to ensure equilibrium thermocouple temperature is achieved [15].

The time required at each measuring point depends on the measuring conditions. The first temperature measurement observes a temperature change from ambient to 1600 (°C) and takes about 3 (min) to achieve an equilibrium temperature value. Once the temperature change reduces to about 100 (°C), the time to achieve equilibrium reduce to approximately 1 (min) per measuring point [15].

2.5. Drop Tube Furnace Experiments

Coal power generating plants in various parts of the world increasingly make use of imported coal as the bulk of their generating fuel. In local context power plants very often source coal from various different surrounding mines with varying coal qualities from location to location and even from seam to seam. This leads to different quality coal being used, often from different geological origins, and an increased demand to establish their different combustion behaviours. The standard proximate and ultimate analysis of coal does not provide enough information to evaluate the particular burnout characteristics of coals and, therefore, additional techniques have been developed [23].

A DTF is a bench scale unit used for studying the combustion behaviour of coal [20]. It is a useful research tool for getting a better insight into the burning characteristics of coals and their dependence on their quality parameters. The coal combustion behaviour during this study was investigated through DTF experiments of volatile yield and char burnout respectively.

Dividing the DTF experiments into coal devolatilization and char burnout respectively was essentially done because of the different surrounding gas environment and residence times required to convert into their subsequent ultimate yield products. Devolatilization occurs at much shorter residence times and has an essential role in stabilizing the flame as it determines the flame ignition behaviour and flame propagation properties [26]. Char combustion, in turn, has a major influence on plant operational costs. The char needs to convert completely into its ultimate combustion products to aid in achieving the most efficient combustion process [34].

2.5.1. Devolatilization

A typical DTF experimental setup is shown in Figure 2-6. This setup was used at the laboratory GRE at the University of Haute-Alsace, France.

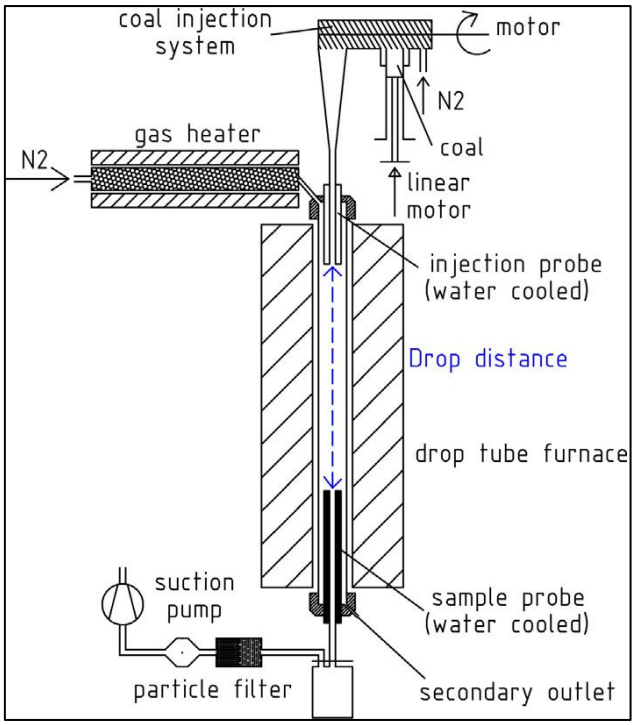


Figure 2-6: DTF facility set up at the laboratory GRE at the University of Haute-Alsace [18]

The DTF mainly consist of a coal injection system, the reactor where the actual mass loss occurs, and a collection system at the bottom collects the products after each experiment. The coal used during DTF experiments are normally crushed to a fine product and sieved to a specific particle size distribution. During this particle experimental setup the coal was sieved to a 40 to 75 micron particle distribution range with an average particle diameter obtained of 50 microns. The coal powder is injected into a nitrogen carrier gas stream at the top of the drop tube furnace and feeds the powder at a constant and uniform rate into the furnace. The coal injection probe is water cooled to ensure the coal does not react before it is injected into the hot reaction zone. A separate nitrogen gas stream is pre-heated to the desired temperature set-point and injected into the top of the drop tube furnace surrounding the injection probe.

The furnace consisted of a vertical cylinder made of alumina/silica with an inner diameter of 50 (mm) and a length of 1.4 (m). The furnace is electrically heated to a maximum operating temperature of 1450 (°C). The reaction distance within the furnace from the injection to the collection probe can be varied from 10 to 70 (cm) depending on the particle residence time required.

The collection probe at the bottom is also water-cooled to ensure rapid cooling of the products at the bottom to ensure further reaction does not take place. The products at the bottom are collected and used for further analysis.

A study done by the University of Haute-Alsace, France [18] found the gas temperature profile within the furnace is not constant and varies with the distance into the furnace tighter with experimental set-point. The gas temperature profiles of the DTF setup found in Figure 2-6 are shown in Figure 2-7.

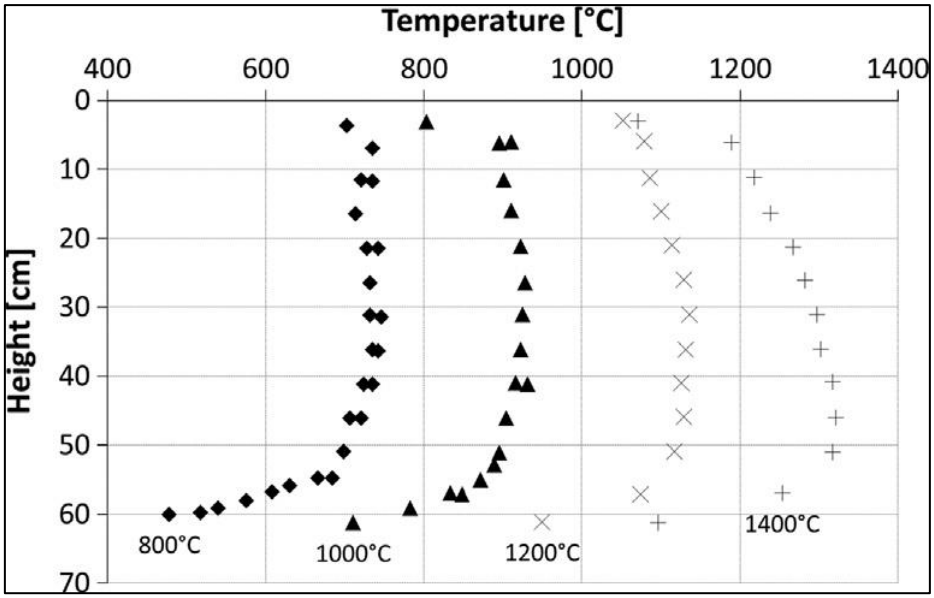


Figure 2-7: Measurement of gas temperature along the DTF heights as a function of reference temperature (from 800 to 1400 (°C)) [18]

The temperature of the gas was measured in the centre of the furnace from the top injection probe going downward. It can be seen that typically the temperatures increase at first then remain rather constant for a while after which the temperatures decrease again. The gas temperatures at all the set-points were found to be substantially lower than the desired temperature set-point.

Two different coal qualities were investigated by the University of Haute-Alsace, France [18] with the experimental setup shown in Figure 2-6 above. The ultimate and proximate analysis of the coals used is shown in Table 2-1 below.

Table 2-1: Coal properties used during DTF experiments [18]

	Anglo-grade/AG-coal	Calenturitas/C-coal
Ultimate analysis (wt% db)		
Carbon	71.4	71.8
Hydrogen	3.8	4.6
Oxygen	6.3	14.1
Nitrogen	2.9	1.3
Sulphur	0.8	0.6
Proximate analysis (wt% db)		
Fixed carbon	61.7	50.5
Volatile matter	23.5	41.9
Ash	14.8	7.6
Moisture (wt% ar)	2.4	6.8

Figure 2-8 and Figure 2-9 shows the dry ash-free weight loss profiles for the two different coals used during the DTF experiments at different experimental temperatures set-points and residence times varying from 0.26 (s) to 2.7 (s). The percentage weight loss of the particle was calculated by the ash tracer method that assumes the ashes from the coal to be inert [18].

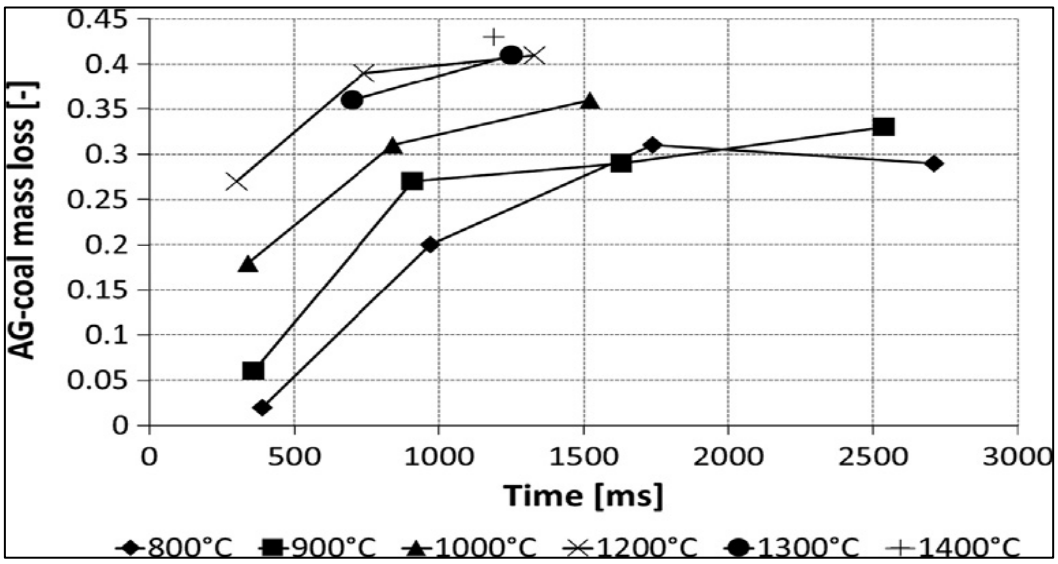


Figure 2-8: AG-coal mass loss as a function of time and reference temperature in DTF [18]

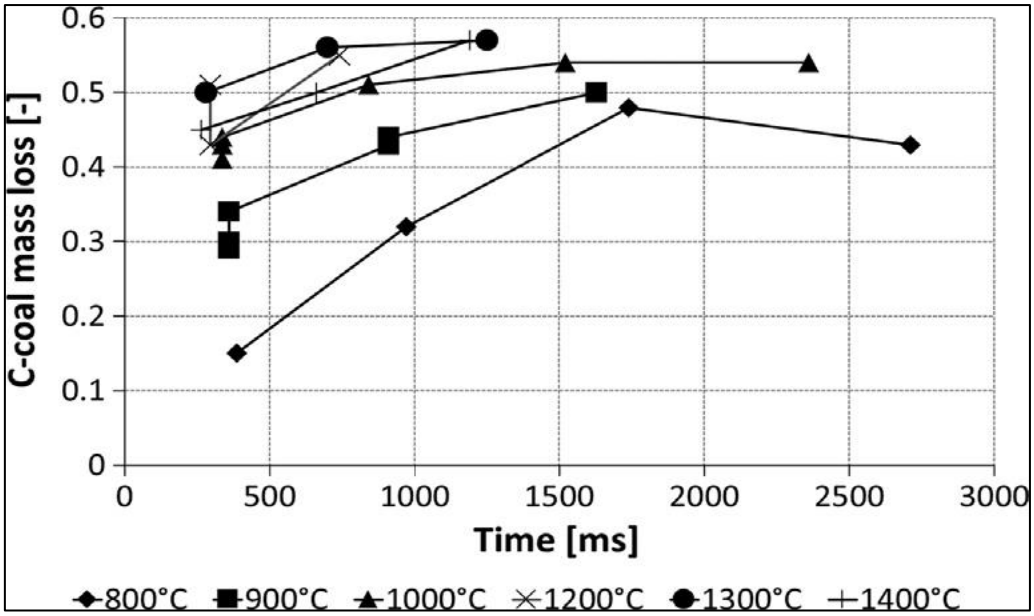


Figure 2-9: C-coal mass loss as a function of time and reference temperature in DTF [18]

Figure 2-8 and Figure 2-9 shows that the weight loss rate of the coal particles increases as the temperature set-point and, therefore, the particle heating rate increases. The figures also show a higher ultimate weight loss percentage achieved at higher particle heating rates. A definite relationship was found between particle temperature and ultimate volatile yield [18].

In another volatile yield study by the department of energy, Pittsburgh Energy Technology Centre, Pittsburg the volatile yield rate of four different coals were obtained by DTF experiments. The coal samples were size graded to a (200 x 400) mesh size and pyrolized in the DTF in a nitrogen only atmosphere at a temperature ranging from approximately 800 (°C) to 1450 (°C). The particle residence times ranged up to 0.9 (s). The coals proximate and ultimate analysis used during the DTF experiments are shown in Table 2-2 below.

Table 2-2: Proximate and ultimate analysis of selected coals [19]

ANALYSIS	TEXAS (WILCOX) ligA		MONTANA (ROSEBUD) subB		ALABAMA (BLACK CREEK) hvAb		PENN (BUCK MT.) an	
	As Rec'd	DAF	As Rec'd	DAF	As Rec'd	DAF	As Rec'd	DAF
Proximate, Wt. Percent								
Moisture (Total)	21.2	--	23.9	--	3.6	--	5.7	--
Volatile Matter	34.7	53.6	30.7	45.0	37.7	40.3	3.5	4.1
Fixed Carbon	30.0	46.4	37.6	55.0	55.8	59.7	83.3	95.9
Ash	14.1	--	7.8	--	2.9	--	7.5	--
Ultimate, Wt. Percent								
Hydrogen	3.5	5.5	3.6	5.3	4.9	5.3	1.7	1.9
Carbon	45.6	70.5	51.6	75.5	78.5	84.0	82.7	95.3
Sulfur	0.6	0.9	0.7	1.0	0.7	0.7	0.4	0.5
Nitrogen	0.8	1.3	0.9	1.3	1.6	1.7	0.7	0.8
Oxygen (Diff)	14.2	21.8	11.5	16.9	7.8	8.3	1.3	1.5
Ash	14.1	--	7.8	--	2.9	--	7.5	--
Higher Heating Value, Btu/lb	7845	12130	8800	12080	13935	14910	12740	14675

The weight loss results obtained (% daf) of each coal are shown in Figure 2-10 below.

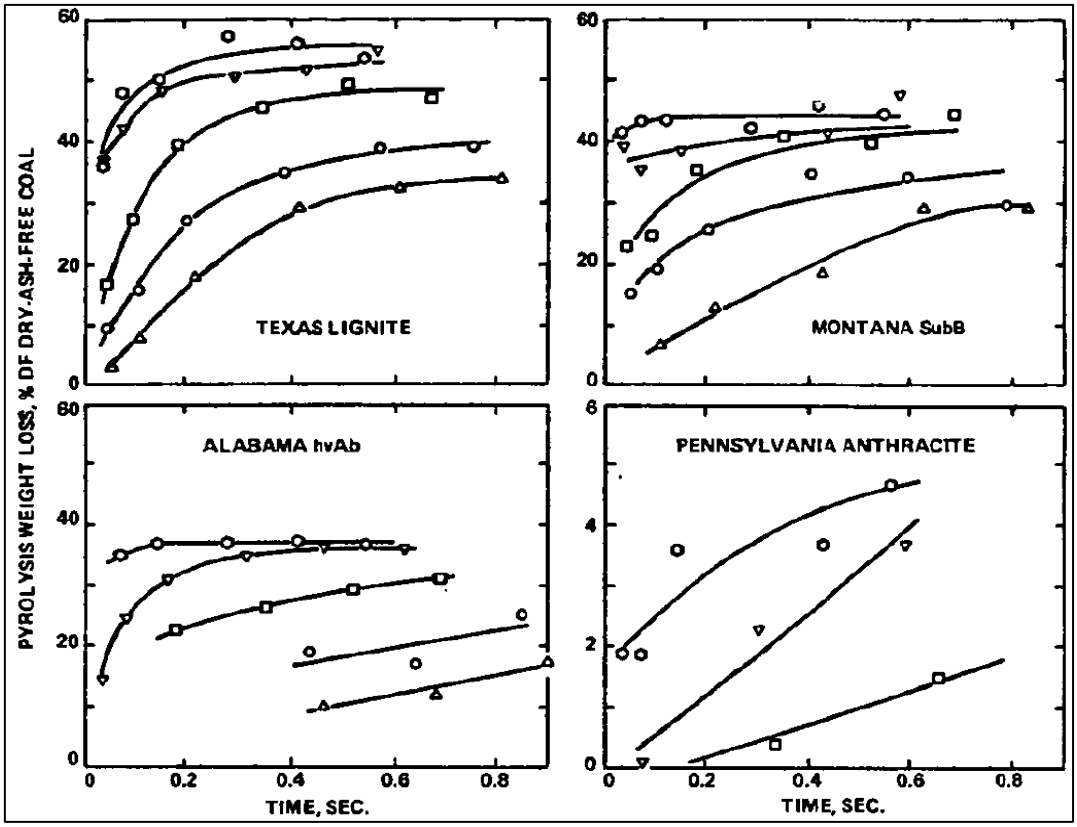


Figure 2-10: DTF volatile yield results at various temperatures (Δ 800 (°C), o 900 (°C), □ 1000 (°C), ᵛ 1300(°C), 0 1450(°C)) [19]

Similar experimental results were achieved when compared to the previous devolatilization DTF study. The volatile yield percentage proved again to be highly temperature dependant. The Texas lignite and Montana sub bituminous coals showed a 12 and 14 (%) ultimate volatile yield increase respectively from their proximate analysis volatile yield (%) [19].

2.5.2. Char Burnout

The Char combustion DTF experiments carried out by the Pittsburgh Energy Technology Centre, Pittsburg on the coal that is being displayed in Table 2-2 followed a slightly different approach when compared to devolatilization experiments [19]. The commercial ground coal was first being pyrolized in a nitrogen environment at high temperature (typically 1400 (°C)) to ensure the sample were free of any contained volatile matter. Thereafter the charred samples were sized (200 x 400 mesh size fraction) and used in the char burnout experiments. The proximate and analysis of the pyrolized coal used by the Pittsburgh Energy Technology Centre during the char combustion experiments are shown in Table 2-3 with the resulting combustion efficiencies obtained at different temperatures shown in Figure 2-11.

Table 2-3: Proximate and ultimate analysis results of charred sample of the selected coals to be used in char burnout experiments [19]

QUANTITY	TEXAS ligA	MONTANA subB	ALABAMA hvAb	PENN. an.
Proximate, Wt.%.				
Volatile Matter	2.3(3.5)*	2.3(2.8)*	1.5(1.6)*	1.3(1.4)*
Fixed Carbon (Diff)	64.3	80.3	94.6	92.1
Ash	31.2	14.9	3.9	5.9
$S_{BET}, m^2/g, daf$	191.3	89.9	16.4	2.6
$S_{CO2}, m^2/g, daf$	210.9	162.9	16.3	1.6
$\sigma_{Hg}, g/cm^3, daf$	0.79	0.69	0.86	1.62
$\sigma_{He}, g/cm^3, daf$	1.71	2.01	1.75	1.86
V_T cm^3/g	0.681	0.952	0.591	0.080
Porosity, %	53.8	65.7	50.9	12.9

*Dry-ash-free-basis

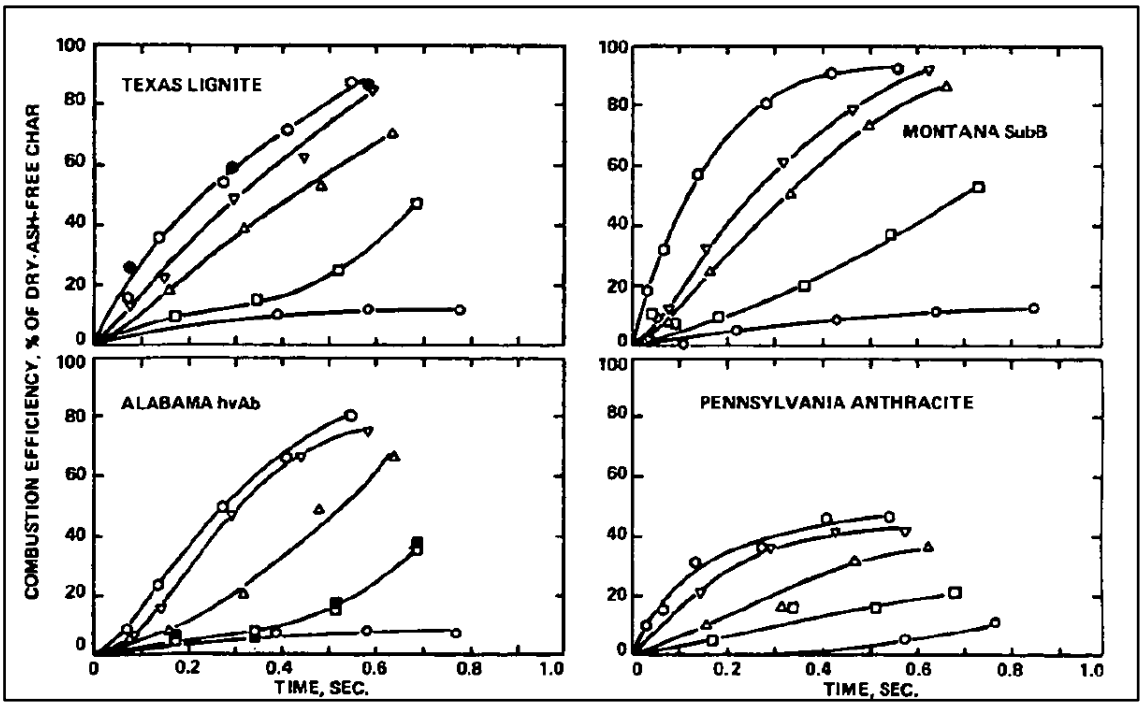


Figure 2-11: DTF char combustion efficiency results at various temperatures (o 900 (°C), □ 1000 (°C), Δ 1200 (°C), ∨ 1300(°C), 0 1450(°C)) [19]

The temperature dependence on combustion efficiency was clearly shown. A 3 (% per volume) oxygen concentration was used in the results obtained in Figure 2-11. Throughout the literature study however, it was found that various oxygen concentrations have been used during combustion experiments. A study at Tampere University of Technology, for instance, investigated the effect different oxygen concentrations had on particle temperature and particle diameter at 3, 6, 12, 25, 35, and 50 (% per volume) oxygen concentrations [24]. Another study at Sandia National Laboratories, USA [25] investigated the effect on the combustion rates of two different coals at 6, 12, 24, and 36 (mol %) oxygen concentrations and gas temperatures ranging from 1320 to 1800 (K). The two coals investigated were a sub bituminous coal from Highvale and a high-volatile bituminous coal from the Eastern United States. The results as a mass fraction of char dry ash free (daf) remaining after each experiment at an intermediate temperature set-point as a function of residence time are shown in Figure 2-12 below. Apart from the temperature dependence of the coal combustion process, the high oxygen dependence was also clearly shown in Figure 2-12. Higher oxygen concentrations result in faster burnout rates [25].

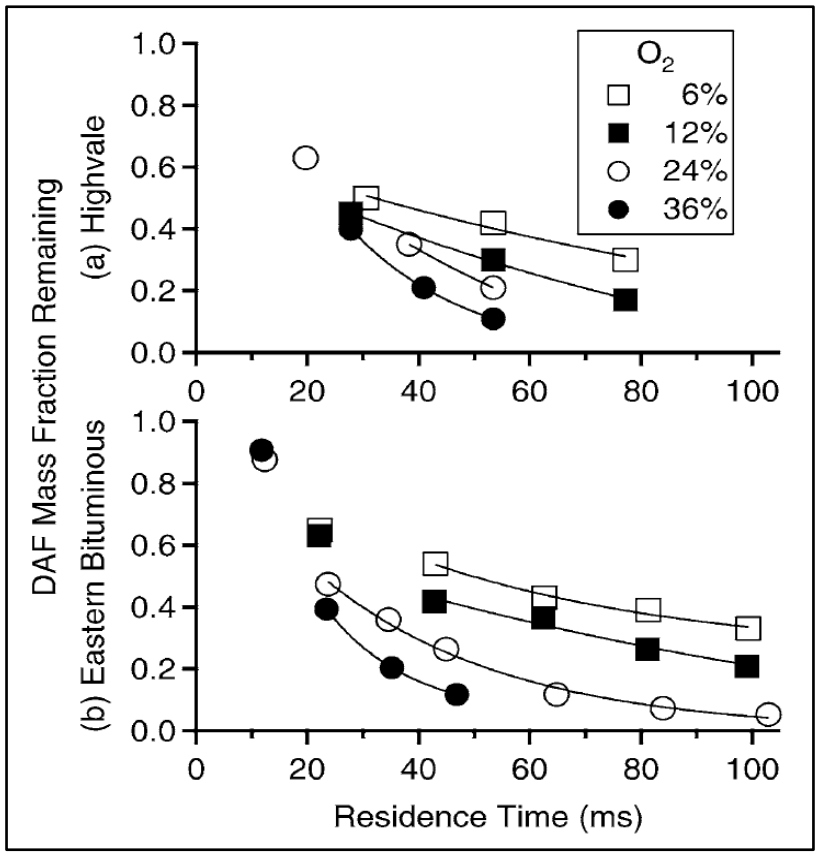


Figure 2-12: Effect of oxygen concentration on the mass fraction of char remaining after each experiment [25]

2.5.3. Ash Tracer Method

The volatile yield and char burnout percentages of the coal particles in DTF experiments are determined by determining the weight loss of the particles during each experiment. This weight loss can be calculated in two ways. In cases where 100 (%) collection efficiency is achieved the mass loss can be determined directly by simply weighing the sample and product before and after each experiment respectively. Another method which is commonly used during DTF experiments where poor collection efficiencies are achieved is the ash tracer method which assumes the ash from the coal to be inert [10][20][21].

The ash tracer weight loss calculation is based on the dry basis ash percentages of the sample before the experiments and dry basis ash percentages of the products collected after each experiment. It was calculated as follow [26]:

$$\% \text{ Particle Mass Loss (daf)} = 100 - \left(\frac{Ai}{100 - Ai}\right)\left(\frac{100 - Ae}{Ae}\right) \quad (2.1)$$

A_i - Initial proximate ash percentage of coal (Dry basis).

A_e - Percentage of ash remaining in coal char each after experiment (Dry basis).

The ash tracer method could be very unreliable for coals used with low ash contents [21]. Fortunately, the coal used during the current study had a high ash content which improves the accuracy of the ash tracer method and was found suitable to be used as a method to calculate the weight loss percentages [26].

The accuracy of the ash tracer method is furthermore dependent on the following three assumptions [22]:

1) The complete conservation of ash throughout the experiment.
2) Identical ash composition of the coal samples used.
3) The products collected after each experiment to consist of only carbon and ash.

2.6. FLASHCHAIN

In modelling coal combustion, one of the most important problems involves the calculation of the coal specific coal combustion rate parameters. The prediction of the kinetic rate parameters of devolatilization and char burnout can be done with several commercial codes such as FG-DVC, FLASHCHAIN or CPD [11][18][33]. These codes only require the coal specific proximate and ultimate analysis together with well-defined operating conditions.

During the present study, FLASHCHAIN was used to calculate the devolatilization and char combustion rate parameters. Since the development of FLASHCHAIN in the early 1980s over 2000 coals with varying coal qualities from different geographical regions worldwide have been examined [36]. The detailed mathematical formulations used are available [38]. The PC coal lab software provides an user interface to utilize FLASHCHAIN

in the form of a user-friendly virtual fuel laboratory. FLASHCHAIN can predict the coal's devolatilization, combustion and gasification behaviour in two kinds of experimental setups. The one is in an electrically heated wire grid and the other one which was used during the current investigations a laminar flow DTF.

2.6.1. Devolatilization

PC coal lab predicts the volatile yield, and the rate of all other products involved with devolatilization for any coal, biomass, or petroleum. The complete list of products available to be included in the results is shown in Table 2-4 below:

Table 2-4: List of products available in PC coal lab [36]

Major Products:	Weight loss. Yields of gas, tar, and char.
Non-condensable Gases:	CO_2, H_2O, CO, hydrocarbons, and HCN.
Hydrocarbons:	CH_4, C_2H_4, C_2H_6, C_3H_6, C_3H_8, H_2, and H_2S.
Nitrogen Species:	Fuel-nitrogen fractions in char, tar, and HCN. Nitrogen contents in char and tar, plus yield of HCN.
Oxygen Species:	Fuel-oxygen fractions in char, tar, and oxygenated gases, plus the oxygen contents in char and tar, plus the yields of CO_2, H_2O, and CO.
Tar Characteristics:	Number-average molecular weight plus tar elemental composition (C,H,O,N, and S).
Char Composition:	Char elemental composition (C,H,O,N, and S).
Char Characteristic:	As-received char mass, scaled particle size and char density.

The thermal history of the particle which gives the particle temperature throughout the devolatilization simulation is calculated through an energy balance for individual particles. This energy balance includes the fuel and temperature-dependent thermophysical properties, the enthalpy requirement for moisture loss, the influence of convective blowing on gas-to-particle heat transfer, and radiant transfer to the channel walls in the limit of a

very large enclosure. The gray-body, total hemispherical emittance of coal is fixed for all temperatures and coal compositions.

2.6.2. Char Combustion

PC coal lab defines the particle temperature, the mass loss of the particle, and the morphological changes which include particle size and bulk density of the particle throughout the char burnout stage. To predict the char burnout rate, particle temperature, and changes in particle diameter and density throughout the combustion process PC coal lab makes use of an expanded version of Prof. Robert Hurt's Carbon Burnout Kinetics (CBK) Model called CBK/E [36]. Char gasification in PC coal lab by H_2O, CO_2, H_2, and CO, in turn, are calculated through Niksa Energy Associates (NEA) uniquely developed model also expanded from the CBK model called CBK/G [39].

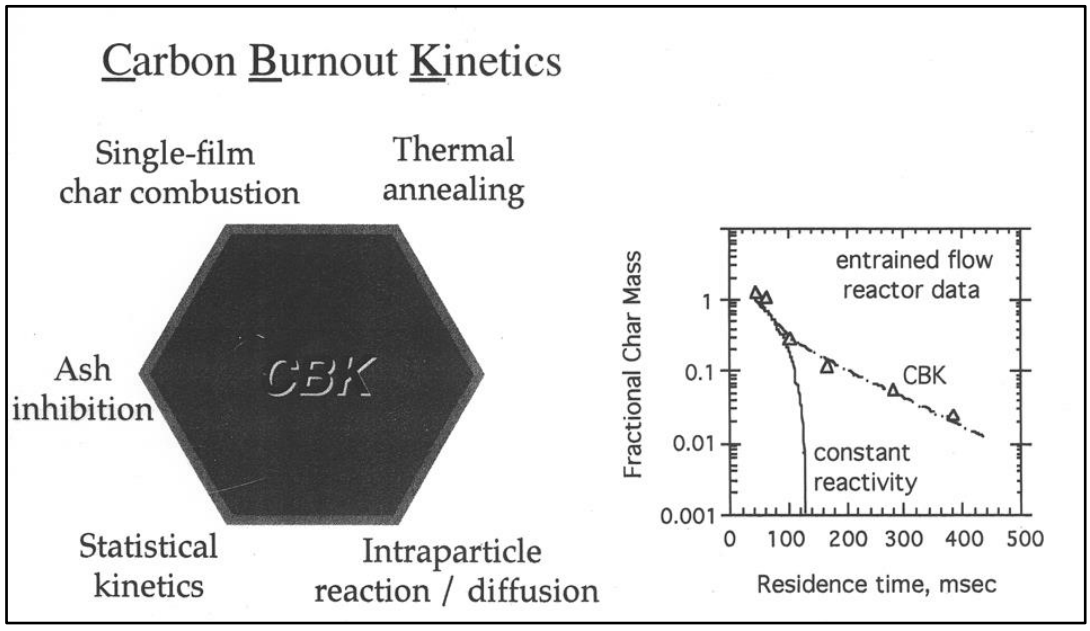


Figure 2-13: Mechanistic features in CBK/E [36]

The main features included in the CBK model are shown in Figure 2-13. Char reactivity is a dynamic function of heat treatment severity, based on a distributed activation energy model of thermal annealing. This standard model of the reaction/ diffusion process within porous char particles and the single film for boundary layer processes are used to predict burning rates over a wide range of conditions. The code also includes a model of the effect

of ash inhibition during the late stages of combustion. In combining the mechanism shown on the left of Figure 2-13 the char burnout rate is significantly reduced during the later stages of combustion. The dotted line on the right of Figure 2-13 is based on the CBK model and correctly predicts the char burnout rate up to the final stages of combustion where the final few percent of char are consumed.

The predicted solid curve on the right of Figure 2-13 is based on a classical single film mechanism for char oxidation, developed by a group at Sandia National Laboratories, Livermore (SNLL). This model significantly overpredicts the char burnout rate especially at the later stages of combustion. The SNLL model ignores all chemistry within the film surrounding a burning char particle and determines the burning rate from a balance between O_2 transport from the free stream to the particle exterior and O_2 consumption by the char oxidation chemistry within the particle's pore network.

Typical PC coal lab combustion results found in the NEA's, user guide and tutorial manual Version 4.3 [36] of three different quality fuels based on the CBK models are shown in Figure 2-14.

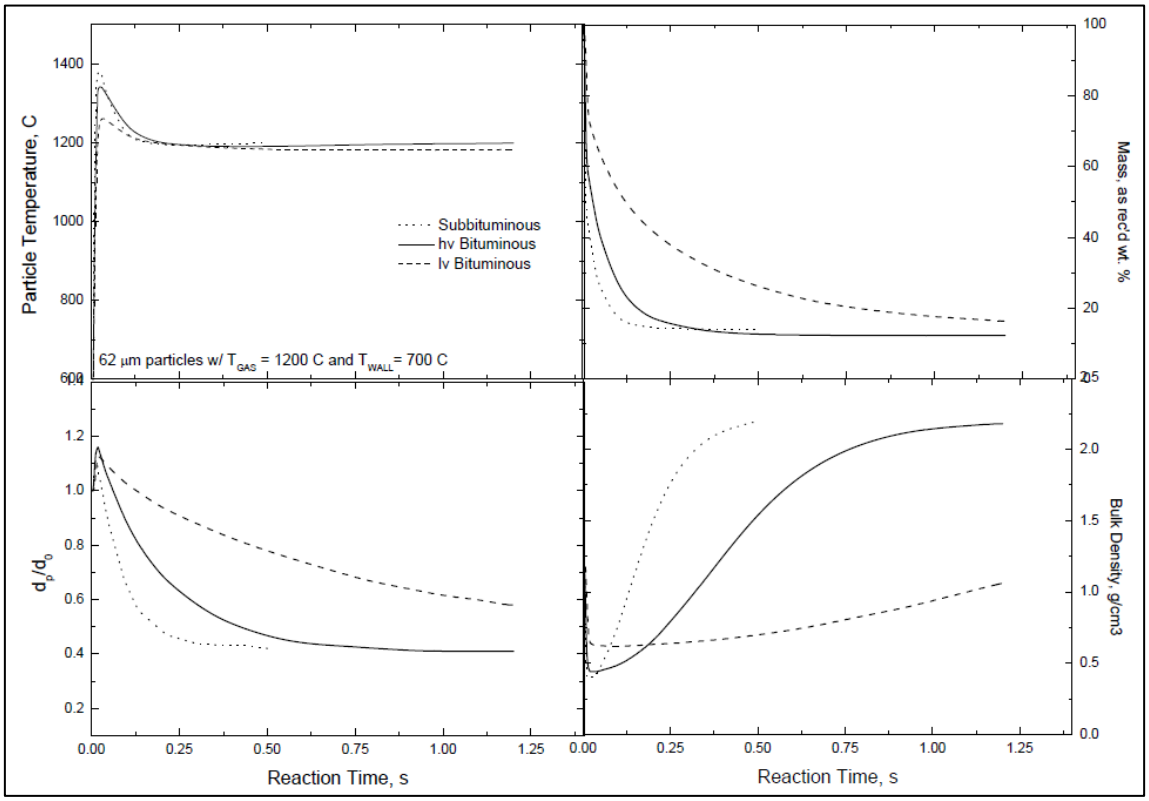


Figure 2-14: PC coal lab coal combustion results for three different quality coals. Showing particle temperatures, mass loss profiles, scaled particle sizes and bulk densities [36]

The CBK model was not specifically designed for conditions far outside the PF combustion regime. It was found however that the model still usefully predicted yield results at temperatures as low as 500 (°C) and was found consistent with Thermal Gravimetric Analysis (TGA) results [40].

2.6.3. Combustion Kinetics Calculation

Combustion kinetics calculations involved the calculation of the devolatilization as well as char burnout rates. Both are calculated since the energy released during coal combustion originates from both the homogeneous combustion of volatiles and heterogeneous combustion of coal [31]. These rates refer to the time rate of change of a product yield. Various different reaction models are available to assign these specific reaction rate parameters to the different combustion stages. Version 4.1 of PC coal lab offers the single first-order reaction, the competing two-step reaction model, and the distributed activation energy model for nominal rate assignments [36].

During the current study, the single first order reaction (SFOR) model has been used. During this model, all reactions are considered to be first order and follow the Arrhenius type law [41]. Arrhenius expressions are used to correlate rates of weight loss with temperature [10].

The Arrhenius equation for specifying SFOR rates are as follow [10][18][25][31][36][41][42]:

$$k_s = A \exp\left(-\frac{Ea}{RT}\right) = \frac{\frac{dV(t)}{dt}}{V^{Ult} - V(t)} \qquad (2.2)$$

k_s	-	Arrhenius rate constant.
A	-	Pseudo-frequency factor (1/s).
E_a	-	Apparent Activation Energy (J/Kmol).
R	-	Universal gas constant (J/mol.K).
T	-	Particle temperature (K).
$V_{(t)}$	-	Instantaneous yield.
V_{ult}	-	Ultimate yield.

In equation 2.2, the frequency factor (A) and the activation energy (E_a) are Arrhenius parameters which can faithfully mimic combustion kinetics provided that they are applied within their range of applicability. The frequency factor, activation energy, and product yields are all adjustable parameters that vary with temperature, heating rate, pressure, and coal type. First, the volatile yield and char burnout rate for the operating conditions specified will be evaluated either through laboratory experiment or numerical simulations. Then the single rate Arrhenius kinetic parameters will be assigned through a mathematical manipulation of the Arrhenius equation.

Taking natural logs of both sides of the equation gives:

$$Ln\ k_s = \left(-\frac{Ea}{R}\right)\frac{1}{T} + Ln\ A \qquad (2.3)$$

The manipulated form of the Arrhenius equation given by equation 2.3 is in the same order as the equation of a straight line y = mx + b. If the dependent y-variable is plotted as a function of the independent x-variable the slope of the line is represented by m and the y-intercept given by b. The same principle can be used to determine E_a and A from equation 2.3. By plotting ln k against 1/T (Arrhenius plot), the single rate Arrhenius parameters can be calculated by the slope of the straight line which gives $-E_a/R$ and the y-intercept which gives ln A. A typical Arrhenius plot is shown in Figure 2-15 below:

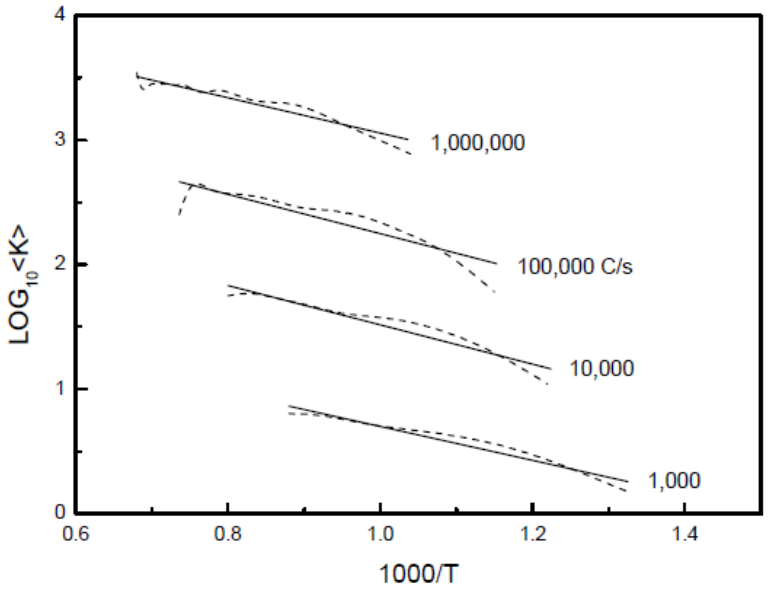


Figure 2-15: Arrhenius plots at increasing heating rates [36]

Figure 2-15 illustrates the effect particle heating rate has on the Arrhenius plot and ultimately the SFOR rates. Typical calculated single first order Arrhenius parameters of a high volatile bituminous Russian coal (proximate and ultimate analyses are shown on the left of Figure 2-16) are shown on the right of Figure 2-16.

Coal type	High-bituminous
Proximate analysis (%)	
Moisture	3.1
Volatile matter	30
Ash	14.9
Fixed carbon	52
Ultimate analysis (%)	
C	66.04
H	4.18
N	1.99
S	2.06
O	7.07

Parameters	
Devolatilization kinetic parameters	
Pre-exponential factor	1.34E4 (s^{-1})
Activation energy	2.41E07 (J/kmol)
Char combustion kinetic parameters	
Pre-exponential factor	4.50E−05 ($kg/m^2/s/P$)
Activation energy	6.90E07 (J/kmol)

Figure 2-16: (Left) - Coal's proximate and ultimate analysis. (Right) - Specific coal's single rate Arrhenius parameters [31]

2.7. Numerical Simulations

Recently, many major technology development efforts are including CFD as a supporting tool for their investigations [34]. With the remarkable progress in the performance of computers (hardware and software), it is strongly expected that CFD will be an important review tool for the design and development technology of combustion furnaces and burners of pulverized coal combustion [27, 28].

Fluid flows are governed by partial differential equations which represent conservation laws in terms of their physical properties such as mass, momentum, and energy. Navier-Stokes equations are the basic differential equations describing the flow of Newtonian fluids in a combination of equations of motion [28]. Combining these conservation laws of the physical properties of fluids with the Navier-Stokes equations of motion, a complete mathematical description of incompressible Newtonian fluids are provided and is able to solve complex fluid flow problems. CFD involves replacing these partial differential equations with discretized algebraic equations (discretization) which approximate the differential equations and then solves them numerically to obtain a complete flow field result throughout the domain. The most well-established and thoroughly validated general purpose CFD discretization technique is the finite volume method. For this method, the

domain is broken into a set of small interlinked cells. An example of a mesh created to be used in CFD analysis is shown on the left of Figure 2-17 below. A finite volume refers to the small volume surrounding each node point of each cell on the interlinked mesh shown on the right of Figure 2-17.

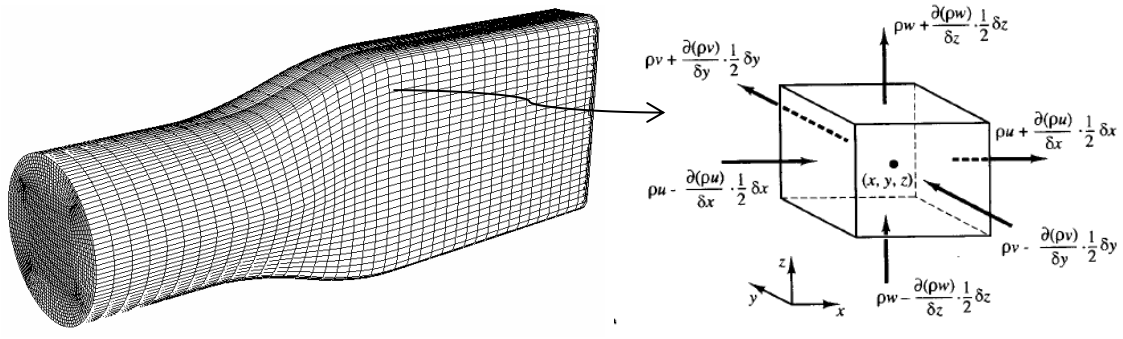


Figure 2-17: (Left) - An example of a typical mesh created for CFD application. (Right) - An example of the conservation of mass on a single cell in the domain [28][29]

The example on the right of Figure 2-17 shows the mass flow conservation throughout a single cell. The conservation equations are written in the appropriate form for each individual cell and the set of algebraic equations are solved numerically and simultaneously throughout the domain with the information of the one cell carried over to the next.

To enable access to the solving power of CFD, commercial CFD codes provides user interfaces where all the relevant information specific to a problem can be specified to be solved and examined. The most commonly used codes on the market all based on the finite volume discretization method are, Phoenics, Ansys Fluent, Flow3D, and Star-CD [27].

2.7.1. Combustion Computational Models

The mathematical modelling of combustion of an industrial coal burner consists of a mixture of turbulent reactive gases and is arguably one of the most challenging aspects of continuum mechanics [11]. CFD solves all the governing equations that describe the combustion process in a number of complex simultaneous coupled phenomena and is

capable of providing detailed information on the required combustion temperature profile and chemical species distribution throughout the domain [9].

Several CFD coal combustion simulations have been developed previously. The respective studies mentioned below all made use of the commercially available CFD code Ansys Fluent.

A study done by Jae Jeong, Kyun Seo, and Hwang at Yonsei University, CFD was used to study the effect coal size has on the gasification performance of an E-GasTM gasifier [30]. Another study done at the Laboratory of Coal Combustion, Huazhong, University of Science and Technology, CFD was used to simulate the ignition process of pulverised coal in oxy-fuel conditions [31]. The numerical simulations were specifically used to obtain profiles of the rate of combustion during the homogeneous and heterogeneous stage of the combustion process. The results were validated by comparison of experimental results with varying temperatures and oxygen mole fractions. A study done by Jovanovic, Milewska, Swiatkowski, Goanta, and Spliethoff, the effect several combustion mechanisms had on ignition point during pulverised coal combustion was numerically determined [32]. A sensitivity analysis on numerical results also done by Jovanovic, Milewska, Swiatkowski, Goanta, and Spliethoff focused mainly on determining the effect different mathematical devolatilization sub-models had on the ignition point during coal combustion [33]. Torresi, Fortunato, Camporeale, and Saponaro developed a full-scale low NO_x coal burner CFD model to investigate the dynamic behaviour of the specific burner [35]. The results of the low NO_x coal burner CFD model are shown in Figure 2-18 below.

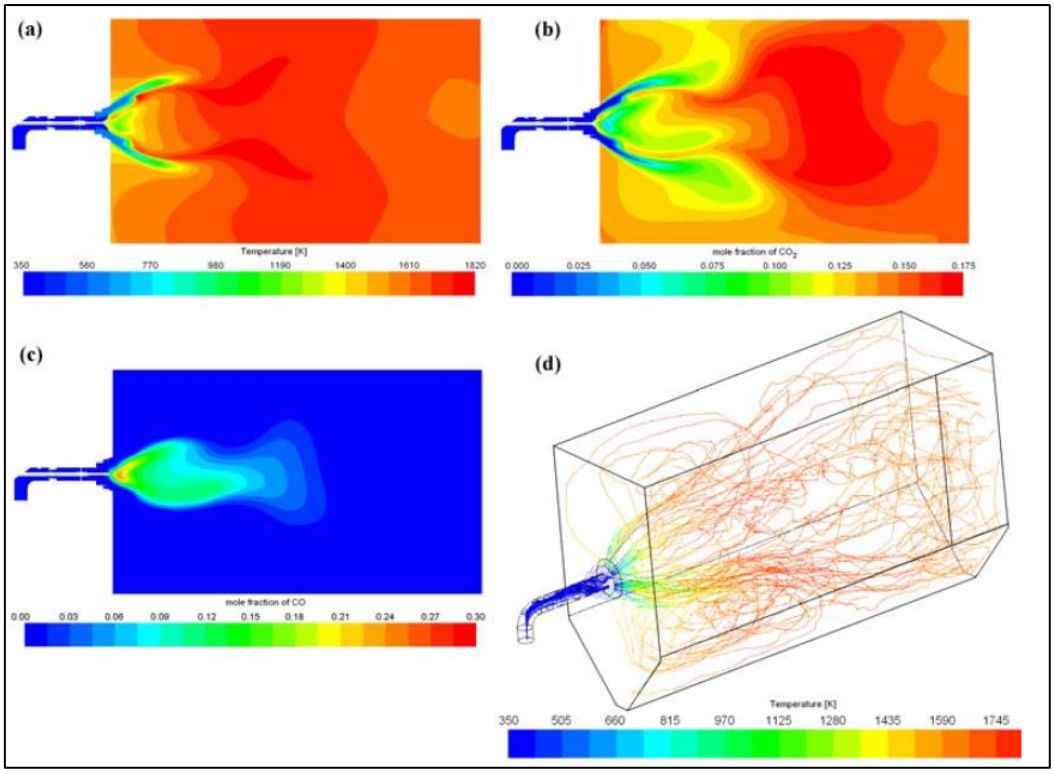


Figure 2-18: Typical CFD results of a low NO_x coal burner. a) Temperature, b) CO_2, c) CO, d) Particle tracks (K) [35]

The results of temperature, CO_2 concentration, CO concentration, and particle tracks with temperature (K) as an index are shown. Throughout the respective CFD simulations above certain common computational models have been used in carrying out the combustion simulations. These common models will be highlighted next and were identified to be appropriated to be used in the current comprehensive combustion CFD model.

Chemical reactions in the gas phase were solved using the finite-rate/eddy-dissipation model and was found to be suitable to successfully predict coal combustion [30][31]. The coal particles were injected into the gas stream as a discrete, secondary phase with stochastic tracking selected as the Lagrangian particle tracking method to account for the turbulent dispersion effect [30][31][33][35]. The char burnout model considers the coal to be composed of porous spherical grains [35]. To take radiation into count the discrete ordinate (DO) radiation model was used [30][31][10][33], together with the weighted-sum-of-gray-gases model (WSGGM) –domain based for radiative properties of the gas [30][31][10][33][35]. A variety of turbulence models were tested to determine the effect of the specific turbulence model selected on the results in order to select the most suitable turbulence model [33]. It was found that no significant change in results occurred between the varying turbulence models. Therefore, the standard k-ε model was used because of its faster convergence

rate [30][31][32][33]. It was found that a good agreement existed between CFD result and operational data especially with improved combustion models used [30].

The following two examples details CFD results found in literature specifically on low NOx burners and gives examples of numerical investigations of the effect different turbulence models and swirl number have on the low NOx burner's flame shape during combustion modelling.

Research done at Hitachi Research Laboratory [63] included a low NOx combustion burner with the furnace geometry shown in Figure 2-19. Circular furnace geometry was used with a diameter of 2 (m). For the burner geometry the flame stabilizing ring was also included and for the fuel source supplied to the burner, pulverized bituminous coal was used with a coal feed rate of approximately 560 (kg/h). Primary air was used in addition to secondary air to transfer the pulverized coal to the burner. The stoichiometric ratio of the furnace was 1.2.

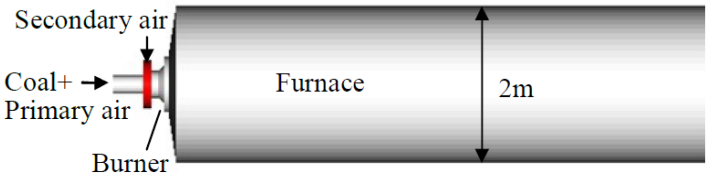


Figure 2-19: Horizontal furnace with low NOx burner [63]

The main aim of the study was to determine the difference in result by using different turbulence models in CFD. The two turbulence models tested during the study was LES (Large Eddy Simulation) and the standard k-ε models. The simulation results of the gas temperatures and oxygen concentrations of the different turbulence models are shown in a cross-section view in Figure 2-20. The instantaneous gas temperature and oxygen concentration calculated by LES are shown in Figure 2-20 (a) with the time averaged LES profiles shown in Figure 2-20 (b) and the standard k-ε model result show in Figure 2-20 (c). The reason for the particular flame profile achieved is as follow:

The low oxygen regions in the cross-sections indicate the recirculation regions of the flame. The temperatures of the flame near the flame stabilizing ring (A) are much higher than those temperatures of the primary air inlet (B) because the stabilizing ring increases the hot gas recirculation flow. This recirculation flow is important as it promote coal

ignition from the onset and therefore increase flame stability. The temperatures of the primary air increase further down into the furnace (D) as it gets heated by radiation and the mixing of hot gases. The temperatures also increase considerably where the coal ignite through the centre line at point (E) and then decreases again shortly after downstream into point (F). The reason for the temperature decrease after point (E) is because of the low oxygen concentration indicated by point (M). Regarding the oxygen concentrations the oxygen concentration is higher near the outlet of secondary air (J) and through the initial stages through the centre line (L) until they decrease downstream (K) by mixing with burned gases. The oxygen lean region which extends beyond point (M) is required for low NOx combustion [8].

The time averaged LES quantities were used to compare with the results of the standard k-ε model.

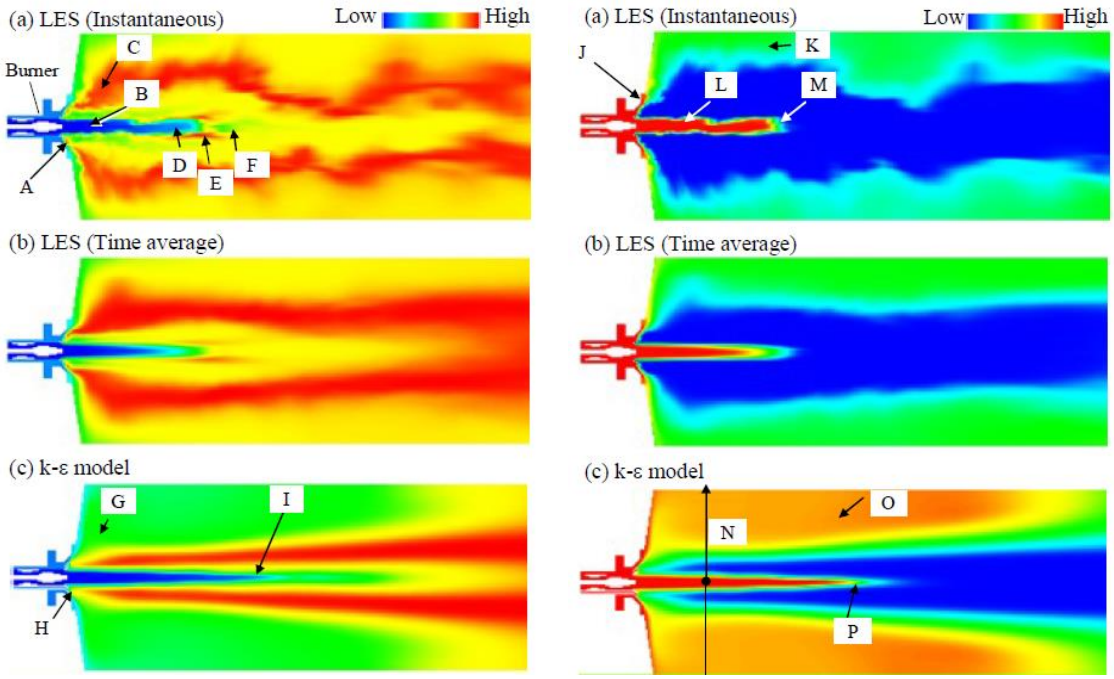


Figure 2-20: (Left) – CFD gas temperature results, (Right) – CFD oxygen concentration [63]

There are three significant differences between the results of LES and the standard k-ε model:

1) The flame width calculated by the standard k-ε model (G) is narrower than that by LES (C).

2) The temperatures on the centre line of the standard k-ε model (I) are lower than those of LES, and the oxygen concentrations on the centre line of the standard k-ε model (P) is higher than those of LES. The oxygen concentration on the outer part of the flame (O) is also higher with the k-ε model as with LES.
3) The temperatures near the flame stabilizing ring of the standard k-ε model (H) are also lower than those of LES [63].

The reason for the differences 1 and 2 is that the standard k-ε model seems to underestimate the decay of primary and secondary jets. The reason for the difference in point 3 is that the standard k-ε model under predicts mixing at the near burner mouth region and overestimates lift-off height. If a combustion model which takes into account local flame structure is coupled with the standard k-ε model, the prediction accuracy near the flame stabilizing ring could be improved [63].

In another study which is also of interest for the research CFD modelling was used to determine initial and optimum burner settings for typical burner retrofits. [64] In order to ensure performance guarantees during low NOx burner retrofits for wall-fired boilers the retrofit requires proper selection of burner size and control settings. Typical boiler performance guarantees usually required are to typically to maintain pre-retrofit boiler efficiency (for example unburned carbon in fly ash (UBC)), super-heater metal temperatures and the required burner pressure differential. As far as emissions goes the performance guarantees usually include and focus primarily on NOx and CO [64]. Aerodynamics-only CFD simulations of the low NOx burner are used as a design tool to estimate changes in flame length, flame attachment and to predict burner settings to achieve optimum near burner aerodynamics for improved low NOx emissions and reduced UBC. [64] These CFD simulations usually make use of a single burner geometry performed in 2D symmetric fashion using a tunnel furnace representing confinement of nearby burners. The characteristics of near burner re-circulation zones are controlled with aerodynamic interactions of swirling air jets in primary, secondary and tertiary form as they enter the furnace. The near burner aerodynamics are qualitatively related to flame behaviour (e.g., flame length and attachment), UBC and NOx emissions values using full-scale burner combustion test results [64].

Figure 2-21 shows the CFD predicted near burner internal re-circulation zones (IRZ) for a typical low NOx coal burner at three different TA vane angles. The predicted streamlines

in the top figure with the highest amount of TA swirl indicate a SA driven external re-circulation zone (ERZ) and a PA driven IRZ. The PA driven IRZ is essential for establishing fuel rich zone during the initial combustion process, a good flame attachment and low fly ash UBC. The CFD results indicate that the PA flow driven IRZ diminishes as TA vane angle changes in the bottom two figures, resulting in less particle capturing by IRZ zone and increased fly ash UBC values [64].

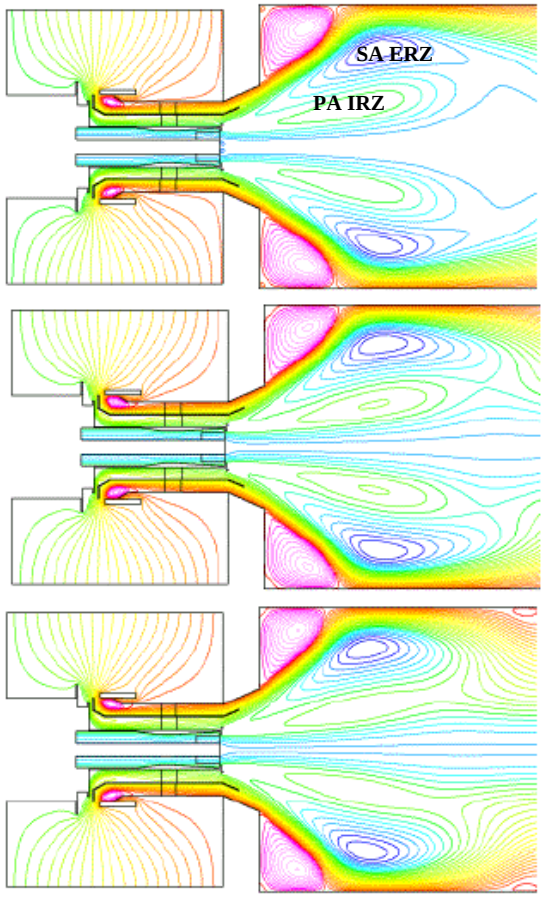


Figure 2-21: Comparison of CFD predictions of near burner flow behaviour and burner performance with a decrease in TA vane angle [64]

CFD modelling can also be used where the flame length becomes critical. To avoid opposite wall flame impingement, the relatively long low NOx coal flame can be reduced through optimization. The CFD result above shows how CFD modelling makes it possible to predict corresponding burner settings to achieve optimum near burner aerodynamics. Predictions of burner settings assist in burner optimization efforts and boiler commissioning.

2.7.2. Ansys Fluent

The code used during the current study was Ansys Fluent and in this section a brief overview of all the governing models identified above and used during the combustion CFD simulations will be discussed. Ansys Fluent provides a complete CFD modelling capability for a wide range of fluid flow problems. Steady-state or transient flow conditions can be simulated with compressible or incompressible and laminar or turbulent fluid flow conditions. Ansys Fluent includes a variety of detailed mathematical models to solve complex problems including pulverized fuel (PF) combustion. Only a brief description of the specific models used in Ansys Fluent will be discussed without the detailed equations involved. The detailed equations can be viewed in the Ansys Fluent theory guide [43].

All fluid flows are solved through the conservation equations of mass and momentum with additional transport equations solved when the flow become turbulent. Turbulence which was accounted for by the standard k-ε model involves a two-equation model to be solved for the turbulence kinetic energy (k) and its dissipation rate (ε) [44]. The semi-empirical model allows for both turbulent length and time scale to be solved, with its derivation relying on both phenomenological considerations and empiricism [43]. The standard k-ε model is valid for turbulent flows only and neglects any affects the molecular viscosity has.

In problems where, heat transfer is included an additional equation for energy conservation is added. Radiation can be included through five radiation models and related submodules which are capable of modelling complex problems such as combustion. The discrete ordinates (DO) radiation model solves a radiative transfer equation for a finite number of discrete solid angles. Each angle consists of a vector direction fixed in a global Cartesian system. The angular discretization fineness of the DO model can be controlled by the user. The DO model solves as many transport equations as there are directions and in principle transforms the radiative transfer equation into a radiative intensity equation in spatial coordinates. The uncoupled energy implementation used during the combustion simulations incorporates a conservative variability of the DO model called the finite-volume scheme [45][46]. The variable absorption coefficient radiative property was calculated through the WSGGM domain based model which provides a reasonable

compromise between an oversimplified gray gas model and a complete model taking particular absorption bands into account.
Ansys Fluent has the ability to model combustion through a variety of reaction models which includes the species transport, non-premixed combustion, premixed combustion, partially premixed combustion, and the composition Probability Density Function (PDF) transport models.

Combustion simulations using the species transport model require additional chemical species conservation equations to be solved. These conservation equations predict the local mass fraction of each species throughout the solution by describing convection, diffusion, and reaction sources for each component species [43].

The volumetric species transport equations, for turbulent flows, are calculated by one of three finite-rate reaction models. The Laminar finite-rate reaction model ignores any turbulent fluctuations and determines the reaction rates solely by taking the Arrhenius kinetic parameters into account. The Eddy-dissipation model ignores any Arrhenius kinetic parameters impact and calculates the reaction rates by only considering turbulence effects [47]. The Eddy-dissipation-concept (EDC) model is the most computationally expensive and includes detailed Arrhenius chemical kinetics incorporated in turbulent flames [43].

Ansys Fluent also provides a variance on the eddy-dissipation model which was the model of choice in the numerical simulations describes in this study called the finite-rate/eddy-dissipation model. This model takes both the rate controlled by turbulent mixing and the Arrhenius reaction rate into account. Ansys Fluent calculates both reaction rates with the net reaction rate taken as the minimum of the two rates. The finite-rate/eddy-dissipation model can be used in both non-premixed and premixed combustion simulations. The Arrhenius rate during the finite-rate/eddy-dissipation model simulations acts as a protection, preventing combustion to take place in the transport medium before it enters the furnace.

The discrete phase coal particles during combustion simulations are being solved through the Lagrangian discrete phase model which follows the Euler – Lagrange approach. The discrete phase is solved tracking the particles through the flow field and can exchange momentum, mass, and energy with the continuum fluid phase. The particle trajectories are

computed individually at specified intervals during the fluid phase calculation and predicted by equating the particle inertia with the forces acting on the particle.

Ansys Fluent provides four different heterogeneous surface reaction rate models for char-combusting particles. After the volatile component of the coal particle has completely evolved, char combustion begins which consumes the combustible fraction, governed by the stoichiometric requirement, of the surface burnout reaction (with the exception of the particle surface model). After the consumption of the combustible fraction, the combusting particle contains the residual ash that reverts to an inert heating law.

The four different char reaction models available in Ansys Fluent are following:

• Diffusion-limited rate model

The diffusion-limited surface reaction rate model ignores any kinetics influence on the char reaction rate and only takes the rate determined by the diffusion of the gaseous oxidant to the surface of the particle into account [54]. The diffusion-limited rate model assumes that the diameter of the particles does not change.

• Kinetics/diffusion-limited rate model

The kinetic/diffusion-limited rate model includes the effect of kinetics and calculates the surface reaction rate either by kinetics or by a diffusion rate. Ansys Fluent uses the model of Baum and Street [54] and Field [55] in which diffusion of the gaseous oxidant and the kinetic rate coefficients are compared to each other to ultimately produce the char combustion rate. The particle size is assumed to remain constant in this model while the density is allowed to decrease.

• Intrinsic model

The intrinsic model is based on Smith's model and assumes the order of particle reaction is equal to unity [56]. Similar to the kinetic/diffusion model, the intrinsic model takes both the effects of bulk diffusion and chemical reaction rates into account in the calculation of the surface reaction rate. The difference is during the intrinsic model the diffusion rate coefficient is calculated the same, but the chemical rate is explicitly expressed in terms of the intrinsic chemical and pore diffusion rates of the particle.

• Multiple surface reactions model

In modelling multiple particle surface reactions, the surface species is considered as "particle surface species". For the mixture material selected, the particle surface species can be depleted or produced by the defined stoichiometry of the particle surface reactions. When the reactive char content of the particle is consumed the particle surface species is set to be depleted and when surface species is produced, it is added to the particle char mass.

Turbulence effects on the dispersion of particles influencing the particles trajectories in the fluid phase can be predicted using the stochastic tracking model. This method also called the random walk model calculates the turbulent dispersion of the discrete phase particles by integrating the trajectory equations for individual particles, using instantaneous fluid velocity, along the particle path during the integration. In the discrete random walk model, the interaction of the particle with a succession of discrete stylized fluid phase turbulent eddies is simulated. Each eddy is characterized by a Gaussian distributed random velocity fluctuation and a timescale [48].

The amount of incident radiation absorbed at the wall surfaces and the amount emitted back depends on the emissivity of the surface. The emissivity of an object is, therefore, the effectiveness in which the wall emits energy as thermal radiation. Emissivity is defined as the ratio of the thermal radiation from a surface to the radiation from an ideal black surface at the same temperature as given by the Stefan–Boltzmann law [53]. The ratio varies from 0.0 to 1.0 with 1.0 being equal to the radiation of a black body. Ansys Fluent assumes the emissivity on the wall boundaries conditions to be 1.0 unless you choose to redefine this boundary treatment. An actual object has an emissivity of less than 1 and emits thermal radiation at corresponding lower rates. An emissivity of 0.8 was defined for all wall boundary conditions during the numerical simulations.

Chapter 3: BURNER IN-FLAME TEMPERATURE MEASUREMENTS

3.1. Introduction

Coal burners found in coal powered generating plants play an important role in producing power efficiently. The flame is the core of the system and largely determines the outcome and the quality of the combustion process. Collecting direct information (temperature and combustion gas composition) of the flame appears as an attractive option to optimize combustion systems. However due to practical difficulties to obtain accurate data during on load conditions burner tests are very seldom done [37]. PF Burners are not easily accessible and the associated high temperatures make it infeasible to perform routine assessments and adjustments on-line to improve combustion efficiency.

This together with power supply and funding constraints limits the opportunity to carry out online burner investigations. Therefore the reason for developing a single burner combustion CFD model described in chapter 8 to support with burner investigations. However, before any conclusions can be made from the CFD results, the accuracy of the model will always be challenged. To have confidence in the combustion CFD model's output, in-flame measurements were carried on a single full-scale industrial coal burner and compared to the CFD results. Once the CFD model compares within reasonable margin against the in-flame measurements the CFD model can be used in burner investigations, eliminating the need for frequent routine online measurements.

3.2. Low NO_x Burner Operation

The main components of a low NO_x coal burner are shown in Figure 3-1 below. The core air tube at the centre of the burner transports core air and fuel oil through a fuel oil lance into the furnace to establish an initial fuel oil flame. The fuel oil ignites with an ignition system containing propane gas located at the burner mouth. A primary air tube transports the PA / PF mixture into the furnace and ignites as soon as the PF particles reach ignition temperatures of approximately 600 (°C) within the fuel oil flame. Once the PF flame is stable the fuel oil supply into the furnace is terminated. The PA / PF mixture flow through a set of flow straighteners and then the flame stabilizing ring situated at the burner mouth of the primary air tube which forces the outer portion of air inwards and pulls the flame closer to the burner mouth. The air entering the burner from the windbox is divided into a secondary and tertiary air stream both containing angled swirl blades to create swirl through the burner before entering the furnace. The amount of swirl through the SA air tube can be adjusted by regulating the amount of air entering the tube as well as the amount of air flowing through the swirling barrel. The blades on the TA air tube are fixed and cannot be adjusted. The low NO_x burners make use of staged air to reduce the peak flame temperature and to create a reducing environment condition throughout the centre-line of the flame. This enables the combustion species to react in an oxygen-lean environment and to reduce NO_x formation within the flame.

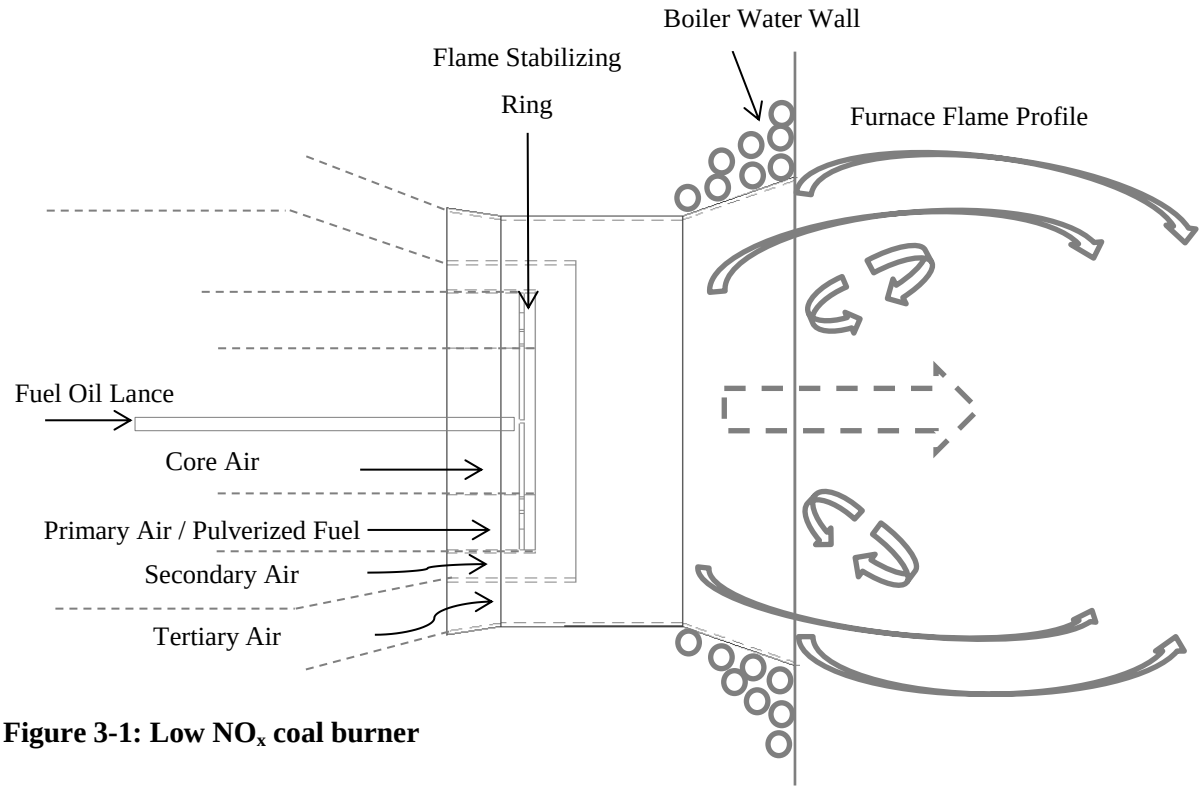


Figure 3-1: Low NO_x coal burner

3.3. In-Flame Burner Measurements:

The complete process of performing the in-flame burner measurements included the following:

- Determination of parameters to be measured.
- Equipment to be used.
- Determination of location through the burner to execute the in-flame measurements.
- Selection of suitable burner.
- Geometrical analysis of measuring points to minimize measurement location uncertainty.
- Burner in-flame measurements procedure together with unit load selection and control during tests.
- Additional supplementary measurements executed.

Each process will be explained in further detail in the following sections.

3.3.1. Parameters Measured

The main parameter of the flame required and used to compare to the CFD model results was the in-flame temperature measurements. The temperature through the centre line was used to establish the flame offset from the burner mouth. Apart from the temperature measurements, combustion product gas species were also measured. This gas species measurement included the concentration of O_2 (Dry Basis), CO, CO_2, and NO_x. The species results did not form part of the current investigation but were still presented in Appendix A for future reference.

3.3.2. Equipment Used

The in-flame measurements were done by a 6 (m) long 50 (mm) in diameter water cooled stainless steel suction probe from Eskom RT&D. The probe is similar to the IFRF standard suction pyrometer [15] with the specific probe used for the measurements shown in Figure 3-2 below.



Figure 3-2: Actual water cooled suction pyrometer used

The working principle of the suction probe is being illustrated by the Computer-aided design (CAD) drawing of the probe in Figure 3-3 below.

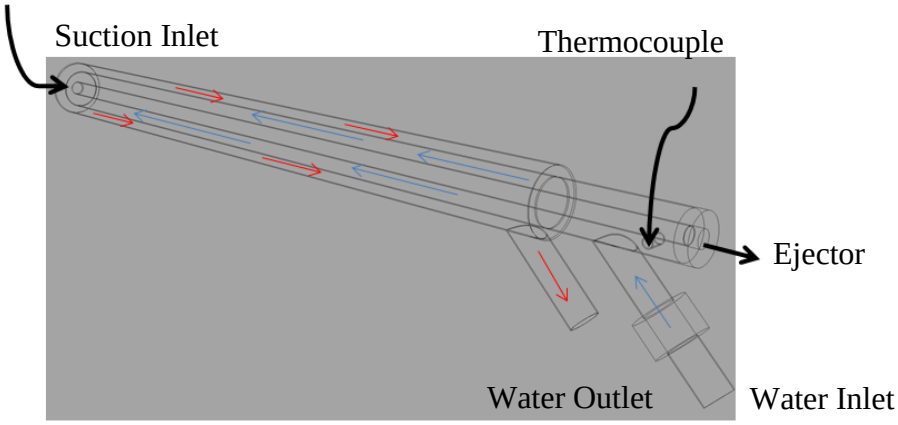


Figure 3-3: CAD of the probe used

An ejector connected at the back of the probe made use of service air from the power plant to create a cyclone and drew the gas through the inlet of the suction probe to the outlet through the ejector. To ensure the probe was protected against the heat from combustion when measuring within the flame, the gas was cooled within the probe to ensure further combustion did not take place within the probe. The probe was cooled throughout the measurements with water received from the fire hydrants located next to the furnace at the burner level. The cooling water flows into the probe through the water-inlet pipe surrounding the centre-line tube where the gas was drawn in. The cooling water then flows to the tip of the probe and returns to the outlet of the probe through an outer water outlet channel.

The same suction pyrometer was used to carry out both temperature and species distribution measurements with the different additional equipment used shown in Table 3-1.

Table 3-1: Instruments used during the in-flame measurements

Measurement	Instrument used
Temperature	HE701 Series Multi-channel thermocouple thermometer
	K - Type (Nickel- Chromium) Thermocouple
Gas Species	Testo 350 XL testo 454 flue gas analyzer

The thermocouple used for the temperature measurements was inserted all the way into the centre-line of the probe until it reached the suction inlet of the probe where an additionally installed radiation shield was added.

3.3.3. Radiation Shield

The thermocouple was shielded from radiation by means of a temporary modification done to the tip of the stainless-steel water-cooled probe. A ceramic tip was added to the front end of the probe to shield and protected the thermocouple from external radiation shown in Figure 3-4 below.

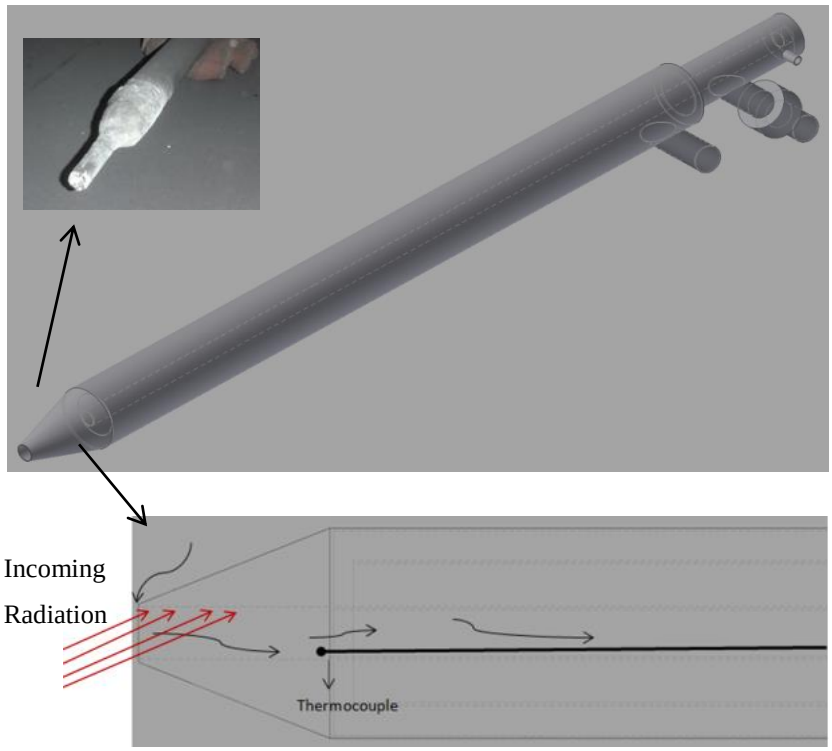


Figure 3-4: Temporary ceramic tip added to the suction probe in order to shield the thermocouple from radiation

Although a certain portion of radiation which came in head on along the axis of the probe possibly still reached to the thermocouple tip it was anticipated that the bulk of the emitted radiation was blocked out and, therefore, shielded from the thermocouple tip.

An added benefit of the ceramic tip was the protection of the thermocouple against the cooling effect of the cooling water flowing over the outer walls of the centre gas suction tube.

3.3.4. Measurement Location

The in-flame temperature measurements were done on a single burner and included measurements through the centre-line and bottom inspection port of the burner in an effort to produce a semi two-dimensional view of the flame. The centre-line measurements were done through the core air tube in the centre of the burner. The measurements through the bottom inspection port were done by inserting the probe through the bottom inspection port at the outer wall of the windbox and through the tertiary burner tube. The entry points on the simplified burner schematic are shown in Figure 3-5 below.

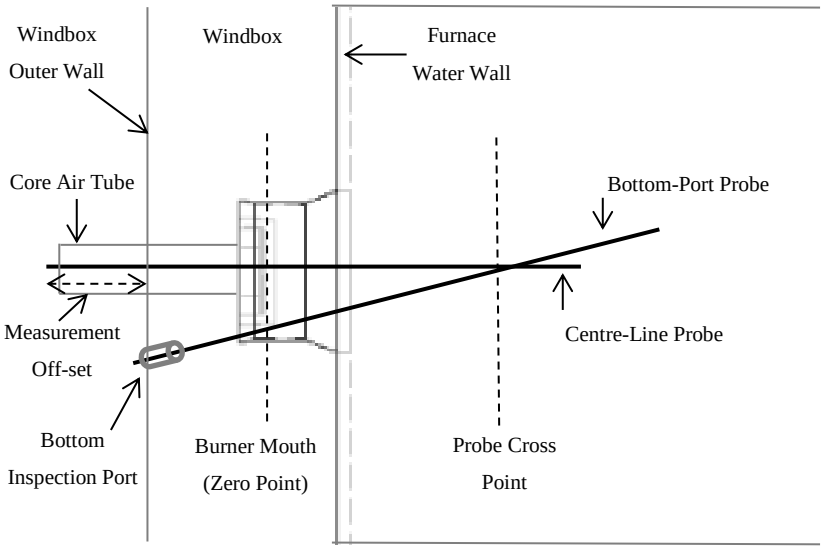


Figure 3-5: Basic burner schematic showing probe entry points into the furnace

The probe through the bottom inspection port could be inserted further into the furnace when compared to the centre line measurements. This was because of the off-set distance that occurred when measuring through the centre-line with the core air tube that extends well beyond the windbox outer wall. It was determined that the two probes cross each other approximately 1994 (mm) from the burner mouth. The method used in determining the probe cross point is being described in section 3.4.3.

3.4. Burner Selection Process

The process of selecting the best suitable burner to perform the measurements on included the following criteria.

- Burner condition.
- PF distribution.
- Geometrical analysis to determine the accessibility of the measurement ports and determining the exact measurement location.
- Location of a fire hydrant.

After the selection process discussed below the best suitable burner selected to perform the in-flame temperature measurements on was burner E3 (Burner in the bottom row, front wall shown in Figure 3-6 below).

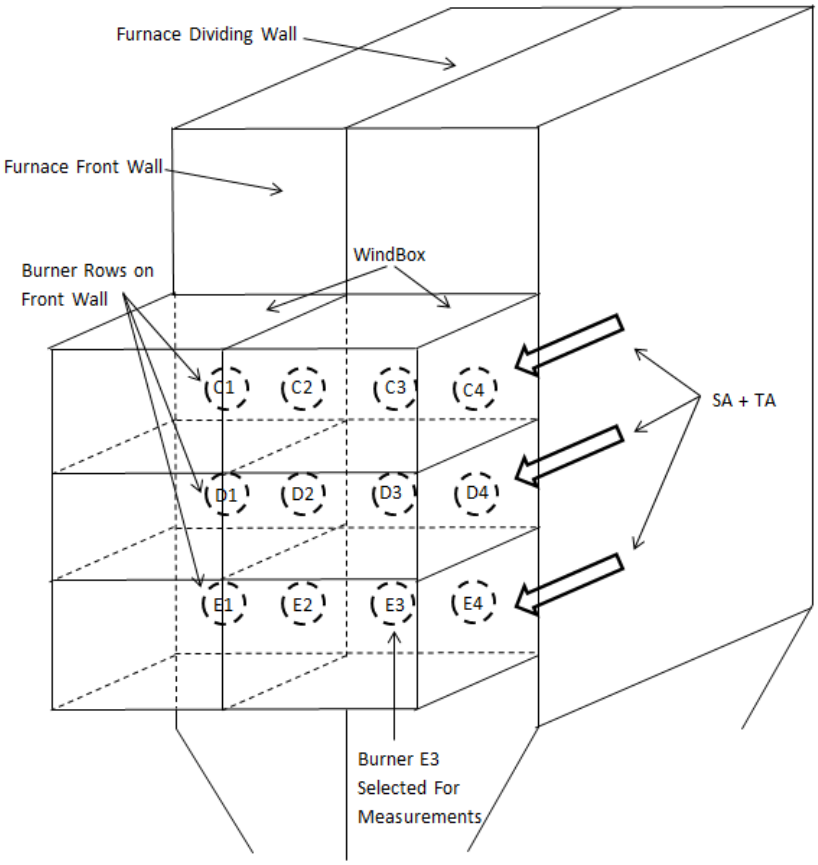


Figure 3-6: Location of burner E3 in relation to furnace front wall and windbox.

3.4.1. Burner Condition

The power plant under investigation has been in operation for a considerable amount of time. Because of the very stringent operating conditions, the possibility existed that some of the burners might have severely worn parts because of the excessive wear exposure. In some instances, erosion could have created holes in the primary and even secondary pipes of the burner. If holes through the burner tubes do exist it could have an impact on the burner aerodynamics and the flame temperature profile achieved. The holes will force a certain portion of the air into the surrounding burner tube which could produce either a reduced or increased amount of swirl depending on the location of the hole. It was, therefore, important that the burner selected to perform the in-flame measurements on had to be in an acceptable operating condition to accurately represent a typical flame profile normally achieved. Burner E3 was found to still be in acceptable condition.

3.4.2. PF Distribution

The PF distribution between the four burners supplied by a mill greatly affects the air / fuel ratio to each burner and influence the actual flame shape achieved. The burner selected to perform the in-flame measurements was required to have a stable flow of PF and air in the correct ratio to ensure representative conditions were achieved. Figure 3-7 below shows the PF distribution of all the mills that was in service during the in-flame temperature measurements. The figure shows the deviation of PF mass flow from the mean value (1.12 (kg/s)) of all the mills combined. To guarantee NOx and carbon burnout targets, Original Equipment Manufacturers (OEM's) typically quote margins of 5-10% deviation from mean primary, secondary, and tertiary air (PA ,SA, and TA) flow and 10-15% deviation from mean pulverized fuel (PF) flow between burners [12]. Although a very poor all-around PF distribution was achieved, burner E3 was found to have an acceptable PF supply and operates well within the 15 (%) acceptable deviation from the mean. The complete PF sampling report of mill E obtained during the in-flame temperature measurements is displayed in Appendix B.

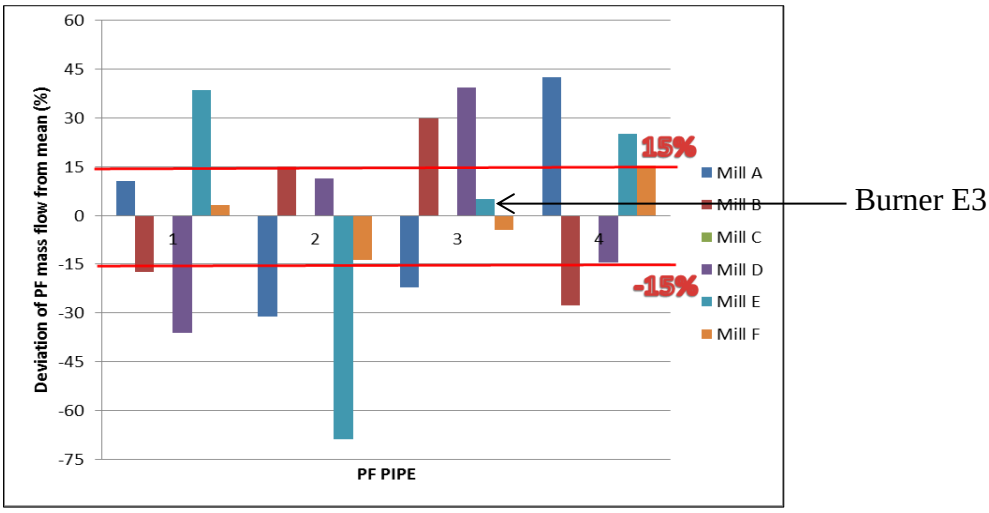


Figure 3-7: Summary of complete PF distribution (21 October 2014) done during measurements

Additionally the typical low NOx burner particle size distribution requirement is as follow [12]:

Particles passing through 75µm: 71% to 80%

Particles passing through 90µm: 80% to 90%

Particles passing through 200µm: 99.4% to 99.95%

Particles passing through 300µm: 100%

The particle size distribution and SA, TA flow distribution was not included in the burner selection process.

3.4.3. Geometric Analysis

The geometric uncertainty of where the measurements took place in the furnace will have an impact on the confidence of the results. To build confidence within the measurement uncertainty an accurate line of measurement had to be established. To determine the exact location of each of the measurement points within the furnace both CAD (from burner design documents) and on-site burner measurements were done. The simplified CAD shown in Figure 3-8 only contained the parts of the burner on which the probes rested on

through the bottom inspection port and burner centre-line while carrying out the in-flame measurements. These parts determined the angle of the probe and included the outer face of the windbox (bottom inspection port) and the tertiary burner tube exactly where the probe cut through the TA swirler. The burner mouth was taken to be at the primary burner tube outlet.

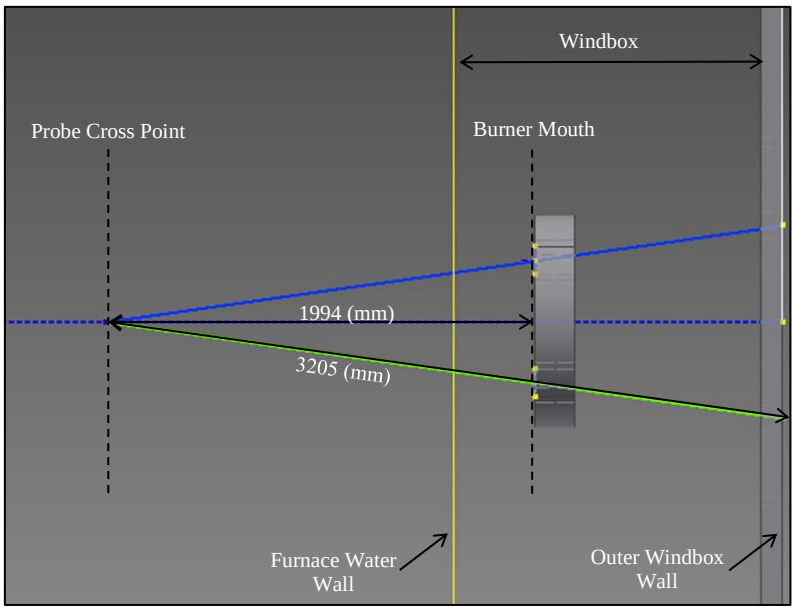


Figure 3-8: CAD distance from burner outlet to probe cross point through centre-line was calculated at 1994 (mm). CAD distance from the outer windbox wall to the probe cross point through the bottom inspection port was calculated at 3205 (mm)

Probes were added in the CAD through the bottom and top inspection ports and through the burner centre-line. From CAD, it was determined that the probes intersect each other at 1994 (mm) from the burner mouth with a total probe length measured from the bottom inspection port to the cross point of 3205 (mm).

To ensure an accurate line of measurement was determined through CAD, physical on-site measurements were also done during a power plant outage. Geometrically the length of the probe caused challenges at some of the burner locations. To ensure a free path of measurement through the centre-line and bottom inspection ports two Polyvinyl Chloride (PVC) pipes with the same dimensions as the actual probe used was fitted beforehand to make sure the probe fits through the burner and the path of entry was clear of any obstructions. The two probes were inserted through the centre-line and bottom inspection port until it crossed in the furnace. The probe cross point is shown in Figure 3-9 viewed from the side furnace inspection door.

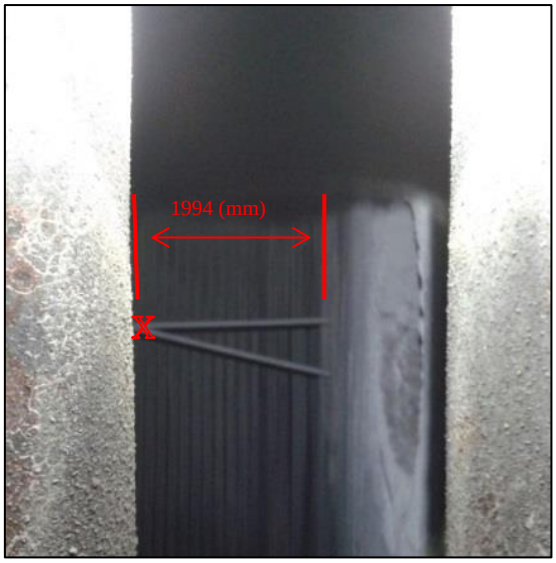


Figure 3-9: Probe cross point in the furnace indicated by point x viewed from the side furnace inspection door

The total probe length which was the distance defined from the outer windbox wall to the probe cross point in the furnace through the bottom inspection port was measured and compared to the CAD results show in Table 3-2 below.

Table 3-2: CAD compared to on-site measurements

	Bottom Inspection Port	
	Measured Distance (mm)	CAD Distance (mm)
Measured from bottom inspection port to the probe cross point in the furnace.	3215	3205

The CAD determined total probe distance of 3205 (mm) very closely predicted the 3215 (mm) which was measured on-site.

3.4.4. Fire Hydrant

If more than one burner would have been found fit for the in-flame temperature measurements the fire hydrant would have been the deciding factor with the burner closest to the fire hydrant to get the first choice.

3.5. Burner In-flame Measurements Procedure:

3.5.1. Swirl Settings

To reduce the amount of variables involved with the in-flame measurements the swirl number of the burners had to be fixed and properly defined. The amount of swirl through the TA tube is fixed with only the SA swirl amount that could be adjusted. The burner SA sleeve setting which controls the amount of air flowing through the secondary burner tube was set at 110 (mm) as shown in Figure 3-10 below:

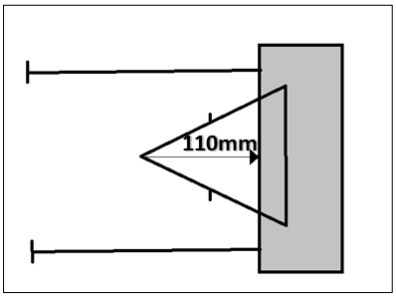


Figure 3-10: Burner sleeve setting

Apart from the burner sleeve setting the amount of swirl through the SA tube can further be controlled by proportioning the quantity of air flowing through the SA swirler and the amount of air bypassing it. The more you retract the swirler the more air bypasses the swirler thus imparting fewer swirl on the air flowing through. The SA air cone during the in-flame temperature measurements was set all the way inwards which drive the largest quantity of air through the SA swirler creating the maximum amount of swirl available.

3.5.2. Operating Procedure

Before any measurements could commence the unit production manager had to be informed of the procedure on how the test was going to be done and the risks involved during the measurements. The in-flame measurements were done under the limited access register (LAR) completed with the unit operator in the control room. This ensures that the unit operator knows exactly what was taking place on the unit, on which level the measurements are taking place, and all the risks involved. If the operator observes any fluctuation in any operational value visualized on the distributed control system (DCS) which could put the unit's production at risk all measurements would've been aborted immediately.

A temporary operating instruction (TOI) was loaded on to the system the day leading up to the measurements and included the following criteria.

- Unit load to be above 90 (%) maximum continuous rating (MCR) from 07:00 to 18:00. The unit should remain stable for the duration of the test.
- The O_2 setpoint to be controlled at 3.5 (%)
- Bottom mills to be in service throughout the test.

To carry out the measurements as accurately as possible it was required that all operating conditions were kept as stable as possible throughout the duration of the measurements. If any operating conditions changed throughout the test period the unit operator would inform the test team to establish what the impact is on the measurements and if the measurements were still valid.

Individuals involved with the in-flame measurements ensured the appropriate safety equipment (Safety hat, goggles, high-temperature face shield, dust mask, high-temperature gloves, ear plugs, safety shoes.) were worn to operate equipment at high temperatures.

3.5.3. Burner In-flame Measurements Method

The Windbox is typically under a positive pressure (gauge pressure) of 700 (Pa) at temperatures close to 250 (°C). This positive windbox pressure created a natural draft out of the inspection port to atmosphere as soon as the port was opened. The hot air at approximately 250 (°C) blowing out of the bottom inspection port created challenging conditions when carrying out the in-flame temperature measurements. Apart from the hot air conditions, dust settling also occurred within the windbox and accumulates heavily within the inspection ports over time. Before the probe could be inserted into the inspection port the dust which had settled in the port first had to be removed. This was done by opening the inspection port a few minutes before the measurements were scheduled to take place. Approximately ten minutes was required to completely clear the port of all accumulated dust. Once the inspection port was clear of dust the probe could be inserted through the port to carry out the measurements. While carrying out the in-flame measurements through the bottom inspection port the entrance into the port surrounding the probe had to be covered with a high-temperature resistant cloth. This was done to reduce the hot air blowing out of the port and to minimize dust emissions into the plant.

The measurements through the centre-line did not impose any of the above implications. The core air tube in which the probe was inserted through the centre-line extended directly into the furnace where a negative furnace pressure (gauge pressure) of approximately 100 (Pa) was obtained. This slightly lower than atmospheric pressure created a natural draft into the furnace and not out of the port as was the case with the bottom inspection port.

The probe was marked with high-temperature tape at the offset value before the probe reached the burner mouth set as the zero point reading. This value was determined as approximately 1500 (mm) for the bottom inspection port and 3000 (mm) for the centre-line measurements. After this zero point reading at the burner mouth the probe was marked every 500 (mm) at which each reading took place respectively. At each marked position, five minutes was allowed for the readings to stabilize before the readings were taken.

3.5.4. Additional Measurements

Apart from the in-flame burner measurements, additional measurements throughout the unit also took place simultaneously by a team from Eskom RT&D. These measurements were mainly done to determine if delayed combustion are taking place affecting the metal temperatures in the super-heaters.

The additional measurements were done at furnace exit, economiser inlet, and economiser outlet. Temperature and species distribution (O_2, CO, CO_2, and NO_x) were measured. The equipment used was the same that was used during the burner in-flame measurements. The results did not form part of the current investigations but were still included in Appendix C for future reference.

3.6. Experimental Error Analysis

3.6.1. Measurement Fluctuation:

Because of the turbulent and dynamic nature of the flame, the readings fluctuated considerably at each measuring point. Errors due to fluctuation in measurement readings are found to be the greatest contributor to measurement uncertainty [37]. The fluctuation percentage was calculated by calculating the average fluctuation from the mean value at each measuring point. Hence, at each measurement location, a number of readings were taken from where the average temperature at each measuring point was calculated. Each reading was then considered as either a larger or smaller deviation from the average. The deviation from the average temperature calculated at each measurement point is shown in Figure 3-11 below.

The mean fluctuation through the bottom inspection port of all the measurement points combined was calculated as 2.64 (%) and was also included in Figure 3-11 to give an indication of the overall fluctuation which occurred during the measurement through the bottom inspection port.

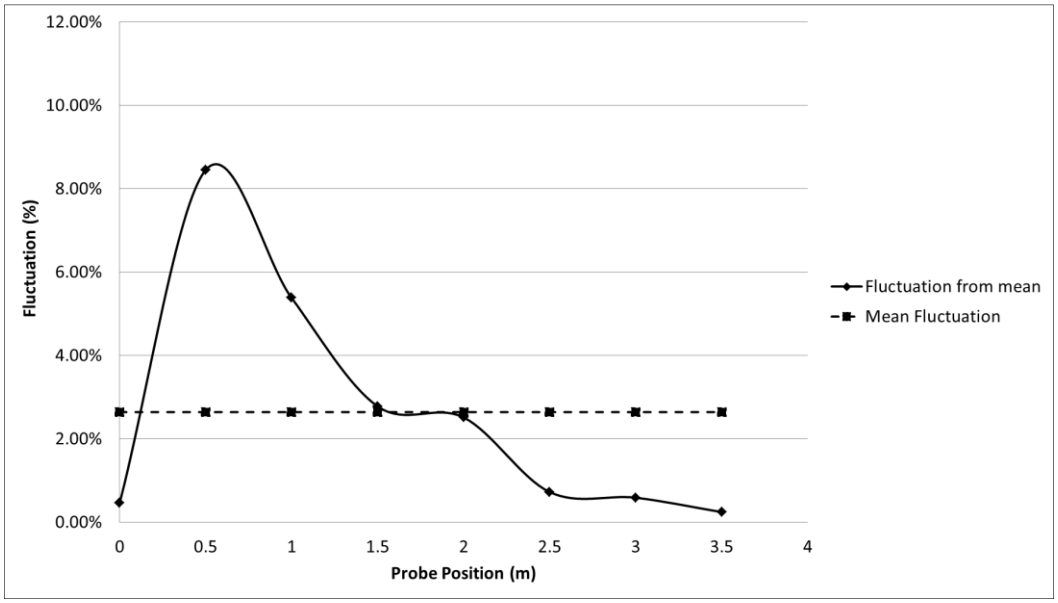


Figure 3-11: Percentage fluctuation from the mean value at each point measured through the bottom inspection port

The percentage fluctuation through the centre-line was calculated in the same way shown in Figure 3-12 below. The mean fluctuation through centre-line off all the measurement points combined was calculated at 5.31 (%) which was almost double than what was observed through the bottom inspection port. This was because of the very high 16 (%) fluctuation observed at one meter into the furnace through the centre-line. The reason for this high fluctuation could be because of the internal recirculation zones created within the flame.

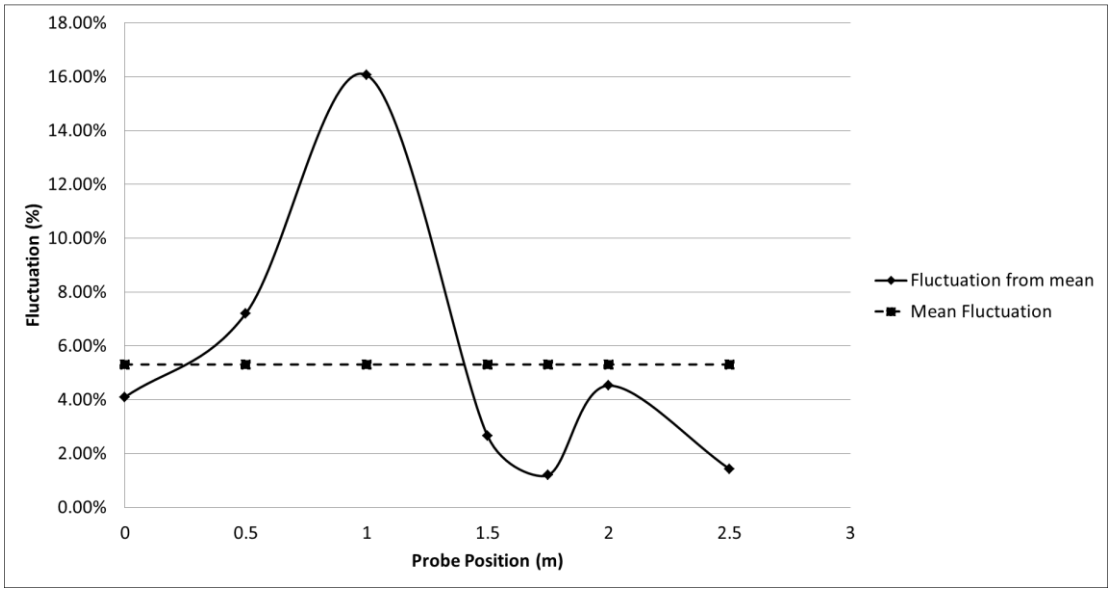


Figure 3-12: Percentage fluctuation from the mean value at each point measured through the burner centre-line

In both cases, high fluctuations in measurements occurred up until 1.5 (m) into the furnace. After 1.5 (m) into the furnace, the temperature reading fluctuations lessened considerably. This could be because after 1.5 (m) into the furnace measurements were taken after the ignition of coal took place with a resulting more uniform temperature distribution.

3.6.2. Measurement Error Analysis

This section describes the methodology involved in estimating the level of uncertainty within the flame temperature measurement results.

The experimental error relates to the measurement uncertainty and included the intrinsic error and any other sources of errors which may occur due to equipment used. The intrinsic error relates to equipment used and measured quantities.

The experimental error was calculated from the methods proposed for the estimation of the uncertainty in the experimental results by the IFRF [15]. The experimental error involved by performing in flame measurements originates from the following sources:

- Incomplete Convective Heat Transfer

Not all the heat in the gas gets transferred to the thermocouple tip and, therefore, the error in the reading because of incomplete convective heat transfer between the surrounding gas and thermocouple tip. The formula expressing the convective heat transfer of a thermocouple in a pyrometer under turbulent conditions was defined as:

$$\frac{(h_c D)}{k} = 0.2 \left(\frac{\rho V D)}{\mu}\right)^{0.8} \quad (3.1)$$

Where:

h_c - Convective heat transfer coefficient (W / m^2.K)

D - Characteristic diameter (m)

V - Fluid velocity (m/s)

k_f - Fluid thermal conductivity (W / m .K)

ρ - Fluid density (kg/m^3)

μ - Fluid viscosity (kg .s / m)

The velocity of the fluid (flue gas) at the inlet of the suction probe plays an important role in the error estimation. If the velocity is too low considerably high measurement error may occur. Throughout the flame temperature measurements, a high suction velocity was maintained (the velocity is expected to be between 60-70 (m/s) as measured by the IFRF on a typical IFRF standard probe) and a conservative 5 (°C) as recommended by the IFRF was considered for ineffective heat transfer between the gas and thermocouple tip [15].

- Difference in gas velocity

The gas velocity within the probe is normally different from the true gas velocity with the velocity in the probe usually higher than the free gas stream. Therefore, the higher kinetic energy of the gas in the probe is transformed into heat energy and could cause an error in measurement. This error is displayed by the following formula:

$$T_g - T_m = \frac{(1-a)\,(V_A^2 - V_G^2)}{2c_p} \qquad (3.2)$$

Where:

T_g - True gas temperature (K)

T_m - Measured gas temperature (K)

C_p - Gas specific heat at constant pressure (J/K)

α - Recovery factor ~ 0.85

V_A - Suction velocity (m/s)

V_G - True gas velocity

The error due to the difference in gas velocity as recommended by the IFRF was conservatively taken as 1 (°C) [15].

- Error due to conduction

Because of the small diameter thermocouple wire used the error due to heat conduction through the thermocouple wires was neglected.

- Insufficient radiation shield

To ensure accurate measurement of true gas temperature by the thermocouple the thermocouple needs to be effectively shielded from radiation. If the thermocouple is not sufficiently shielded from radiation the thermocouple will not only reach equilibrium with the convective heat provided by the gas as required but also with the radiative heat flux from the surroundings. This error can be reduced by the efficiency of the radiation shield in terms of the design of the shield, thickness of the materials used, and selecting materials with low emissivity and conductivity. The temporary radiation shield added to the suction probe inlet made use of a ceramic material, so that the error due to radiation, provided that the suction velocity was high enough, was considered negligible [57].

- Thermocouple accuracy

The accuracy of a thermocouple depends on many factors including but not limited to electrical interference and the purity of the metals used. The percentage error is not linear and increases with an increase of temperature. This enables a higher error expected to measure in the high-temperature regions of the flame. The error due to thermocouple used can range from 2.2 (°C) at 250 (°C) to 9.75 (°C) at 1300 (°C). A value of 5 (°C) was incorporated throughout the measurement range.

- Thermometer accuracy

The voltmeter used to read the signal from the thermocouple was a HE701 series multi-channel thermocouple thermometer. The thermometer has an accuracy and thus estimated error of ± 0.1(%). A conservative 9 (°C) has been used.

- Probe location uncertainty

The exact location of measurements within the flame plays an important part in the determining the measurement accuracy. On-site measurements and CAD was used to eliminate any error that may occur. The probe location uncertainty was therefore neglected during the error analysis.

3.6.3. Final Error Percentage

The combined error due to measurement and fluctuation at each measurement point was translated into error bars added to the temperature measurements shown in Figure 3-13. The highest error percentage was obtained at the 1 (m) traverse point into the furnace through both the centre-line and bottom inspection port. Through the centre-line, the error percentage at 1(m) was calculated as 16 (%) and through the bottom inspection port as 8.5 (%). The lowest error percentage through the centre-line was calculated as 1.53 (%) at 2.5 (m) and through the bottom inspection port as 0.25 (%) at 3.5 (m).

3.7. Results

3.7.1. Operational Values

All operational values while carrying out the in-flame temperature measurements were extracted from the Honeywell Uniformance process history database (PHD) after the measurements were done. Only the main parameters involved were extracted and their average values throughout the measurement period are shown in Table 3-3 below. The complete sets of values are shown in Appendix D. Mill combination was kept the same throughout the measurements with all operating conditions kept as stable as possible. The unit load was controlled at 93 (%) MCR.

Table 3-3: Operational data

Parameter	Unit	Average Value
Unit Load	MW	184.99
Total Air Flow	kg/s	274.55
Total Fuel Flow	MJ/s	577.47
RH Furnace Gas Pressure	Pa	-105.68
RH Front WB Hot Air Pressure	kPa	0.45
Front WB Pressure between E3&E4	kPa	0.43
Burner E3 Tertiary Pressure	kPa	-0.41
E3&4 Promecon Air Flow	kg/s	14.44
Mill E Outlet Temp	℃	85.25
PA Fan E PA Air Flow	kg/s	9.46
RH Air Heater Air Outlet Temperature	℃	256.43

The total air flow delivered by both left and right hand FD fans was approximately 275 (kg/s). The furnace pressure was controlled at -100 (Pa). The PA/PF mixture mill outlet temperature was controlled at 85 (℃) with a PA mass flow of 9.46 (kg/s). The air into the windbox supplying SA and TA into the burner was approximately 256 (℃) calculated from the air heater air outlet temperature.

3.7.2. Temperature Results

3.7.2.1. Combined Result

The burner in-flame gas temperature results obtained through the centre-line and bottom inspection port are shown in the combined Figure 3-13 below. The complete set of values can be seen in Appendix C.

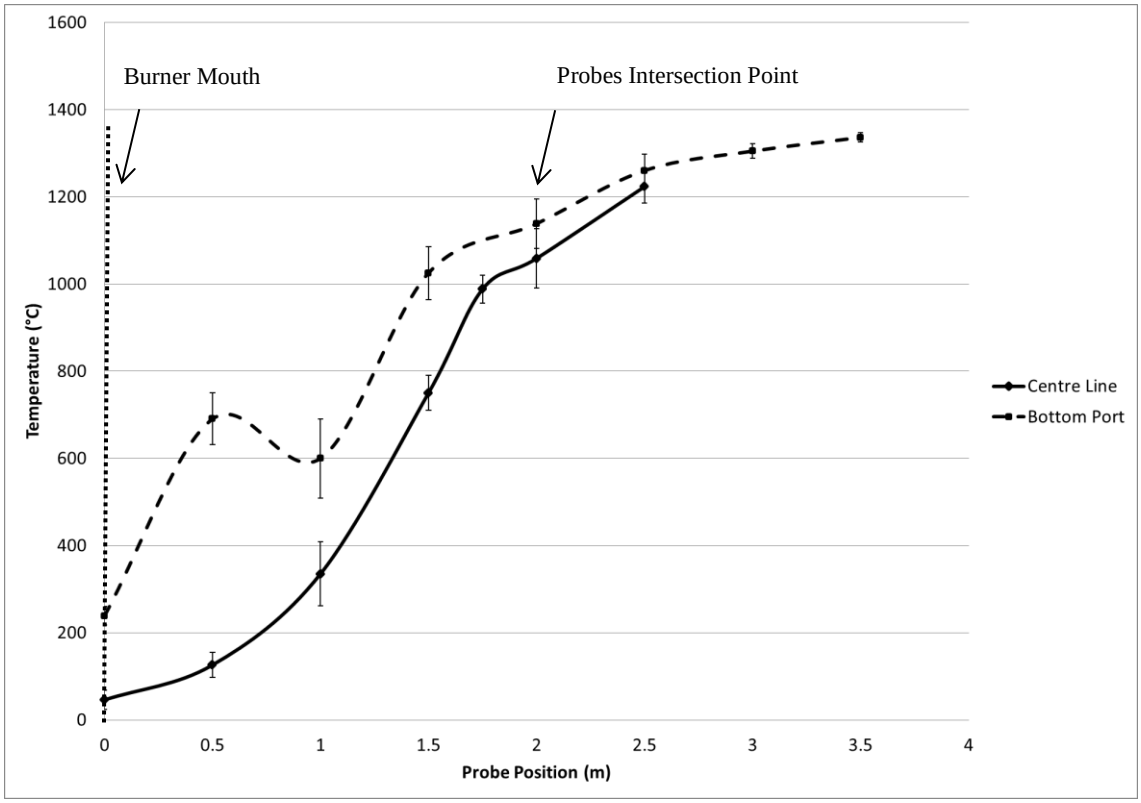


Figure 3-13: Burner in-flame temperature measurement results through the centre-line and bottom inspection port combined

The measurement values in Figure 3-13 started off from the zero point which was at the burner mouth and extends into the furnace in increments of 500 (mm). Another reference point of the measurement results was the intersection point of the probes. This point was where the centre-line and bottom-port measurements intersected each other in the furnace at approximately two meters from the burner mouth through the centre-line. The temperature at the intersection point through the bottom inspection port was slightly higher than the temperature through the centre-line. The error bar at each measuring point indicates the error involved due to the fluctuation in the measurement data as well as the experimental error due to the equipment used. With the experimental error taken into consideration, the values at the probe intersection point were found to be within acceptable margins of each other.

3.7.2.2. Bottom Port

The temperature readings at the burner mouth started off at 238 (°C) as expected and were in the range of typical windbox operating temperatures. From there the temperatures gradually increased to a maximum temperature of 1336 (°C). There was a sudden increase in temperature at 0.5 (m) into the furnace up to 690 (°C) from where it dropped back to 600 (°C) again at 1 (m) in.

This sudden increase could be as a result of the expected highly turbulent conditions where the measurement took place. These turbulent conditions together with dynamic flame operating conditions constantly varying the flame offset from the burner mouth, possibly contributed to the high fluctuation in temperature values observed at this certain measuring point.

3.7.2.3. Centre-Line

The temperature readings through the centre-line increased gradually from 46 (°C) to 1223 (°C). The flame off-set was determined to be between 1 and 1.5 (m) into the furnace which was the point where the temperatures exceeded 600 (°C).

The amount of fluctuation at each measuring point will be discussed further in the succeeding experimental error analysis section.

3.8. Flame Profile Measurement Discussion

Temperature measurements were done through the centre-line and through the bottom inspection port of the burner to obtain a semi two-dimensional view of the flame. The flame offset from the burner mouth through the centre-line of the burner was found to be between 1 and 1.5 (m) into the furnace. An error analysis was done to establish the amount of uncertainty that occurred during the measurements. The error analysis included the error occurred due to fluctuation in readings together with the error due to measurement accuracy at each measurement point. Fluctuations in the temperature readings were found to be the leading contributor to the measurement error percentage.

These temperature results obtained in Chapter 3: were required to be compared to the full-scale single burner combustion CFD model presented in Chapter 8: .

Chapter 4: DEVOLATILIZATION DTF EXPERIMENTS

4.1. Introduction

Chapter 4: describes the process involved in evaluating the volatile yield mass fraction of the specific coal used. This evaluation relates to different heating rates and varying residence times.

The DTF experiments allow for a common basis to be derived for comparison between different quality fuels and allow one to draw useful conclusions about the coal's specific combustion characteristics.

The DTF experimental results were also used to be compared to the numerical calculations in Chapter 5: in order to calculate the coal specific single rate combustion kinetic parameters. This served as a computational input to improve on the default values used in CFD to improve on the full scale single-burner combustion CFD model results described in Chapter 8: .

4.2. Experimental Setup

The complete setup of apparatus used during the drop tube furnace devolatilization experiments is shown in Figure 4-1 below.

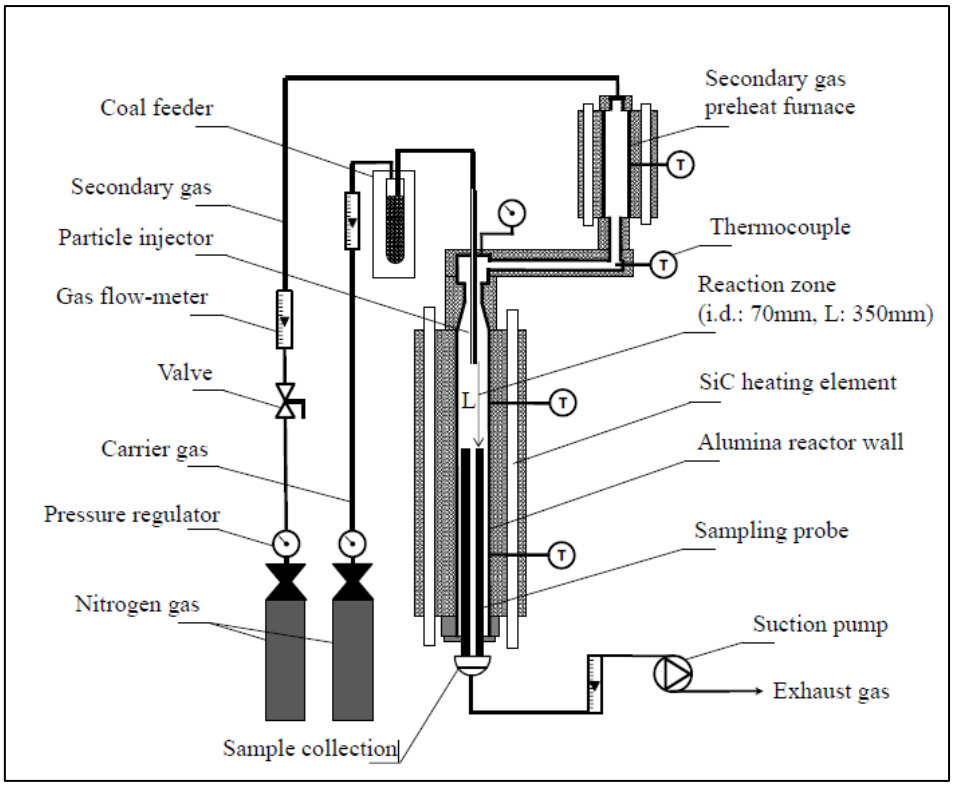


Figure 4-1: DTF experimental setup [26]

The DTF furnace consisted of a 70 (mm) internal diameter vertical alumina tube displayed on the right of Figure 4-3 below. The tube was heated to the desired set point (maximum 1500 (°C)) electrically with six silicon carbide elements equally spaced surrounding the alumina tube.

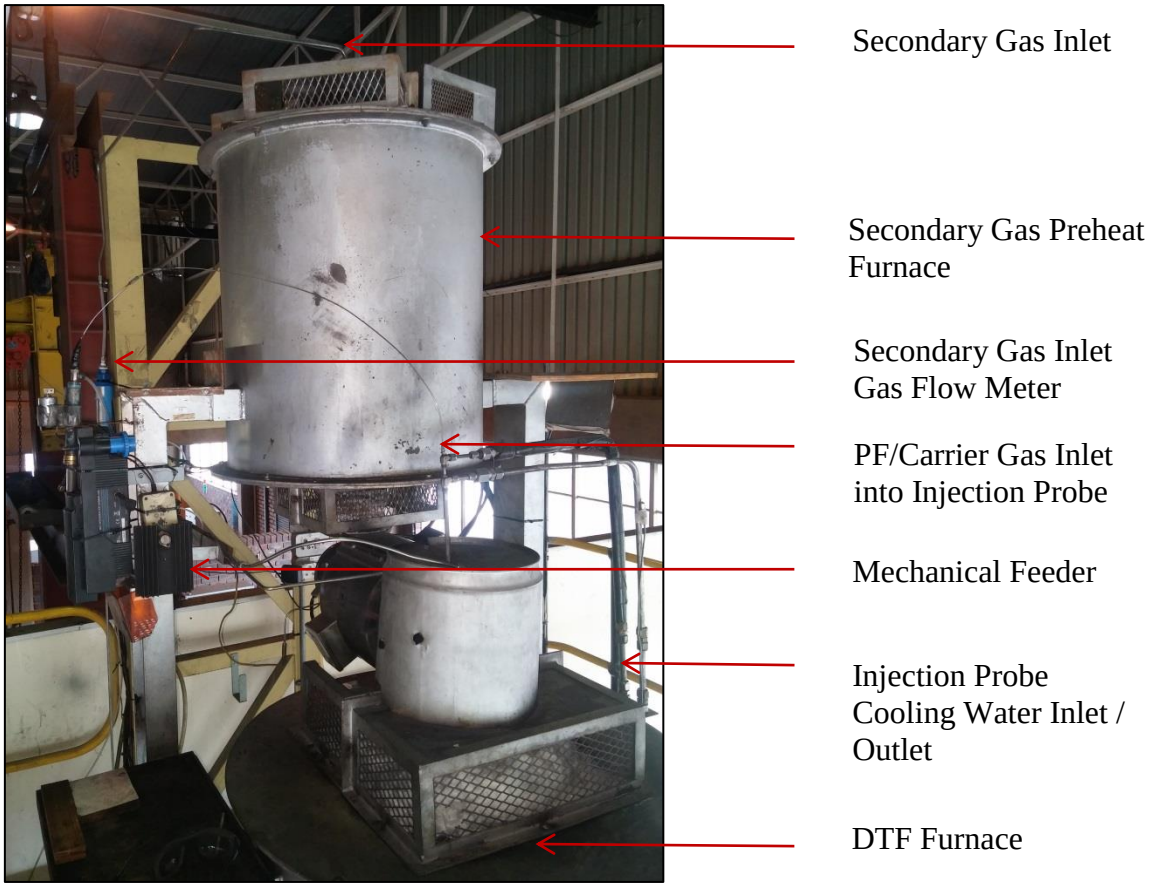


Figure 4-2: DTF gas inlet experimental setup



Figure 4-3: (Left) - Mechanical feeder. (Right) - Alumina tube together with the six surrounding heating elements

The coal sample in the form of a finely crushed pulverised fuel of below 150 (µm) was injected into the furnace by means of a water-cooled injection probe. A mechanical feeder displayed on the left of Figure 4-3 above fed the PF at an average rate determined by the feeder speed into the primary carrier gas stream at atmospheric temperature. The carrier gas stream served as a transport medium to transport the PF from the feeder into the injection probe at the inlet of the DTF furnace.

A separate secondary gas stream allowed for gas preheating by means of an electrically heated furnace which preheated the gas to the prescribed desired set point before it was introduced into the furnace surrounding the injection probe. (Preheat furnace displayed in Figure 4-2 above)

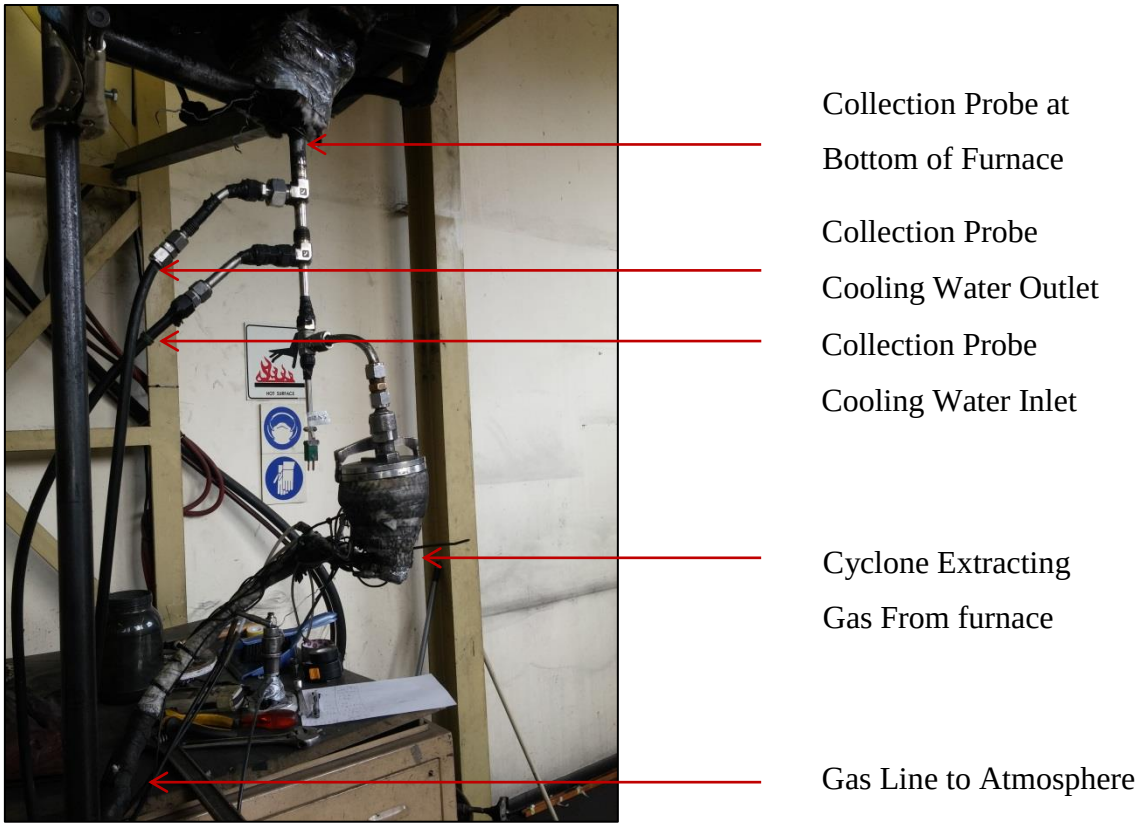


Figure 4-4: DTF gas outlet experimental setup

On the bottom of the combustion furnace, a water cooled collection probe displayed in Figure 4-4 above withdrew the gas from the furnace and separated the solids remaining after the devolatilization process from the gas which was then extracted to atmosphere. The water cooled collection probe at the bottom of the furnace could be inserted into the furnace at any depth required to achieve the desired particle residence times. Depending on

the desired temperature set point together with physical properties of the coal, heating rates of approximately 10000 (°C/s) are usually achieved during DTF experiments. This is typical the heating rate achieved in industrial coal combustion furnaces and was very important to realistically analyse the combustion performance of the coal particles during the DTF experiments.

4.3. Coal Properties & Preparation:

The coal used for the devolatilization experiments was the same coal that was supplied to the unit while performing the burner in-flame temperature profile measurements discussed in Chapter 3: . This was to ensure that a common base was being kept between practical experiments and numerical simulations. Table 4-1 below provides the proximate analysis of the PF used during the devolatilization experiments.

Table 4-1: Devolatilization experiment coal proximate analysis

	Unit	Air Dried	Dry Basis	Dry Ash Free
Moisture	%	3.30	0.00	0.00
Volatile Matter	%	20.50	21.20	30.33
Ash	%	29.10	30.09	0.00
Fixed Carbon	%	47.10	48.71	69.67
Total	%	100.00	100.00	100.00

In preparation of the PF for the devolatilization experiments the PF was sieved to below 150 (μm). This was done to ensure a particle diameter which could accurately be monitored within the given time frame of the furnace and to avoid particle feeder blockages. Figure 4-5 below shows the particle diameter distribution of the PF used during the devolatilization experiments calculated by a Malvern Mastersizer 2000 E Ver. 5.60.

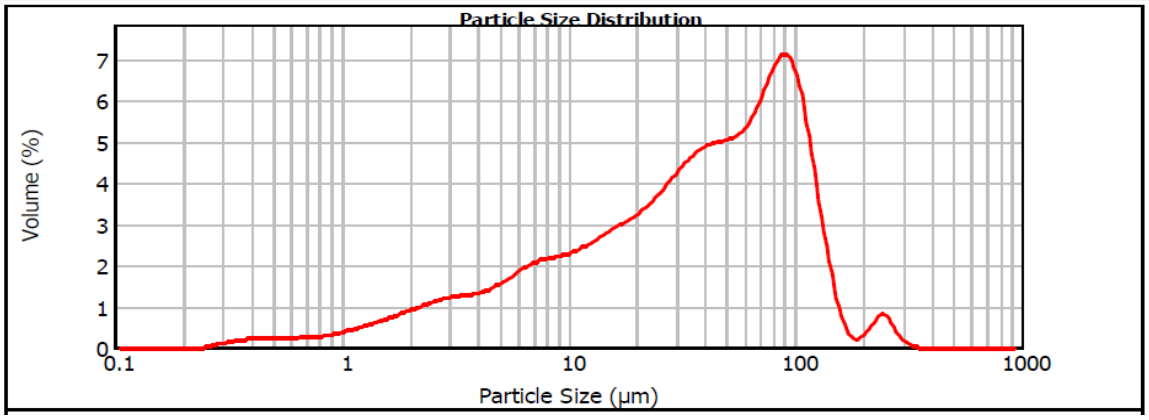


Figure 4-5: DTF experimental particle distribution

The bulk of the particles were found to be in the 90 (µm) range with 98 (%) of the particle below 150 (µm).

4.4. Devolatilization Experimental Procedure

The coal devolatilization experiments determined the volatile yield mass percentages of the PF particles at different heating rates and varying particle residence times. The PF particles were pyrolized in a nitrogen only atmosphere at three temperature set points i.e. 1000, 1200 and 1400 (°C). The particle residence times ranged from 92 (ms) to 192 (ms). Inert nitrogen gas was used to avoid char oxidation within the DTF furnace, to ensure only the devolatilization stage of the combustion process was being looked at. In an attempt to achieve the relatively short particle residence times typically involved with the devolatilization process the collection probe was fixed and fully inserted into the furnace achieving the shortest possible distance between the injection and collection probe of 400 (mm). To vary the particle residence times throughout the experiments the secondary nitrogen gas velocity was adjusted between a minimum of 1.9 (m/s) to a maximum of 6.4 (m/s). The maximum gas velocity was set to ensure laminar conditions were maintained within the DTF furnace. The flow is laminar if the Reynolds number is less than approximately 2100. If the Reynolds number is above 4000 the flow is defined to be fully turbulent. For a Reynolds number between 2100 and 4000 the flow may switch between laminar and turbulent conditions defined as transitional flow [61].

The Reynolds number was calculated as follow [61]:

$$Re = \frac{\rho V D}{\mu} \quad (4.1)$$

Re - Reynolds number

ρ - Density of fluid ($kg.m^{-3}$)

V - Velocity of fluid ($m.s^{-1}$)

D - Inner Diameter of pipe (m)

μ - Dynamic Viscosity of fluid ($kg.m^{-1}s^{-1}$)

The Reynold number for the 6.4 (m/s) flow limit was calculated to be:

$$Re = \frac{(0.2317)(6.4)(0.07)}{(5.022 * 10^{-5})}$$

$Re = 2066$

The density and dynamic viscosity of Nitrogen were obtained from an engineering calculator at an average centre-line temperature of 1200 (°C).The value of 2066 is just below the laminar limit of 2100 and therefore regarded as the upper limit of the flow range.

The mechanical feeder feeding the PF into the DTF furnace was set to achieve an average particle mass flow of 3.9E-05 (kg/s). The carrier nitrogen gas transporting the PF from the feeder into the injection probe and finally into the DTF furnace was kept at a constant rate of approximately 0.25 - 0.3 (NL/min).

The samples were weighed and collected in a glass tube before it was inserted into the mechanical feeder. Each experiment required approximately 40 (g) of the PF sample to produce enough products for a proximate analysis to be done. The solid products remaining in the container at the bottom of the collection probe after each experiment were collected and sealed in a glass container to be analysed by the coal laboratory. After each experiment, the DTF furnace and collection probe's walls had to be cleaned with compressed air to ensure all the trapped particles inside the DTF furnace and collection probe was removed, and could not influence the subsequent experimental results.

4.5. DTF Experiments Results

The DTF furnace wall temperature profile achieved at the specified temperature set points was obtained from the DTF history. The wall temperature achieved during the experiments was not constant throughout the DTF furnace. Figure 4-6 shows the results obtained from the measured wall temperature profiles for the 400 (mm) DTF furnace at the three different experimental temperature set points [26]. The wall temperature measurements were done with an R-type thermocouple and were conducted from the injection probe at the top of the furnace going downward against the furnace wall until the collection probe at the bottom of the furnace was reached in increments of 100 (mm). The temperature increased moving downward from the top of the furnace until it reached the maximum desired set point further down into the furnace. The wall temperature profiles were measured and defined to be implemented in all the subsequent numerical simulations to ensure the most accurate numerical results were achieved.

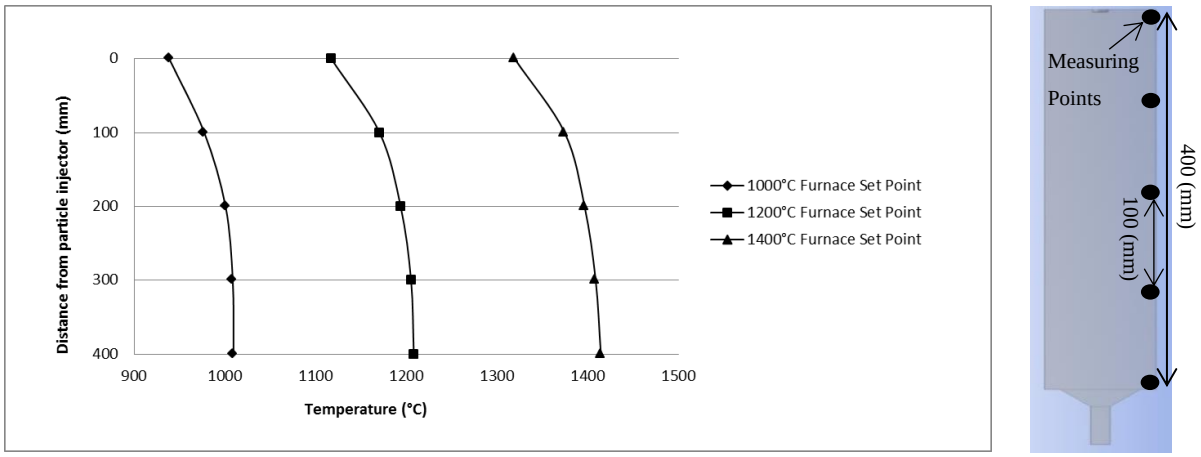


Figure 4-6: (Left) - DTF devolatilization experiment wall temperature profiles [26], (Right) - Illustration of measuring points down the furnace wall

Poor collection efficiency was achieved during the experiments due to some of the particles collecting on the furnace and collection probe walls during the experiments. To accurately calculate the particle mass loss during the DTF experiments the ash tracer method was used. Table 4-2 below shows the proximate analysis ash percentages of the samples collected after each experiment.

Table 4-2: Proximate ash percentages (dry basis) of product remaining after each DTF experiment

Flow	Particle Residence Time (ms)	1000 (°C) Ash (%)	1200 (°C) Ash (%)	1400 (°C) Ash (%)
20%	192.094	38.76	38.67	41.92
40%	136.703	37.08	38.09	40.57
60%	107.323	32.74	36.26	39.77
80%	91.706	31.79	37.70	39.61

The dry ash free particle mass loss percentage calculated by the ash tracer method was calculated as follow:

$$\% \text{ Particle Mass Loss (daf)} = 100 - 100\left(\frac{Ai}{100 - Ai}\right)\left(\frac{100 - Ae}{Ae}\right) \quad (4.1)$$

A_i - Initial proximate ash percentage of coal (dry basis).

A_e - Percentage of ash remaining in coal char each after experiment (Dry basis).

$$\% \text{ Particle Mass Loss (daf)} = 100 - 100\left(\frac{30.09}{100 - 30.09}\right)\left(\frac{100-38.76)}{38.76}\right) \quad (4.2)$$

$$= 31.98\ \%$$

The particle mass loss percentages (daf) approximating the volatile yield mass percentage of each experiment are shown in Table 4-3 below. The coal devolatilization curves obtained during the experiments for each temperature set point are shown in Figure 4-7 below:

Table 4-3: Particle volatile yield percentage (ash tracer method)

Flow	Particle Residence Time (ms)	1000 °C Particle Mass Loss % (DAF)	1200 °C Particle Mass Loss % (DAF)	1400 °C Particle Mass Loss % (DAF)
20%	192.094	31.98	31.74	40.36
40%	136.703	26.97	30.05	36.95
60%	107.323	11.55	24.32	34.80
80%	91.706	7.65	28.86	34.37

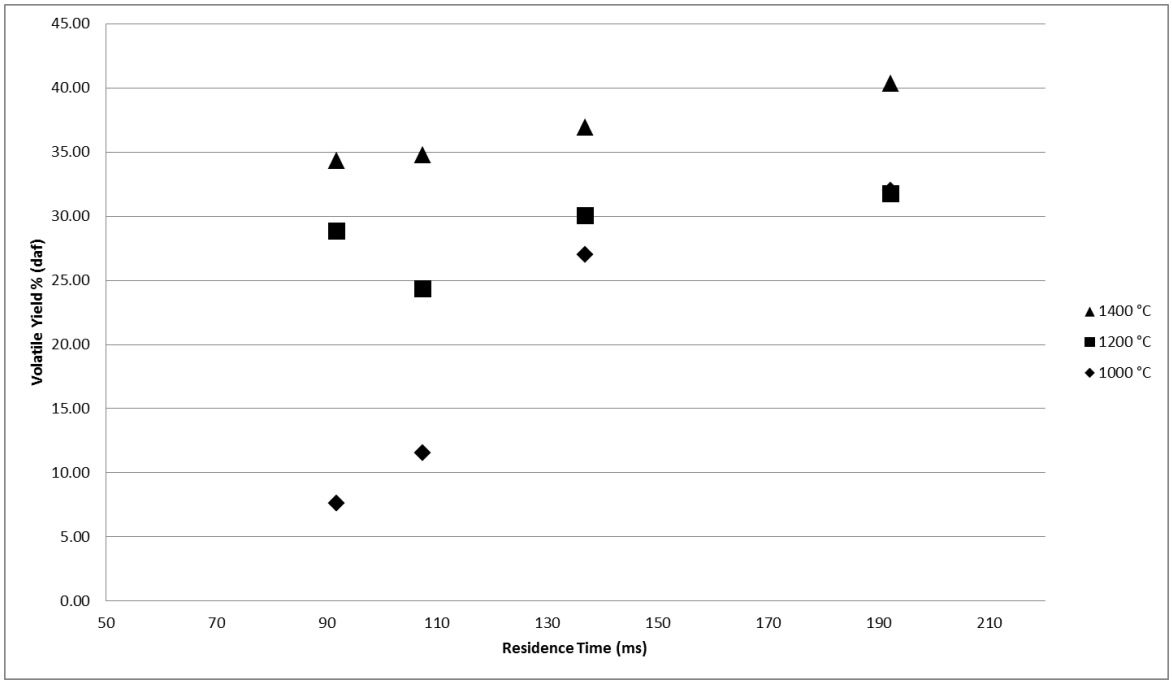


Figure 4-7: DTF volatile yield experimental results

Figure 4-7 shows that at higher particle heating rates more volatiles are released from the coal, achieving a higher ultimate volatile yield percentage. The ultimate volatile yield percentage is defined as the largest mass fraction of volatiles release achieved. During the 1400 (°C) set point experiments the measured ultimate volatile yield was substantially higher than what the proximate analysis predicted. The ultimate volatile yield at 1400 (°C) was 40.36 (% daf) compared to the 30.33 (%) volatiles in the proximate analysis. This indicated that at higher heating rates typically experienced in power plant coal combustion processes, the mass percentage of volatiles released from the coal could be higher than what the proximate analysis predicts.

4.6. DTF Devolatilization Discussion

The secondary gas flow was varied between 1.9 (m/s) achieving 192 (ms) particle residence times and 6.4 (m/s) achieving the shortest possible particle residence times of 91.7 (ms). During the experiments at the 91.7 (ms) residence time, the secondary gas line was opened to 80 (%) flow control indicated by the additionally installed gas flow meter.

This very high gas flow used within the DTF furnace negatively affected certain operating parameters within the furnace. Apart from the very high gas usage during the experiments which led to the need to change the nitrogen gas supply bottles after each experiment the aerodynamics of the gas flow through the furnace was also affected. The laminar gas flow conditions required within the DTF furnace were being at risk of shifting to turbulent flow conditions at very high velocities. The Reynolds number throughout the experiments has to be kept below 2100, or else the DTF gas flow will become turbulent, with associated inaccurately calculated residence times. Therefore, the upper limit was set on a gas flow of 80 (%) achieving approximately 6.4 (m/s). Another operating parameter influenced by the high gas flows were the secondary gas preheat temperatures. The secondary gas pre-heaters could not reach the desired temperature set points as a result of the high mass flows of gas used during the experiments. These lower actual temperatures achieved compared to the temperature set points during the experiments affected the particle heating rate and were accounted for in the numerical simulations to follow.

The 1400 (°C) set point case was used to calculate the single rate combustion parameters for the coal's devolatilization stage. From Figure 4-7 it can be seen that at the shortest residence time achieved of 91.7 (ms) an ultimate volatile yield of 33.92 (%) was already obtained. To calculate the single rate kinetic parameters accurately from the graph it was necessary to obtain a complete spectrum of volatile yield percentages, especially at even shorter residence times. This very short residence times required to predict the volatile yield below 33.92 (%) could not be achieved by means of experiments. The same phenomena were also experienced through a previous study by S. Peta who investigated the ignition characteristics of low volatile high ash quality coal [26]. Apart from a complete spectrum of volatile yield percentages required, to calculate the single rate devolatilization kinetic parameters from the experimental data the particle temperatures at each point were also required which could not be obtained easily from the DTF experiments. Therefore to provide a complete spectrum of volatile yield percentages at residence times faster than what could be achieved during the experiments and to determine the particle temperatures during the DTF experiments a numerical analysis was done.

Chapter 5: DEVOLATILIZATION DTF NUMERICAL ANALYSIS

5.1. Introduction

Chapter 5 describes the method used in determining the coal's single rate devolatilization combustion kinetic parameters by means of numerical analysis.

Lower actual temperatures were achieved during the experiments compared to the theoretical set points. Therefore, the highest temperature set point of 1400 (°C) for the wall and gas temperatures were used in all subsequent numerical simulations to still realistically simulate heating rates commonly found in combustion furnaces. The same principles used in during the 1400 (°C) set point simulations can be applied to calculate the volatile yield for the 1200 (°C) and 1000 (°C) set points as well. The residence time used during the numerical simulations was the longest residence time achieved during the experiments of 192 (ms). This input ensured a complete devolatilization curve was obtained from the onset of devolatilization up until 192 (ms). The main purpose of the numerical coal devolatilization simulations was to obtain an accurate set of devolatilization kinetics especially at residence times shorter than what could be obtained during the devolatilization experiments to be used to improve on the full-scale single coal burner combustion CFD model. Numerical analysis of coal devolatilization process involved a combination of CFD and PC coal lab simulations shown in Figure 5-1.

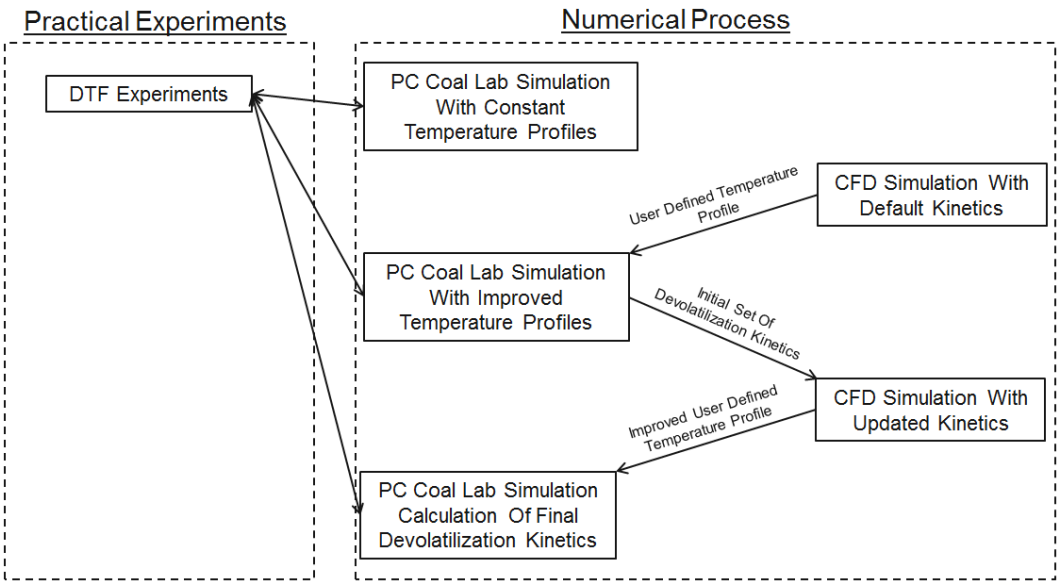


Figure 5-1: Method followed in the numerical calculation of devolatilization reaction kinetics

An initial PC coal lab simulation was done with constant temperature profiles defined for the DTF wall and gas centre-line temperatures. PC coal lab, however, gives the user the option to insert an user defined temperature profile instead of a constant profile throughout the DTF's furnace for the centre-line gas and furnace wall temperature. The user defined temperature profiles describe the temperatures obtained during the experiments more accurately and improves on the calculated heat transfer to the particles resulting in an improved result. The user defined DTF furnace wall temperature was obtained by measurement and the user defined gas centre-line temperature profile by making use of CFD. The method of using CFD to obtain user defined gas centre-line temperature profiles was found to be very effective from previous studies [26].

An initial CFD simulation made use of Ansys Fluent's default kinetics to calculate a centre-line gas temperature profile of the DTF's furnace to better define and improve on the initial PC coal lab simulation. After specifying this user defined temperature profiles into PC coal lab the improved devolatilization result from PC coal lab was subsequently used to calculate an initial set of devolatilization single rate kinetic parameters to improve on the initial CFD result. The CFD model with the updated kinetics was then used to calculate a final and even more accurately defined centre-line gas temperature profile to be used as an updated user defined temperature profile in PC coal lab to calculate a final set of devolatilization kinetics.

CFD in addition to the centre-line temperature calculation was also used to determine the particle residence time together with the particle temperature achieved during the DTF experiments.

All the numerical results were compared to the experimental data obtained in chapter 4 to ensure accurate result were obtained. The CFD package used during the numerical process was Ansys Fluent R15.0 Academic. The development of the numerical results by means of iterating between CFD and PC coal lab were shown from the most elementary initial simulation through to the final most accurately defined result.

5.2. PC Coal Lab Simulation (Initial Run)

To start with the volatile yield numerical iteration process, PC coal lab was used to obtain an initial volatile yield and particle temperature result. This first initial run of PC coal lab was done without any user defined temperature profiles from CFD. The simulation assumed a constant temperature profile for the DTF walls and centre-line gas temperature. This most elementary PC coal lab simulation only required the proximate and ultimate analysis of the coal obtained from the coal laboratory report, and certain DTF operating parameters which could easily be obtained from the DTF experiments done in chapter 4.

The PC coal lab input files for the initial run are shown in Figure 5-2 below. The simulation assumed a constant defined DTF wall and centre-line gas temperature of 1400 (°C).

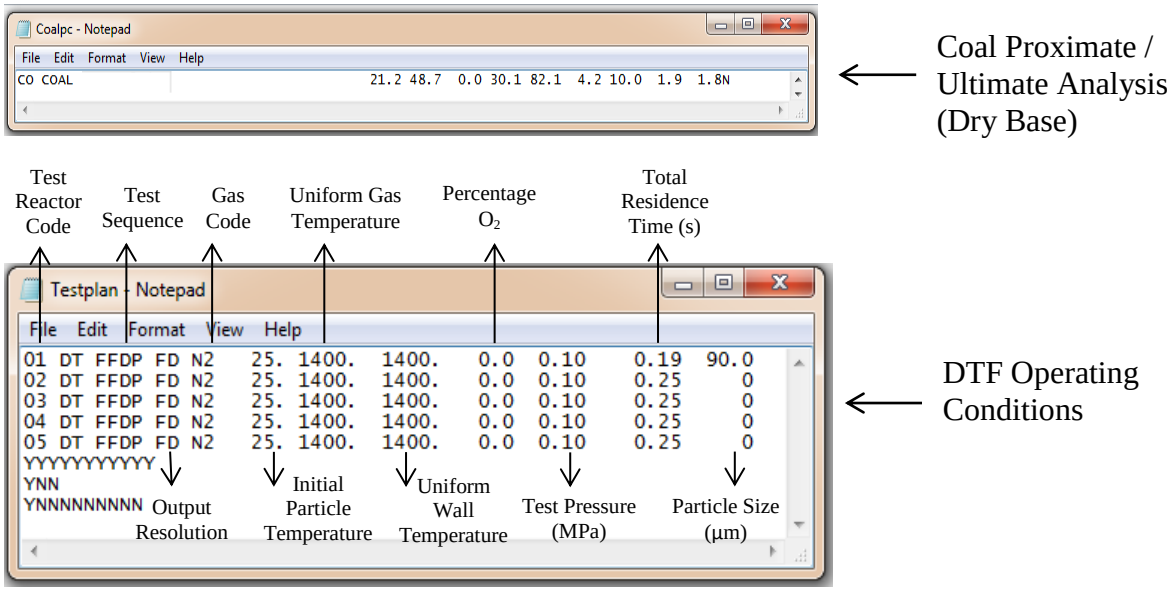


Figure 5-2: PC coal lab devolatilization simulation input values

The PC coal lab result for the particle temperatures achieved at the corresponding particle residence times are shown in Figure 5-3 below.

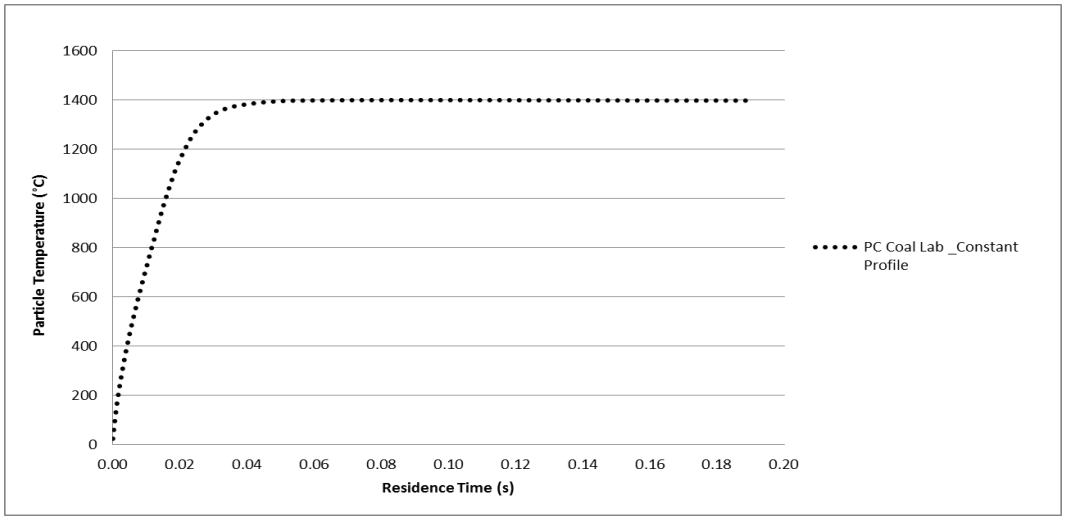


Figure 5-3: PC coal lab particle temperature result @ 1400 (°C) (initial run)

The particle temperature results in Figure 5-3 showed a very high particle heating rate achieved resulting in a very steep particle temperature increase at residence times of below 0.02 (s). An unrealistic particle heating rate of approximately 35000 (°C /s) was achieved. This was because of the way in which the input values were defined. The simulation assumed the coal particle was exposed to 1400 (°C) from the onset into the DTF furnace. It

was therefore expected that the initial PC coal lab simulation would over-predict the particle temperature. This expected over prediction of particle temperature also affect the predicted volatile yield of the particle. The result of the initial PC coal lab volatile yield prediction compared to the DTF experiments are shown in Figure 5-4 below.

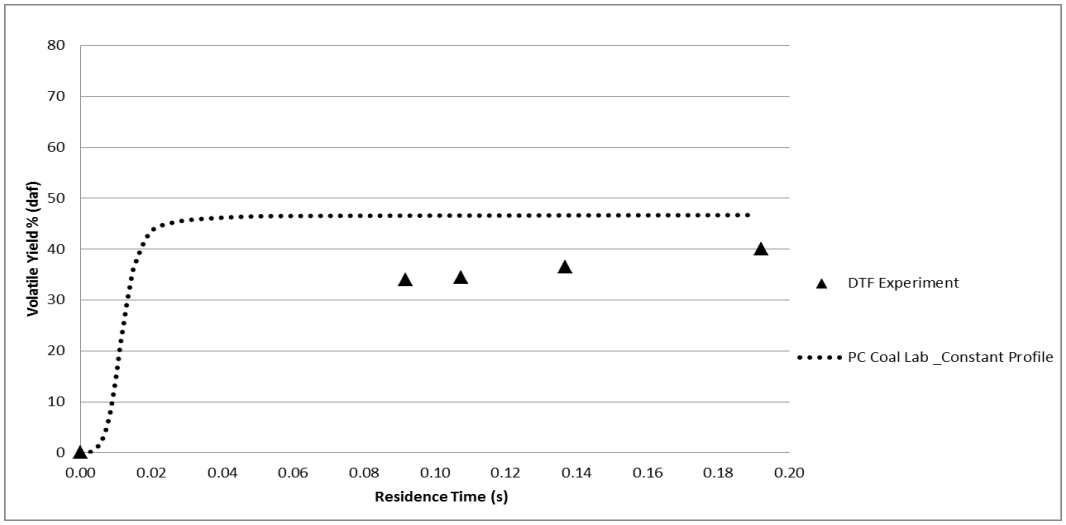


Figure 5-4: PC coal lab volatile yield compared to DTF experimental results at 1400 (°C) set point

As expected, PC coal lab over predicted the volatile yield and the ultimate yield when compared to the DTF experiments. The ultimate yield is defined as the maximum amount of volatiles released during the PC coal lab simulation. The ultimate volatile yield approached 50 (%) were the expected ultimate volatile yield obtained from the DTF experiments were in the range of 40 (%).

To improve on this initial PC coal lab result, CFD was used to determine an improved user-defined centre-line gas temperature profile to be used in the PC coal lab simulations. The following sections describe the complete process involved in how the final kinetics was achieved together with an eventual comparison between measurement and CFD, and measurement and PC coal lab results.

5.3. DTF CFD Model

5.3.1. Geometry

The geometry of the DTF CFD simulations was simplified to include only the furnace part of the DTF together with its corresponding inlet and outlet boundaries. The CAD was created in Autodesk Inventor Professional 2014. The geometry created for the devolatilization experiments is shown in Figure 5-5 below:

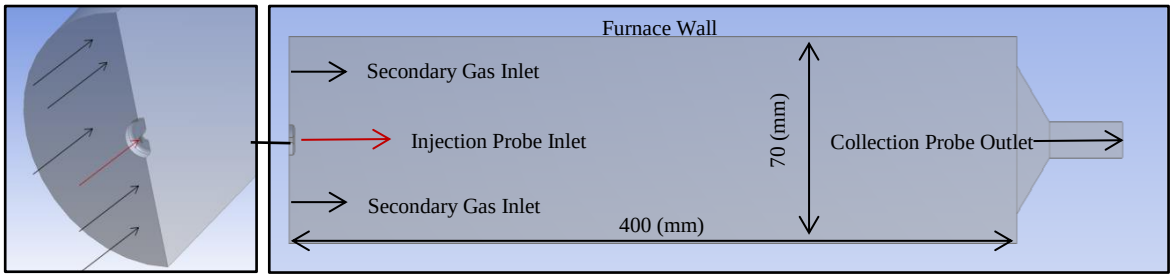


Figure 5-5: DTF CAD

For the ease of presentation, the furnace of the DTF together with the CFD results are shown horizontal however the orientation of the DTF furnace during the CFD simulations was simulated as vertical with gravity applied in the direction of flow. The distance between the water-cooled injection and collection probe was fixed at 400 (mm). The Black arrows on the inlet boundaries indicate the secondary surrounding nitrogen gas supplied into the DTF furnace and the red arrow indicates the carrier nitrogen gas injected into the DTF furnace.

5.3.2. Mesh

To solve the CFD equations throughout the domain, it was necessary to divide the geometry into very small interlinked cells called a mesh. The mesh was created in the Ansys Mesh working directory file obtained in the Ansys Workbench folder. The global mesh was created through the patch conforming method producing a tetrahedral mesh with

a locally defined boundary layer on the DTF walls. The mesh of the complete DTF furnace created in Ansys Fluent is shown on the right of Figure 5-6 below:

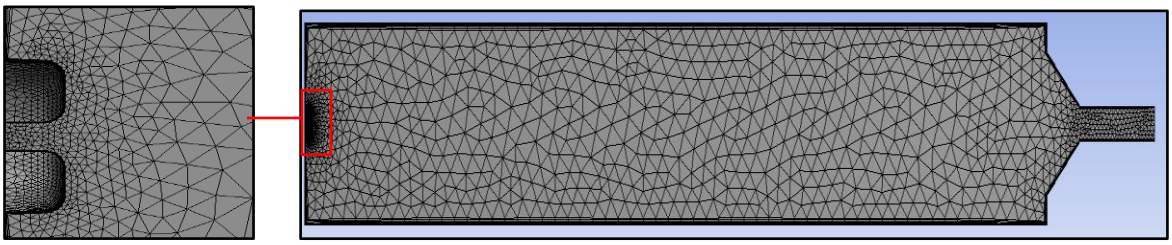


Figure 5-6: (Left) - Expanded view of mesh at the injector inlet. (Right) – Mesh of the complete DTF furnace

Only the devolatilization stage of the combustion process was solved in this instance which resulted in less computational time required to reach convergence when compared to a complete combustion simulation. The mesh created consisted of 84626 cells with a minimum orthogonal quality of 0.3066. The minimum value for orthogonal quality is important and should not fall below 0.05. The minimum orthogonal quality for this mesh was, therefore, acceptable. The locally defined inflation layer at the furnace walls consisted of 5 layers with a growth rate specified at 1.2. The global sizing selection used an advanced sizing function on proximity a curvature with a fine relevance centre specified. The maximum face size was determined at 1.345e-02 (m). The picture on the left in Figure 5-6 shows an expanded view of the injection probe inlet boundary to illustrate the increased amount of cells created with the proximity and curvature function selected in the global mesh setting.

5.3.3. CFD Simulation Model Setup

After the mesh was created in Ansys Workbench the mesh was imported into Ansys Fluent with the model setup as follow: The pressure-based solver was selected with steady state operating conditions defined. Turbulence was accounted for through the standard k-epsilon turbulence model with standard near-wall treatment specified. To solve the gas phase devolatilization stage of the combustion process the species transport model has been used with finite-rate/eddy-dissipation turbulence-chemistry interaction. Radiation was accounted for through the DO method and the absorptivity of the gas phase was described through the WSGGM – domain based model.

The specified boundary conditions are shown in Table 5-1 below.

Table 5-1: Devolatilization CFD model input boundary conditions

Boundary Condition	Unit	Value
Injection Probe Velocity Inlet		
Velocity Magnitude	(m/s)	1.59
Turbulent Intensity	%	5
Hydraulic Diameter	(m)	0.002
Temperature	(K)	298.15
Nitrogen Concentration	(%)	100
Secondary Surrounding Gas Velocity Inlet		
Velocity Magnitude	(m/s)	1.9
Turbulent Intensity	%	5
Hydraulic Diameter	(m)	0.06
Temperature	(K)	1443
Nitrogen Concentration	%	100
Collection Probe Pressure Outlet		
Gauge Pressure	(pa)	0
Turbulent Intensity	%	5
Hydraulic Diameter	(m)	0.012
Backflow Total Temperature	(K)	1400
DTF Furnace Wall		
Temperature	(K)	UDF
Internal Emissivity		0.8
Injector / Collector Wall		
Temperature	(K)	298.15
Internal Emissivity		0.8
PF Injection		
Diameter	(m)	9.00E-05
Temperature	(K)	298.15
Velocity Magnitude	(m/s)	1.59
Total Flow Rate	(kg/s)	1.96E-05

A separately defined surface injection was created to inject the discrete PF particles into the furnace. The PF was released from the injection probe inlet boundary. The Ansys Fluent solver solves two modules during the iterative process. The first module solves the gas flow through the domain in an Eulerian framework whereas a second module solves the discrete PF particles in a Lagrangian framework.

The bulk of the particle diameters in the particle distribution during the DTF experiments were in the range of 90 (μm) found in Figure 4-5 from the Malvern Mastersizer results. Therefore, a uniform particle diameter of 90 (μm) was used to enable the results to be accurately compared to the PC coal lab simulations which can only simulate a uniform particle diameter during each simulation. To ensure only the devolatilization stage of the combustion process has been simulated in Ansys Fluent, custom reaction laws were specified. The reaction laws allowed for the inert heating of the particle, followed by the devolatilization of coal, followed by the inert heating of the products to be solved. The discrete random walk model was used under stochastic tracking in the turbulent dispersion tab. During the discrete phase model (DPM) iteration, 580 particles were injected into the furnace. The turbulence intensity for all inlet and outlet boundary conditions was kept at a default value of 5 (%).

5.3.4. CFD Wall Temperature User Defined Function

Although the wall temperature of the DTF during the experiments was set at 1400 (°C) a constant and uniform wall temperature of 1400 (°C) could not be achieved. The wall temperature of the DTF at the injection probe inlet was measured at 1320 (°C) and only achieved the desired set point of 1400 (°C) approximately 300 (mm) down into the furnace from the injection probe inlet. To improve the numerical model accuracy the measured wall temperature profile of the DTF at 1400 (°C) set point obtained from the DTF experiments shown in Figure 4-6 was used rather than a constant wall temperature in all subsequent numerical simulations. The non-uniform wall temperature profile was included and interpreted into Ansys Fluent by means of a wall temperature profile UDF (User Defined Function) in a C^{++} code format shown in Figure 5-7 below:

Wall_Temp_UDF@1400.c - Notepad

File Edit Format View Help

```
#include "udf.h"
#include <cmath>

DEFINE_PROFILE(Wall_Temp_Profile,thread,position)

{ real pos[ND_ND];

real z;

face_t f;

begin_f_loop(f,thread)

{

F_CENTROID(pos,f,thread);

z=pos[2];

F_PROFILE(f, thread, position) = (2208.3*pow(z,3)) - (2099.3 * pow(z,2)) + (723.63 *z) + 1592.5;

}

end_f_loop(f,thread)

}
```

Figure 5-7: C^{++} UDF Interpreted Into CFD

5.3.5. CFD Inlet Temperature Calculation

As already mentioned during the DTF experiments the high nitrogen gas velocities used to achieve the shorter residence times associated with coal devolatilization, negatively affected the gas temperature achieved at the secondary gas inlet boundary. The gas pre-heaters could not reach the 1400 (°C) preheat gas temperature set point during the devolatilization experiments. The temperatures reached during each experiment were measured at the collection probe inlet and is shown in Figure 5-8 below:

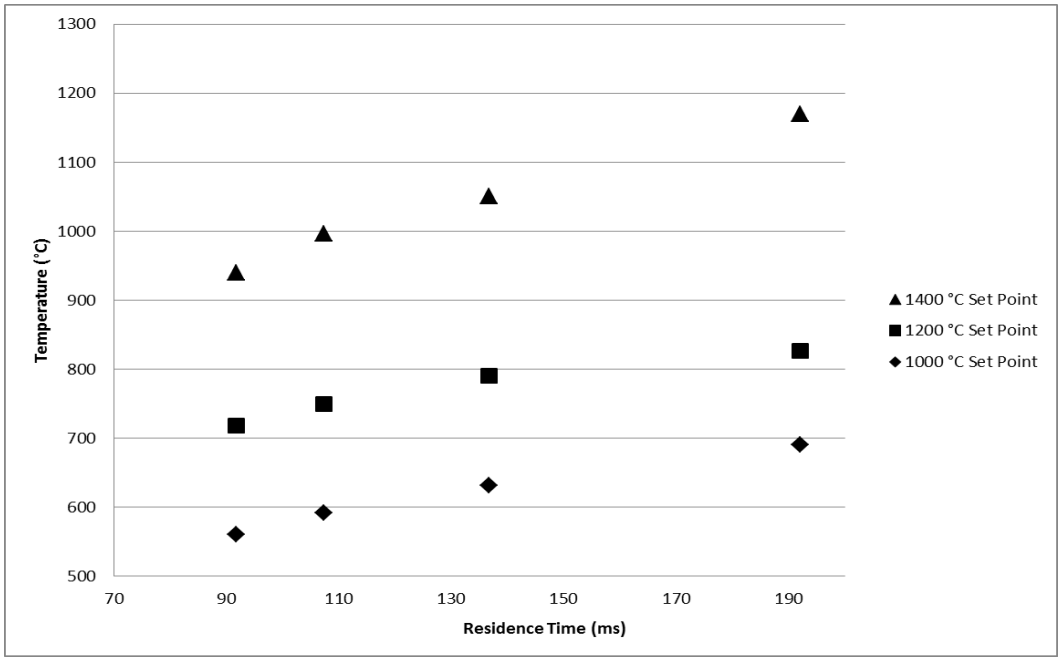


Figure 5-8: Secondary gas temperatures measured at the collection probe inlet during the experiments

These actual secondary gas temperatures measured during the experiments were used during the numerical simulations instead of the theoretical maximum set point temperatures to ensure the most accurate numerical results were obtained. From Figure 5-8 it can be seen that for the 1400 (°C) set point case the highest temperature achieved during the experiments was 1170 (°C) which was at the 192 (ms) particle residence time experimental set point.

5.4. CFD Results – Default Kinetics (Initial Run)

Because of the lack of information on the volatile yield at shorter residence time during the DTF experiments, an initial set of devolatilization kinetic parameters could not be calculated directly from the DTF experiments. Therefore, default devolatilization kinetic parameters were used in Ansys Fluent initially to produce an initial CFD result. This served as an initial CFD iteration to calculate the volatile yield, particle temperature and centreline gas temperature of the DTF at the required experimental operating conditions. The default devolatilization kinetics input into Ansys Fluent assumed a constant devolatilization rate of 50 (s^{-1}). To ensure the wall temperature UDF was correctly

interpreted into the simulation the furnace wall temperature was plotted against furnace position in Figure 5-9.

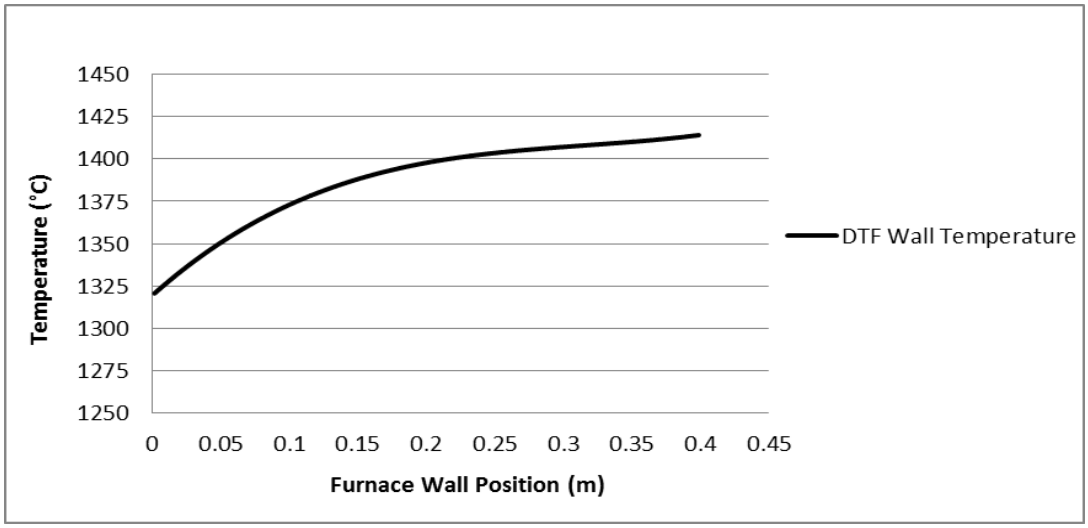


Figure 5-9: CFD Wall Temperature UDF Result

The wall temperature profile calculated in Ansys Fluent was confirmed to display the same profile measured during the DTF experiments.

The next result required from the CFD model was the centre-line gas temperature profile of the DTF furnace. The temperature contours of the complete furnace are shown in Figure 5-10 below.

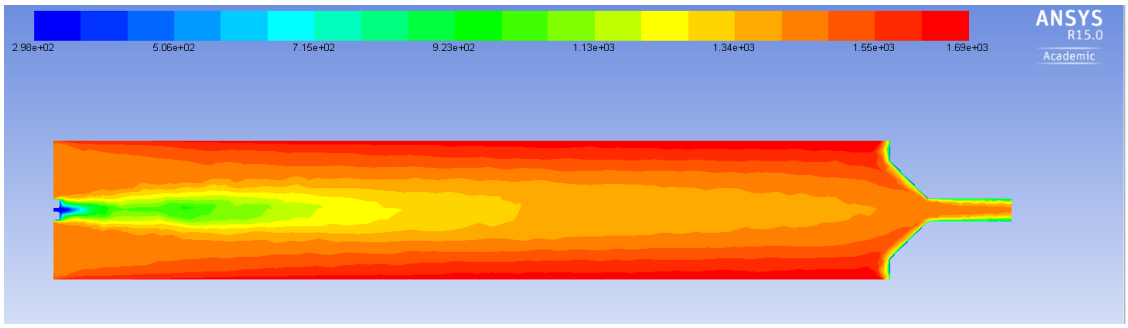


Figure 5-10: Temperature Contours (K)

From Figure 5-10 it can be seen that the centre-line temperature of the gas in the furnace increased throughout the furnace until it reached the collection probe at the bottom. The effect of the carrier inlet gas temperature being at room temperature affecting the centre-line temperature profile can also seen. The Centre line temperature of the DTF started off

at 25 (°C) which was the carrier gas inlet temperature set point and then gradually increased to a maximum temperature of 1224 (°C). This temperature correlated well with the maximum measured temperature of 1170 (°C) during the experiments at the collector probe inlet reference point. The temperature contours showed no steep increase in the location were devolatilization took place confirming that only the coal decomposition into volatiles has been simulated and not the combustion of the volatile products.

The effect of the temperature profile obtained in Figure 5-10 on the calculated CFD particle temperature is shown in Figure 5-11 below. The temperature profile through the centre-line resulted in a lower particle heating rate achieved when compared to the initial PC coal lab simulation.

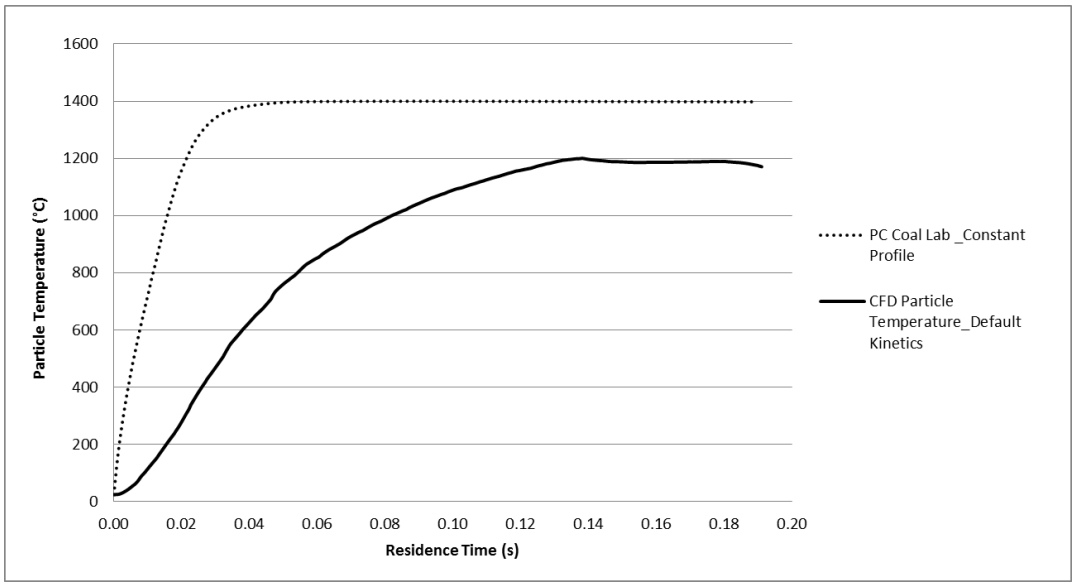


Figure 5-11: CFD particle temperature compared to PC coal lab @ 1400 (°C) - initial run

This lower particle heating rate of approximately 8600 (°C/s) achieved during the CFD simulation also greatly affected the volatile yield percentage obtained through the initial CFD simulation. The volatile yield mass fraction contours displayed in Figure 5-12 also showed that with the current models used and with the nitrogen only conditions specified the coal particles does break down into its volatile component but does not break down further into its subsequent devolatilization products (CO, CO_2, H_2O and N_2). This was because in Ansys Fluent the volatiles released from the coal particle needs to react with oxygen before it will break down into its devolatilization products and combust.

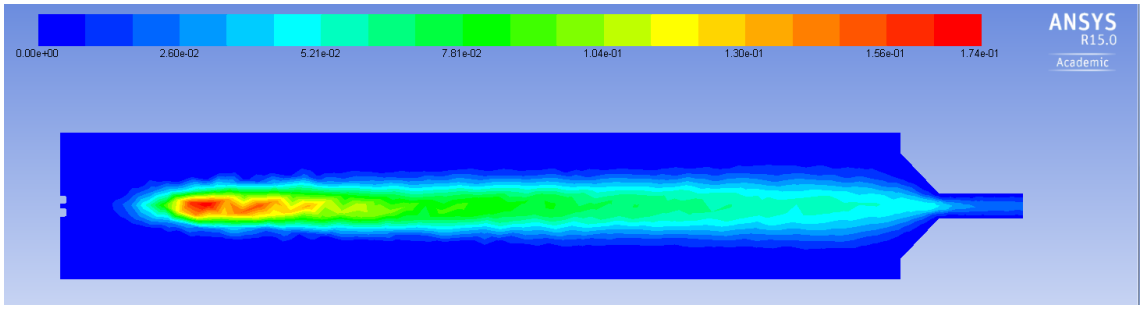


Figure 5-12: Volatile yield mass fraction contour

The volatile yield percentage obtained from the CFD simulation with default kinetics compared to the experimental results and the previous initial PC coal lab result is shown in Figure 5-13 below:

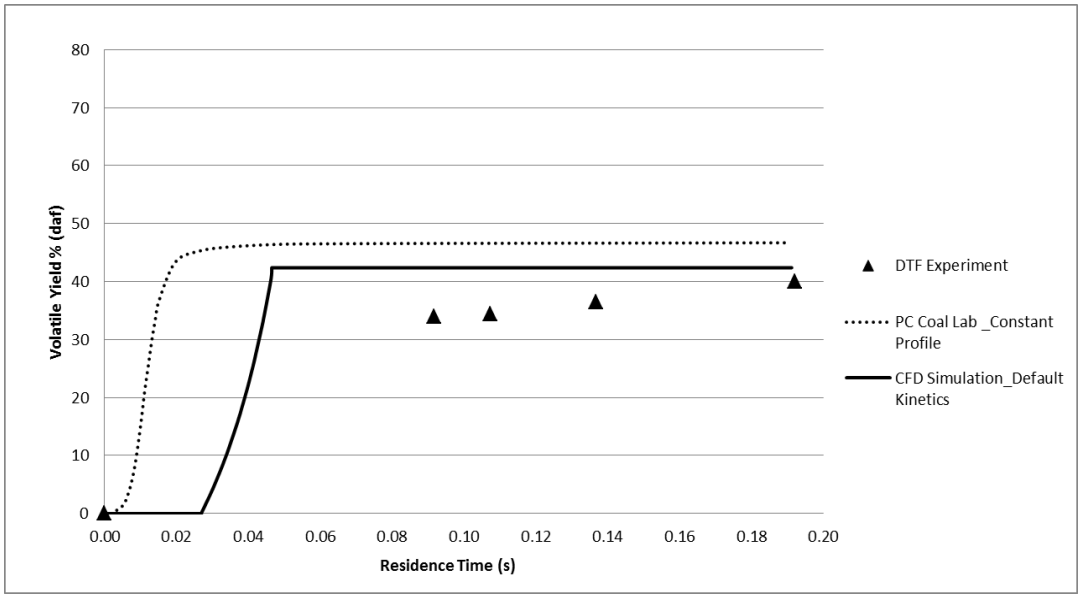


Figure 5-13: CFD volatile yield (%) result compared to PC coal lab and experimental results @ 1400 (°C) (initial run)

An ultimate volatile yield of 42.4 (%) was achieved during the default kinetics CFD simulation. The CFD predicted volatile yield even though default kinetics was used, already showed an improvement in the volatile yield percentage obtained from the initial PC coal lab simulation. This was because the CFD model used the measured wall temperature from the experiments and a more accurately defined centre-line temperature profile. These profiles related to a more accurately defined heat transfer rate to the particles. The CFD volatile yield result displayed a rather straight line during the

devolatilization process compared to the expected more curved volatile yield profile found in the literature. This straight line was a result of the constant rate kinetic model used.

After this initial CFD iteration, the next section involved a PC coal lab simulation with user defined temperature profiles defined for the centre-line gas temperature obtained from the initial CFD simulation and the DTF wall.

5.5. PC Coal Lab Simulation (Improved User Defined Profile)

The user defined wall and gas temperature profiles obtained from the initial CFD simulation were defined into PC coal lab's "DVOL.inp" file. The input profiles are shown in Figure 5-14 below:

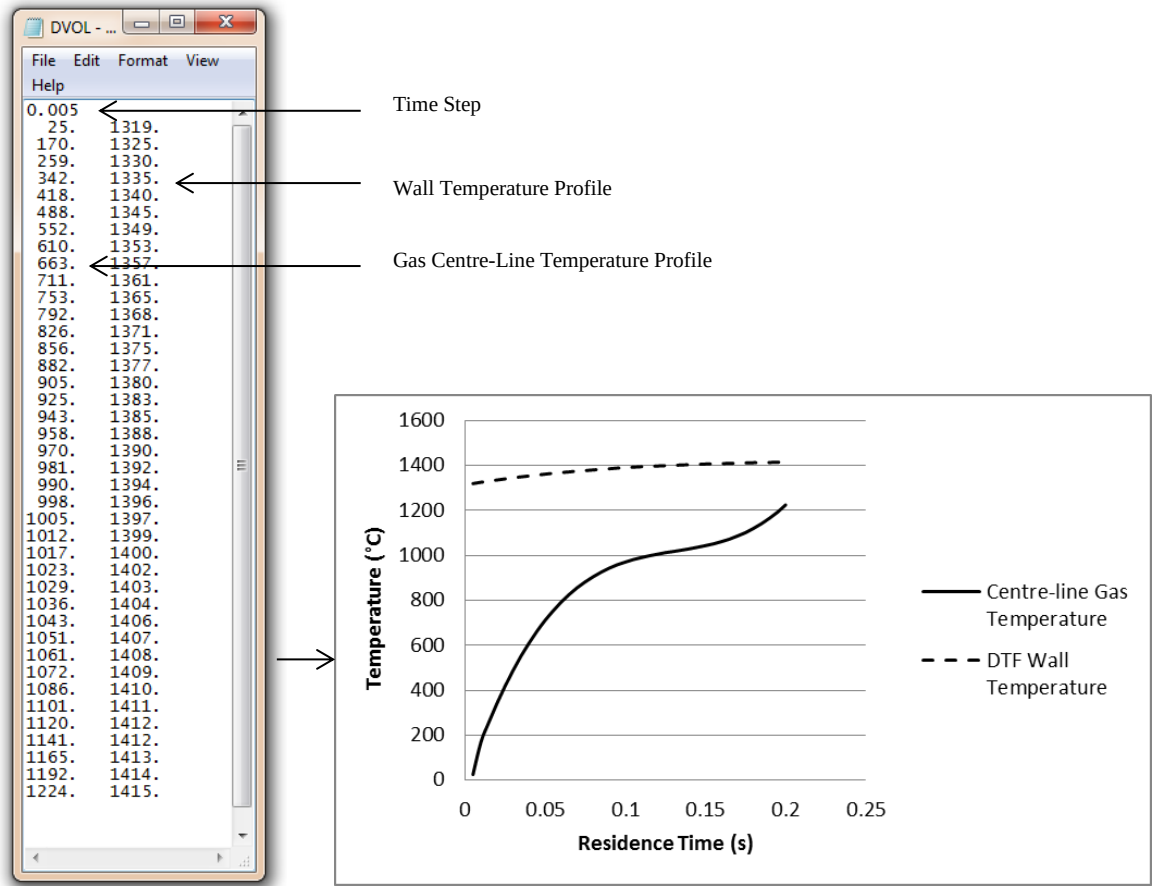


Figure 5-14: (Left) - PC coal lab user defined profiles for the DTF wall and centre-line gas temperatures - ("Dvol.inp"), (Right) – Complete profile obtained from CFD

All the other input values into PC coal lab were kept the same with only the above user defined temperature profiles incorporated into the simulation. The effect on the PC coal lab particle temperature result by defining the user defined temperature profiles for the centre-line gas obtained from CFD and furnace wall obtained from measurements are shown in Figure 5-15 below.

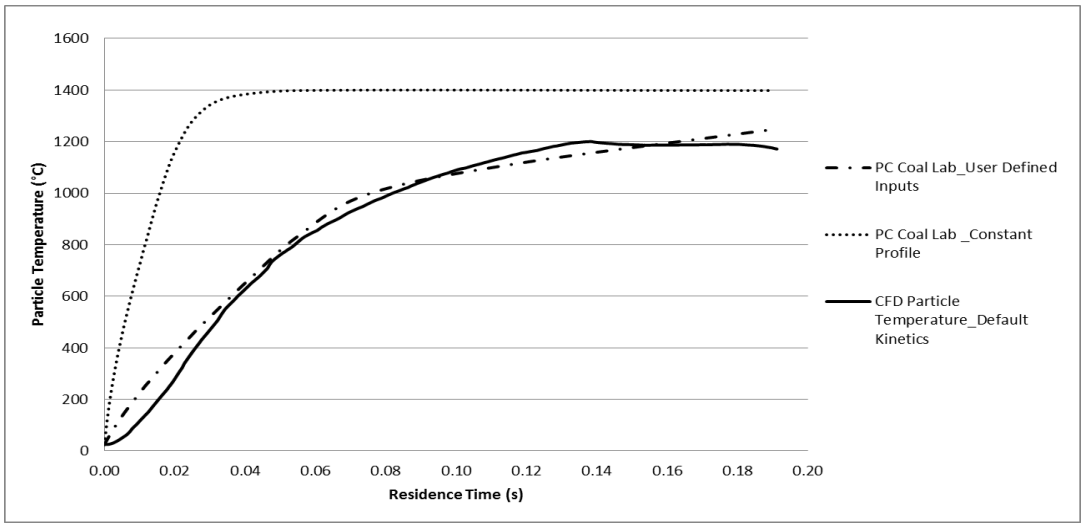


Figure 5-15: Improved PC coal lab result compared to initial PC coal lab and CFD results @ 1400 (°C) (UDF defined)

Figure 5-15 shows how the results improved by defining user-defined temperature profiles. The PC coal lab calculated particle temperature used a centre-line gas temperature profile obtained from the initial CFD simulation and therefore very closely followed the initial CFD particle temperature result in Figure 5-15. This indicated that PC coal lab and Ansys Fluent use similar heat transfer models with resulting similar results. The improved calculated particle temperature from the initial PC coal lab result also had an impact on the volatile yield result. The updated PC coal lab volatile yield result compared to the previous initial PC coal lab and CFD results are shown in Figure 5-16.

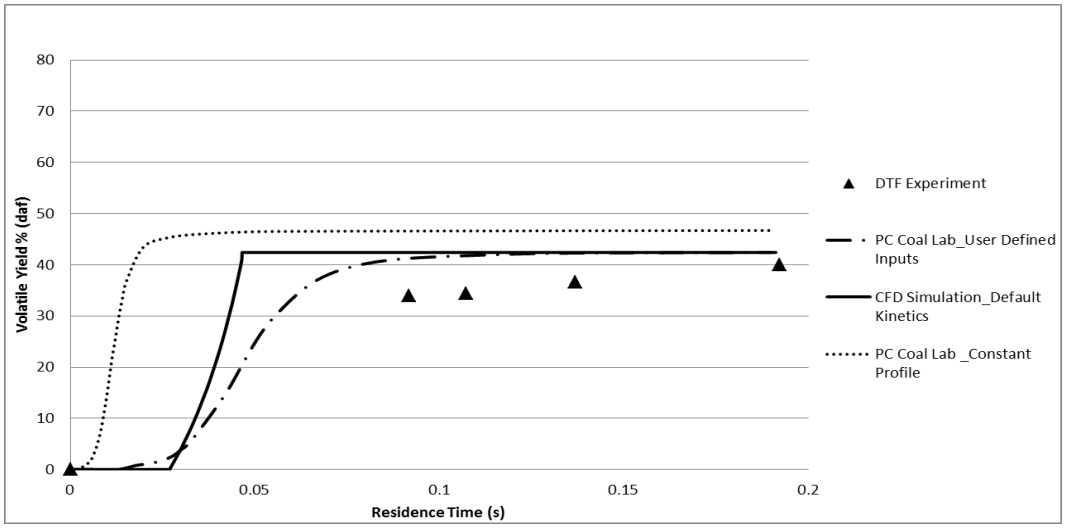


Figure 5-16: Improved PC coal lab volatile yield (%) compared to initial PC coal lab simulation, initial CFD results, and experimental results @ 1400 (°C)

The coal particles during the updated PC coal lab simulation started to release the volatiles very closely to where the initial CFD simulation predicted. Because the initial CFD model released its volatiles at a constant default volatile release rate of 50 (s^{-1}), a discrepancy existed between the CFD and PC coal lab curve shapes. The 50 (s^{-1}) can be calculated from the graph by taking the inverse of the time difference between the time to reach ultimate volatile yield and the time at the onset of devolatilization. The PC coal lab result after specifying user-defined temperature values into the "DVOL.inp" file showed an improvement on the volatile yield result. From this improved PC coal lab result an initial set of single rate devolatilization kinetic parameters were calculated and specified into CFD to improve on the initial CFD result.

The single rate devolatilization kinetics calculated through PC coal lab is shown in Figure 5-17.

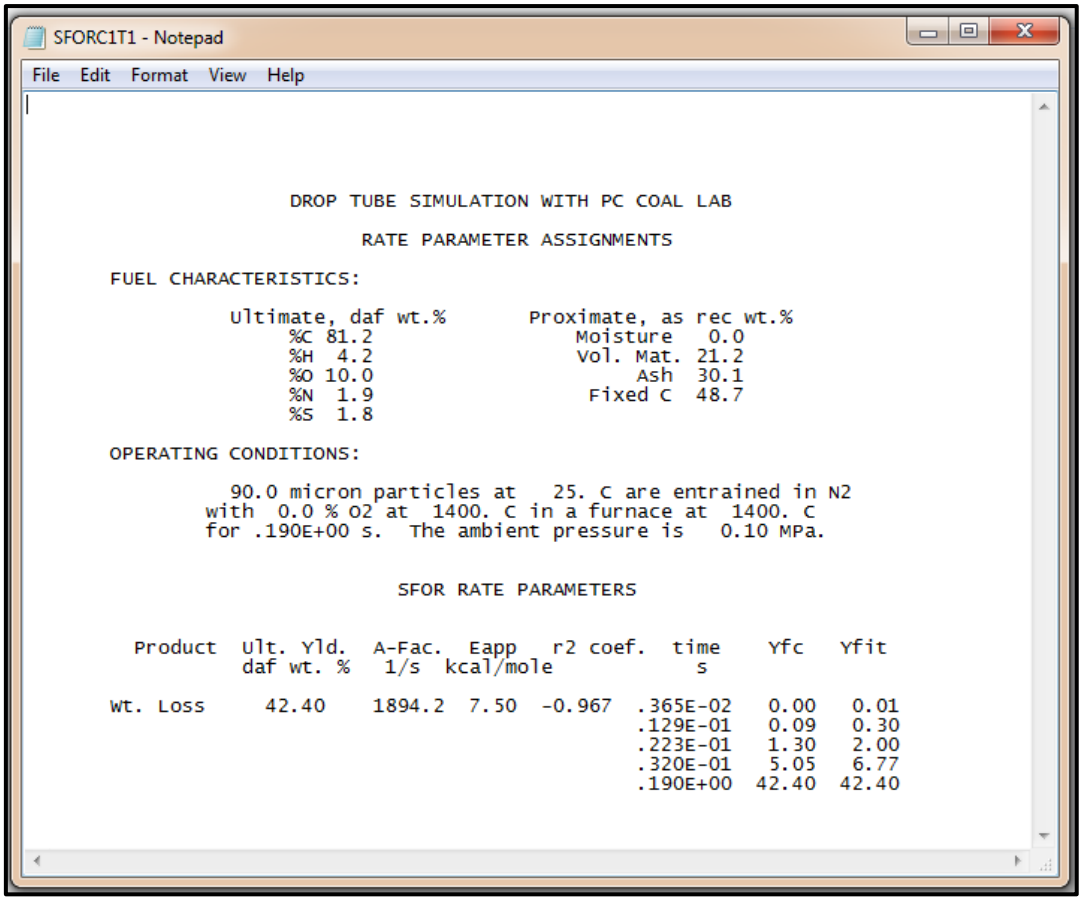


Figure 5-17: PC coal lab single rate parameters

To verify the PC coal lab single rate kinetic parameters results a manual calculation was done.

The Arrhenius equation was solved by producing an Arrhenius plot shown in Figure 5-18. The data required to be able to perform the plot are shown in table Appendix E.

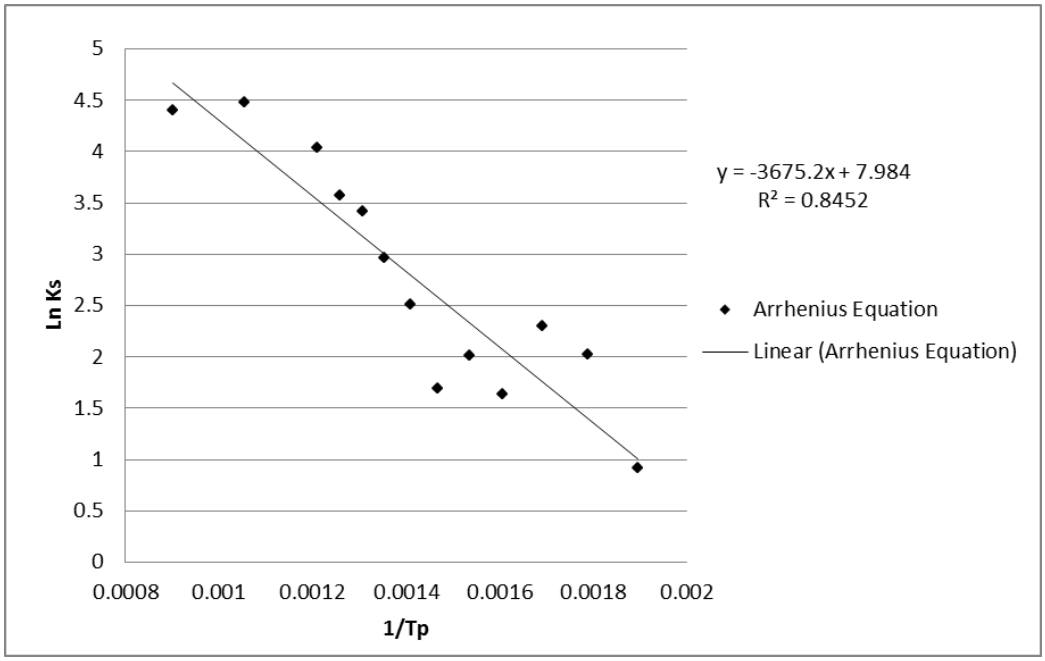


Figure 5-18: Arrhenius plot

The calculated Arrhenius single rate parameters are shown in Table 5-2 below.

Table 5-2: Single rate kinetic parameters

Paramter	Value
Ea / R	3675
R (J / mol-K)	8.31
Ea (J/mol)	30557
Ea (kJ/mol)	31
Ea (J/Kmol)	30557311
ln A	8
A(1/s)	2934

A comparison between the PC coal lab calculated kinetic parameters and the manual calculation of the kinetic parameters are shown in Table 5-3 below. Units displayed are the same units that were required for the CFD input.

Table 5-3: Single rate kinetic parameters comparison

	PC Coal Lab	Manual Calculation	Difference
Activation Energy Ea (J/Kmol)	3.14E+07	3.06E+07	0.08E+07
Frequency Factor A (1/s)	1.89E+03	2.93E+03	-1.04E+03

The manual calculation compared well with the PC coal lab result. The PC coal lab calculated single rate kinetic parameters shown in Table 5-3 were used in the updated kinetics CFD simulation.

5.6. CFD Results – Updated Kinetics

To further improve on the coal devolatilization numerical simulations the previously calculated set of single rate kinetic parameters calculated from PC coal lab were inserted back into the initial CFD simulation. This was done to improve on the default volatile release rate of 50 (s^{-1}) used during the initial CFD simulation. All other specified boundary conditions were kept the same with only the calculated single rate devolatilization kinetics specified. The newly developed volatile yield mass fraction contour plot is shown in Figure 5-19 below.

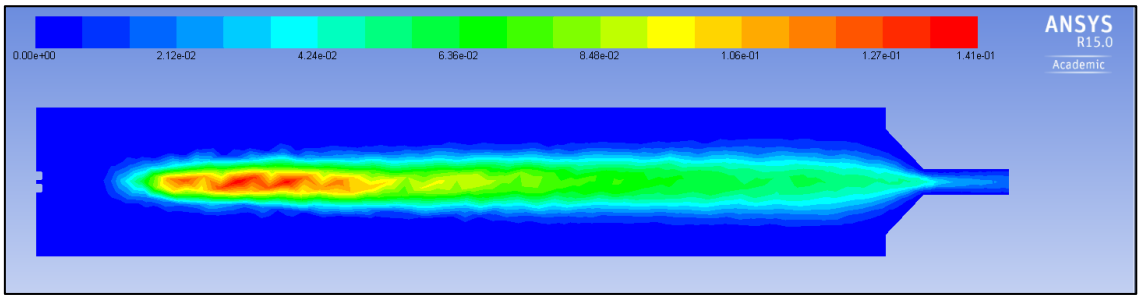


Figure 5-19: Updated volatile yield mass fraction contour @ 1400 (°C)

The volatile yield contour plot, when compared to the initial result, showed a different volatile release profile. The mass fraction of volatile's released shifted further down into the furnace indicating that the volatiles were released at a slower rate compared to the default kinetics simulation. The effect on the volatile yield result when specifying single

rate kinetics as compared to the initial constant rate default kinetics input are shown in Figure 5-20 below:

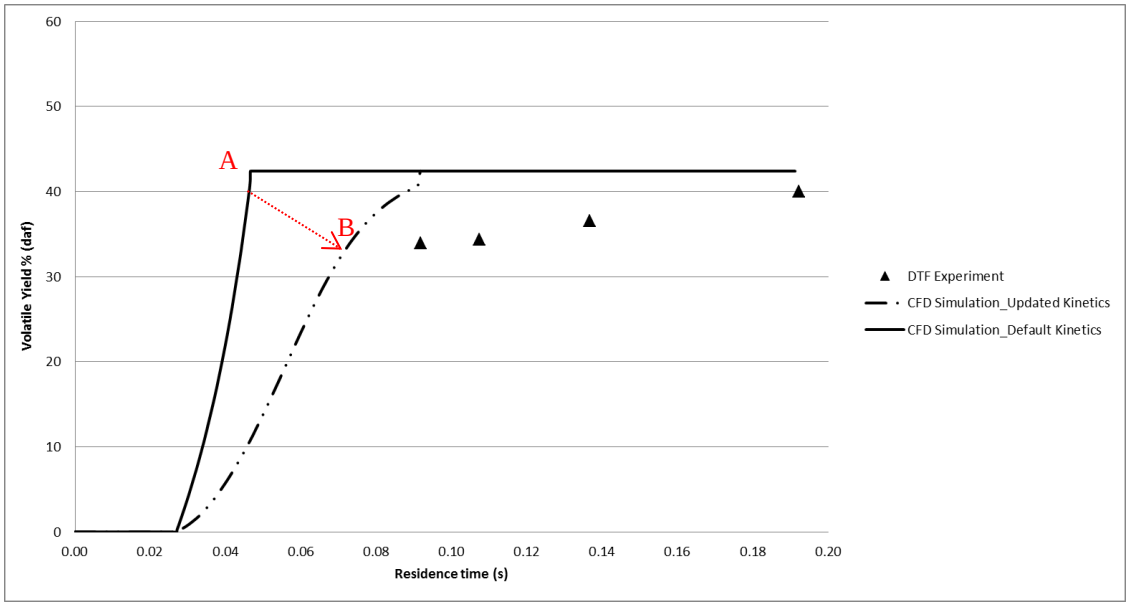


Figure 5-20: Single rate kinetics CFD volatile yield (%) compared to default kinetics CFD volatile yield (%) @ 1400 (°C)

By using the updated calculated kinetics from PC coal lab there was a definite improvement on the CFD results. The volatile yield rate improved from point "A" to point "B" indicated in Figure 5-20. The curve with the single rate kinetics specified into CFD resembled a volatile yield curve similar to what was expected from literature. The CFD simulation still slightly over predicted the volatile yield obtained during the experiments. This could be because of the uniform 90 (μm) in diameter particle used during the numerical simulations compared to the complete particle diameter distribution used during the DTF experiments. The possibility also existed that the measurements during the DTF experiments were not 100 (%) accurate with a certain experimental error percentage involved.

The slower volatile release rate within the furnace affected the centre-line gas temperature profile which in turn affected the PC coal lab simulation results. This improved CFD centre-line gas temperature profile was defined back into PC coal lab to calculate a final set of devolatilization kinetics.

5.7. PC Coal Lab Simulation (Final Kinetics Calculation)

The final Devol.inp file obtained from the updated kinetics CFD simulation together with all the relevant PC coal lab results can be seen in Appendix F.

Figure 5-21 below shows the development of the PC coal lab results compared to the DTF experiments. Figure 5-21 demonstrates how the devolatilization results continuously improved throughout the numerical development.

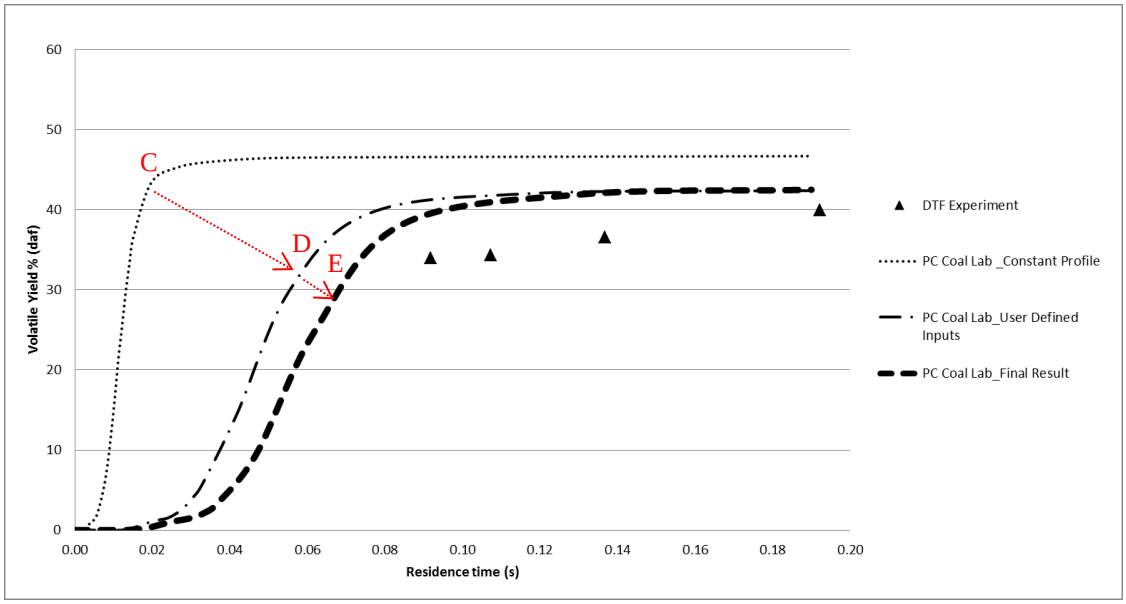


Figure 5-21: Complete development of the numerical volatile yield (%) results compared to experimental result @ 1400 (°C)

Point "C" in Figure 5-21 indicates the initial PC coal lab devolatilization result. After this initial result point "D" indicates the improved PC coal lab devolatilization result with an user defined DTF wall temperature and centre-line gas temperature obtained from the initial CFD simulation defined as a user defined input. Point "E" shows the final most accurate PC coal lab result with an user defined centre-line gas temperature profile defined obtained from the improved CFD simulation with updated devolatilization kinetics. From this final PC coal lab result a final set of single rate devolatilization kinetic parameters was calculated and used in the single burner CFD model described in chapter 8. The final calculated single rate devolatilization kinetic parameters are shown in Table 5-4 below. Additional iterations were not required as the results after the above mentioned iterations did not change significantly from the final result shown.

Kinetic Parameter	Value
Ea (J/Kmol)	3.06E+07
A (1/s)	1.53E+03

Table 5-4: Final single rate kinetic parameters

5.8. Devolatilization Numerical Analysis Discussion

PC coal lab was used to calculate the single rate devolatilization kinetic parameters required for combustion CFD simulations. The complete numerical process of iterating between PC coal lab and CFD before the final set of single rate devolatilization kinetic parameters could be calculated was shown. A comprehensive study has been done on how the PC coal lab results improved with more accurately defined user temperature input profiles. An ultimate volatile yield value of 42.7 (%) was achieved during the final PC coal lab result. This value compared well to the 40.36 (%) achieved during the DTF experiments.

The continuous improvement in the volatile yield prediction showed the importance CFD had in obtaining a final set of kinetic parameters by means of numerical simulation. The final PC coal result showed a significant improvement when compared to the initial PC coal lab and experimental results. The reason for the slight over-prediction during the final numerical result could be because of the uniform particle diameter used in the numerical process compared to the particle distribution used during the experiments. Another reason could also be an experimental error percentage involved with the experimental result obtaining lower than actual values.

Chapter 6: CHAR BURNOUT DTF EXPERIMENTS

6.1. Introduction

Following the coal devolatilization experiments, the second part of the drop tube furnace experiments included the heterogeneous char burnout phase of the combustion process. The objective of the experiments was to obtain char burnout rates for the specific coal at different particle heating rates and varying residence times. Unlike the devolatilization stage of coal combustion where below 200 milliseconds at 1400 (°C) were required to obtain a complete volatile yield curve, the subsequent char burnout phase of the combustion process required much longer residence times and, therefore, a different experimental approach was used. The char burnout percentages were obtained at three different heating rates.

6.2. Char Burnout Procedure

The experiments made use of a pre-mixed gas stream of oxygen and nitrogen within the combustion furnace. The pre-mixed gas stream consisted of a 3 % (by volume) oxygen and 97 (%) nitrogen concentration. A 3 % (by volume) oxygen concentration was used to create an oxygen environment approximately what is achieved in practice. Three different heating rates were used with temperature set points at 1000, 1200 and 1400 (°C) and particle residence times ranging from 0.9 to 3 (s) respectively.

The primary gas flow was maintained between 0.25 - 0.3 (NL/min) with an average particle feeding rate via the mechanical feeder of 1.9E-06 (kg/s). The different particle residence times were achieved by keeping the secondary gas flow constant at 20 (NL/min) and varying the bottom collector probe's position through 52, 92 and 132 (cm) from the injection probe. The combustion products after each experiment were sealed in a container and send to the coal laboratory to be analysed. The char burnout percentages at each sampling point were calculated by means of the ash tracer method.

6.3. Coal Properties & Preparation

The coal used for the char burnout experiments was the same coal that was supplied to the burner while performing the burner in-flame temperature measurements and also the same coal that was used during the devolatilization experiments.

Before the char burnout experiments could commence, the coal sample first had to be charred (Pyrolized) in a nitrogen only environment at an elevated temperature of 1400 (°C) and residence times of approximately 2 (s) to ensure the coal sample released all of its contained volatile matter.

After pyrolysis of the coal, the remaining content was sieved to a 38 – 75 (μm) particle distribution range with an average particle diameter of 47 (μm). The coal sample used during the char burnout experiments after pyrolysis proximate analysis is shown in Table 6-1 below:

Table 6-1: DTF sample proximate analysis

	Unit	Dry Basis	Dry Ash Free
Moisture	%	0.00	0.00
Volatile Matter	%	0.80	1.29
Ash	%	37.95	0.00
Fixed Carbon (By difference)	%	61.25	98.71
Total	%	100.00	100.00

The dry basis proximate analysis confirms that only 0.8 (%) volatiles remained in the sample after pyrolysis and mainly contained carbon (source intended for char burnout) and ash.

6.4. DTF Experiment Equations

The already developed DTF program was used to calculate the particle residence time and particle temperature at each sampling point. The program calculated the particle residence times by a combination of the gas and particle free-fall velocities, and the particle temperatures through a combination of the thermal properties of the gas and particles at each sampling point. The equations used to solve these two parameters are displayed below. These parameters had to be calculated to be used together with the Arrhenius equation to solve for an initial set of single rate kinetic parameters. All equations were obtained from the drop tube furnace kinetic theory manual compiled by M. Van der Riet, April 1998 [58].

6.4.1. Calculation of particle temperature (Tp):

The particle surface temperature at each probe position was calculated through an equilibrium heat balance were the heat gain by the particle equals the heat loss:

$$(\boldsymbol{H_g}) = (\boldsymbol{H_l}) \qquad (6.1)$$

H_g - Heat gained ($J.m^{-2}.s^{-1}$)

H_l - Heat Lost ($J.m^{-2}.s^{-1}$)

The heat gained by the combusting coal particle was calculated as follow:

$$\boldsymbol{H_g} = \mathbf{9791} * \boldsymbol{q} \qquad (6.2)$$

q - Rate of Carbon removal per unit surface area ($g.m^{-2}.s^{-1}$)

9797 - Enthalpy oxidation of Carbon @ 1800 (K) (J/g)

The rate of carbon removal per unit surface area was calculated as follow:

$$\boldsymbol{q} = \frac{\mathbf{3}\,(\mathbf{1}-\boldsymbol{U}^{\mathbf{0.33}})}{\boldsymbol{So}*\boldsymbol{t}} \tag{6.3}$$

U - Unburnt fraction (1 – B)

B - Fractional burn-off

S_o - Initial surface area ($m^2.g^{-1}$)

t - Residence time (s)

With the initial surface area given as:

$$\boldsymbol{S_o} = \frac{\boldsymbol{6}*\boldsymbol{U}}{\boldsymbol{X}*\boldsymbol{P_c}} \tag{6.4}$$

X - Particle diameter (m)

P_c - Particle density ($g.m^{-3}$)

And the heat loss of the combusting particle by:

$$\boldsymbol{H_l} = \boldsymbol{H_c} + \boldsymbol{H_r} \tag{6.5}$$

H_c - *Heat gained by conduction ($J.m^{-2}.s^{-1}$)*

H_r - *Heat gained by radiation ($J.m^{-2}.s^{-1}$)*

Heat gained by conduction:

$$\boldsymbol{H_c} = \frac{\mathbf{2}*\boldsymbol{\lambda}\,(\boldsymbol{Tp}-\boldsymbol{Tb})}{\boldsymbol{D}} \tag{6.6}$$

λ - *Thermal conductivity of reactant gas ($J.m^{-1}.s^{-1}.K^{-1}$)*

T_p - *Particle surface temperature (K)*

T_b - *Local bulk gas temperature (K)*

D - *Particle diameter (m)*

Heat gained by radiation:

$$\boldsymbol{H_r = \varepsilon_s * \sigma\,(Tp^4 - Tw^4)} \quad (6.7)$$

ε_s - *Emissivity of surface*

σ - *Stefan-Boltzmann constant*

T_w - *Local DTF wall temperature (K)*

Thus the particle temperature at equilibrium was calculated as follow:

$$\boldsymbol{9791 * q - \frac{2*\lambda\,(Tp-Tg)}{X} - \varepsilon * \sigma\,(Tp^4 - Tw^4) = 0} \quad (6.8)$$

x - *Mean particle diameter of coal fired (m)*

The equation was solved iteratively to find T_p at each probe position and operating condition. The value of T_p at each operating condition is shown in Table 6-2.

Table 6-2: DTF calculated particle temperature and particle residence time at each operating condition

Particle Residence Time - t (s)	DTF Gas Temperature Set Point (°C)	DTF Particle Temperature - Tp (°C)
0	1000	25
2.087	1000	1005
2.999	1000	998
1.036	1200	1216
1.829	1200	1229
2.63	1200	1215
0.925	1400	1423
1.635	1400	1438
2.35	1400	1420

The particle residence time through the DTF furnace at each operating condition shown in Table 6-2 was calculated as follow:

6.4.2. Calculation particle residence time:

The residence time of the particles at each probe position was calculated as a cumulative residence time as follow:

$$\boldsymbol{t} = \boldsymbol{\Sigma}^{(l=1-n)} \left(\frac{\boldsymbol{Li}}{\boldsymbol{vg+vp}}\right) \quad (6.9)$$

t - *Particle residence time (s)*

L_i - *Length of slice (m)*

V_g - *Linear Velocity of gas ($m.s^{-1}$)*

V_p - *Free fall velocity in gas ($m.s^{-1}$)*

The length of the DTF furnace was divided into small increments with each increment considered as a slice out of the total length of the furnace.

The linear velocity of the gas was calculated by:

$$\boldsymbol{v_g = \frac{F}{R_v}} \tag{6.10}$$

F - *Volumetric flow ($m^3.s^{-1}$)*

R_v - *Reactor volume per meter ($m^3.m^{-1}$)*

Where the Volumetric Flow were calculated as:

$$\boldsymbol{F = F_0 \left(\frac{P_0}{P_1}\right)\left(\frac{T_1}{T_0}\right)} \tag{6.11}$$

F_0 - *Inlet volumetric flow ($m^3.s^{-1}$)*

P_0, T_0 - *Gas inlet pressure (atm), temperature (K)*

P_1, T_1 - *Gas outlet pressure (atm), temperature (K)*

The free fall terminal velocity of the spherical particle was calculated by:

$$\boldsymbol{vp = g * x^2 \left(\frac{\rho_p - \rho_g}{18 * \delta_g}\right)} \tag{6.12}$$

g - *Gravitational acceleration ($m.s^{-2}$)*

x - *Average particle diameter (m)*

ρ_p - *Particle Density ($kg.m^{-3}$)*

ρ_g - *Gas density ($kg.m^{-3}$)*

δ_g - *Gas Viscosity ($kg.m^{-1}.s^{-1}$)*

6.5. Measured Wall Temperature

The wall temperature profile measured from the top of the DTF furnace at the injection probe inlet expanding downward into the furnaces to the bottom collection probe measured in increments of 100 (mm) are displayed in Figure 6-1 below. These profiles were measured by a previous author with an R-type thermocouple extended through the bottom opening of the DTF furnace [26].

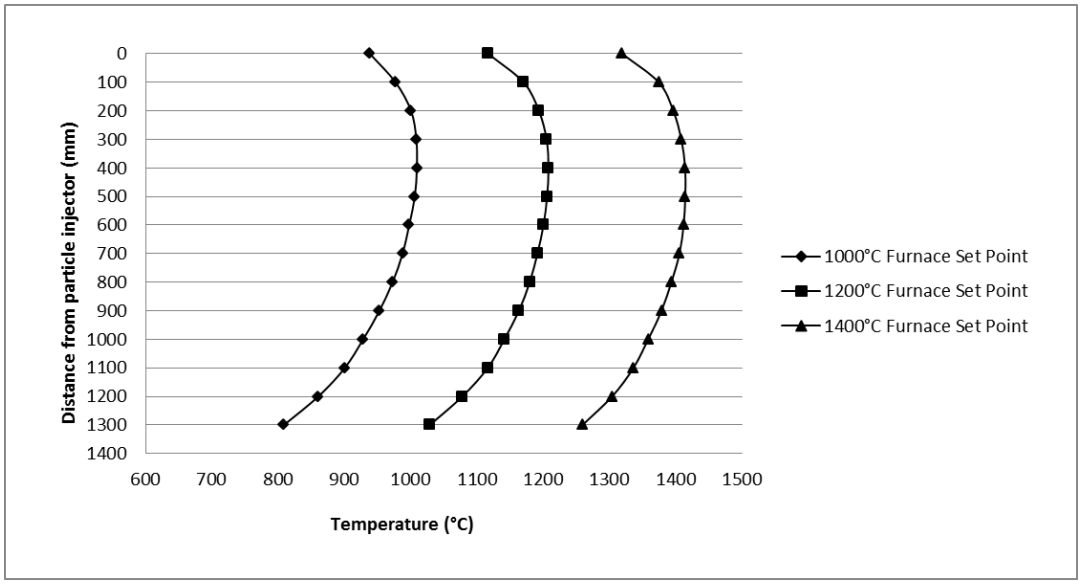


Figure 6-1: DTF char burnout experiments wall temperature profile [26]

The wall temperature only reached the target value about 300 (mm) into the furnace. The temperature then remained rather constant until it started to decay again after 800 (mm) inwards. These temperature profiles were included into the numerical simulations to ensure the most accurate results were obtained.

6.6. Char Burnout Results

The percentage ash contained in the products after each experiment are displayed in Table 6-3 below.

Table 6-3: DTF experimental results

Residence Time (s)	Temperature (°C)	Ash (%) - Dry Basis
2.087	1000	42
2.999	1000	45.5
1.036	1200	45
1.829	1200	56.7
2.63	1200	78
0.925	1400	52
1.635	1400	84.1
2.35	1400	90.7

From the dry basis ash percentages the char burnout resembling the combustion efficiency of the char particle was calculated by using the ash tracer method. The char burnout percentages are shown in Figure 6-2 below.

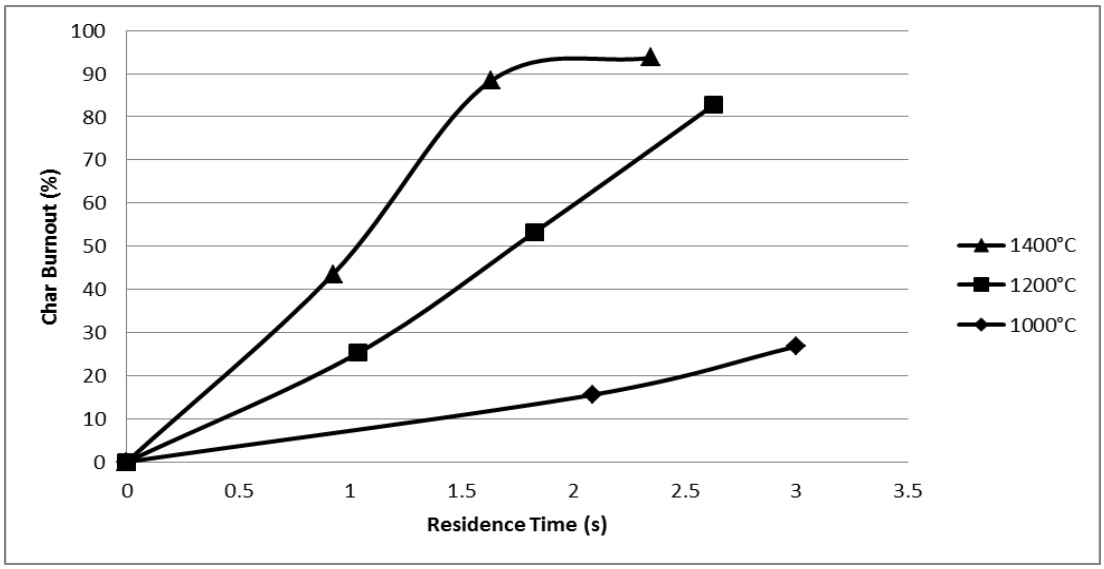


Figure 6-2: DTF experiments char burnout percentage

From Figure 6-2 it can be seen that for the 1400 (°C) set point case 94 (%) burnout was achieved. Because a complete burnout curve from the onset could be obtained using the char burnout experiments, compared to the devolatilization experiments in chapter 4 where

the shorter residence times were problematic, an initial set of single rate char burnout combustion kinetics could directly be calculated from the experimental results. The method of calculating the char single rate combustion kinetic parameters from the experimental results follows.

6.7. DTF Experiment Char Burnout Kinetics

An initial set of char single reaction kinetics was calculated by using a combination of all the experimental results ranging from 1000 (°C) through to 1400 (°C). The Arrhenius plot generated from the data obtained through the experiments are shown is Figure 6-3 below.

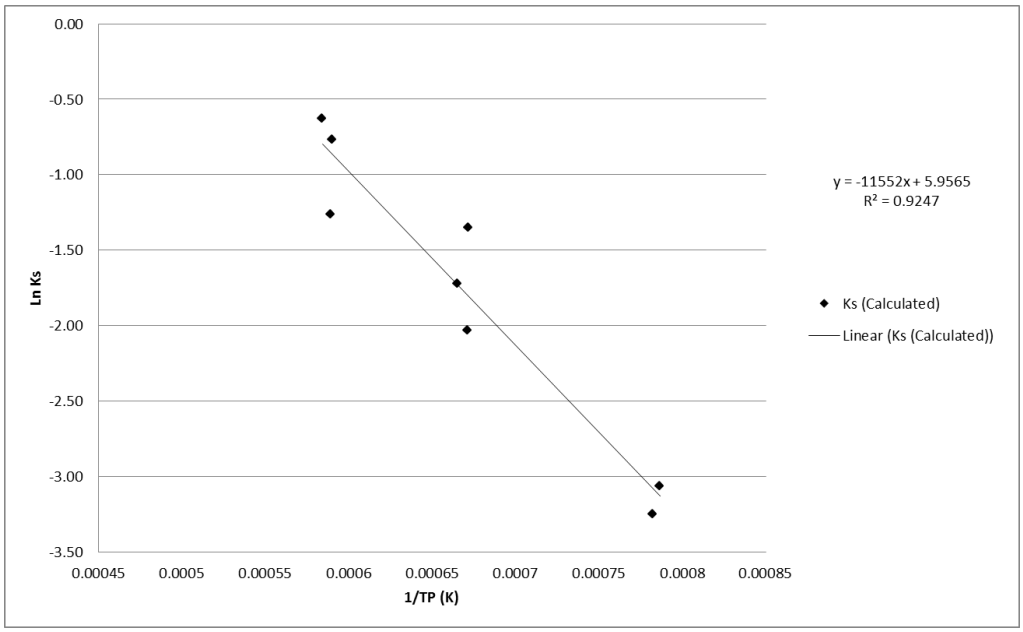


Figure 6-3: Arrhenius plot (char burnout)

The slope of the linear fitted curve was calculated as -11552 and the curve intersected the y-axis at 5.9565. From the Arrhenius equation the single rate Arrhenius reaction kinetic parameters were calculated as follow:

$$\boldsymbol{Ea = 11552 * R} \qquad (6.13)$$

R - *Universal gas constant ($J.mol^{-1}.K^{-1}$)*

E_a - *Activation Energy ($J.mol^{-1}$)*

$$\boldsymbol{LnA = 5.9565} \quad (6.14)$$

A - *Pre-exponential factor (1/s)*

The calculated Arrhenius reaction kinetic parameters calculated are shown in Table 6-4 below.

Table 6-4: Arrhenius single rate kinetic parameters

Activation Energy (J/Kmol)	9.60E+07
Frequency Factor (1/s)	3.86E+02

6.8. DTF Char Burnout Discussion

The char burnout percentages obtained through the DTF experiments were used to calculate an initial set of Arrhenius single rate char combustion kinetic parameters. The particle temperature and particle residence times required solving the Arrhenius equation was calculated by the already developed DTF program.

This calculated set of char reaction kinetics was mainly used to improve on the initial char burnout CFD simulation. The results of all subsequent char burnout DTF numerical simulations in Chapter 7: were compared to the experimental results to ensure accurate numerical results were achieved.

Chapter 7: CHAR BURNOUT DTF NUMERICAL ANALYSIS

7.1. Introduction

All numerical simulations for the char burnout phase were done for the 1400 (°C) temperature set point case. The method followed in calculating the char single rate kinetic parameters are shown in Figure 7-1. The numerical method of obtaining the char reaction kinetic parameters similar to the devolatilization simulations involved a combination of CFD and PC coal lab simulations. PC coal lab which was used to calculate the char kinetic parameters required user defined temperature profiles. This temperature profiles again similar to the devolatilization experiments included a DTF furnace wall temperature profile obtained through measurements and a centre-line gas temperature profile obtained from CFD simulations. For the char burnout simulations however, an additional user defined input was required for the centre-line oxygen concentration which was not required during the devolatilization experiments. Furthermore different from the devolatilization simulations, less iteration was necessary between CFD and PC coal lab to reach a final set of kinetic parameters. The longer residence times associated with char burnout as oppose to the short residence times during devolatilization was well within the DTF capability and therefore, a complete char burnout curve could be obtained during the experiments. This experimental char burnout curve was then used to calculate an initial set of char kinetic parameters directly from the experiments to be used in the initial CFD simulation.

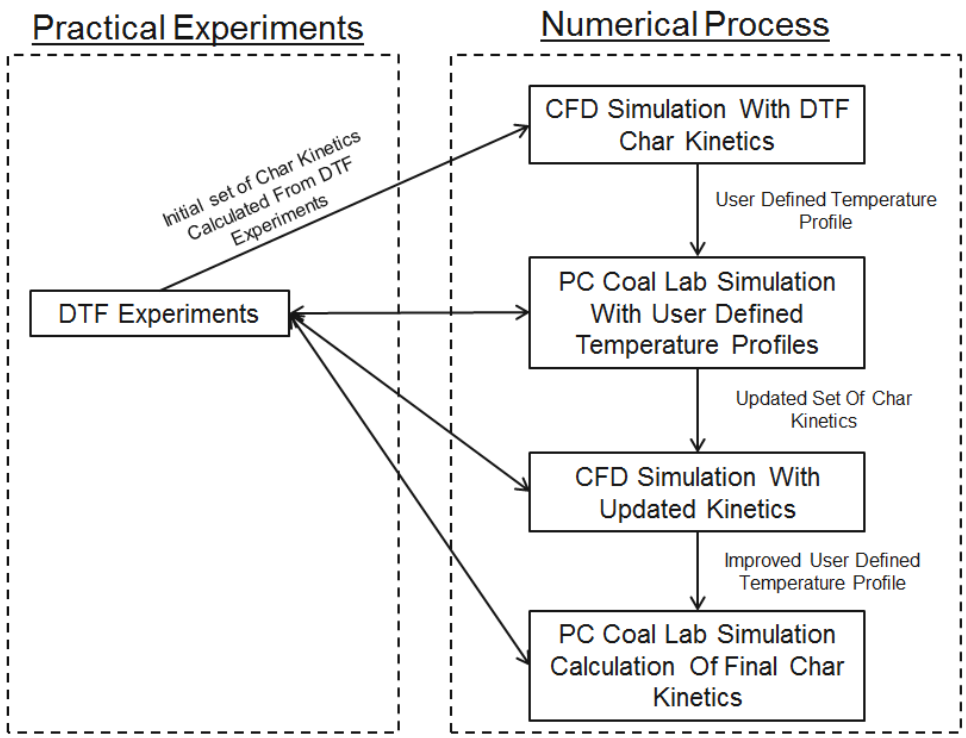


Figure 7-1: Numerical calculation of char reaction kinetics method followed

The initial CFD simulation, in turn, was then used to calculate user defined input profiles for the centre-line gas temperature and centre-line oxygen concentration which was required for the PC coal lab simulations. This PC coal lab simulation was then used to calculate an improved updated set of char reaction kinetic parameters to improve on the initial CFD simulation results for the centre-line gas temperature and centre-line oxygen concentration. Finally, the improved user-defined profiles were used in PC coal lab to calculate a final set of char reaction kinetic parameters.

Although an initial PC coal lab simulation without user-defined profiles and a CFD simulation with default Ansys Fluent kinetics were not required in the method followed it was still included in the development to show the results step by step from the initial most basic type of simulation through to the final most accurately obtained result.

7.2. PC Coal Lab Char Burnout Simulation – Initial Run

This basic initial PC coal lab simulation only required the proximate and ultimate analysis of the coal and constant values for the DTF operating conditions in terms of temperature, oxygen concentration, reactor pressure, particle residence time, and particle diameter. The input files for the initial case are shown in Figure 7-2 and Figure 7-3 below.

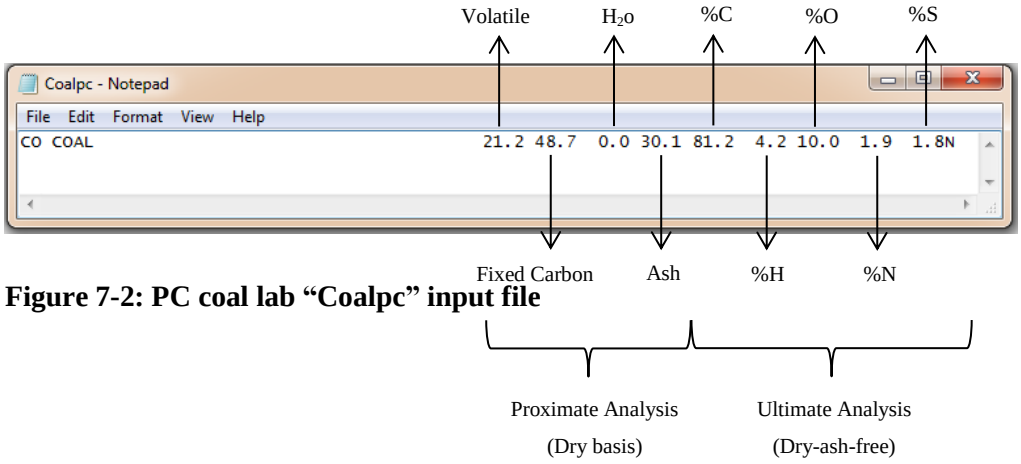


Figure 7-2: PC coal lab "Coalpc" input file

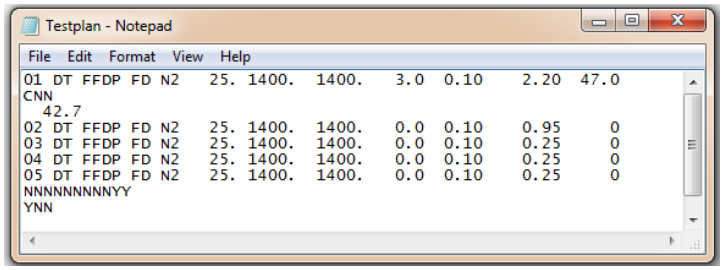


Figure 7-3: PC coal lab "Testplan" input file

Notice that a constant 3 % (by volume) oxygen concentration was used during this simulation. The addition line added after the first entry was as a result of the non-zero value specified for the inlet oxygen concentration. The three letter code (CNN) in the additional line specifies the required calculations to be performed:

- "C" indicates only char oxidation was considered with the CBK/E model.
- The first "N" indicates that uniform constant temperatures were used during this simulation. All subsequent PC coal lab simulations after this initial simulation will use a "Y" letter code for this entry specifying user-defined values in the CBKE.inp file.

- The last code letter enables a particle distribution to be specified. This feature was not yet active with version 4.2 and, therefore, specified as "N". Because only the char burnout phase was simulated the previous ultimate volatile yield value of 42.7 (daf wt. %) was also required.

The CBK/E model contains an intrinsic formulation that allows a transition phase, in which the O_2 completely penetrates the internal pore structure and both external film and intra-particle diffusion resistances are negligible. This addition is useful especially at the later stages of combustion or at lower temperatures when overall burning rates are slow and particle diameters are small. The intrinsic formulation allows more accurate extrapolation of the primary high temperature data on which CBK is based to lower temperatures. CBK/E also includes a sub model of the effect of ash on heat transfer during the late stages of combustion. Taken together, these features provide a better description of extinction phenomena during the later stages of burnout [32].

The initial simulation results of the char burnout percentage achieved are shown in Figure 7-4 below:

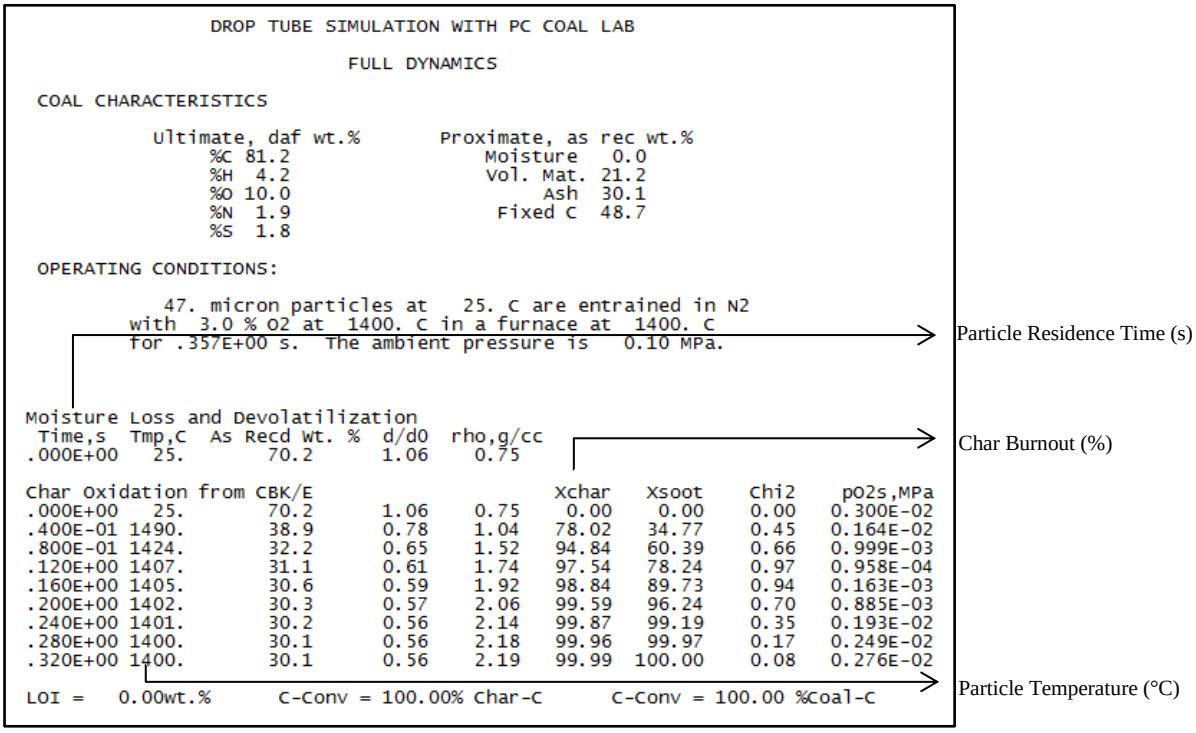


Figure 7-4: PC coal lab char burnout (%)

These results were also plotted against residence time to be able to compare to the experimental data in Figure 7-5.

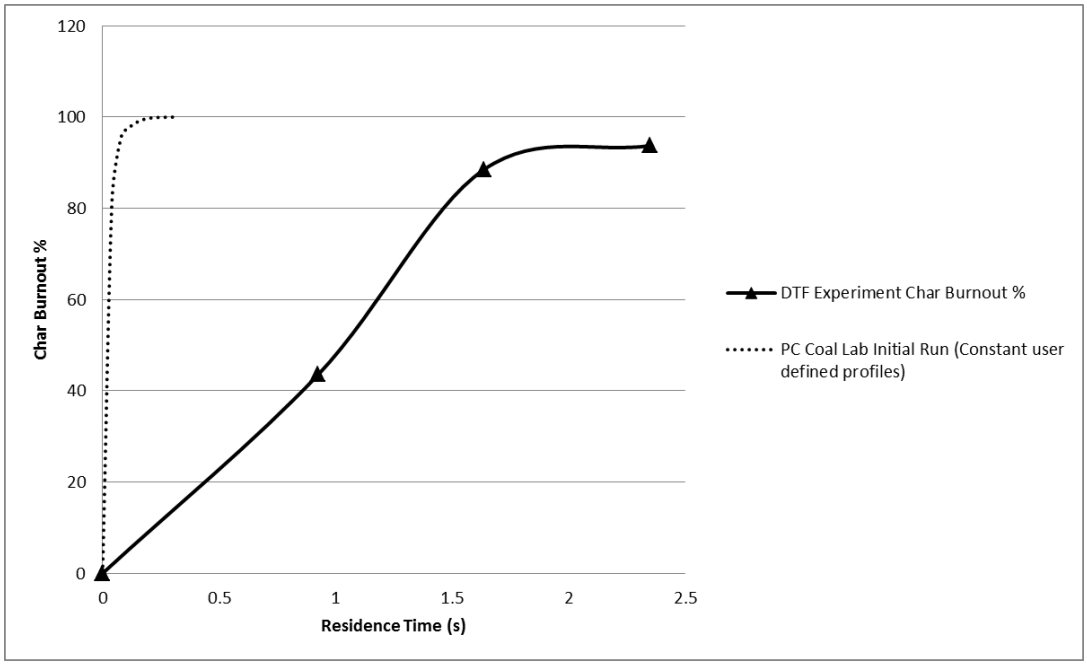


Figure 7-5: PC coal lab initial run char burnout (%) compared to experimental results @ 1400 (°C) (initial run)

The char burnout rate obtained from the initial input values showed a very prompt and unrealistic char burnout rate together with a particle heating rate of up to 35000 (°C/s). The expected particle heating rate is in the range of 10000 (°C/s); clearly an incorrect initial result was achieved. In an attempt to improve on the initial PC coal lab char burnout simulation CFD was incorporated to calculate an additional input file called "CBKE.inp". This file contained more accurately defined user input values for the wall temperature, and centre-line gas temperature profiles similar to the devolatilization simulations. The only difference was that for the char burnout simulations an additional input profile was required for the centre-line oxygen concentration.

The next section gives the techniques used in obtaining the input profiles required for the "CBK.inp" file by means of CFD.

7.3. DTF CFD Char Burnout Model

7.3.1. Geometry & Mesh

The geometry created for the char burnout numerical simulations was mainly the same as the geometry used during the devolatilization simulations with the only difference the furnace length shown on the right of Figure 7-6. The furnace length was increased from 400 (mm) to 1320 (mm). Half of the furnace was modelled around the symmetry plane. Because the char burnout process required more complex equations to be solved a much finer mesh were required to accurately solve the char burnout rate. A global mesh was created through the patch conforming method producing a tetrahedral mesh with a locally defined boundary layer on the DTF walls. After the tetrahedral mesh was created in the Ansys Mesh working directory the mesh was imported into Ansys Fluent and converted to a polyhedral mesh. This method of converting the tetrahedral mesh to polyhedral allowed the cells to be reduced from 1499563 to 425391 with an improved and acceptable orthogonal quality from 0.15 to 0.2905. The locally defined inflation layer at the furnace wall consisted of 5 layers with a growth rate specified at 1.2. An expanded view of the furnace inlet showing the polyhedral mesh created in the Ansys Fluent is shown on the left of Figure 7-6 below:

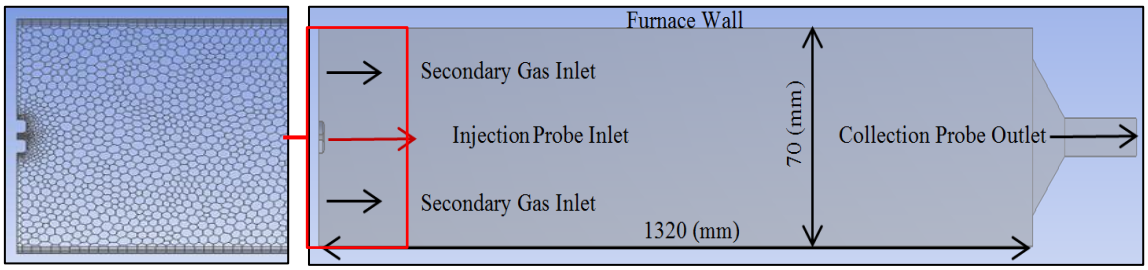


Figure 7-6: (Left) - Expanded view of injection probe inlet showing the polyhedral mesh, (Right) - DTF char burnout furnace CAD

The global sizing used an advanced size function on proximity a curvature and relevance centre set at fine. The maximum face size was additionally specified as 2.049e-03 (m). For the ease of presentation, the furnace of the DTF together with the CFD results are shown in the horizontal direction however the orientation of the DTF furnace during the CFD simulations was simulated as vertical with gravity applied in the direction of flow.

7.3.2. Model Boundary Conditions

Table 7-1: Char CFD model boundary conditions

Boundary Condition	Unit	Value
Injection Probe Mass-Flow Inlet		
Velocity Magnitude	(m/s)	1.59
Turbulent Intensity	(%)	5
Hydraulic Diameter	(m)	0.002
Temperature	(K)	298.15
Oxygen Concentration	(%)	3.4
Secondary Surrounding Gas Velocity Inlet		
Velocity Magnitude	(m/s)	0.53
Turbulent Intensity	(%)	5
Hydraulic Diameter	(m)	0.06
Temperature	(K)	1669
Oxygen Concentration (Mass Fraction)	(%)	3.4
Collection Probe Pressure Outlet		
Gauge Pressure	(pa)	0
Turbulent Intensity	(%)	5
Hydraulic Diameter	(m)	0.012
Backflow Total Temperature	(K)	1669
DTF Furnace Wall		
Temperature	(K)	UDF
Internal Emissivity		0.8
Injector / Collector Wall		
Temperature	(K)	298.15
Internal Emissivity		0.8
PF Injection		
Diameter	(m)	47E-05
Temperature	(K)	298.15
Velocity Magnitude	(m/s)	1.59
Total Flow Rate	(kg/s)	9.5E-07

7.3.3. CFD Wall Temperature User Defined Function

To improve the numerical model accuracy the wall temperature profile measured during the 1400 (°C) experiments shown in Figure 6-1 was implemented during all subsequent numerical simulations as oppose to a constant defined temperature on the wall. The wall temperature profile for the 1320 (mm) furnace length was included and interpreted into Ansys Fluent by means of a wall temperature profile UDF in C++ format shown in Figure 7-7:

Wall_Temp_UDF@1400 char - Notepad

File Edit Format View Help

```
#include "udf.h"

DEFINE_PROFILE(Wall_Temp_DTF132,thread,position)
{ real pos[ND_ND]; /* this will hold the position vector */
real z;
face_t f;
begin_f_loop(f,thread)
{
F_CENTROID(pos,f,thread);
z=pos[2];
F_PROFILE(f, thread, position) = (76.273 * pow(z,3)) - (420.58 * pow(z,2)) + (368.75 *z) + 1603.7;
}
end_f_loop(f,thread)
```

Figure 7-7: 1320 (mm) char DTF experiments furnace wall temperature UDF

The furnace wall temperature UDF interpreted into Ansys Fluent produced a wall temperature profile shown in Figure 7-8. This profile accurately followed the profile obtained during the experiments.

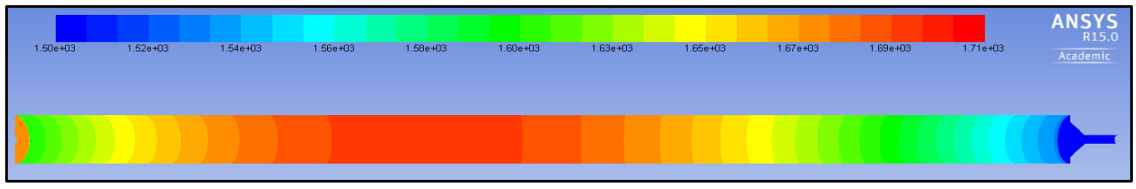


Figure 7-8: Temperature contours (K) of the furnace wall

The temperature contours on the cylindrical DTF wall display how the temperature on the furnace wall increased from the injection probe inlet until it reached the desired temperature set point of 1400 (°C) at about 300 (mm). Thereafter at about 800 (mm) the wall temperature decreases again up until the collection probe outlet.

7.4. CFD Char Burnout Results – Default Kinetics (Initial Run)

An initial CFD simulation with default kinetics specified in Ansys Fluent served as a baseline simulation to be compared to an updated kinetics simulation thereafter. The reason why this initial simulation was included in the development of the char kinetic calculations was to illustrate the effect char kinetics had on the char burnout simulations.

The default Ansys Fluent single rate Arrhenius parameters are shown in Table 7-2 below:

Table 7-2: Default single rate char combustion kinetic parameters

	Unit	Value
Activation Energy (Ea)	(J/Kmol)	7.90E+07
Frequency Factor (A)	(1/s)	2.00E-03

The CFD default kinetics char burnout rate compared to the DTF experiments are shown in Figure 7-9 below:

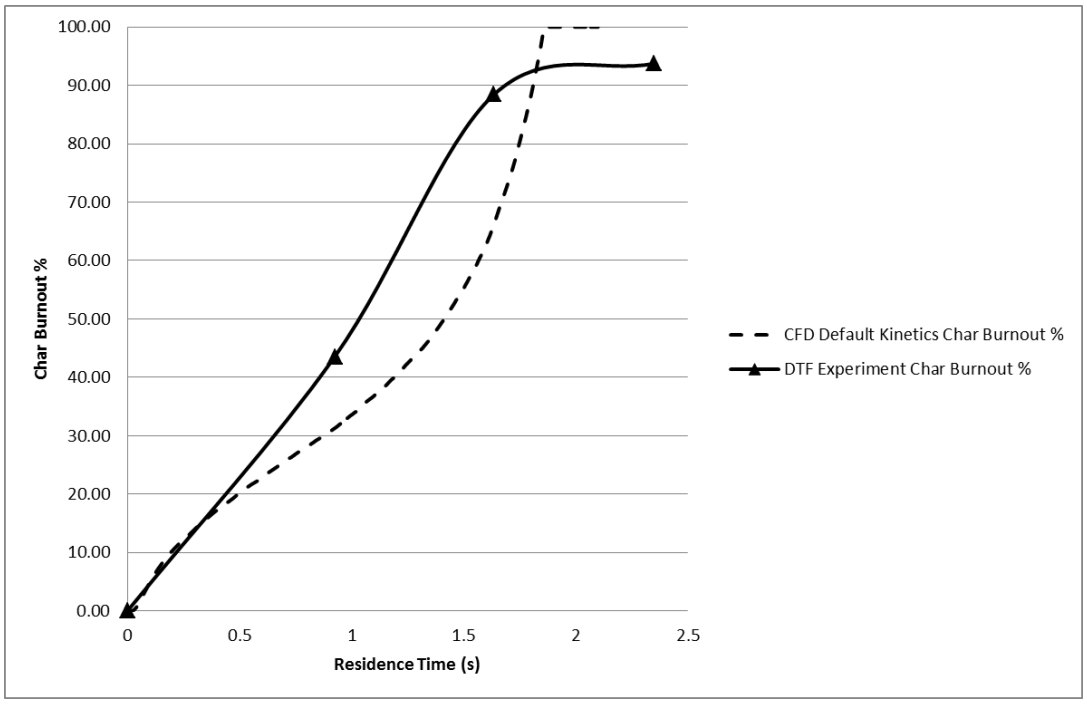


Figure 7-9: CFD initial char burnout result compared to experimental data @ 1400 (°C)

The results are shown of a single particle track of the average particle burnout rate achieved. The CFD simulation with default kinetics under predicted the char burnout percentage between 0.5 and 1.8 (s) with an achieved complete burnout time of 1.86 (s).

The oxygen concentration obtained through the DTF furnace as a result of the current burnout percentages is shown in Figure 7-10 below. A definite reducing atmosphere was created especially along the centre line of the furnace. There was a direct relationship between coal mass flow and oxygen consumption through the DTF furnace.

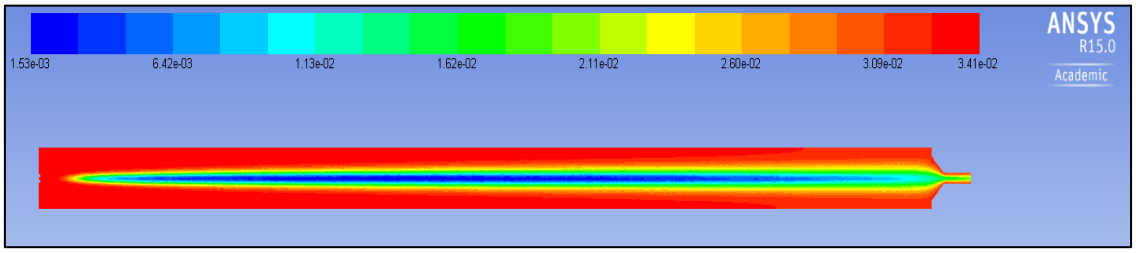


Figure 7-10: Mass fraction percentage oxygen concentration contour - default kinetics

The depletion of oxygen concentration through the centre-line was created because of the char oxidation (char combustion) reactions that took place. The char combustion reactions consumed the available oxygen through the centre-line where the particles were located.

The next section demonstrates the effect the single rate kinetic inputs calculated from DTF experiments had on the CFD char burnout results.

7.5. CFD Char Burnout Results – Updated Kinetics

All the model parameters were kept the same with only the kinetic input values updated with the values calculated from the DTF char experiments. The char burnout results by specifying updated kinetics compared to the default kinetics and experimental results are shown in Figure 7-11. The particle heating rate achieved during the updated CFD simulation was approximately 10560 (°C/s).

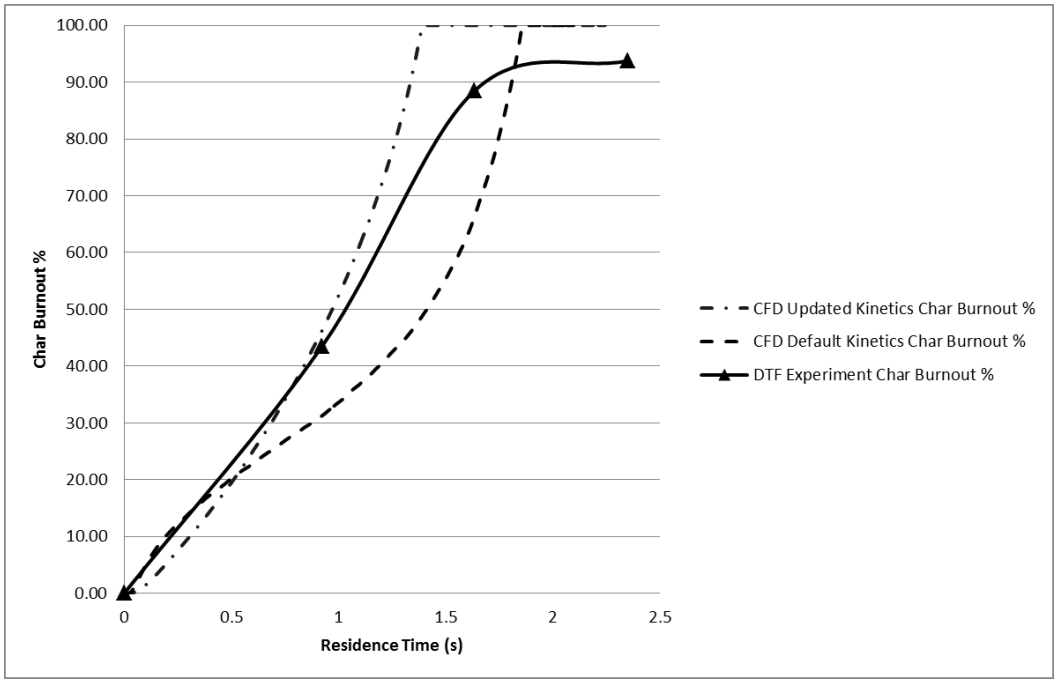


Figure 7-11: CFD char burnout (%) result with updated kinetics compared to initial CFD result, and experimental data @ 1400 (°C)

The char burnout rate increased with the updated set of kinetics compared to the initial CFD simulation. The updated kinetics simulation very closely predicted the char burnout achieved during the DTF experiments. The slight overprediction and possibly the 100 (%) burnout achieved was because of the uniform constant average particle diameter used compared to the particle distribution used during the experiments. The effect a larger uniform particle diameter has on char burnout percentage will be shown in the final PC coal lab simulation hereafter. The faster burnout rate achieved with the improved kinetics influenced the way in which the oxygen was consumed through the DTF furnace. The oxygen concentration obtained as a result of the updated kinetics simulation is shown in Figure 7-12:

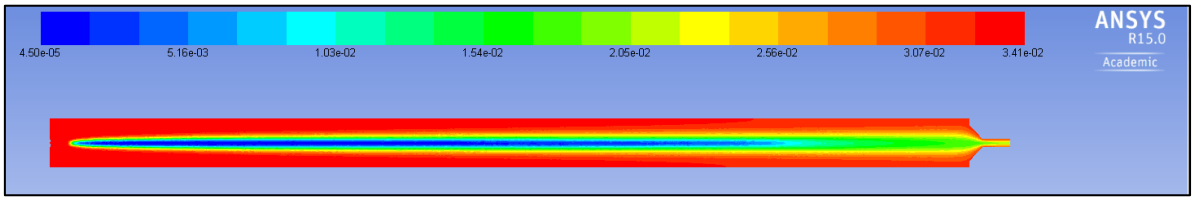


Figure 7-12: Mass fraction percentage oxygen concentration contour - updated kinetics

Because the char burnout rate increased during this simulation, the available oxygen concentration was consumed earlier in the furnace with a resulting shorter depletion zone through the centre-line compared to the default kinetics simulation. The centre-line oxygen concentration profile obtained during the updated kinetics CFD simulation was used to be specified in PC coal lab to improve on the initial PC coal lab result.

7.6. PC Coal Lab Char Burnout Simulation – User Defined Conditions

From the updated kinetics CFD simulation, the profiles shown in Figure 7-13 were obtained and defined as a "CBKE.inp" file into PC coal lab. Only the first few lines of the defined profiles into the "CBKE.inp" file are shown in Figure 7-13. The complete profile of each parameter found in the "CBKE.inp" file is being displayed in Figure 7-14.

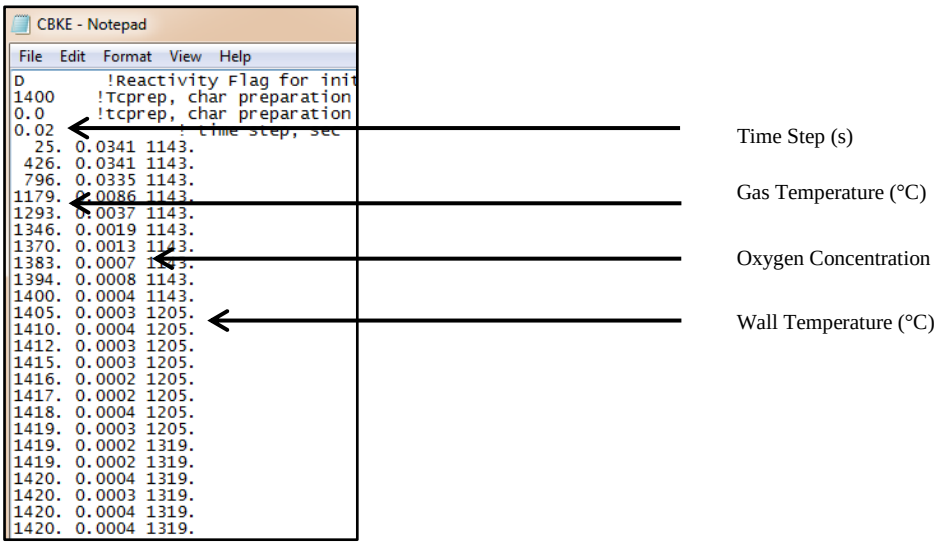


Figure 7-13: PC coal lab "CBKE.inp" input file created for char burnout simulation

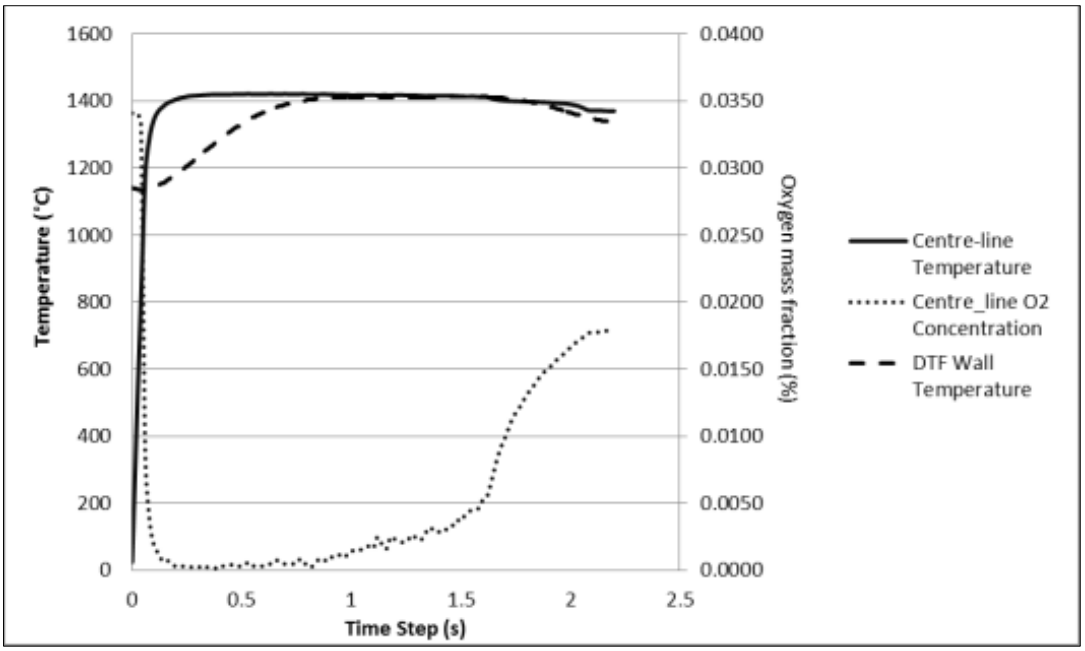


Figure 7-14: Complete user defined input profiles for the centre-line temperature, centre-line oxygen, and wall temperature

The depletion of oxygen through the centre-line of the furnace was further being illustrated by Figure 7-14.

The char burnout CFD input into PC coal lab consisted of a minor devolatilization part. This was because of the 0.8 (%) volatile matter which still remained in the coal after pyrolysis. Therefore, the results obtained in the time frame of devolatilization were removed from the PC coal lab simulations to ensure only the char burnout results were investigated. The PC coal lab results compared to the previous initial PC coal simulation, and the experimental data are shown in Figure 7-15.

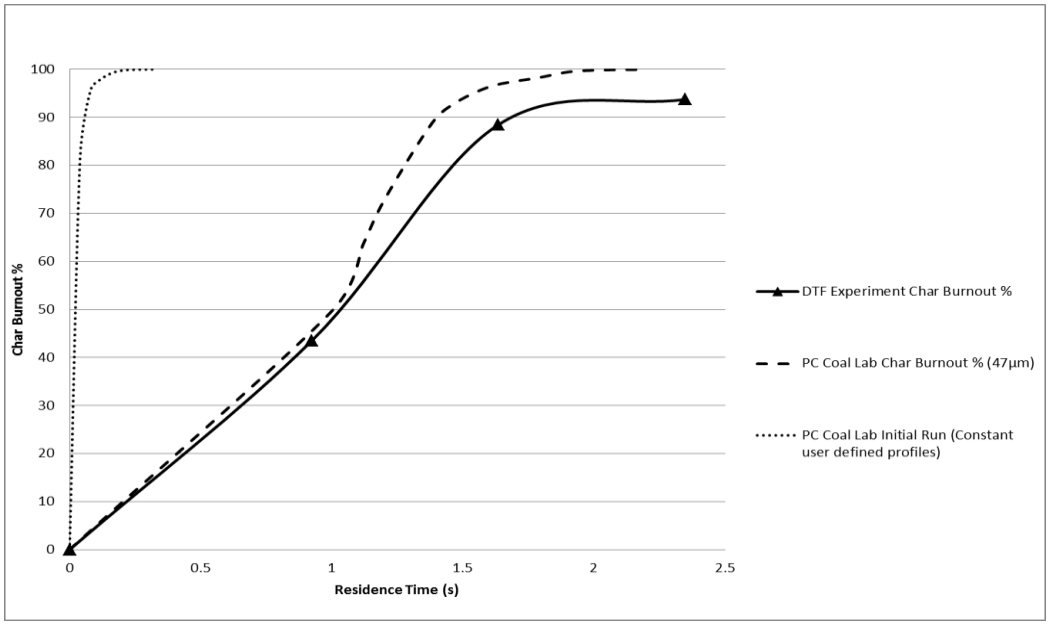


Figure 7-15: PC coal lab char burnout % result with user defined input profiles compared to initial PC coal lab result, and experimental data @ 1400 (°C)

The PC coal lab result with user defined profiles defined displayed an improvement from the initial simulation. The improved PC coal lab result closely predicted the char burnout rate obtained during the DTF experiments. The final set of kinetic parameters calculated from the improved PC coal lab result is shown in Table 7-3 below:

Table 7-3: Final char combustion single rate kinetic parameters

	Unit	Value
Activation Energy (Ea)	(J/Kmol)	1.67E+08
Frequency Factor (A)	(1/s)	4.81E+07

7.7. Char Burnout Numerical Analysis Discussion

This chapter showed the development and throughout improvement of the char burnout numerical simulations. CFD was used to better define PC coal lab's input values to improve on the char kinetics results. Throughout the development of the simulations, the results were compared to the experimental results to ensure the results were properly validated.

The initial PC coal lab simulation made use of constant profiles for the wall temperature, centre-line gas temperature, and centre-line oxygen concentration through the DTF's furnace. This initial PC coal lab simulation showed an unrealistic char burnout result. For this reason, char burnout CFD simulations were incorporated into the numerical process to obtain more accurately defined input profiles into the PC coal lab simulations. Although it was not necessary to develop a CFD simulation with default single rate char kinetics, it was still included in the numerical iteration process to demonstrate the development of results and the effect the kinetic inputs had on the combustion CFD results.

To conclude on the char burnout numerical simulations the complete numerical result comparing the initial PC Coal lab simulation, the final PC coal simulation with a constant 47 (μm) particle, the final PC coal simulation with a constant 75 (μm) particle, and the final CFD result to the experimental data are shown in Figure 7-16.

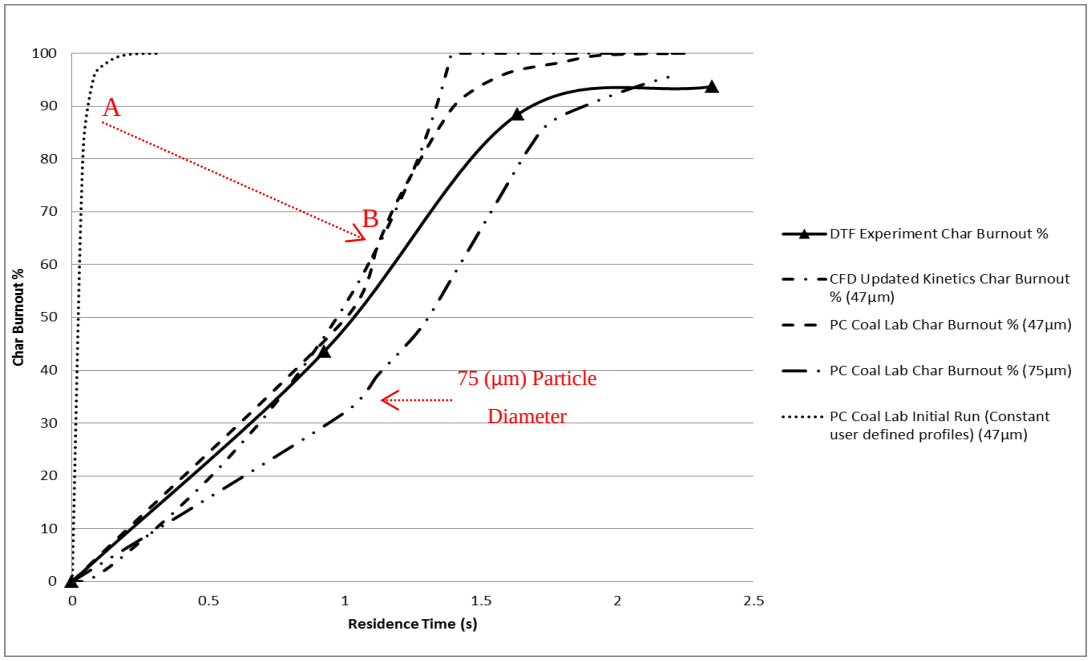


Figure 7-16: Complete development of numerical char burnout results compared to experimental data @ 1400 (°C)

In Figure 7-16 the arrows show how the PC coal lab results improved from point "A" to point "B" by defining user-defined temperature and oxygen profiles when compared to both the final CFD simulation and experimental data. To illustrate the effect particle diameter has on the char burnout simulations a 75 (µm) particle diameter (largest particle size in the particle distribution) was included in the final illustration displayed in Figure 7-16. The larger particle size followed a slower char burnout rate and under-predicted the actual burnout rate achieved. The larger particle diameter also indicated incomplete combustion within the given time frame which explained the incomplete char burnout obtained during the experimental results.

The result was satisfactory and the kinetic parameters obtained from the final PC coal lab simulation were used in the full-scale combustion burner model developed in Chapter 8: .

Chapter 8: LOW NO_x BURNER COMBUSTION CFD SIMULATION

8.1. Introduction

The final chapter describes the method involved in modelling combustion of a full scale single low NO_x coal burner. The software used to develop the burner CFD model was the same that was used during the DTF simulations - Ansys Fluent R15.0 Academic.

Combustion of pulverized coal is a very complicated phenomenon, in which the maximum flame temperature could exceed 1500 (°C) which together with some of its releasing species are very difficult to measure accurately. Because of the challenging conditions that exist to perform in-flame measurements frequently, the trend in the industry and academy shifted to simulating coal combustion by means of CFD to get solutions faster, easier and at much lower costs involved. CFD over the last couple of years played a major role in optimizing combustion processes.

The single burner CFD model was mainly used to investigate the burner flame profile achieved during different air flow conditions. The flame of the burner was investigated in terms of velocity, temperature, and main species distribution achieved. The effect different combustion kinetic parameters had on the combustion performance of the burner were also included. In the final case study, the effect of increased swirl through the TA burner tube on the aerodynamic flame profile of the burner was numerically investigated.

The CFD flame temperature results were compared to the in-flame temperature measurements described in Chapter 3: to ensure a realistic numerical result was achieved.

8.2. CFD Geometry

To save on numerical simulation expense the burner geometry was simplified to include only the inlet annular faces shown in Figure 8-1 below. The geometry included the burner part 0.136 (m) upstream of the flame stabilizing ring shown in Figure 8-2. The burner was attached to a 15 x 8 (m) combustion furnace with a circular furnace outlet boundary on the opposed side of the inlet boundary. An initial CFD simulation with default values was first used to optimize the dimensions of the furnace to ensure the furnace size was sufficient to capture the complete profile of the flame with the minimum amount of surrounding cells required. The Inlet boundary conditions were defined on the three annular burner inlet faces, defined as a PA, SA, and TA inlet mass flow streams shown in Figure 8-2.

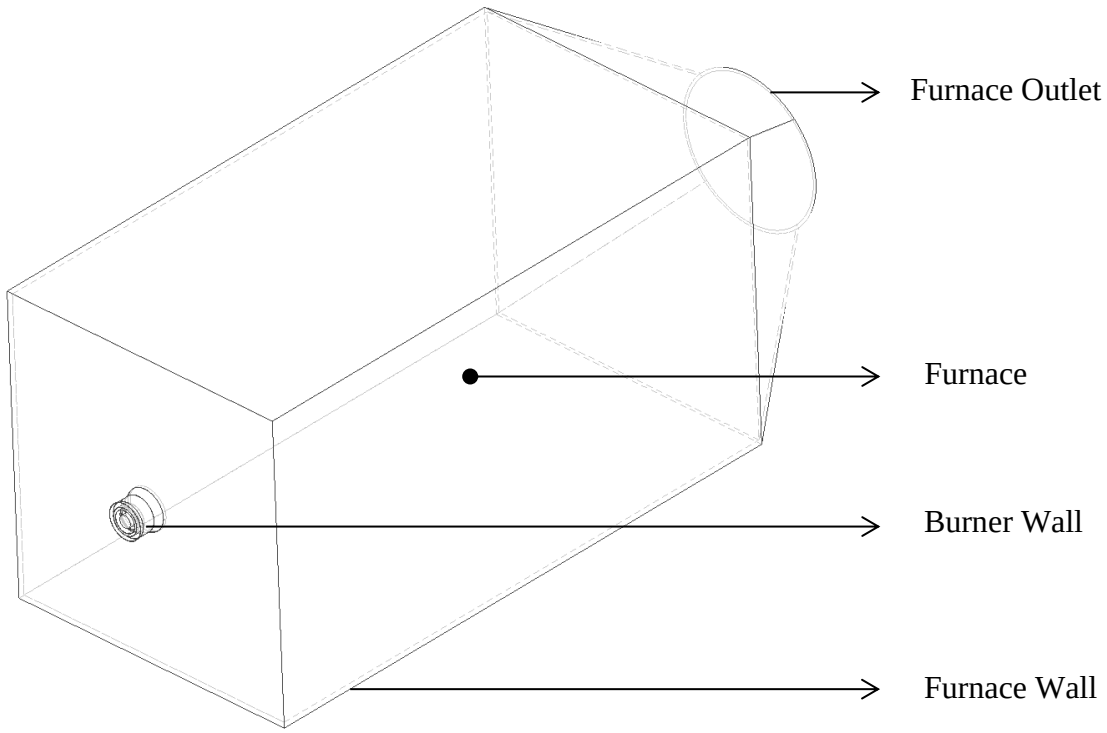


Figure 8-1: Simplified single burner geometry

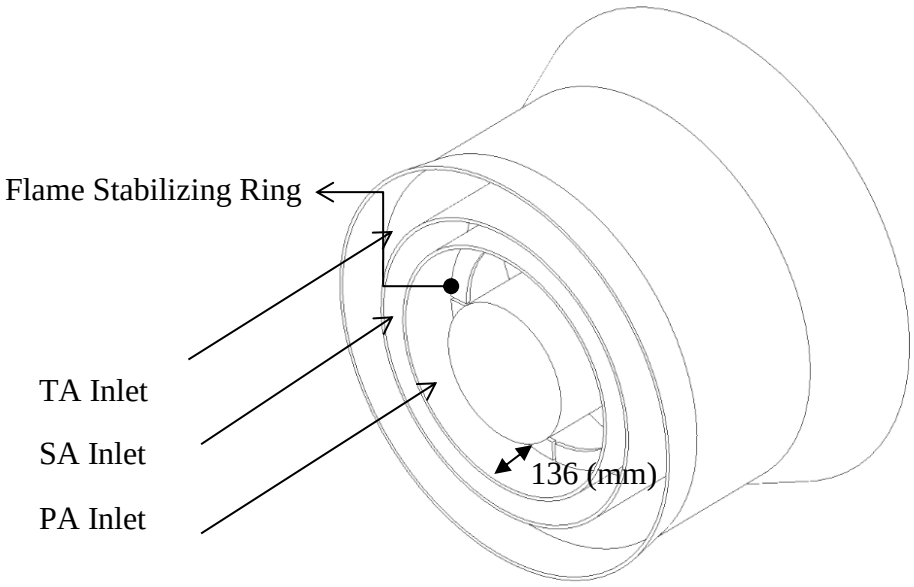


Figure 8-2: Single burner geometry inlet boundaries expanded

The outer diameter of the burner tubes were defined as follow:

TA Tube	=	909 (mm)
SA Tube	=	710 (mm)
PA Tube	=	584 (mm)
Core Air Tube	=	324 (mm)

The wall thickness of all the burner tubes was assumed to be 8 (mm).

8.3. Mesh

The complete combustion CFD model required complex species transport equations to be solved and a rather fine mesh to be used. The global mesh was created through the patch conforming method producing a tetrahedral mesh through the domain. In the combustion zone of the furnace an increased mesh count was required which was done by using the body sizing meshing technique [62]. There are three types of body sizing which are element size, sphere of influence, and body of influence [43]. The body of influence type was used

with a separate body sizing defined shown on the left of Figure 8-3. The body of influence sizing tool was used to increase the cell count around the combustion zone to ensure the mesh was fine enough to accurately solve through the boundary layers of the combustion process.

The finer mesh size of the body of influence was not used throughout the domain to save on numerical solving expense.

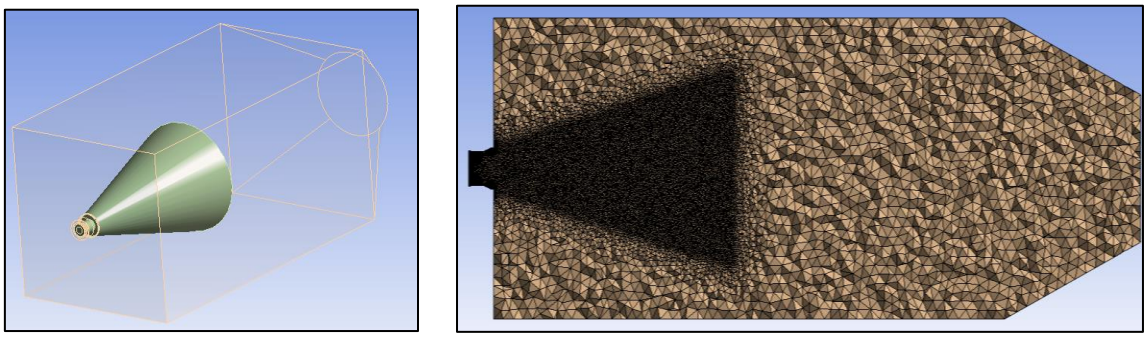


Figure 8-3: (Left) - Body of influence added, (Right) – Tetrahedral mesh created as a result of body of influence

The body of influence at the combustion zone was locally defined with a maximum element size of 0.05 (m) and the remaining domain with a maximum element size of 0.3 (m). The tetrahedral mesh created in the Ansys Mesh working directory contained 6 423 703 cells with an orthogonal quality of 0.21 shown on the right of Figure 8-3.

After the tetrahedral mesh was created the mesh was imported into Ansys Fluent and the domain converted to a polyhedral mesh. This method of converting the tetrahedral mesh to polyhedral allowed the cell count to be reduced to 1 181 769 with an improved orthogonal quality of 0.26. The final mesh created in the Ansys Fluent is shown in Figure 8-4 below:

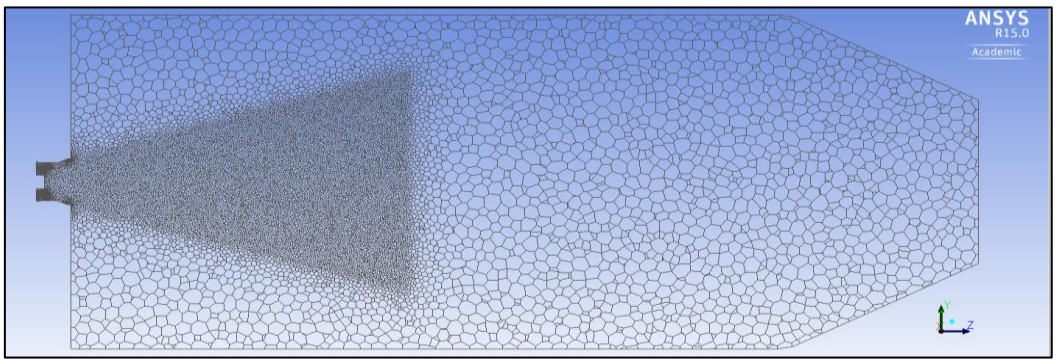


Figure 8-4: Final polyhedral mesh created

8.4. Model Physics

The pressure-based solver was used under steady state operating conditions with an atmospheric operating pressure of 84 000 (Pa). Turbulence was accounted for through the standard k-epsilon turbulence model with advanced near-wall treatment, and radiation through the (DO model with the absorptivity of the gas phase described through the WSGGM – domain based.

To solve for coal combustion the species transport combustion model was selected with a finite-rate/eddy-dissipation turbulence-chemistry interaction. The coal-volatiles-air mixture material, together with the combusting-particle inputs required for all injections was created through the coal calculator.

A separately defined surface injection was created to inject the discrete PF particles into the furnace. The discrete phase 75 (μm) PF particles were injected as a surface injection released from the PA inlet boundary into the combustion furnace. The velocity and PF mass flow rate of the PF injection were obtained from the PF sampling report found in appendix A. The PF proximate and ultimate analysis was the same as what was used during all previous DTF experiments.

The coupled pressure-velocity scheme was used as a solution method. A very specific modelling approach had to be used to solve the equations throughout the domain. The simulation initially was solved with air-only inlet conditions without combustion to make sure the velocity profile were established before the particles were injected into the furnace. After the air-only simulation converged, a cylindrical region was marked, and a temperature of 2000 (K) patched approximately where the PF particles should ignite within the furnace. The immediate iteration thereafter, the PF particles were injected into the furnace. This was done to ensure the particles reached the specified vaporization temperature and ignite. The DPM particles were injected every 30 iterations with 34 600 particles injected during each DPM iteration.

The turbulence intensity percentages for the inlet and outlet boundary conditions were obtained from suggested values during an Ansys Fluent combustion tutorial [52]. The PA inlet turbulence intensity was set at 10 (%) because of the normal to boundary inlet direction. The SA and TA inlet turbulence intensities were set at 12 (%) because of the additional swirl velocity defined.

The core air tube which supplies air to the burner when the fuel oil burner is in service was neglected during the simulations and was inserted as a blank body with a zero defined air flow.

8.5. Boundary Conditions

Table 8-1: Combustion CFD boundary conditions

Burner Wall	Unit	Value
Temperature	(K)	508
Internal Emissivity		0.8
DPM Boundary Condition Type		Reflect
Furnace Wall		
Temperature	(K)	1000
Internal Emissivity		0.8
DPM Boundary Condition Type		Escape
PA Inlet		
Mass Flow Rate	(kg/s)	2.2
Turbulent Intensity	(%)	10
Hydraulic Diameter	(m)	0.244
Temperature	(K)	358
O2 (By weight)	(%)	23
SA Inlet		
Mass Flow Rate	(kg/s)	1.56
Turbulent Intensity	(%)	12
Hydraulic Diameter	(m)	0.11
Temperature	(K)	508
O2 (By weight)	(%)	23
TA Inlet		
Mass Flow Rate	(kg/s)	5.72
Turbulent Intensity	(%)	12
Hydraulic Diameter	(m)	0.183
Temperature	(K)	508
O2 (By weight)	(%)	23
Collection Probe Pressure Outlet		
Gauge Pressure	(pa)	0
Turbulent Intensity	%	10
Hydraulic Diameter	(m)	3.84
Backflow Total Temperature	(K)	1400
PF Injection		
Diameter	(m)	7.50E-05
Temperature	(K)	353
Velocity Magnitude	(m/s)	23
Total Flow Rate	(kg/s)	1.2

The boundary conditions in Table 8-1 above were defined for the baseline solution. The kinetics used for the baseline simulation for the devolatilization and char combustion stage was the kinetics determined from the DTF experiments summarized in Table 8-2 below:

Table 8-2: Final combustion kinetics during the baseline CFD simulations

	Unit	Devolatilization	Char
Activation Energy - Ea	J/Kmol	3.06E+07	1.67E+08
Pre-Exponential Factor - A	1/s	1.53E+03	4.81E+07

8.6. Stoichiometric Air Calculation

A basic calculation was done to determine the stoichiometric air requirement for the fuel supplied. The stoichiometric air requirement is the precise theoretical amount of air required in an ideal combustion process where the fuel is burned completely without any excess air supplied. The ultimate analysis of the coal used for the stoichiometric air requirement calculation is shown in Table 8-3 below.

Table 8-3: Coal ultimate analysis (as received)

Ultimate Analysis	As Received (%)
Nitrogen	1.21
Oxygen	6.43
Carbon	52.89
Ash	27.73
Sulphur	1.16
Hydrogen	2.73
Total Moisture	7.85
Total	100.00

The calculation anticipated for a complete combustion process to convert all the carbon to CO_2, all the hydrogen to H_2O, and all the sulphur to SO_2. From the ultimate analysis of the coal, it was determined per 100 (kg) coal supplied, 52.89 (kg) consisted of carbon, 2.73 (kg) consisted of hydrogen, and 1.16 (kg) consisted of sulphur.

The combustion reactions responsible for consuming oxygen during the combustion process are defined below:

C	+	O_2	=	CO_2	(8.1)
12	+	*32*	=	*44*	*(Molecular weight (g/mole) of each of the elements)*
1	+	*2.667*	=	*3.667*	*(Air requirement per kg carbon)*
52.89	+	*141.04*	=	*193.92*	*(Air requirement per 52.89 kg carbon found in ultimate analysis)*

The carbon calculation above showed that for 52.89 (kg) of carbon found in the ultimate analysis 141.04 (kg) of oxygen is required to produce 193.92 (kg) of CO_2.

The same can be done for the hydrogen and sulphur reactions. The hydrogen requirement is:

$2H_2$	+	O_2	=	$2H_2O$	(8.2)
4	+	*32*	=	*36*	*(Molecular weight (g/mole) of each of the elements)*
1	+	*8*	=	*9*	*(Air requirement per kg hydrogen)*
2.73	+	*21.84*	=	*24.57*	*(Air requirement per 2.73 kg hydrogen)*

The hydrogen calculation above showed that for 2.73 (kg) of hydrogen found in the ultimate analysis 21.84 (kg) of oxygen is required to produce 24.57 (kg) of H_2O.

The sulphur requirement is:

S	+	O_2	=	SO_2		(8.3)
32	+	*32*	=	*64*	*(Molecular weight (g/mole) of each of the elements)*	
1	+	*1*	=	*2*	*(Air requirement per kg hydrogen)*	
1.16	+	*1.16*	=	*2.32*	*(Air requirement per 2.73 kg hydrogen)*	

The sulphur calculation above showed that for 1.16 (kg) of sulphur found in the ultimate analysis 1.16 (kg) of oxygen is required to produce 2.32 (kg) of SO_2.

The total amount of O_2 required for combustion was:

O2 required	=	*O2 required for carbon +*	(8.4)
		O2 required for hydrogen + O2 required for sulphur	
	=	*141.04 + 21.84 + 1.16*	
	=	*164.04 (kg O_2)*	

The total amount of O_2 required for combustion per 100 kg coal was calculated as:

Total O2 required	=	*O2 required - O2 contained in coal*	(8.5)
	=	*164.04 – 6.42*	
	=	*157.61 (kg O2 / 100 kg PF)*	

The oxygen percentage in the air is given as 23.20 % (by weight). Therefore the stoichiometric amount of air required per 100 (kg) coal was:

Air Required = *Total O2 required / Percentage O2 in air (% by weight)*

= *157.61 / 0.2320* (8.6)

= *679.35 (kg Air / 100 kg PF)*

Or

= *6.79 (kg Air/ kg PF)*

For each kilogram of coal supplied to the burner, 6.79 (kg) of air is theoretically required to ensure complete combustion. The theoretical air to fuel ratio was therefore calculated as 6.79. The stoichiometric mass flow of air required for the 1.2 (kg/s) mass flow of coal achieved during the combustion CFD simulations was calculated as 8.12 (kg/s).

In practice where the conditions are far from ideal, excess air is required to ensure complete combustion. The total amount of air supplied to the burner was 9.44 (kg/s) which means about 16 (%) excess to the amount of theoretical air was supplied.

8.7. Inlet Swirl Calculation

To save on numerical computational expense the complete burner geometry was not included in the single burner combustion CFD simulations. Since the complete in-detail geometry of the burner was not included into the single burner combustion simulations it was necessary to accurately determine the amount of swirl created on the outlet of the secondary and tertiary burner tubes of detailed burner geometry to be defined as inlet into the simplified model. These swirl angles were calculated by means of a separate already developed air only (without any chemical reactions simulated) CFD simulation in Star CCM^{+} [59]. This air flow only CFD model included a detailed windbox model which involved the complete windbox geometry of a burner pair shown in Figure 8-5.

The detailed CFD model gave the structure of the flow through the burner. This model was used to calculate the mass flow split between a burner pair, the mass flow split between SA

and TA per burner, and the velocity components of the SA and TA to be used in the simplified geometry CFD simulation.

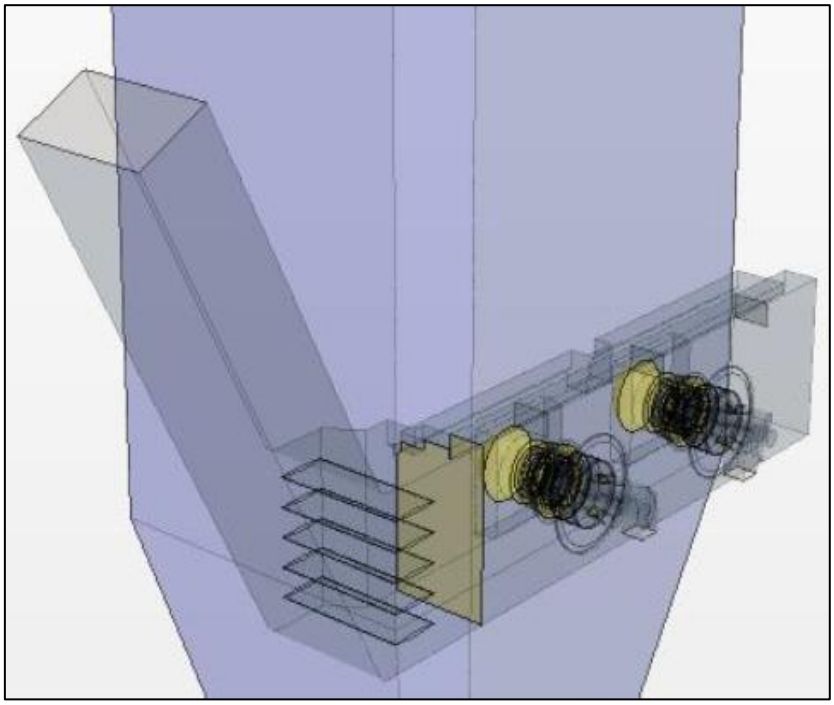


Figure 8-5: Detailed burner CFD model geometry per burner pair [59]

The velocity profile required a direction vector in a local cylindrical coordinate system and required the radial, tangential, and axial velocity components do be defined. The Radial velocity was insignificant and neglected during the simulations.

The velocity components on average calculated from the detail full-scale model of the PA, SA, and TA outlets are shown in Table 8-4:

Table 8-4: Velocity components calculated from detailed geometry CFD model [59]

	Velocity Magnitude (m/s)	Axial Velocity (m/s)	Tangential Velocity (m/s)
PA Inlet	Normal to Boundary		
SA Inlet	30.43	23.88	17.71
TA Inlet	45.60	41.86	19.12

These velocity components were defined in the mass flow boundary inlet conditions of the simplified model and accurately followed the velocity profile obtained in the detailed model. The final velocity profiles achieved by the simplified CFD model used for the combustion simulations are shown in Figure 8-6 below.

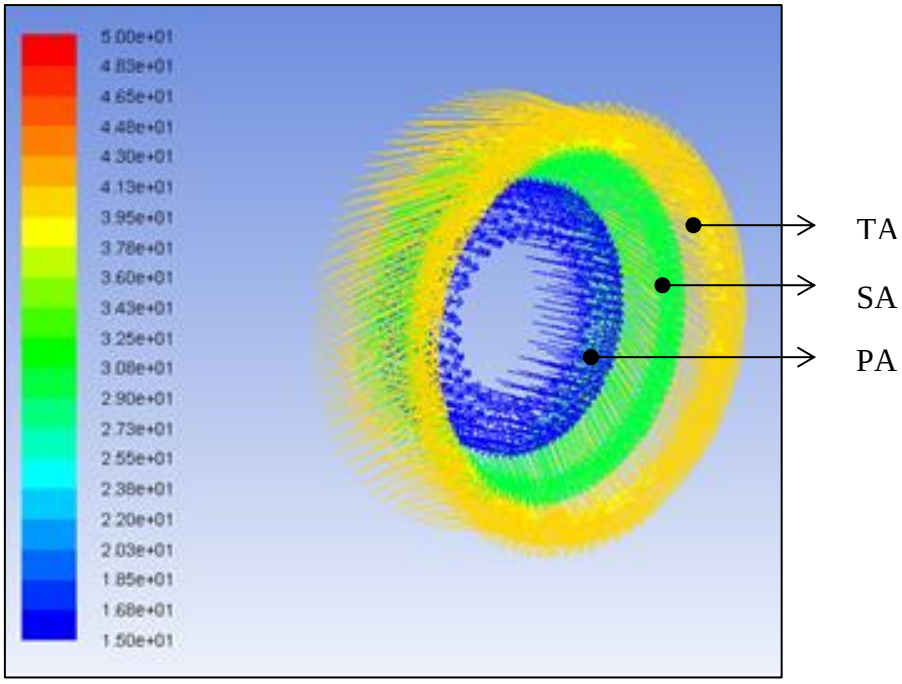


Figure 8-6: Final velocity vectors (m/s) achieved with simplified geometry (isometric view)

The Isometric view of Figure 8-6 illustrates the swirl angle of the air on the TA and SA inlets. The isometric view also illustrates the normal to boundary inlet condition on the PA tube. The detailed windbox CFD model was also used to determine the aerodynamic flow profile of the burner during design conditions to be compared to the baseline simulation.

8.8. Single Burner Combustion CFD Results

A case study investigating two different air flow conditions were investigated by making use of the simplified single burner geometry. These two air flow conditions included a CFD simulation with design air flows and a baseline CFD simulation with a reduced amount of air which was the same air flows achieved on the power plant during the in-flame temperature measurements detailed in Chapter 3: The difference in mass flow achieved during design conditions when compared to the baseline simulation are shown in Table 8-5. Approximately 2.04 (kg/s) in total less air through the burner was considered during the baseline simulation of which 1.76 (kg/s) less air was received through the secondary and tertiary burner tubes and 0.28 (kg/s) through the primary burner tube.

Table 8-5: Design vs baseline simulation single burner flow [3][12]

	SA + TA (kg/s)	PA (kg/s)
Design Flow	9	2.48
Baseline Flow	7.24	2.2
Difference	1.76	0.28

8.8.1. Baseline vs Design Simulation Results

The complete velocity profile obtained during the baseline solution is shown in Figure 8-7 below.

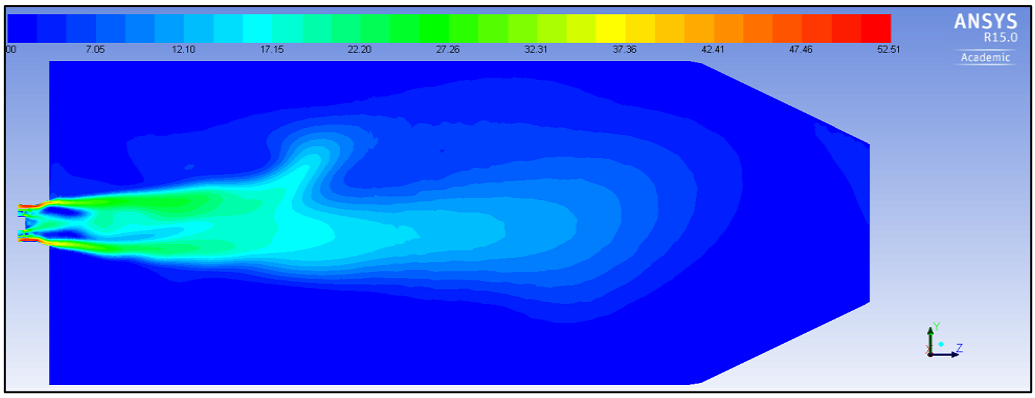


Figure 8-7: Contours of velocity magnitude (m/s) during baseline simulation, reduced flow

The maximum velocity achieved during the baseline simulation was 52.51 (m/s) through the TA swirl. A very prominent and high centre-line velocity profile can be seen in Figure 8-7 during the baseline flow simulation. This could increase the particle velocity through the centre-line and produce a delayed combustion effect.

To further investigate the flame profile achieved during the baseline simulation the velocity result of Figure 8-7 was compared to the flame velocity profile achieved during design flows. Figure 8-8 shows the velocity contours (m/s) of the velocity profile achieved during design conditions.

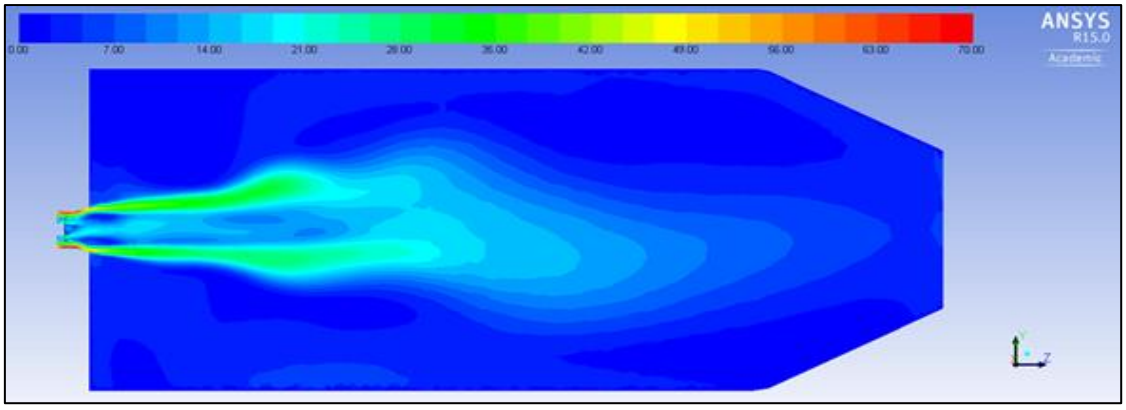


Figure 8-8: Contours of velocity magnitude (m/s) during design flows

The maximum velocity obtained during design conditions was approximately 70 (m/s) found at the TA inlet into the furnace. The higher velocity obtained during design conditions resulted in an increased amount of swirl created through the TA tube. This increase in swirl velocity through the TA burner tube lowered the centre-line velocity.

The baseline solution result in Figure 8-7 showed a different velocity profile achieved compared to design. The baseline solution with the lower than design mass flow of air achieved a maximum TA velocity of only 52.51 (m/s) compared to 70 (m/s) during design conditions. The lower velocity through the burner's SA and TA tube inlets affected the amount of swirl created by the burner. From Figure 8-7 it can be seen that with a reduced amount swirl created through the burner during the baseline solution high centre-line velocity was achieved creating a jet-like profile as opposed to the swirl profile obtained during design flows.

The temperature profile obtained from the combustion CFD simulation during baseline conditions compared to design flows are showed in Figure 8-9.

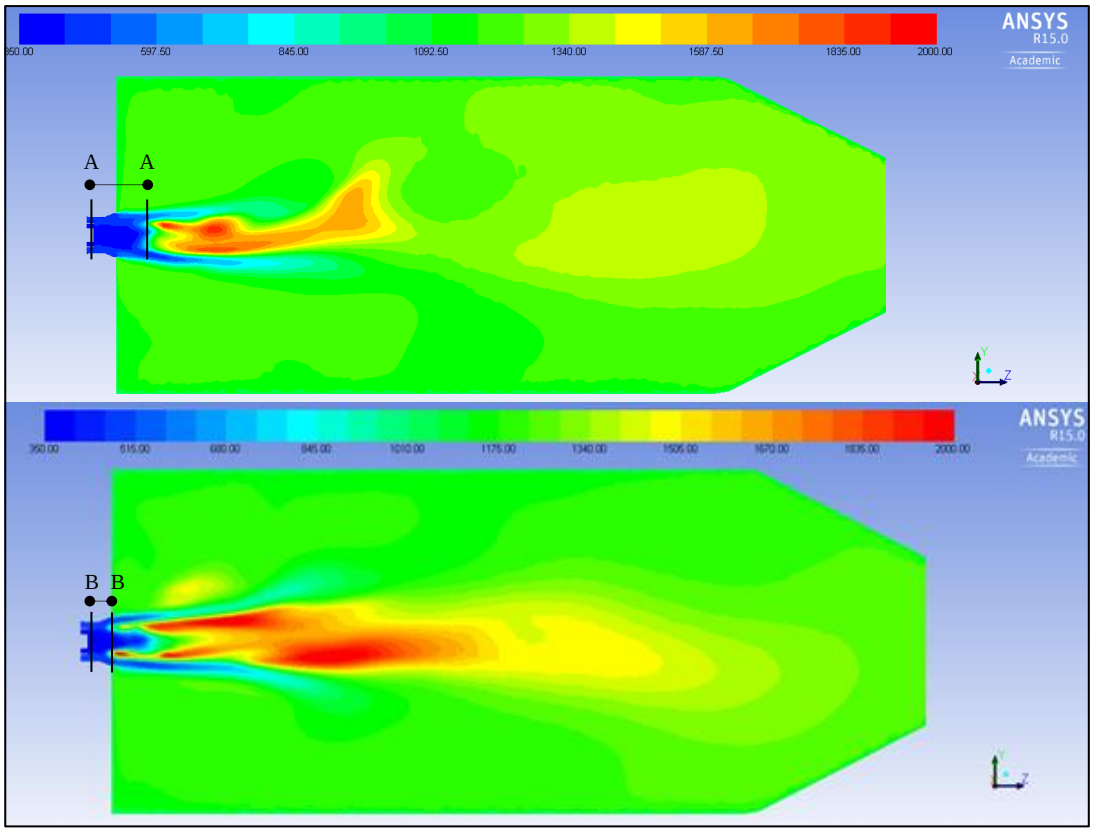


Figure 8-9: (Top) - Contours of static temperature (K) during baseline flows. (Bottom) - Contours of static temperature (K) during design flows

The offset of the flame from the burner mouth is defined as the distance from the burner mouth which was at the front end of PA tube to the closest temperature increase of above 600 (°C). The offset of the flame from the burner mouth are indicated by the two vertical lines in figure 8-9. This offset is not necessarily through the centre line of the burner. The offset for the baseline simulation, however, was measured through the centre-line and was determined to be approximately 1.2 (m) from the burner mouth indicated by offset A-A on the top of Figure 8-9. The design flow simulation result on the bottom of Figure 8-9 showed an improved flame distance from the burner mouth of approximately 0.4 (m) indicated by offset B-B. The hot zones during design flows are drawn closer to the burner mouth and are formed off-centre of the burner centre-line.

The resulting species (O_2, CO,) distribution obtained during the baseline and design simulations have also been included and are shown in APPENDIX I.

8.8.2. Comparison to Measurements

To ensure realistic values were obtained through the numerical simulations the numerical results were compared to the experimental in-flame temperature measurements. Figure 8-10 below shows the in-flame temperature measurements described in Chapter 3: (Figure 3-13) compared to an expanded view of the temperature contours obtained during the baseline simulation in Figure 8-9. The probe measurement direction and the location of where the measurements took place in CFD was the same as the direction of the in-flame measurements shown on the bottom of Figure 8-10.

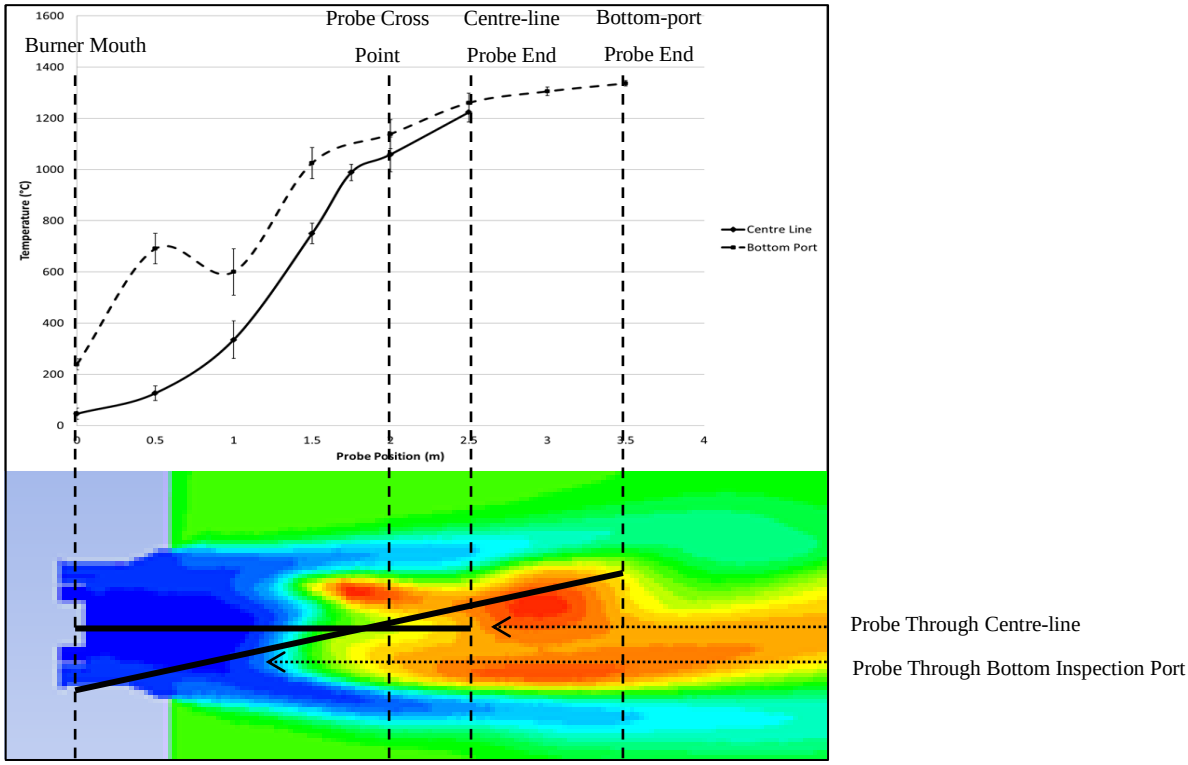


Figure 8-10: (Top) - Measurement results obtained in Chapter 3: . (Bottom) – Expanded view of temperature contour showing probe angles used in CFD to compare to measurements taken

The CFD temperature data along the centre-line probe and the bottom inspection port were extracted and compared to the measurements individually in Figure 8-11 and Figure 8-12 below.

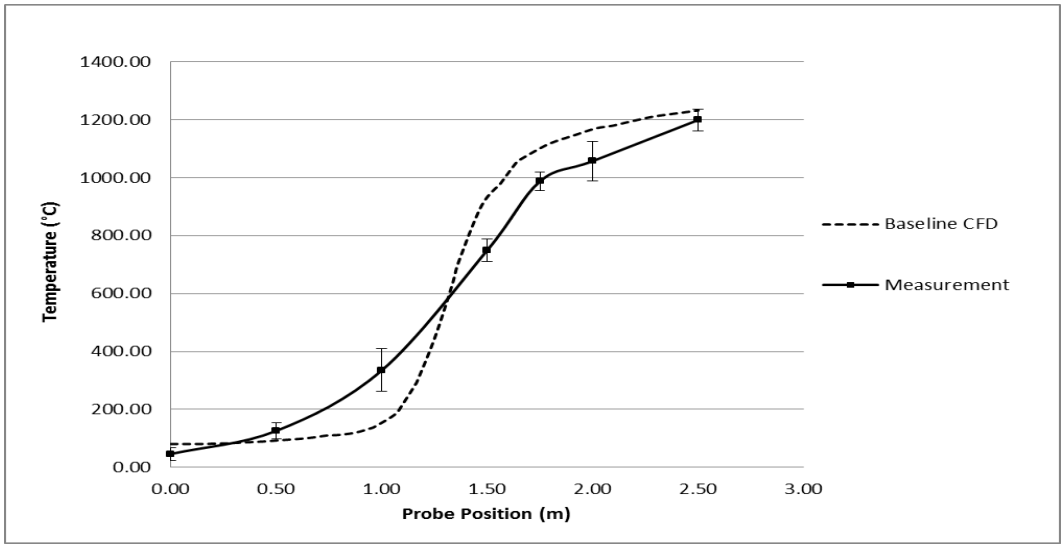


Figure 8-11: Numerical result with probe inserted through centre-line compared to in-flame measurements

Figure 8-11 shows the numerical CFD result compared to in-flame temperature measurements through the centre-line of the burner. The results showed that the CFD simulation predicted the temperature through the centre-line fairly accurately in the designated areas. Initially up until 1.2 (m) into the furnace CFD under predicted the temperature profile through the centre-line after which the temperature increased to above the measurements until the 2.5 (m) mark. This was where ignition took place and confirmed the flame off-set from the burner mouth. The initial discrepancy between the CFD and measured temperatures could be because of the initial under prediction of air and fuel mixing during the CFD simulation or the accuracy of the in-flame temperature measurements. During the measurements the thermocouple although it was shielded, could possibly still absorb a minor percentage of radiation and therefore measured temperatures slightly higher than what the actual temperature was.

The numerical CFD result compared to in-flame temperature measurements through the bottom inspection port of the burner are displayed in Figure 8-12 below:

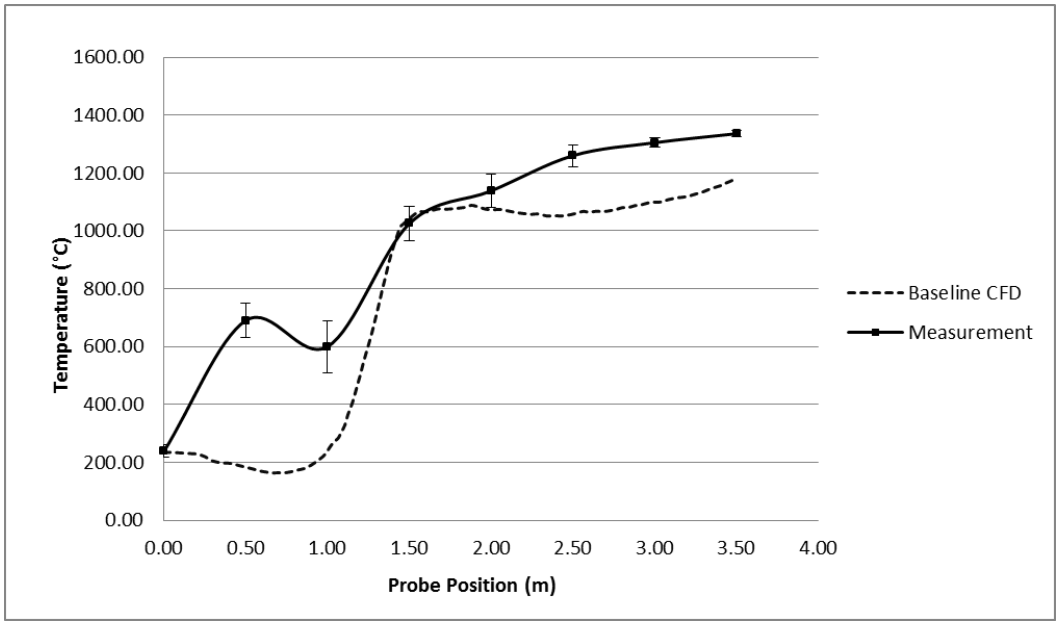


Figure 8-12: Numerical result with probe inserted through bottom-port compared to in-flame measurements

Greater discrepancies were found between CFD and the in-flame temperature measurement through the bottom inspection port. It could be that the CFD simulation again under predicted the amount mixing that took place during the initial stages of combustion especially through the bottom inspection port where the high swirling TA air enters the furnace. Furthermore measuring through the bottom inspection port at the lower flow rates it could also be that the flame was not 100 (%) stable, particularly at the hot gas recirculation zones. The CFD simulation with steady state operating conditions will most probably not pick this up. A transient CFD simulation, therefore, might be able to predict this phenomenon better.

Overall a very good relationship was found between the CFD simulations and the in-flame temperature measurements. The CFD simulation accurately followed the profiles obtained during the measurements with an acceptable margin of error. Typically during CFD simulations, one would strive to have a margin of error between the CFD simulation and measurements of between 5 and 10 (%) [60]. These percentages are strongly dependent on the type of simulation. During combustion simulations, one would expect the margin of error to be at the higher end of the acceptable range. A mass and energy balance was done to ensure conservation throughout the simulation and are shown in APPENDIX J.

8.8.3. Case Study 1: Kinetics Input Effect on Numerical Result

To illustrate the effect combustion kinetics had on the combustion simulation results a case study was done comparing the results of three different kinetic inputs into CFD to the in-flame temperature measurements. A simulation with default Ansys Fluent kinetics, a simulation without kinetics specified (diffusion limited), and the baseline simulation with the final calculated single rate combustion kinetics from the DTF experiments were modelled. A summary of the default kinetic values used during the case study is displayed in Table 8-6 below. All other inputs into the simulations were kept the same as the baseline simulation.

Table 8-6: Summary of the different single rate kinetic input values used

Kinetic Parameter	Default Value	Diffusion Limited	Final Calculated Value (Baseline)
Devolatilization			
Ea (J/Kmol)	7.40E+07	-	3.06E+07
A (1/s)	3.82E+05	-	1.53E+03
Char			
Ea (J/Kmol)	7.90E+07	-	1.67E+08
A (1/s)	2.00E-03	-	4.81E+07

The temperature results obtained through the burner centre-line are displayed in Figure 8-13 and through the burner bottom-port in Figure 8-14

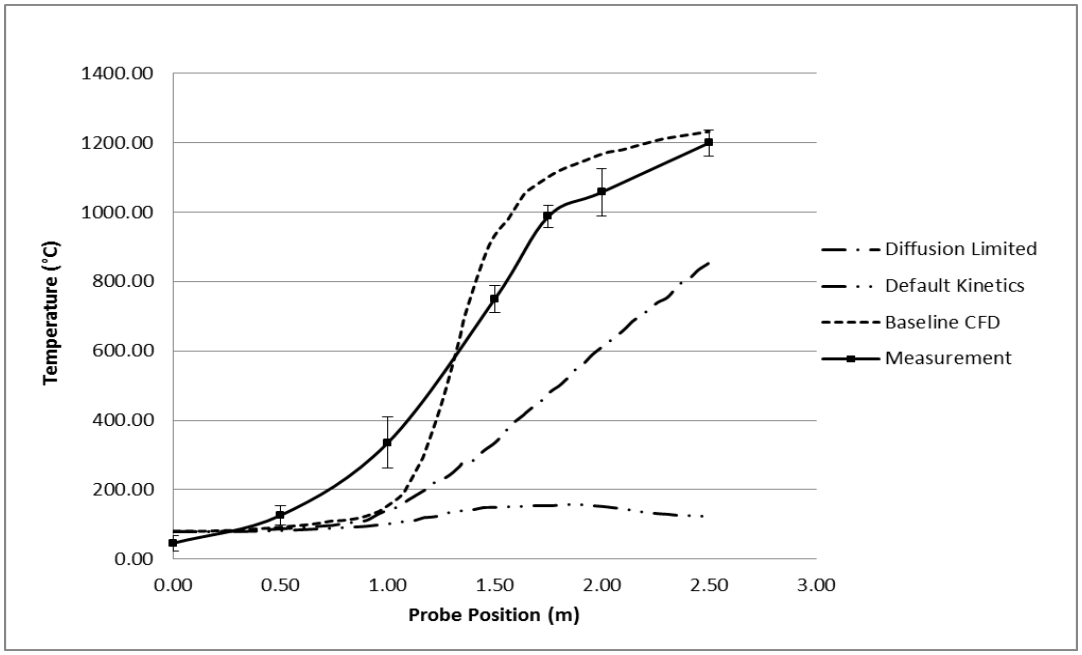


Figure 8-13: Kinetic input results through burner centre-line

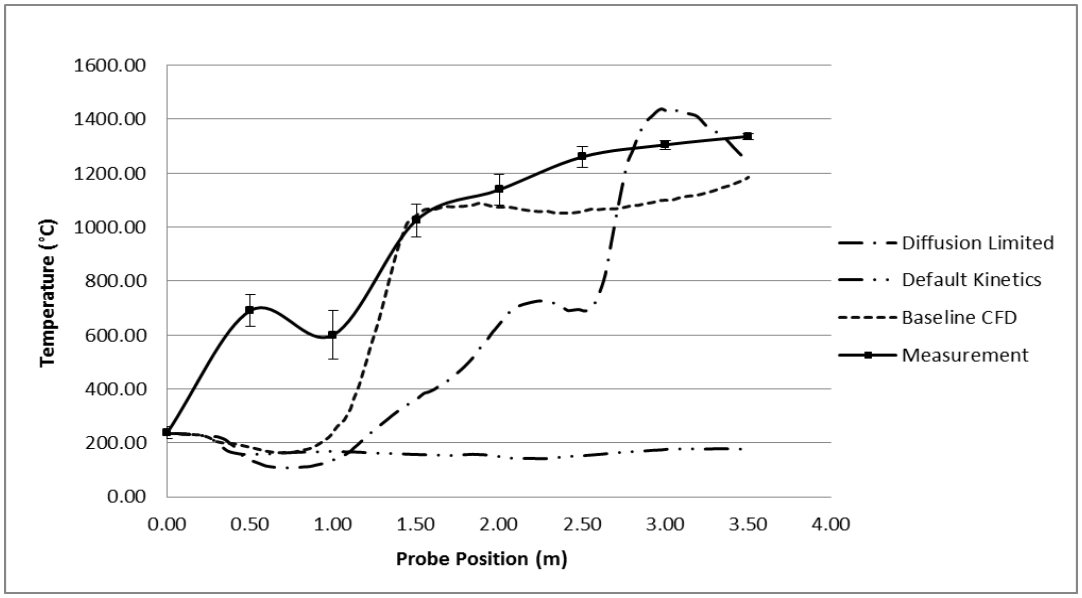


Figure 8-14: Kinetic input results through burner bottom-port

In Figure 8-13 and Figure 8-14, the effect of the different kinetic inputs can be seen. The distance into the furnace displayed is the same distance measured during the in-flame temperature measurements. The default Ansys Fluent kinetics CFD simulation displayed a highly inaccurate result with a longer delayed combustion effect. This was because of the different coal quality used during the simulation as oppose to the default quality coal in

Ansys Fluent for which the default kinetics were calculated. The coal particles during the default kinetics simulation although not shown in the figures did ignite and combust about 4.3 (m) into the furnace. The Diffusion limited case study without any kinetics specified into the simulation provided a more realistic result compared to the default kinetics case but was still fairly inaccurate. The baseline simulation with the improved calculated combustion kinetic parameters defined into the simulation provided the most accurate results when compared to the in-flame measurements. The Flame temperature profiles of the different case studies can be seen in Appendix G.

8.8.4. Case Study 2: Swirl Effect on Numerical Result

From the baseline simulation results, it became evident that the amount of swirl through the burner was reduced because of the decrease mass flow of air when compared to the design profile. The reduced mass flow resulted in a drop in velocity through the burner and affected the flame temperature profile achieved. This case study was done to determine if by changing the burner geometry i.e. TA swirl angle, a better flame temperature profile could be achieved under the reduced air flow conditions available on the plant.

Essentially the case study investigated the effect swirl angle has on a low NOx burner flame profile and, therefore, the aerodynamic flame shape achieved. The mass flow of air was kept the same as the reduced mass flow during the baseline simulation. Only the TA inlet swirl angle was increased as the TA tube received the highest mass flow of air with the most predominant effect. The swirl angle of the baseline simulation was increased until a maximum swirl velocity of approximately 70 (m/s) was achieved through the TA inlet tube. This 70 (m/s) is the same velocity obtained during design conditions. The effect on the velocity profile, temperature distribution, and CO formation was investigated.

The velocity profile obtained with the baseline reduced air flow but with an increased swirl number is shown in Figure 8-15.

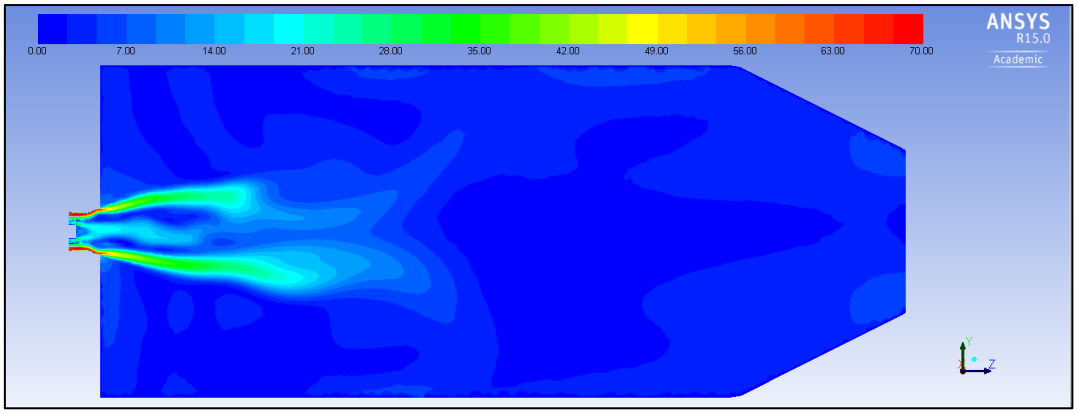


Figure 8-15: Contours of velocity magnitude (m/s) of baseline simulation with an increased amount of swirl through tertiary burner tube

With the increased swirl number on the TA tube, a different aerodynamic flow profile was achieved. An improvement from the baseline simulation can be seen regarding the centre-line velocity achieved. With an increase swirl number on the TA tube, the centre-line velocity decreases similar to what was happening during the design flow simulation.

An extended view of the improved velocity profile achieved compared to design are shown in Figure 8-16 below:

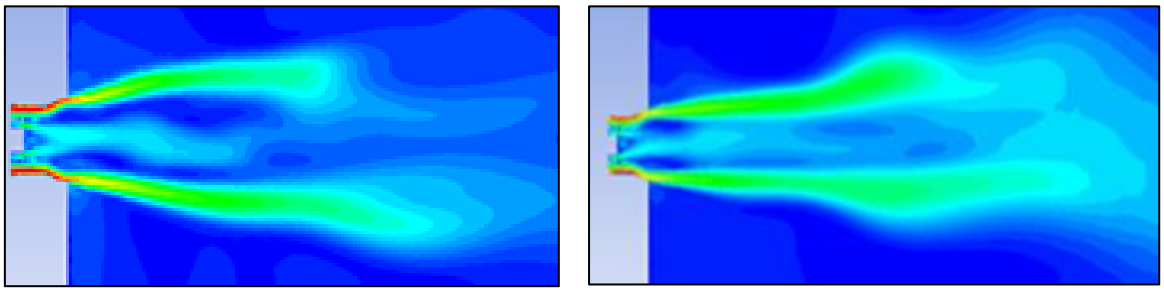


Figure 8-16: (Left) – Extended view of the increased swirl simulation velocity magnitude (m/s) result. (Right) – Design flow CFD velocity results (m/s)

Figure 8-16 shows that a similar to design flow velocity profile can be achieved with the reduced baseline simulation by increasing the amount of swirl through the TA tube. The velocity vectors of the baseline flow simulation with increased swirl compared to the baseline simulation are shown in Figure 8-17 below.

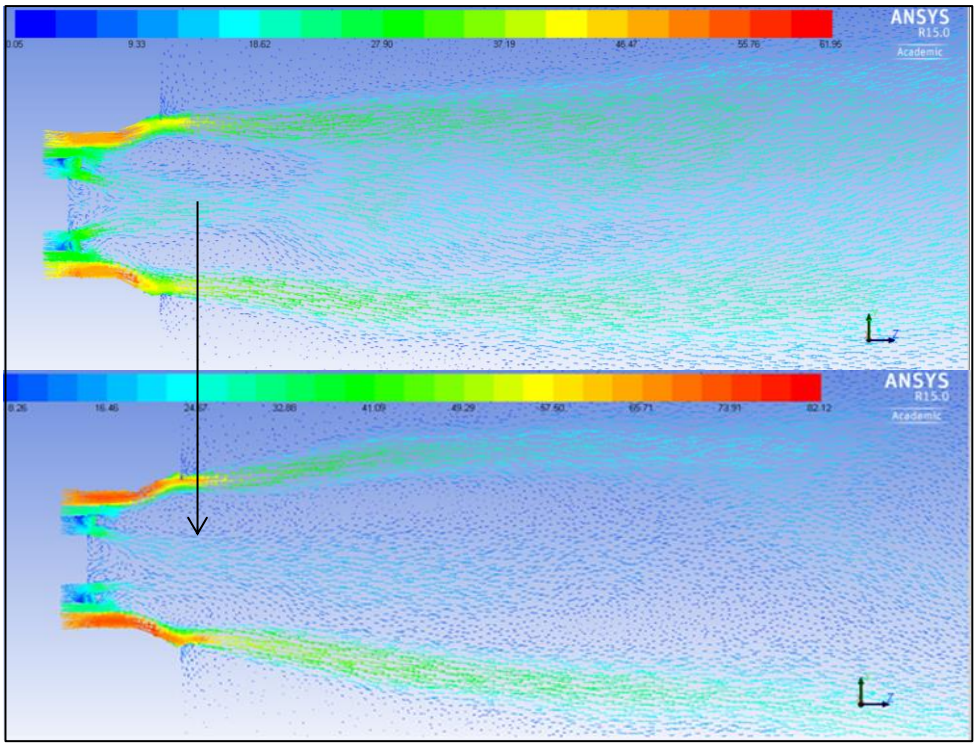


Figure 8-17: (Top) - Velocity vectors coloured by velocity magnitude (m/s) baseline simulation. (Bottom) - Velocity vectors coloured by velocity magnitude (m/s) increased swirl

The increased swirl simulation on the bottom of Figure 8-17 displayed a different velocity vector profile achieved when compared to the baseline simulation. The increased amount of swirl shortened the jet like profile created through the centre-line and should produce better mixing of species and oxygen within the flame

The temperature profile obtained as a result of the increased swirl simulation compared to the previous baseline and design flow solutions are shown in Figure 8-18 below.

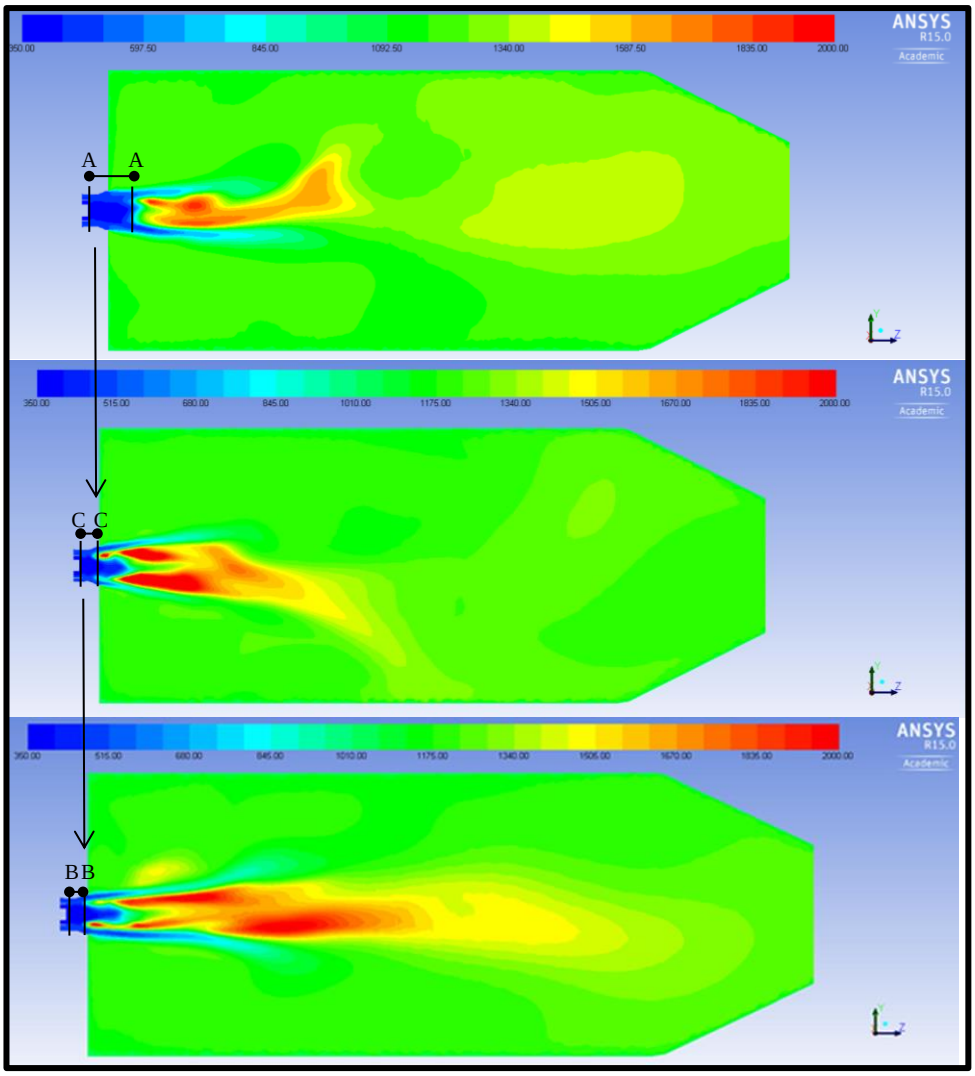


Figure 8-18: (Top) - Contours of static temperature (K) during baseline simulation. (Middle) - Contours of static temperature (K) with an improved swirl. (Bottom) - Contours of static temperature (K) during design simulation

An improvement can be seen in terms of flame offset displayed by offset C-C when compared to the baseline result offset A-A. The temperature profile achieved during the increased swirl simulation showed the hot zones of the flame are created towards the TA outlet of the burner very similar to what was obtained during the design flow simulation result B-B. The flame offset in this scenario was not determined through the centre-line and rather through the TA tube of the burner. The flame offset decreased to approximately 0.4 (m) from the burner mouth compared to the previous 1.2 (m). The improved flame temperature result in Figure 8-18 showed that during reduced air flow conditions through the burner a flame profile similar to design can still be obtained by increasing the swirl created through the burner. This will have a positive impact on flame ignition, char burnout, NOx emissions, and flame stability.

The particle concentration through the furnace during the improved swirl simulation compared to the baseline simulation is shown in Figure 8-19 below. The increased swirl simulation on the bottom of Figure 8-19 showed an improvement of the particle distribution and a shorter burnout time achieved. The baseline simulation shown on the top of Figure 8-19 with its jet-like profile showed a longer particle burnout through the furnace.

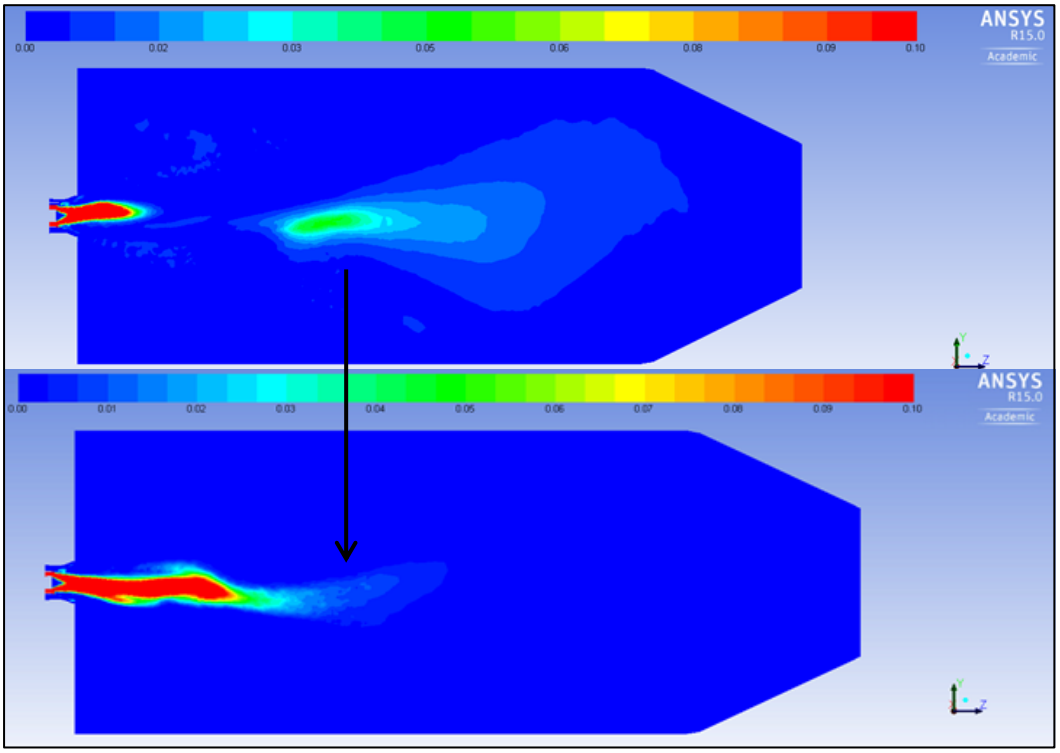


Figure 8-19: (Top) Contours of DPM concentration during baseline simulation. (Bottom) - Contours of DPM concentration with an improved swirl

The CO formation obtained as a result of the increased swirl on the TA inlet compared to the previous baseline simulation is shown in Figure 8-20 below.

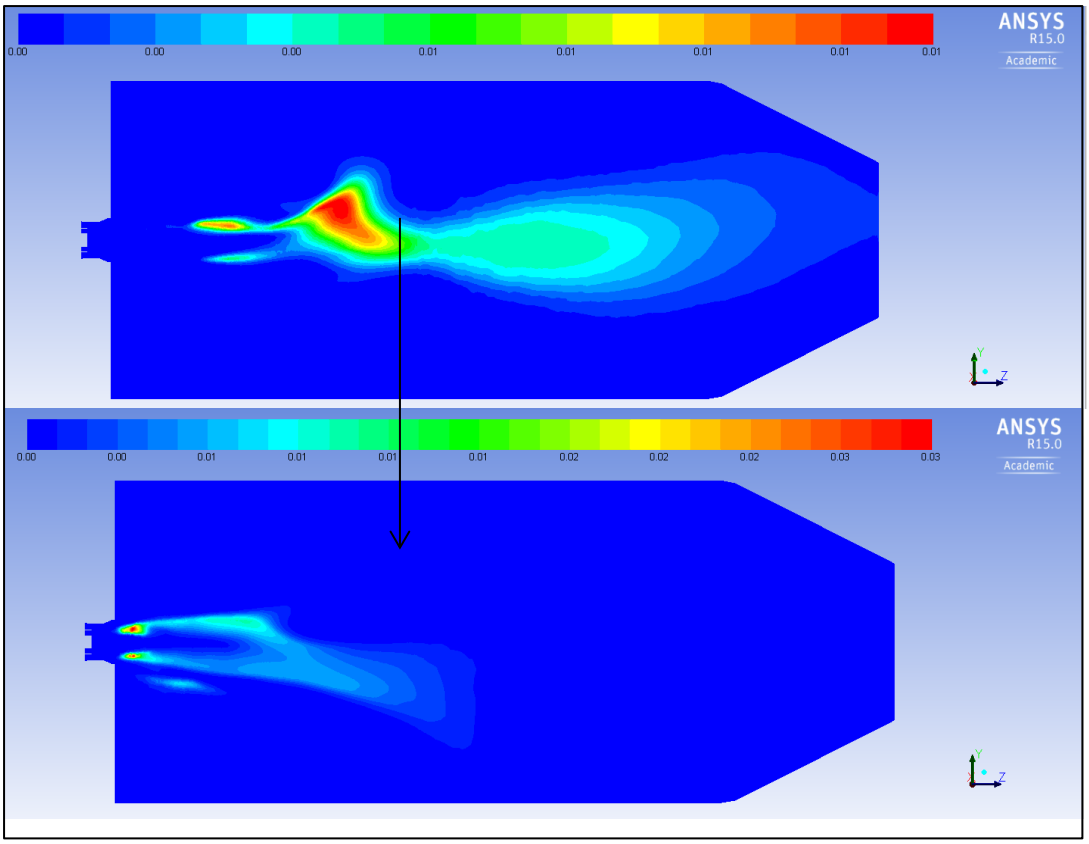


Figure 8-20: (Top) - Contours of mass fraction of CO during baseline simulation. (Bottom) - Contours of mass fraction of CO with an improved swirl

As a result of the improved mixing rate between the available oxygen and combustion species during the increased swirl simulation, the amount of incomplete combustion resulting in CO reduced. The mass fraction of CO calculated as a mass-weighted average on the outlet boundary was 8.25E-09 which was a major improvement from the baseline's simulation 0.000407.

The current swirl angle was adjusted in cylindrical coordinates until design velocities were obtained though the TA outlet of the burner. In order to identify an optimum swirl angle for possible implementation various other angles can be similarly investigated and the resulting velocity, temperature distribution, and species distribution compared to each other. The stakeholder will then be able to determine a suitable angle for their specific requirements. Once the optimum angle in cylindrical coordinates is identified the exact angle in degrees can be calculated for implementation purposes.

8.9. Mesh Sensitivity

To ensure the results were independent of the mesh, a mesh sensitivity was done. Four different mesh sizes and different adjustments were used to perform the mesh sensitivity analysis. The four different mesh sizes used during the analysis are displayed in Appendix H. A summary of the mesh size, orthogonal quality, and peak temperatures are shown in Table 8-7 below.

Table 8-7: Mesh sensitivity information

	Cells	Orthogonal Quality	Peak Temperature (K)
Mesh 1	200665	0.25	1816
Mesh 2	490943	0.259	2097
Mesh 3	1181769	0.261	2091
Mesh 4	1942582	0.237	2031

The mesh count started off with 200 665 cells and then doubled up until almost 2 million cells were created. The temperature profile measured through the centre-line showing the ignition point of the flame through the centre-line was used to perform the mesh sensitivity analysis. The results of the 4 different mesh sizes used are shown in Figure 8-21 below.

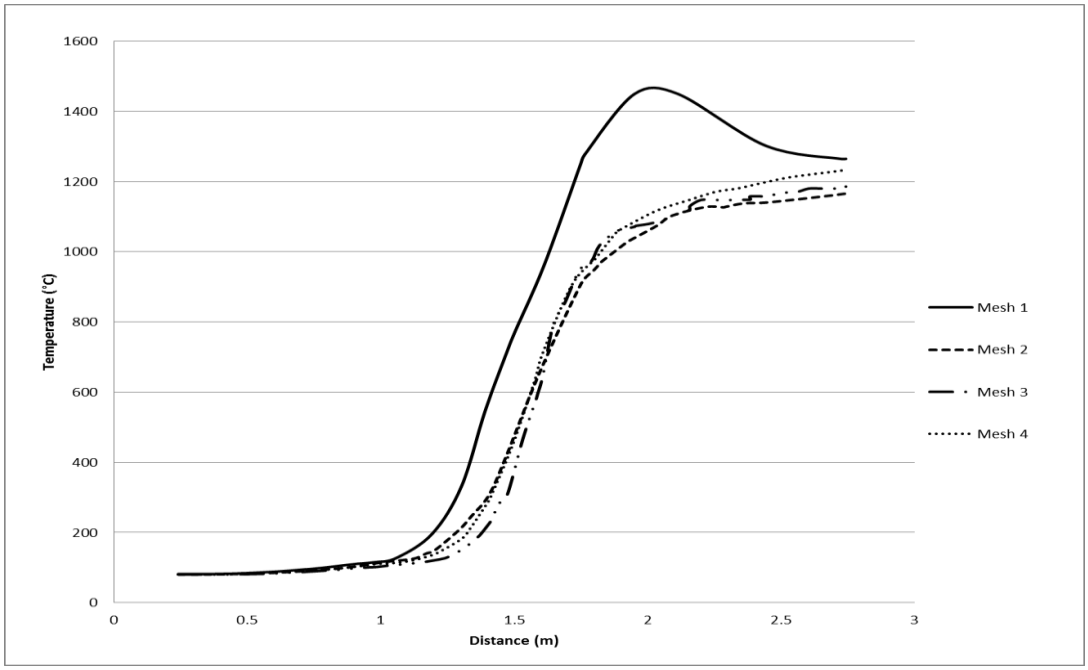


Figure 8-21: Temperature obtained through burner centre-line

It can be seen that mesh 1 with 200 655 cells showed a completely different result when compared to the other 3 mesh sizes. The results of a mesh size larger than 200 655 cells stayed fairly constant with a negligible difference in the temperature result through the centre-line. Mesh 3 was used during all numerical simulations because of the highest orthogonal quality achieved at a reasonable mesh count of 1181769 cells.

8.10. CFD Results Discussion

A baseline CFD simulation was done under the same operating conditions found during the in-flame temperature measurements. This was done to compare the CFD temperature results with the in-flame temperature measurements. A very good relationship was found between CFD and measurements with the CFD simulation which accurately followed the measurement profiles achieved.

During the combustion CFD simulations it was found that with the lower than design air flow through the burner, the velocity through the burner was affected with a reduced amount of swirl created. This, in turn, affected the aerodynamic profile of the burner and consequently the temperature profile achieved. The reduction in swirl tends to produce a more of jet like velocity profile through the centre-line when compared to the design flow simulation and influenced the way in which the combustion species were brought together. This mixing of species, in turn, affected the combustion process and, therefore, the temperature distribution within the flame. At current operating conditions the specific air plume created pushed the flame away from the burner mouth with an achieved flame offset of about 1.2 (m) away from the burner mouth.

In an attempt to improve the aerodynamic profile of the burner at the reduced mass flow baseline conditions a burner geometry change was considered. It was found that during design flows a swirl velocity of 70 (m/s) was achieved through the tertiary burner tube. Therefore, for the burner geometry change the TA swirl angle was increased until the same swirl velocity of approximately 70 (m/s) was achieved during the baseline flow conditions. This required approximately 30 (%) more swirl to be added on the TA inlet. An improved result was obtained. The increased swirl on the TA inlet of the burner reduced the jet created through the centre-line and improved the aerodynamic profile of the flame. This

improved velocity profile promoted the mixing rate of the combustion species and improved the rate and manner in which the species were brought together. The increase in swirl number had a significant impact on the temperature distribution within the flame. The increased swirl drew the hot zones of the flame closer to the burner mouth with an achieved flame offset reduced to approximately 0.5 (m) compared to 1.2 (m).

The effect of the increased swirl on the temperature profile of the flame showed how aerodynamically driven the flame is. Because of the improved mixing of species within the flame, the CO formation also showed an improvement with basically not any CO concentration contained on the furnace outlet.

Three different heterogeneous surface reaction rate models for char combustion has been used during the CFD simulations and compared to each other. These models included the diffusion limited, kinetics/diffusion-limited with default Ansys Fluent kinetics, and kinetics/diffusion-limited with improved calculated kinetics. The kinetics/diffusion-limited rate model with improved calculated kinetics gave the most accurate results when compared to the in-flame measurements. The CFD simulations also showed an improvement in results with the updated calculated homogenous devolatilization kinetics used. These result emphasized the importance of calculating the devolatilization and char kinetic parameters when performing combustion CFD simulations.

Chapter 9: CONCLUSION AND RECOMMENDATION

9.1. Conclusion

The temperature profile of an industrial low NO_x coal burner was evaluated through a combination of experimental and numerical techniques. The experimental part involved in-flame temperature measurements on the utility-scale low NO_x coal burner. The measurements were done with a 6 (m) long, 50 (mm) in diameter suction pyrometer and were conducted through the centre-line and bottom inspection port of the burner. The numerical part involved a fully developed full-scale single burner combustion CFD model of a low NO_x burner.

To improve on the burner CFD model results the coal devolatilization and char burnout combustion kinetics were also determined through a combination of experimental and numerical techniques. The experimental part involved DTF experiments to determine the volatile yield and char burnout rate of the specific coal used under three different defined particle heating rates. The DTF results were mainly used to validate the numerical simulations. The numerical part involved the calculation of the coal's specific devolatilization and char single rate kinetic parameters through an iteration process between CFD and PC coal lab. CFD was mainly used to accurately calculate user defined input profiles to be inserted into PC coal lab to improve on the PC coal lab result. It was found that once the CFD determined user-defined profiles are used in PC coal lab a much improved and very realistic result was obtained when compared to the DTF experiments. The final PC coal lab simulation was used to determine the devolatilization and char single rate kinetic parameters which were used during the single burner combustion CFD model. In obtaining accurate and realistic combustion CFD results it was crucial that the devolatilization and char single rate kinetic parameters had to be determined accurately. The method used in calculating the devolatilization and char single rate kinetic parameters through CFD and PC coal lab was very effective and accurate.

The single burner CFD model compared well with the in-flame temperature measurements once the calculated coal combustion kinetic parameters were defined. The effect of different flow conditions and swirl numbers were thoroughly investigated. The single

burner CFD model showed that during reduced flow conditions a reduced amount of swirl was created compared to the design flow simulation. The reduction in swirl produced a jet-like flame with a resulting increase in flame offset distance from the burner mouth. The flame offset distance from the burner mouth during the baseline simulation was calculated to be approximately 1.2 (m). During a case study, it was determined that the flame offset can be improved by increasing the swirl number on the TA tube. It was shown that with the baseline flows and an increased amount of swirl the flame offset from the burner mouth can be decreased from 1.2 (m) to approximately 0.5 (m) away. This flame offset was very similar to the 0.4 (m) achieved during the design flow simulation.

The combustion CFD model showed a direct relationship between the aerodynamic profile of the flame and temperature distribution achieved.

9.2. Recommendations

From the outcomes of the present study, the following potential future work is recommended.

Recommendations for future experimental work:

- Regarding the in-flame temperature measurements, it is recommended that a modification needs to be done to permanently add an appropriate radiation shield to the suction pyrometer tip. This will ensure accurate temperature readings especially when measuring in high radiation environments such as in a burner's flame.
- An investigation needs to be done to determine the possibilities of adding additional flame measurement angles to produce an improved 2-dimensional profile of the flame to study flame structures.
- During the DTF devolatilization experiments even shorter particle residence times were required in obtaining a complete devolatilization curve. This can be achieved by increasing either the injection or collection probe length in order to decrease the particle travelling distance. By decreasing the particle travelling distance the gas flow can be kept constant ensuring laminar flow conditions are maintained and the gas pre-heaters to reach the desired temperature set point at furnace inlet. To

implement the modification further calculations are required to determine heat transfer effects.

- During the char burnout experiments, the chemical composition of the resulting gas as a product of char combustion could not be analysed. Analysing the chemical composition of the resulting gas could be fundamental in analysing the combustion performance during each experiment. By measuring the O_2 concentration at the outlet of the collection probe the CFD centre-line O_2 results can also be validated which was an important input into PC coal lab. Therefore, a gas analyser needs to be fitted to the current DTF set up to expand on the current available DTF results.

Recommendations for future CFD work:

- The detailed effect devolatilization kinetic parameters have on the full combustion process of a single burner or/and the complete furnace needs to be investigated to determine the importance of calculating devolatilization kinetics for combustion CFD modelling.
- The effect different particle size distributions have on the full combustion process results can be further investigated.
- The effect swirl has on the flame temperature profile has been showed by increasing the amount of swirl created through the burner TA tube. It was shown that by increasing the swirl through the TA tube the flame offset from the burner mouth can be reduced. Further investigation has to be done to determine the effect different swirl numbers has on the flame shape at different flow conditions. This can be used to suggest optimum swirl angles during different flow conditions.
- Other geometrical considerations can also be included into the simulated to determine the effect on the flame temperature profile achieved. The diameter of the burner flame stabilizing ring, for instance, can be increased to determine the effect it has on the flame offset from the burner mouth.
- The influence the amount of swirl through the burner has on NO_x formation need to be investigated. The use and testing of the Ansys Fluent NO_x model to predict NO_x, therefore, needs to be further investigated.

- Finally, the single burner combustion CFD model can be expanded to a complete furnace combustion CFD model. This model can be used and is not limited to assist with investigations on the following parameters:
    - The influence of the surrounding burners on the specific individual flame profile achieved.
    - Effect of different mill combinations on furnace outlet temperature.
    - Determination of resulting gas composition at the furnace outlet.
    - Determination of char burnout rate at different operating conditions.

Chapter 10: REFERENCES

[1] Govindsamy, R., (2012). Eskom Combustion Reliability Improvement Project. Eskom Group Technology Division Investigation Report.

[2] "Environmental Management: Air Quality Act" (No 39 of 2004)

[3] U.S. Department of Energy (2001). Evaluation of Gas Re-burning and Low-NO_x Burners on a Wall-Fired Boiler A DOE Assessment. *National Energy Technology Laboratory*. DOE/NETL-2001/1143.

[4] Matsumoto, K., Domoto, K., Fujimura, K., Abe, N., Hirahara, H., Kasai, J. (2013). Development of Ultra-low NO_x Coal-firing Burner. *Mitsubishi Heavy Industries Technical Review*. (50) no. 3, p. 11-17.

[5] Wang, J., Fan, W., Li, Y., Xiao, M., Wang, K., Ren, P. (2012). The effect of air staged combustion on NO_x emissions in dried lignite combustion. *Energy, vol.* 37, pp. 725-736.

[6] Hesselmann, G., Rivas, M. (2001). What are the main NO_x formation processes in combustion plant? *IFRF Online Combustion Handbook*. (66) ISSN 1607-9116.

[7] Baukal, C., Zinc, J. (2005) Everything You Need to Know About NO_x. *Pollution Control*. p18-24.

[8] Ochi, K., Kiyama, K., Yoshizako, H., Okazaki, H., Taniguchi, M. (2009). Latest Low-NO_x Combustion Technology for Pulverized-coal-fired Boilers. *Hitachi Review*. (58) no. 5, p. 187-193.

[9] Kurose, R., Watanabe, H., Makino, H. (2009). Numerical Simulations of Pulverized Coal Combustion. *KONA Powder and Particle Journal*. (27) p. 144-156.

[10] Álvarez, L., Gharebaghi, M., Jones, J.M., Pourkashanian, M., Williams, A., Riaza, J., Pevida, C., Pis, J.J., Rubiera, F. (2012). CFD modelling of oxy-coal combustion: Prediction of burnout, volatile and NO precursor's release. *Applied Energy,* vol. 104, pp. 653-665.

[11] Constenla, I., Ferrín, J.L., Saavedra, L. (2013). Numerical study of a 350 MWe tangentially fired pulverized coal furnace of the As Pontes Power Plant. *Fuel Processing Technology,* vol. 116, pp. 189-200.

[12] Peta, S., (2013). Preliminary Low NO_x burner design and operation review. *Eskom Group Technology Division*.

[13] Kychakoff, G., Hollingshead, A.F., Stewart, P.B. (2005). Use of Acoustic temperature measurements in the cement manufacturing pyroprocess. *Penta Engineering*, Enertechnix Inc. 0-7803-9107-1/05.

[14] Rinaldi, F., Najafi. B. (2013). Temperature measurement in WTE boilers using suction pyrometers. *Department of Energy*, Sensors, vol. 13, pp. 15633-15655.

[15] Parente, A., Coraggio, G., Galletti, C., Tognotti, L. (2010). Verification, validation and uncertainty quantification in industrial combustion modelling: some practical tools. *Livorno*. IFRF Doc. No G25/y/01 - 15.

[16] MICRO-EPSILON. Basics of non-contact temperature measurement. Y9766331-A021021DGO.

[17] Collective of authors, IMPAC Infrared GmbH. (2004). *Pyrometer Handbook*. Frankfurt am Main Germany.

[18] Authier, O., Thunin, E., Plion, P., Schönnenbeck, C., Leyssens, G., Brilhac, J., Porcheron, L. (2014). Kinetic study of pulverized coal devolatilization for boiler CFD modelling. Fuel, vol. 122, pp. 254-260.

[19] Nsakala, N.Y., Goetz, G.J., Pate1, R.L., Lao, T.C. Pyrolysis and combustion characterization of pulverized coals for industrial applications. *Department of Energy*. Combustion Engineering.

[20] Li, H., Elliott, L., Rogers, H., Wall, T. (2013). Coal burnout in a pilot-scale rig simulating pulverised coal injection and a laboratory drop tube furnace. *10th Australian Coal Science Conference.*

[21] Man, C.K., Gibbins, J.R., Cashdollar, K.L. Effect of coal type and oxyfuel combustion parameters on pulverised fuel ignition. *Dept. of Mechanical Engineering, Pittsburgh Research Laboratory.*

[22] Li, S. (2010). Char-slag transition during pulverized coal gasification. Doctor of Philosophy. *Department of Chemical Engineering: The University of Utah.*

[23] Cloke, M., Lester, E., Thompson, A.W. (2002). Combustion characteristics of coal using a drop tube furnace. Fuel, vol. 81, pp. 727-735.

[24] Rodriguez. M., Raiko, R. Effect of O_2 and CO_2 content on particle surface temperature and size of coal char during combustion. *Department of Energy and Process Engineering (EPR): Tampere University of Technology.*

[25] Murphy, J.J., Shaddix, C.R. (2006). Combustion kinetics of coal chars in oxygen-enriched environments. Combustion and Flame, vol. 144, pp.710-729.

[26] Peta, S. (2014). Ignition characteristics of low volatile quality high ash coal. MSc. Dissertation. Johannesburg: *University of Witwatersrand*.

[27] Versteeg, H.K., Malalasekera, W. (1995). An introduction to Computational Fluid Dynamics the Finite Volume method. United States: *John Wiley & Sons Inc*.

[28] Zuo, W. Introduction of Computational Fluid Dynamics. *St. Petersburg*

[29] Bekker, A. (2002). Applied Computational Fluid Dynamics. Lecture 1 - Introduction to CFD. *Fluent Inc.*

[30] Jeong, H.J., Seo, D.K., Hwang, J. (2014). CFD modelling for coal size effect on coal gasification in a two-stage commercial entrained-bed gasifier with an improved char gasification model. *Applied Energy*, vol. 123, pp. 29-36.

[31] Zou, C., Cai, L., Zheng, C., (2014). Numerical research on the homogeneous / heterogeneous ignition process of pulverized coal in oxy-fuel combustion. *International Journal of Heat and Mass Transfer*, vol. 73, pp. 207-216.

[32] Jovanovic, R., Milewska, A., Swiatkowski, B.,Goanta, A., Spliethoff, H. (2011). Numerical investigation of influence of homogeneous/heterogeneous ignition/ combustion mechanisms on ignition point position during pulverized coal combustion in oxygen enriched and recycled flue gases atmosphere, Int. J. Heat Mass Transfer, vol. 54, pp. 921-931.

[33] Jovanovic, R., Milewska, A., Swiatkowski, B., Goanta, A., Spliethoff, H. (2012). Sensitivity analysis of different devolatilisation models on predicting ignition point position during pulverized coal combustion in O_2/N_2 and O_2/CO_2 atmospheres. *Fuel*, vol. 123, pp. 23-37.

[34] Niksaa, S., Liua, G., Hurt, R.H. (2003). Coal conversion submodels for design applications at elevated pressures. Part I. devolatilization and char oxidation. *Progress in Energy and Combustion Science*, vol. 29, pp. 425-477.

[35] Torresi, M., Fortunato, B., Camporeale, S.M., Saponaro, A. Numerical simulation of a Low-NOx burner for coal firing. Meeting of the Italian Section of the Combustion Institute.

[36] Niksa Energy Associates, (1997-2015). User Guide and Tutorial, PC Coal Lab, Version 4.3.

[37] Le Bris, T., Cadavid, F., Caillat, S., Pietrzyk, S., Blondin, J., Baudoin, B. (2007). Coal combustion modelling of large power plant, for NOx abatement. *Fuel*, vol. 86, pp. 2213–2220.

[38] Niksa, S., Kerstein, A.R. (1991). Flashchain Theory for Rapid Coal Devolatilization Kinetics. Part 1. Formulation. *Energy and Fuels*, vol. 5(5), pp. 647-664.

[39] Liu, G., Niksa, S., Hurt, R.H. (2004). Coal Conversion Submodels for Design Applications at Elevated Pressures. Part II. Char Gasification. *Prog. Energy Combust. Sci*. vol. 30(6), pp. 697- 717.

[40] Niksa, S., Liu, G., Hurt, R.H. (2003). Coal Conversion Submodels for Design Applications at Elevated Pressures. Part I. Devolatilization and Char Oxidation. *Prog. Energy Combust. Sci*. vol. 29, pp. 425-477.

[41] Maffei, T., Frassoldati, A., Cuoci, A., Ranzi, E., Faravelli, T. (2013). Predictive one step kinetic model of coal pyrolysis for CFD applications. *Proc Combust Inst*. vol. 34, pp. 2401–2410.

[42] Jovanovic, R., Milewska, A., Swiatkowski, B., Goanta, A., Spliethoff, H. (2011) Numerical investigation of influence of homogeneous/heterogeneous ignition/ combustion mechanisms on ignition point position during pulverized coal combustion in oxygen enriched and recycled flue gases atmosphere. Int. J. Heat Mass Transfer, vol. 54, pp. 921-931.

[43] ANSYS. (2012) ANSYS FLUENT Theory Guide. Version 14.5.

[44] Launder, B.E., Spalding, D.B. (1972). Lectures in Mathematical Models of Turbulence. England: Academic Press.

[45] Chui, E.H., Raithby, G.D. (1993). Computation of Radiant Heat Transfer on a Non Orthogonal Mesh Using the Finite-Volume Method. *Numerical Heat Transfer, Part B*. vol. 23, pp 269-288.

[46] Raithby, G.D., Chui, E.H. (1990). A Finite-Volume Method for Predicting a Radiant Heat Transfer in Enclosures with Participating Media. *Heat Transfer*. vol. 112, pp. 415-423.

[47] Magnussen, B.F., Hjertager, B,H. (1976). On mathematical models of turbulent combustion with special emphasis on soot formation and combustion. *In 16th Symp. on Combustion*. The Combustion Institute.

[48] Gosman, D., Ioannides, E. (1983). Aspects of computer simulation of liquid-fuelled combustors. *J. Energy*. vol. 7(6), pp. 482-490.

[49] De Soete, G.G. (2005). Kinetics of the nitrogen oxides formation and destruction, related to the combustion of pulverised solid fuel. *In: International symposium on strategic approach for implementation of primary de NO_x measures in large EU pulverised coal and lignite fired units 2008–2015 and after 2015*. Greece.

[50] Monat, J.P., Hanson, R.K., Kruger, C.H. (1978). Shock tube determination of the rate coefficient for the reaction $O + N_2 \rightarrow N + NO$. Pittsburgh: *The Combustion Institute*. p. 543.

[51] "World Energy Outlook 2009" International Energy Agency (IEA) Report (WEO-2009), ISBN 978-92-64-06130-9, OECD/IEA.

[52] ANSYS FLUENT 14.5 Tutorial Guide. (2012) *Tutorial: Coal Combustion with Eddy Break Up (EBU) Model.* ANSYS, Inc.

[53] Bransden, B.H., Joachain, C.J. (2000). Quantum Mechanics. 2nd ed. Pearson.

[54] Baum, M.M., Street, P.J. (1971). Predicting the Combustion Behavior of Coal Particles. *Combust. Sci.Tech.* vol. 3(5), pp. 231-243.

[55] Field, M.A. (1969). Rate of Combustion of Size-Graded Fractions of Char from a Low Rank Coal between 1200 K–2000 K. *Combustion and Flame*. vol. 13, pp. 237-252

[56] Smith, I.W. (1982). The Combustion Rates of Coal Chars: A Review. *In 19th Symp. (Int'l.) on Combustion*. The Combustion Institute. pp. 1045-1065.

[57] Chedaille, J., Braud, Y. (1972). Measurements in flames. IFRF. vol. I, Edward Arnold.

[58] Van der Riet, M. (1998). Drop tube furnace (DTF) kinetic theory.

[59] Naidoo, R., Schmitz, W. (2010). Low NOx burner flow characterisation using CFD. *Eskom Technical Report*.

[60] Bicsák, G., Hornyák, A., Veress, A. (1992). Numerical Simulation of Combustion Processes in a Gas Turbine. *Budapest University of Technology and Economics*. Hungary.

[61] Munson, B.R., Young, D.F., Okiishi, T.H. (2006). Fundamentals of Fluid Mechanics. 5th ed. *John Wiley & Sons, Inc*.

[62] Noor, M.M., Wandel, A.P, Yusaf, T. (2013). Detail guide for CFD on the simulation of Biogas combustion in bluff-body mild burner. *International Conference on Mechanical Engineering Research (ICMER2103).* Paper ID: P342.

[63] Yamamoto, K., Kina, D., Okazaki, T., Taniguchi, M., Okazaki, H. (2011). LES of pulverized coal combustion furnaces. *Proceeding of the ASME 2011 Power Conference.* USA.

[64] Yilmaz, A., Davé, P. (2003). Individual burner air flow measurement and CFD modelling expedites low NOx burner optimization boiler commissioning. *Riley Power Inc*. Florida.

APPENDIX A

Centre Line		Bottom Port	
Probe postion from burner mouth (m)	Temperature (°C)	Probe postion from burner mouth (m)	Temperature (°C)
0.00	46.00	0.00	238.92
0.50	126.10	0.50	690.40
1.00	335.20	1.00	600.00
1.50	750.20	1.50	1025.42
1.75	988.33	2.00	1138.50
2.00	1058.86	2.50	1260.40
2.50	1223.42	3.00	1305.00
		3.50	1336.40

Table 10-1: In-Flame burner temperature results

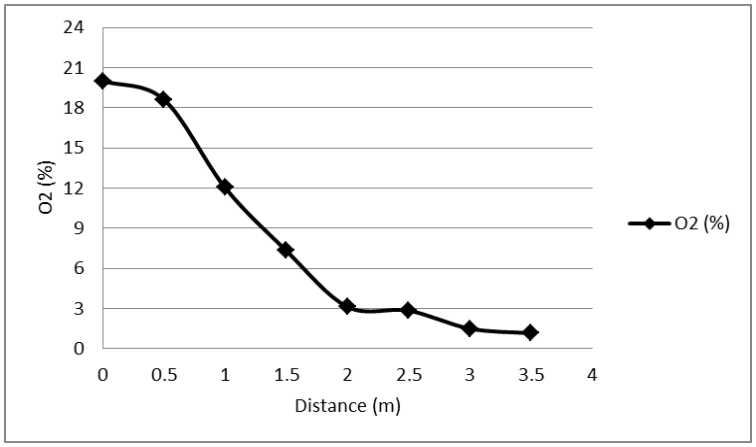


Figure 10-1: Oxygen concentration through bottom-port

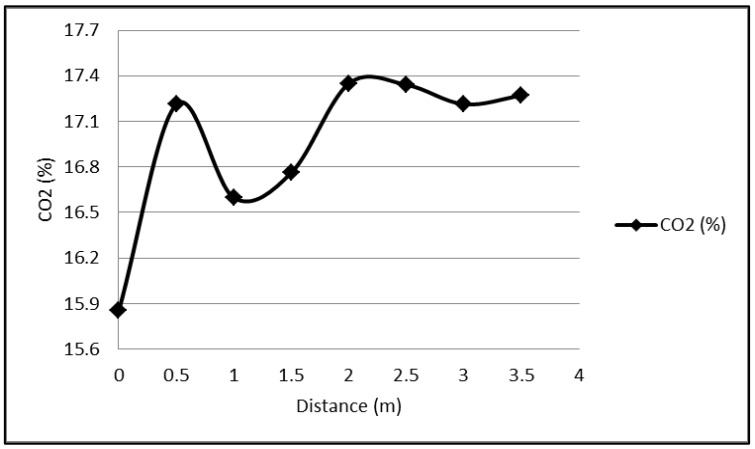


Figure 10-2: Carbon dioxide concentration through bottom-port

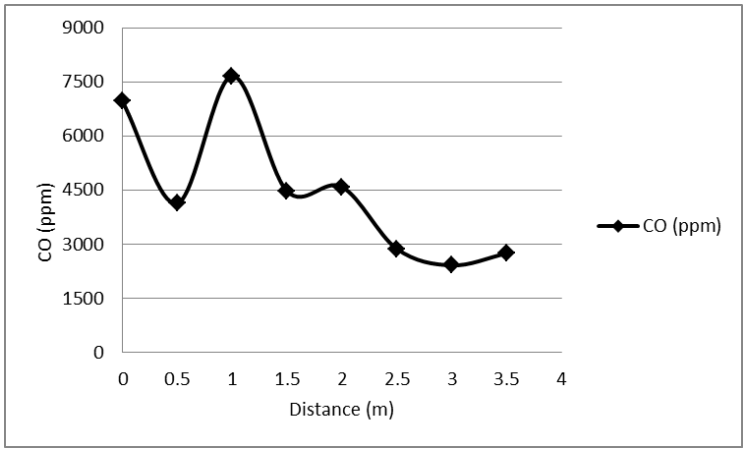


Figure 10-3: Carbon monoxide concentration through bottom-port

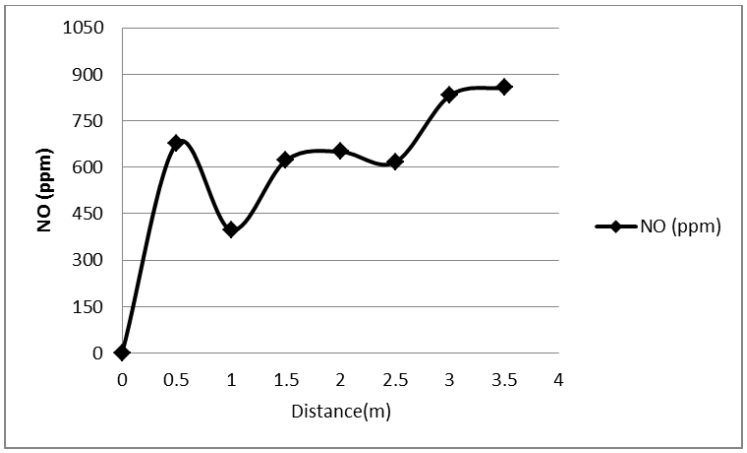


Figure 10-4: NOx concentration through bottom-port

APPENDIX B

TEST MEASUREMENTS

TEST No. 1

DATE 21/10/14

Mill Running Hours

start test 14H00

end test 14H15

PANEL

PRIMARY AIR FLOW (kg/s)	9.5
COAL FLOW (kg/s)	
FEEDER SPEED rpm	
MILL INLET TEMP. °C	220
MILL OUTLET TEMP. °C	85.3
MILL DIFF. PRESSURE (kPa)	4.1
GAS LOADING PRESSURE Mpa	1.05

COAL

CLASSIFIER		
VANES POSITION	35	
BALL TIME (sec)	94	
BIN MASS (kg)	37.4	
Coal BULK DENSITY	961.1	(kg/m3)
Primary Air DENSITY	0.621	(kg/m3)
PA DIFF. (kPa)	0.34	
PA K- factor	17.4	

MILL INLET MEASUREMENTS

PRIMARY AIR (kg/s)	8.0
FEEDER COALFLOW (kg/s)	5.0
AIR / FUEL RATIO	1.6

PF SAMPLES

Sampling time : 15 sec per point x 32 points per pipe — Masses in grams

PF PIPE	1	2	3	4
container + sample	870	204	663	786
Mass of Container	10.4	10.4	10.4	10.4
Mass of Sample	859.9	193.7	652.1	776.0
Average	620.4			
% deviation from mean	38.6	-68.8	5.1	25.1

% coal total moisture	8.0
% moisture evaporated	6.5
Coalflow to burners (kg/s)	4.7

Each sample is reduced to a representative sample

60 grams of sample is Dried in oven @ 110 °C for one hour				
DRY MASS grams	59.1	58.9	59.2	59.1
% PF MOISTURE	1.5	1.8	1.3	1.5

SIEVING

50 grams sieved

PF PIPE	1	2	3	4
Retained PF mass > 300 um	0.2	0.4	0.4	0.2
Retained PF mass > 150 um	1.7	0.6	1.3	2.0
Retained PF mass > 106 um	5.3	1.7	3.7	4.9
Retained PF mass > 75 um	9.2	6.1	8.4	10.1
Collected in the receiver	33.6	41.3	36.5	32.9
Sum totals	50.0	50.1	50.3	50.1

PF PIPE MEASUREMENTS

PIPE No.	Velocity Pressure	Static Pressure	Temp	Atmos Pressure	Density
	kPa	kPa	C	kPa	kg/m3
1	0.38	0.8	84	84.0	0.8373
2	0.38	1.1	78		0.8444
3	0.32	0.7	77		0.8430
4	0.34	0.8	78		0.8410

Figure 10-5: PF sampling & grading

DATE 21/10/14

LOAD HIGH

PA flow 9.5 kg/s

CONDITIONS :

Vanes position 35 degrees

PF PIPE MEASUREMENTS						PF GRADING RESULTS			
PIPE No.	Coalflow kg/s	% Deviation	Airflow kg/s	Temp °C	Velocity m/s	% Passing 300 u	% Passing 150 u	% Passing 106 u	% Passing 75 u
1	1.6	38.6	2.4	84	26	99.6	96.2	85.6	67.2
2	0.4	-68.8	2.2	78	25	99.2	98.0	94.6	82.4
3	1.2	5.1	2.2	77	23	99.2	96.6	89.2	72.4
4	1.5	25.1	2.2	78	24	99.6	95.6	85.8	65.6

TOTAL	4.7	TOTAL	9.0
tons/hr	16.8	tons/hr	32.5

WEIGHTED AVERAGE FOR THE MILL			
% Passing 300 u	% Passing 150 u	% Passing 106 u	% Passing 75 u
99.5	**96.3**	**87.3**	**69.3**

Figure 10-6: PF sampling results

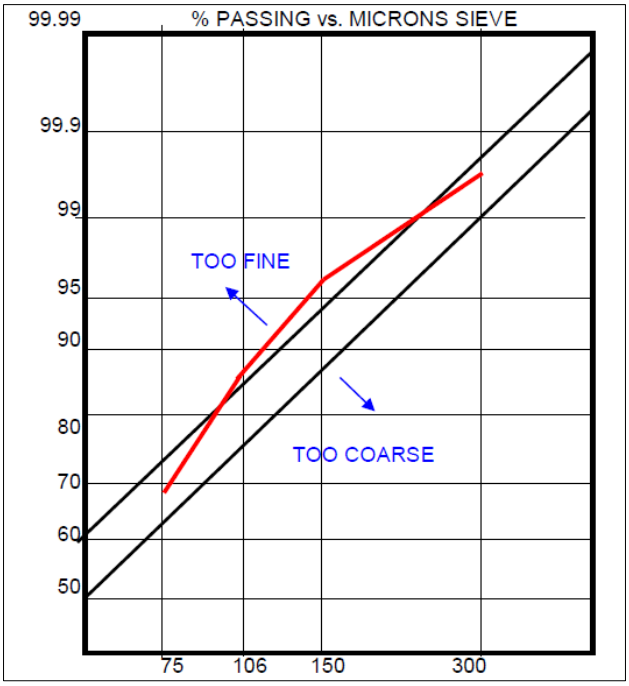


Figure 10-7: Rosin-Rammler graph

APPENDIX C

SAMPLING LEVEL	UNITS	LHS	RHS
FURNACE EXIT			
Flue Gas Temperature	(°C)	1103	1113
Oxygen Concentration	%	2.17	2.39
Carbon Monoxide Concentration	ppm	522	86
Carbon Monoxide Concentration	ppm @ 6% O_2	416	70
Carbon Dioxide Concentration	%	17.30	17.09
Carbon Dioxide Concentration	% @ 6% O_2	13.77	13.77
Nitrogen Concentration	ppm	856	846
Nitrogen Concentration	ppm @ 6% O_2	682	682
Average Nitrogen Concentration	mg/Nm^3 @ 6% O_2	913	
Combustion Efficiency	%	98.11	99.28
Average Combustion Efficiency	%	99	
SUPERHEATER BOTTOM BANK	(°C)		
SUPERHEATER TOP BANK	(°C)		
ECONOMISER INLET			
Flue Gas Temperature	(°C)	597	610
Oxygen Concentration	%	2.32	2.43
Carbon Monoxide Concentration	ppm	97	140
Carbon Monoxide Concentration	ppm @ 6% O_2	78	113
Carbon Dioxide Concentration	%	17.27	17.12
Carbon Dioxide Concentration	% @ 6% O_2	13.86	13.82
Nitrogen Concentration	ppm	860	851
Nitrogen Concentration	ppm @ 6% O_2	690	687
Average Nitrogen Concentration	mg/Nm^3 @ 6% O_2	923	
LEAKAGE BETWEEN FURNACE EXIT AND ECO-INLET	%	0.83	0.22
ECONOMISER OUTLET			
Flue Gas Temperature	(°C)	313	309
Oxygen Concentration	%	3.85	3.65
Carbon Monoxide Concentration	ppm	24	12
Carbon Monoxide Concentration	ppm @ 6% O_2	21	10
Carbon Dioxide Concentration	%	15.82	16.01
Carbon Dioxide Concentration	% @ 6% O_2	13.83	13.84
Sulphur Dioxide Concentration	ppm	1068	947
Sulphur Dioxide Concentration	ppm @ 6% O2	932	819
Average Sulphur Dioxide Concentration	mg/Nm^3 @ 6% O_2	2504	
Nitrogen Concentration	ppm	789	795
Nitrogen Concentration	ppm @ 6% O_2	689	687
Average Nitrogen Concentration	mg/Nm^3 @ 6% O_2	922	
Combustion Efficiency (Cegrit Sampler)	%		
Average Combustion Efficiency	%		
LEAKAGE BETWEEN ECO-INLET AND ECO-OUTLET	%	8.94	7.07
LEAKAGE BETWEEN ECO-OUTLET AND FURNACE EXIT	%	9.85	7.30

Figure 10-8: Measurements carried out by Eskom RT&D

APPENDIX D

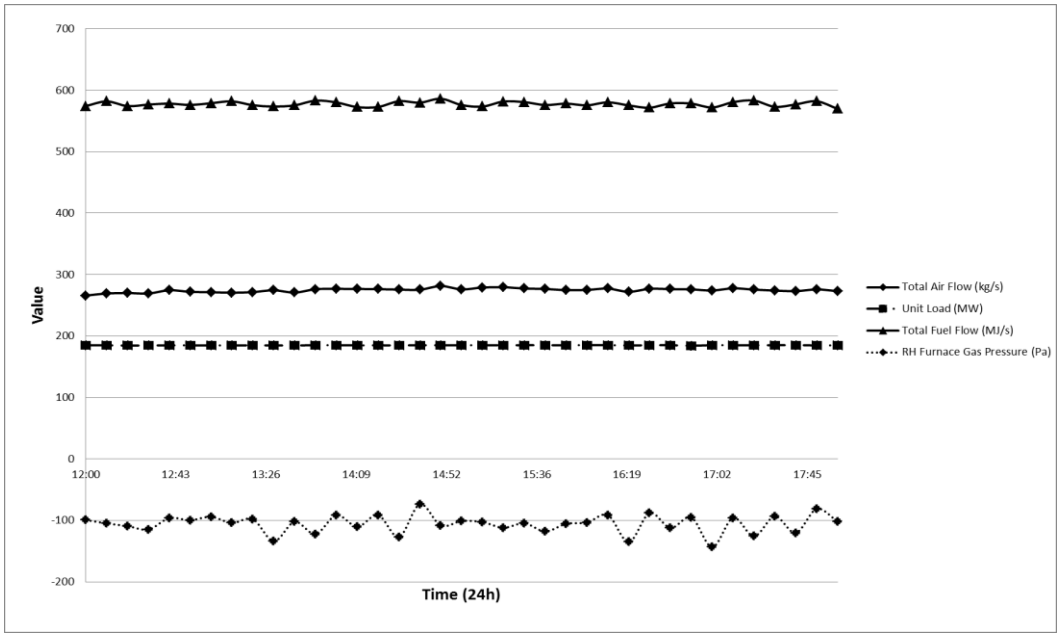


Figure 10-9: Unit critical operating values

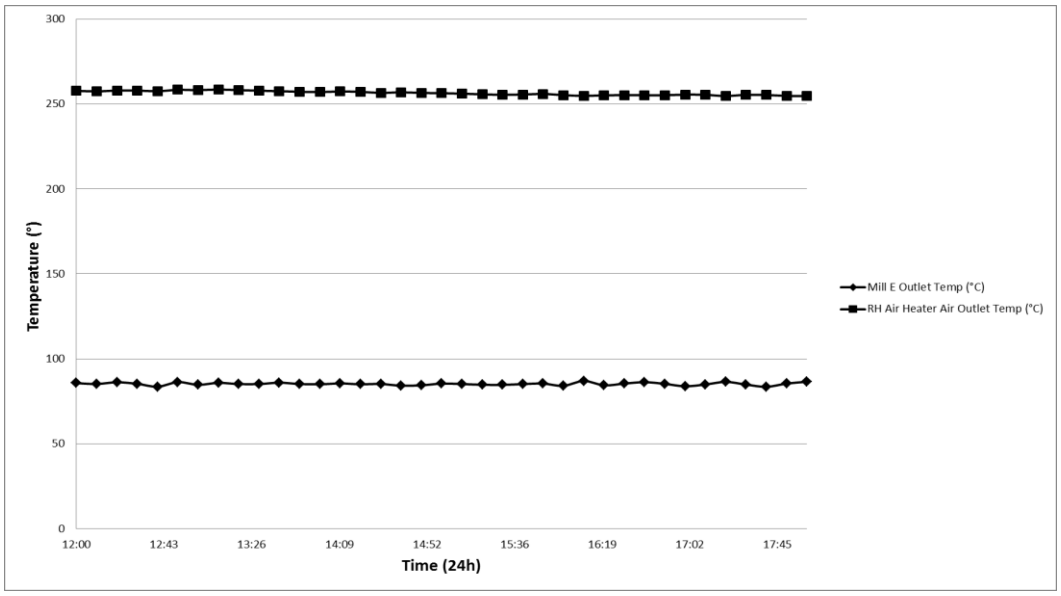


Figure 10-10: Mill E & RH Air Heater outlet temperatures

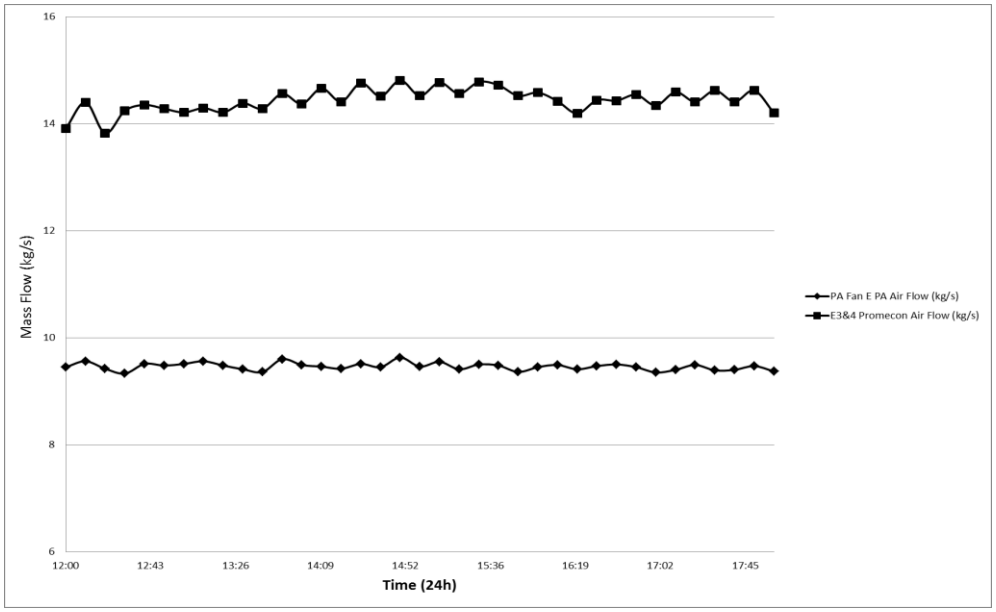


Figure 10-11: PA fan E PA air flow per burner pair

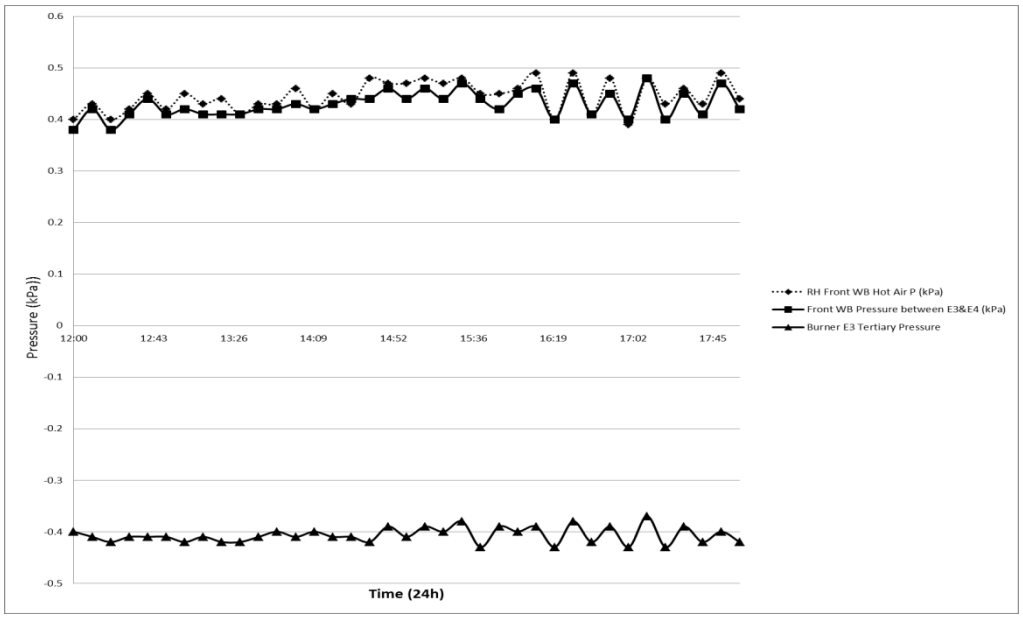


Figure 10-12: Winbox & burner pressure

APPENDIX E

d(V(t) / dt)	V(ult) - V(t)	Ks	Ln Ks	Tp (K)	1 / Tp
0.000	42.4	0.000	0.000	298.15	0.0034
0.000	42.4	0.000	0.000	337.15	0.0030
0.000	42.4	0.000	0.000	381.15	0.0026
0.000	42.4	0.000	0.000	421.15	0.0024
0.000	42.4	0.000	0.000	458.15	0.0022
0.000	42.4	0.000	0.000	493.15	0.0020
105.263	42.4	2.483	0.909	527.15	0.0019
315.789	42.3	7.465	2.010	559.15	0.0018
416.667	42	9.921	2.295	591.15	0.0017
210.526	41.6	5.061	1.622	622.15	0.0016
306.122	41.4	7.394	2.001	651.15	0.0015
222.222	41.1	5.407	1.688	681.15	0.0015
500.000	40.9	12.225	2.503	709.15	0.0014
777.778	40.4	19.252	2.958	738.15	0.0014
1200.000	39.7	30.227	3.409	765.15	0.0013
1363.636	38.5	35.419	3.567	794.15	0.0013
2068.182	37	55.897	4.024	826.15	0.0012
2428.571	27.9	87.046	4.466	947.15	0.0011
1021.277	12.6	81.054	4.395	1108.15	0.0009
134.715	3	44.905	3.805	1270.15	0.0008
2.954	0.4	7.386	2.000	1385.15	0.0007

Table 10-2: Arrhenius equation parameters used in devolatilization kinetics calculation

APPENDIX F

DVOL - Notepad

File Edit Format View Help

```
0.005
  25.    1319.
  99.    1323.
 170.    1327.
 239.    1331.
 305.    1335.
 369.    1338.
 429.    1342.
 488.    1346.
 544.    1350.
 597.    1354.
 648.    1358.
 696.    1361.
 741.    1365.
 784.    1369.
 824.    1372.
 862.    1376.
 897.    1379.
 930.    1382.
 960.    1386.
 988.    1389.
1013.    1392.
1035.    1394.
1055.    1397.
1072.    1400.
1086.    1402.
1098.    1404.
1108.    1406.
1115.    1408.
1119.    1410.
1121.    1411.
1120.    1412.
1116.    1413.
1110.    1414.
1102.    1414.
1090.    1415.
1077.    1415.
1060.    1414.
1041.    1414.
1020.    1413.
1020.    1412.
```

FDC1WT1 - Notepad

File Edit Format View Help

```
                    DROP TUBE SIMULATION WITH PC COAL LAB

                                FULL DYNAMICS

 COAL CHARACTERISTICS:

          Ultimate, daf wt.%        Proximate, as rec wt.%
               %C 81.2                   Moisture   0.0
               %H  4.2                   Vol. Mat. 21.2
               %O 10.0                       Ash  30.1
               %N  1.9                    Fixed C  48.7
               %S  1.8

 OPERATING CONDITIONS:

          90.0 micron particles at   25. C are entrained in N2
        with  0.0 % O2 at  1400. C in a furnace at  1400. C
        for .190E+00 s.  The ambient pressure is   0.10 MPa.


   **User-specified conditions were implemented during devolatilization.**

  Thermal History  Wt.Loss     Products, daf wt.%
   Time,s  Tmp,C   daf wt.%    Ygas   Ytar   Ychr

 .000E+00   25.      0.0        0.0    0.0  100.0
 .173E-02   60.      0.0        0.0    0.0  100.0
 .392E-02  100.      0.0        0.0    0.0  100.0
 .611E-02  137.      0.0        0.0    0.0  100.0
 .830E-02  171.      0.0        0.0    0.0  100.0
 .105E-01  203.      0.0        0.0    0.0  100.0
 .127E-01  234.      0.0        0.0    0.0  100.0
 .149E-01  263.      0.1        0.0    0.0   99.9
 .171E-01  291.      0.2        0.0    0.1   99.8
 .192E-01  319.      0.5        0.1    0.4   99.5
 .214E-01  345.      0.8        0.1    0.7   99.2
 .236E-01  372.      1.0        0.2    0.9   99.0
 .258E-01  398.      1.2        0.2    1.0   98.8
 .280E-01  423.      1.4        0.3    1.1   98.6
 .302E-01  449.      1.8        0.4    1.3   98.2
 .325E-01  475.      2.3        0.6    1.8   97.7
 .351E-01  505.      3.3        0.8    2.5   96.7
 .451E-01  618.      9.8        2.3    7.5   90.2
 .597E-01  781.     25.1        7.1   18.0   74.9
 .812E-01  987.     38.2       11.6   26.7   61.8
 .125E+00 1180.     42.0       14.1   27.9   58.0
 .190E+00 1145.     42.7       14.8   27.9   57.3
```

Figure 10-13: (Left) – "Dvol.inp" file containing wall and gas temperature profiles. (Right) - PC coal lab volatile yield result

SFORC1T1 - Notepad

File Edit Format View Help

```
                    DROP TUBE SIMULATION WITH PC COAL LAB

                          RATE PARAMETER ASSIGNMENTS

 FUEL CHARACTERISTICS:

          Ultimate, daf wt.%        Proximate, as rec wt.%
               %C 81.2                   Moisture   0.0
               %H  4.2                   Vol. Mat. 21.2
               %O 10.0                       Ash  30.1
               %N  1.9                    Fixed C  48.7
               %S  1.8

 OPERATING CONDITIONS:

          90.0 micron particles at   25. C are entrained in N2
        with  0.0 % O2 at  1400. C in a furnace at  1400. C
        for .190E+00 s.  The ambient pressure is   0.10 MPa.


                            SFOR RATE PARAMETERS

   Product  Ult. Yld.  A-Fac.  Eapp   r2 coef.  time    Yfc   Yfit
            daf wt. %   1/s  kcal/mole           s

 Wt. Loss     42.73    1454.5  7.23  -0.956  .392E-02   0.00   0.01
                                             .140E-01   0.04   0.25
                                             .241E-01   1.06   1.58
                                             .345E-01   3.09   5.25
                                             .190E+00  42.73  42.73
```

Figure 10-14: PC coal lab devolatilization coal combustion kinetics result

APPENDIX G

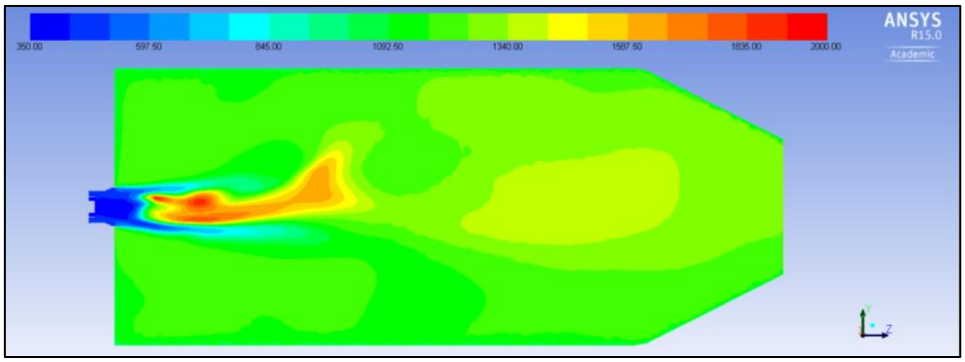


Figure 10-15: Contours of static temperature (K) - updated kinetics

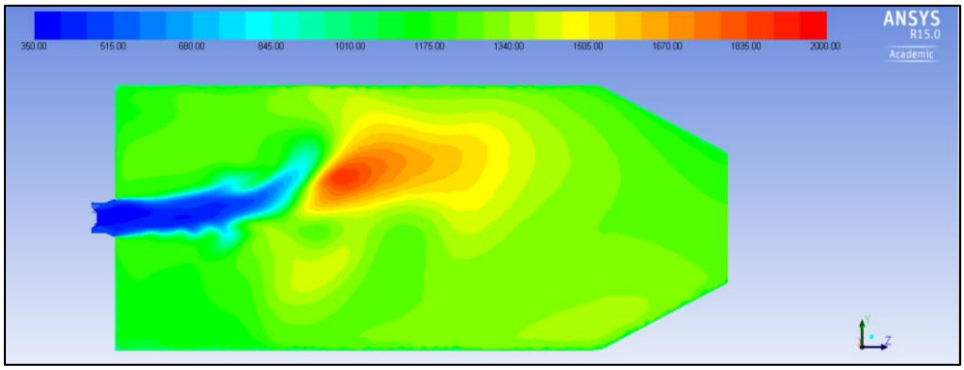


Figure 10-16: Contours of static temperature (K) - default kinetics

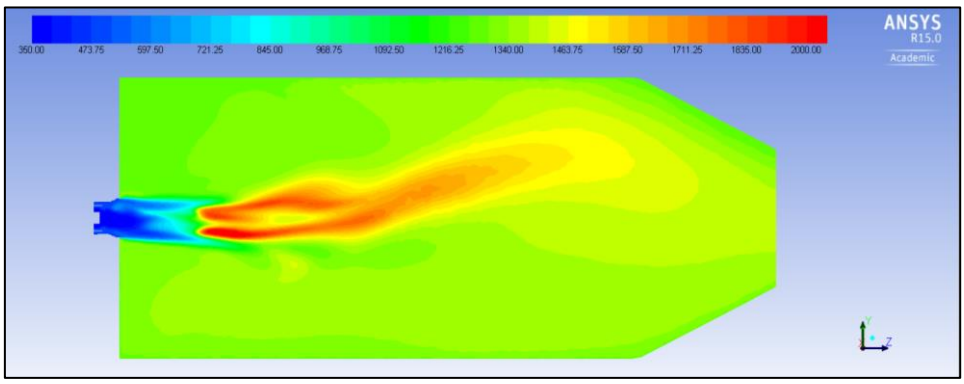


Figure 10-17: Contours of static temperature (K) - diffusion limited

APPENDIX H

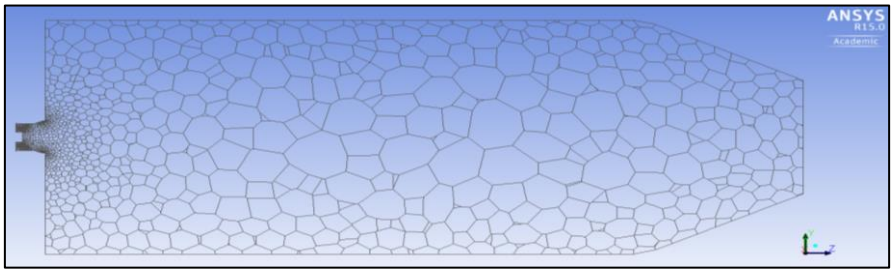


Figure 10-18: Mesh 1

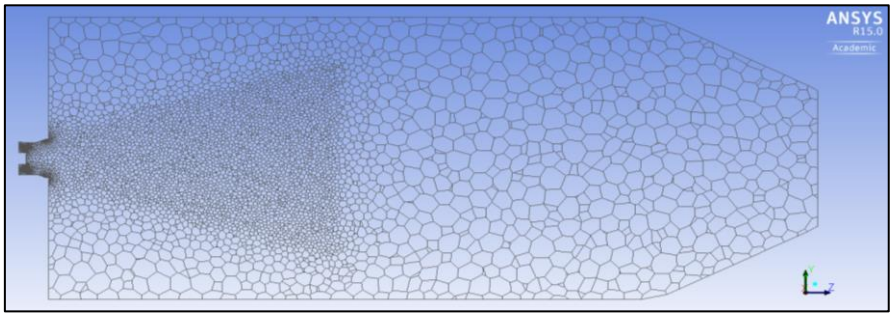


Figure 10-19: Mesh 2

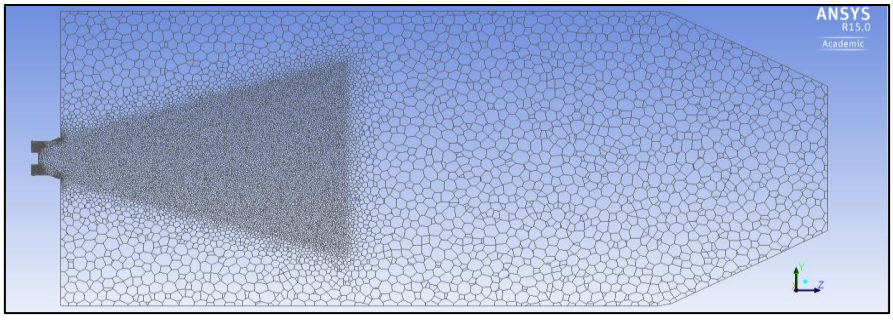


Figure 10-20: Mesh 3

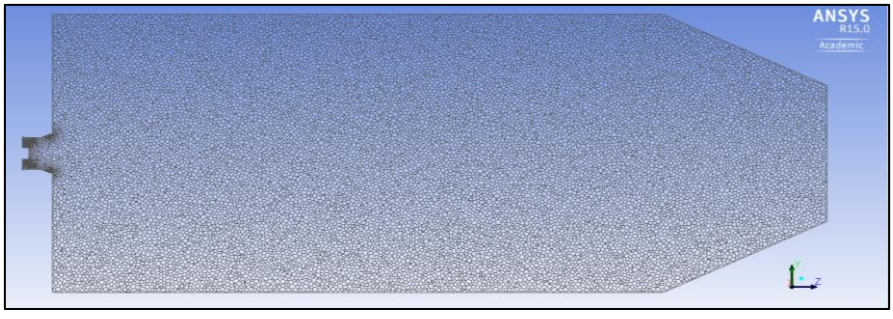


Figure 10-21: Mesh 4

APPENDIX I

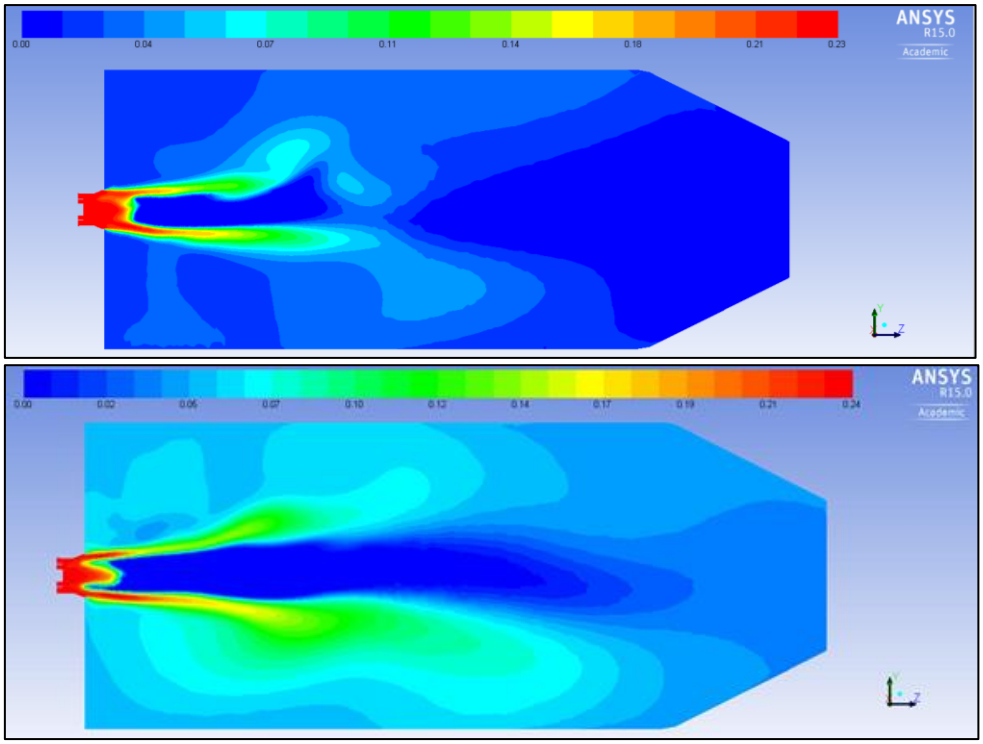


Figure 10-22: (Top) - Contours of mass fraction of O_2 during baseline flows. (Bottom) - Contours of mass fraction of O_2 during design flows

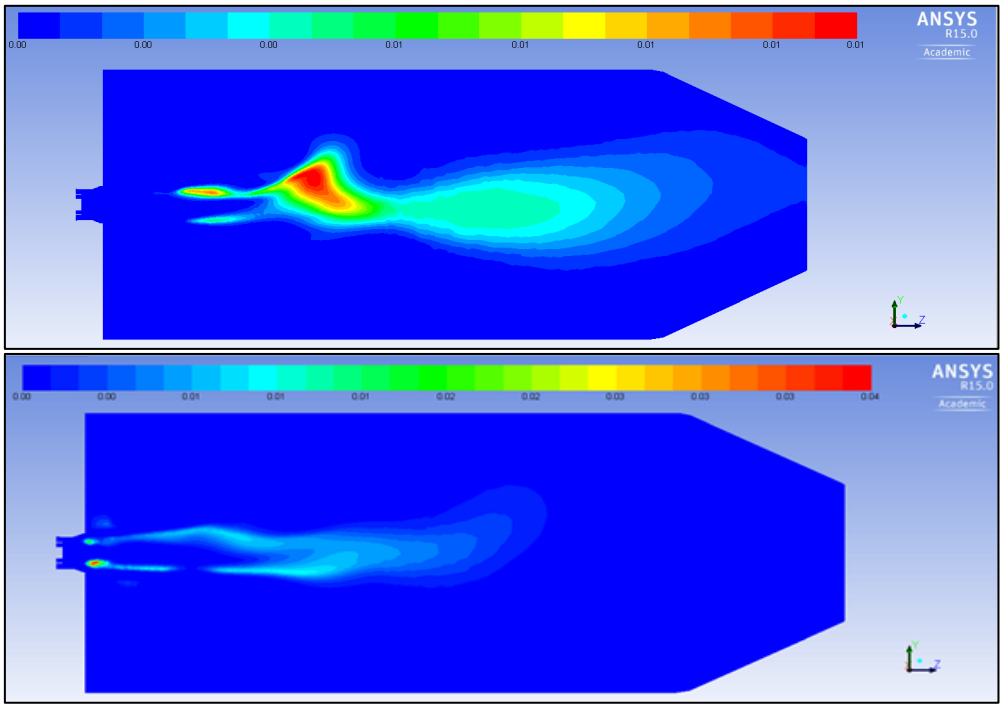


Figure 10-23: (Top) - Contours of mass fraction of CO during baseline flows. (Bottom) - Contours of mass fraction of CO during design flows

APPENDIX J

To ensure mass was conserved throughout the simulation a mass balance was done for the gas phase during the baseline solution. The mass flow of gas at the inlet and outlet surfaces was calculated through a surface report calculation. The inlet gas mass flow of the discrete phase was calculated as follow:

$$PF_{gas} = 1.2 * (1 - Ash\ \%) \quad \text{(J1)}$$

PF_{gas} = *Product available for combustion excluding inert ash (%)*

1.2 = *Mass flow of particles (kg/s)*

(1 – Ash %) = *Percentage of particles converted to the gas phase*

Ash % (Dry basis) = *0.2925*

The gas phase values assuming complete combustion with only ash remaining as product are shown in Table 10-3 below.

Table 10-3: Gas phase mass balance

	Inlet (kg/s)	Outlet (kg/s)
PA_in	2.2	
SA_in	1.56	
TA_in	5.72	
PF_gas	0.84906	
	10.329	10.360
Net		0.031

The gas phase outlet mass flow of 10.360 was calculated by means of CFD by using the mass flow outlet surface report. The net flow of 0.031 kg/s on the outlet surface showed that mass was conserved throughout the simulation.

To establish an estimated theoretical peak flame temperature that should be achieved through the CFD simulation a basic energy balance was generated. The control volume was focused on the combustion zone with the energy balance broken down into its most elementary form and adiabatic conditions assumed. The conservation of energy was defined as:

$$E_{in} = E_{out} \quad \text{(J2)}$$

The energy into the control volume was simplified to consider only the most influential heat input identified as the heat available from the combusting reactants. The heat available from the combustion reactants was calculated from the gross calorific heating value of the coal.

The maximum energy available into the control volume $E_{in} = m_{coal} * CV_{coal}$ (J3)

m_{coal} - *Mass flow of coal (kg/s)*

CV_{coal} - *Gross Calorific value of coal (kJ/kg)*

Thus:

E_{in} = *(1.2) (20899)*

= *25068 (kJ/s)*

This energy value represents the maximum heat available to heat the combusting products to the peak flame temperature.

The energy out of the control volume considered was the energy loss due to the increase of temperature of the combustion products. The combustion products were simplified to the flue gas containing all the combusting gas species and ash respectively.

The energy out of the system considered was:

$$E_{out} = Heat_{flue\ gas} + Heat_{ash} \quad \text{(J4)}$$

$$Heat_{flue\ gas} = m_{flue\ gas} * Cp_{flue\ gas} * \Delta T \quad \text{(J5)}$$

$m_{flue\ gas}$ - *Mass flow of flue gas (kg/s)*

$Cp_{flue\ gas}$ - *Specific heat of flue gas (kJ/kg.K)*

ΔTf - *Flue gas temperature increase (K)*

The specific heat of the flue gas was determined as follow:

From the stoichiometric air calculations assuming complete combustion the flue gas consist of CO_2, SO_2, and H_2O. With associated mole ratios of:

$CO_2 = 0{,}878$

$SO_2 = 0.011$

$H_2O = 0.111$

Therefore the specific heat of the flue gas was calculated as a collective value of the products of flue gas as follow:

$$Cp_{flue\ gas} = 0.878(Cp_{CO2}) + 0.011(Cp_{SO2}) + 0.111(Cp_{H2O}) \quad \text{(J6)}$$

The specific heat value of CO_2, SO_2, and H_2O were obtained from an engineering calculator with the $Cp_{flue\ gas}$ to be:

$$Cp_{flue\ gas} = 0.878(1.348) + 0.011(0.9) + 0.111(2.711)$$

$$= 1.4944$$

$$Heat_{ash} = m_{ash} * Cp_{ash} * \Delta T \quad \text{(J7)}$$

m_{ash} - *Mass flow of flue gas (kg/s)*

Cp_{ash} - *Specific heat of ash (kJ/kg.K)*

ΔTa - *Ash temperature increase (K)*

The specific heat of ash was obtained from an engineering calculator and was determined to be 0.84.

The energy out was calculated as:

$$E_{out} = (10.329)*(1.494)*(Tp - 430) + (0.35)*(0.84)*(Tp - 353) \quad \text{(J8)}$$

$$= 15.73\ Tp - 6741.11$$

From conservation of energy the theoretical peak flame temperature was calculated as:

$$25068 = 15.73\,Tp - 6741.11$$

$$\boldsymbol{Tp = 2022\ (K)}$$

The CFD calculated peak flame temperature was 2091 (K) and was well within the range of the calculated temperature.

To obtain a more accurate and realistic result the energy balance could further be expanded to follow a far more detailed approach. Expanding the energy balance to include a complete set of inlets and outlet energy sources into and out of the control volume but did not form part of the current study.